

# **Development of Catalysts for Hydriodic Acid Decomposition Reaction for Hydrogen Generation from Thermochemical Cycles**

By  
**DEEPAK TYAGI**

CHEM01201004010

Bhabha Atomic Research Centre, Mumbai

*A thesis submitted to the  
Board of Studies in Chemical Sciences*

*In partial fulfillment of requirements  
for the Degree of*

**DOCTOR OF PHILOSOPHY**

*of*

**HOMI BHABHA NATIONAL INSTITUTE**



**August, 2015**

# Homi Bhabha National Institute

## Recommendations of the Viva Voce Committee

As members of the Viva Voce Committee, we certify that we have read the dissertation prepared by **Deepak Tyagi** entitled “**Development of Catalysts for Hydriodic Acid Decomposition Reaction for Hydrogen generation from Thermochemical Cycles**” and recommend that it may be accepted as fulfilling the thesis requirement for the award of Degree of Doctor of Philosophy.

Chairman - **Dr. D. Das**

Date:

*D. Das.*

23/05/2016

Guide / Convener - **Dr. S. R. Bharadwaj**

Date:

*S. R. Bharadwaj*

23/5/2016

Examiner - **Dr. Raj Ganesh Pala**

Date:

*Raj Ganesh Pala*

23/5/16

Member 1- **Dr. A. K. Tripathi**

Date:

*A. K. Tripathi*

23/05/2016

Member 2- **Dr. P. A. Hassan**

Date:

*P. A. Hassan*

23/05/2016

Member 3- **Dr. V. Sudarsan**

Date:

*V. Sudarsan*

23/05/2016

Tech. Advisor: **Dr. S. C. Parida**

Date:

*S. C. Parida*

23/05/2016

Final approval and acceptance of this thesis is contingent upon the candidate's submission of the final copies of the thesis to HBNI.

I/We hereby certify that I/we have read this thesis prepared under my/our direction and recommend that it may be accepted as fulfilling the thesis requirement.

Date: 23/5/2016

Place: Mumbai

*S. R. Bharadwaj*

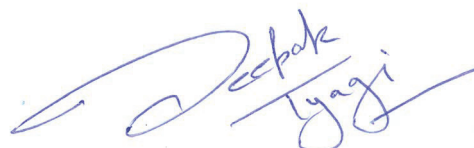
Dr. (Mrs.) S. R. Bharadwaj

Guide

## STATEMENT BY AUTHOR

This dissertation has been submitted in partial fulfillment of requirements for an advanced degree at Homi Bhabha National Institute (HBNI) and is deposited in the Library to be made available to borrowers under rules of the HBNI.

Brief quotations from this dissertation are allowable without special permission, provided that accurate acknowledgement of source is made. Requests for permission for extended quotation from or reproduction of this manuscript in whole or in part may be granted by the Competent Authority of HBNI when in his or her judgment the proposed use of the material is in the interests of scholarship. In all other instances, however, permission must be obtained from the author.



**(Deepak Tyagi)**

## DECLARATION

I, hereby declare that the investigation presented in the thesis has been carried out by me.

The work is original and has not been submitted earlier as a whole or in part for a degree/diploma at this or any other Institution / University.



**(Deepak Tyagi)**



## List of Publications arising from the thesis

### Journal:

1. Development of Pt-carbon catalysts using MCM-41 template for HI decomposition reaction in S-I thermo-chemical cycle; **Deepak Tyagi**, K. Scholz, S. Varma, K. Bhattacharya, S. Mali, P. S. Patil and S. R. Bharadwaj, *International Journal of Hydrogen Energy*, 37 (2012) 3602-3611.
2. Iodine speciation studies on Bunsen reaction of S-I cycle using spectroscopic techniques; **Deepak Tyagi**, Salil Varma, K. Bhattacharya, D. Jain, A. K. Tripathi, C. G. S. Pillai and S. R. Bharadwaj, *International Journal of Hydrogen Energy*, 37 (2012) 3621-3625.
3. Pt/zirconia catalyst for hydrogen generation from HI decomposition reaction of S-I cycle; **Deepak Tyagi**, Salil Varma and S. R. Bharadwaj, *International Journal of Energy Research*, 39(2015) 484-493.
4. Pt/graphite catalyst for HI decomposition reaction in sulfur - iodine thermo-chemical cycle; **Deepak Tyagi**, Salil Varma and S. R. Bharadwaj, *International Journal of Energy Research*, 39(2015) 2008-2018.
5. Mesoporous carbon supported platinum nano-catalyst: Application for Hydrogen production by HI decomposition reaction in S-I cycle; **Deepak Tyagi**, S. Varma and S. R. Bharadwaj, *Journal of Nanoscience and Nanotechnology*, (doi:10.1166/jnn.2016.12812)
6. Pt catalysts supported on carbon derived from rice: Application for HI decomposition reaction of S-I cycle; **Deepak Tyagi**, Salil Varma and S. R. Bharadwaj, *International Journal of Green Energy* (Submitted)

7. Comparative activity and stability of oxide supported platinum catalysts for HI decomposition reaction of S-I cycle; **Deepak Tyagi**, Salil Varma and S. R. Bharadwaj, *International Journal of Energy Research* (To be submitted)

**News Letter/Bulletin:**

8. Development of Catalysts for Various Applications Related to DAE Programs", S. R. Bharadwaj et al, *BARC Newsletter, Founder Day Special Issue*, October 2012, 142-145
9. Pt/Carbon Catalysts with Varying Porosity for Hydrogen Generation Reaction by HI Decomposition Reaction of S-I Thermochemical Cycle Deepak Tyagi, Salil Varma, S. R. Bharadwaj, *SMC Bulletin* 6 (2015) 37-44.

**Conference:**

1. Development of Pt- Carbon Catalysts for HI Decomposition Reaction in S-I thermochemical Cycle Using Hard Templating Route ; D. Tyagi, K. Scholz, S. Varma, K. Bhattacharyya, and S.R. Bharadwaj; Proc. of 3rd International Symposium on Materials Chemistry, BARC, Mumbai December 2010. Page- 317.
2. Iodine speciation studies on Bunsen Reaction of S-I cycle using Spectroscopic techniques; Deepak Tyagi, Salil Varma, K. Bhattacharya, D. Jain, A. K. Tripathi, C. G. S. Pillai and S. R. Bharadwaj; International conference on Renewable Energy ( ICRE-2011) , Jaipur, Jan 2011
3. Development of Pt-Carbon Catalysts using MCM-41 template for HI decomposition reaction in S-I Thermochemical Cycle; Deepak Tyagi, K. Scholz, S.

Varma, K. Bhattacharya, S. Mali, P. S. Patil and S. R. Bharadwaj; International conference on Renewable Energy (ICRE-2011) , Jaipur, Jan 2011

4. Pt-Carbon catalysts by hard templating route; Deepak Tyagi, Salil Varma, A. N. Shirsat and S. R. Bharadwaj; Proceedings of the 18th International Symposium on Thermal Analysis (THERMANS-2012). Page 239-245

5. Pt/Graphite catalyst for HI decomposition reaction in Sulphur - Iodine thermochemical Cycle; Deepak Tyagi, Salil Varma, S. R. Bharadwaj, Proceedings of National conference on Carbon Materials 2012 (CCM12), Page 64.

6. Mesoporous Pt/carbon catalyst by Hard Templating Route using SBA-15 as a Template; Deepak Tyagi, Salil Varma, W.-D. Einicke, S. R. Bharadwaj and R. Gläser; Proceedings of National conference on Carbon Materials 2012 (CCM12), Page 159.

7. Nanocasting: A Versatile Tool for Preparation of Porous Pt/C Catalyst For HI Decomposition in S-I Thermochemical Cycle; Deepak Tyagi, Salil Varma and S. R. Bharadwaj; Proc. of 4th Interdisciplinary Symposium on Materials Chemistry (ISMC-2012), BARC, Mumbai December 2012, Page- 385

8. Pt/Titania catalyst for liquid phase HI decomposition reaction of Sulphur - Iodine Thermochemical Cycle, Deepak Tyagi, Salil Varma, Shyamala R. Bharadwaj Paper presented at 21st National Symposium on Catalysis “Catalysis for Sustainable Development” (CATSYMP-21) at IICT, Hyderabad during 10 to 13 Feb 2013, Page-75

9. Development of Pt/Zirconia catalyst for liquid phase HI decomposition reaction in S-I cycle Deepak Tyagi, Alisha Gogia, Salil Varma, A. K. Tripathi, S. R. Bharadwaj,

Proc.4th Int. Conf. on Advances in Energy Research, IIT, Bombay, Dec. 10 -12, 2013, page 57.

10. Role of Carbon support on Activity and Stability of Pt/C catalyst for Hydrogen production by S-I thermochemical cycle; D. Tyagi, S. Varma, S. R. Bharadwaj, Materials Challenges in Alternative and Renewable Energy (MCARE-2014) February 17-20, 2014 | Hilton Clearwater Beach Resort, Clearwater, Florida, USA

11. Development of Novel Catalytic systems for reactions involved in Hydrogen generation from Thermochemical Cycles presented at 26th Research Scholars' Meet 2014 (RSM-2014) organized by Indian Chemical Society at C.K.T, College, Panvel during February 21-22,2014.

12. A Comparative Study of Pt catalysts supported on different oxide supports for HI decomposition: The Hydrogen producing step in S-I Thermochemical Cycle Proc. of 5th Interdisciplinary Symposium on Materials Chemistry (ISMC 2014), BARC, Mumbai December 2014.

13. Pt/Carbon catalyst for Hydrogen production by S-I thermochemical cycle: Effect of Pore structure of Carbon support; Deepak Tyagi, Salil Varma, S. R. Bharadwaj; 22st National Symposium on Catalysis “Catalysis for Better Tomorrow” (CATSYMP-22) at CSIR-CSMCRI , Bhavnagar during 07 to 09 Jan 2015, Page-125-126.



(Deepak Tyagi)

*Dedicated to.....*

*My Parents*

*(A constant source of endless love and  
unconditional support in my life)*

*&*

*My Teachers*

*(Everything I know today is because of them)*

## ACKNOWLEDGEMENTS

At this juncture of my career, I take this opportunity to look back and place on record my sincere gratitude to number of people to whom I am indebted to for their guidance, motivation, help and support during my career and life. This thesis would not have been possible without their support and encouragement.

First and foremost, I wish to record my deep sense of gratitude and sincere thanks to my research guide **Prof. S. R. Bharadwaj**, Outstanding Scientist and Head, Fuel Cell Materials & Catalysis section, Chemistry Division, Bhabha Atomic Research Centre (BARC) for her unstinted guidance, constant support and encouragement throughout this tenure. Her illuminating guidance and assistance helped me to prepare this thesis.

I feel short of words in expressing my sincere gratitude my immediate supervisor **Dr. Salil Varma**, who introduced me to the field of heterogeneous catalysis. His support in carrying out the various experiments, discussing the results on daily basis during the experiments, in documenting the results is gratefully acknowledged. I could not have imagined having a better advisor and mentor for my Ph.D. study.

Chairman (Dr. D. Das) members (Dr. P.N. Bajaj, Shri C.S.R. Prasad, Dr. A. K. Tripathi, Dr. S.C. Parida, Dr. P.A. Hassan and Dr. V. Sudarsan) of the doctoral committee are gratefully acknowledged for their review and suggestions during progress review and pre-synopsis viva-voce. I am thankful to Dr. S. K. Ghosh Former Dean Academic, Chemical Sciences, HBNI and Dr. B. S. Tomar, Dean Academic, Chemical Sciences, HBNI for their help and support.

I sincerely acknowledge the support and encouragement rendered to my research work by Dr. B. N. Jagatap, Director, Chemistry Group and Dr. T. Mukherjee, former Director, Chemistry Group, Dr. V.K. Jain, Head, Chemistry Division and Dr. D. Das, former Head, Chemistry Division.

I express big thanks to Dr. B. N. Wani for giving me help and advice, whenever I needed. I would like to thank all my colleagues from Fuel Cell Materials & Catalysis section. I express thanks to



my colleagues Dr. K. Bhattacharyya, Dr. A. M. Banerjee and Dr. A. N. Shirsat for useful scientific discussions with them and maintaining a cordial environment. I wish to thank my friends from BARC, Kiran, Pooja, Farheen, Asheesh, Priyanka, Archana, Bandhan and Ganesh for all the good times we had together. Nice and congenial environment provided by all members of Division is also worth mentioning.

I wish to thank a lot of people for their timely help in providing various characterization techniques. I thank Mr. N. Manoj and Dr. R. K. Vatsa, Chemistry Division for his help in SEM-EDS analysis and Dr. Pushan Ayyub of TIFR for TEM analysis. I thank Dr. Rashmi Singh, RRCAT, Dr. A. Sakthivel, Delhi University and Dr. W. D. Einicke and Dr. R. Gläser, Institute of Chemical Technology, Universität Leipzig, Leipzig, Germany for N<sub>2</sub> adsorption measurements. I thank colleagues from Analytical Chemistry Division for their help in ICP-OES analysis.

I would like to acknowledge all my teachers since childhood who taught me everything I know. I would not have been here without their guidance, blessings and support.

I have been fortunate to have so many good friends who have always believed in me. I would like to acknowledge them for their moral support and motivation, which drives me to give my best. My childhood friends Gaurav, Anshul and Vaibhav, Post-graduation seniors Rahul, Sushil and Arun, Post-graduation friends Sandeep, Rajan, Sudhir, Anuj, Meenakshi and Kalpna, all my training school (OCES-2008) batch mates specially Ashish, Ruma, Apurav, Mohini and Amit.

Finally, my deepest gratitude goes to my family for their unflagging love and unconditional support throughout my life. My mother (Anita Tyagi), father (Suresh Chand Tyagi) and brother (Devanshu Tyagi) have been pillars of my strength. I would take this occasion to thank my wife (Parul Tyagi) for all her support, care, understanding and love. Finally I thank my wonderful daughter Kashvi, for her endless unconditional love, for always making me smile and for understanding on those weekends when I was writing this thesis instead of playing with her.

**(Deepak Tyagi)**

# CONTENTS

	Page No.
<b>SYNOPSIS</b>	xix
<b>LIST OF FIGURES</b>	xxx
<b>LIST OF TABLES</b>	xxxvii
 <b>Chapter 1: Introduction</b>	 <b>1-34</b>
<b>1.1 Hydrogen Production</b>	1
<b>1.2 Hydrogen as an Energy Carrier: Solution to the current energy and environmental problems</b>	4
<b>1.3 Hydrogen Production: Present Status</b>	5
<b>1.4 Hydrogen Production</b>	5
<b>1.5 Hydrogen Production from water</b>	6
<b>1.6 Thermochemical Cycles for Hydrogen production</b>	7
<i>1.6.1 Copper chlorine cycle</i>	10
<i>1.6.2 UT-3 (Ca-Br-Fe) Cycle</i>	11
<i>1.6.3 Ispra Mark cycles</i>	12
<i>Ispra Mark 1 cycle</i>	12
<i>Ispra Mark 15 cycle</i>	13
<i>Ispra Mark 13 cycle (Sulfur-Bromine cycle)</i>	13
<i>1.6.4 Hybrid Sulfur (Westinghouse) cycle</i>	14
<i>1.6.5 Sulfur-Iodine cycle</i>	14
<b>1.7 HI<sub>x</sub> Section of S-I Cycle</b>	17

<b>1.8 HI Decomposition Reaction</b>	<b>18</b>
<b>1.9 Catalyst requirement for HI Decomposition Reaction</b>	<b>19</b>
<b>1.10 Brief history of catalysis</b>	<b>19</b>
<b>1.11 Classification of Catalysts</b>	<b>24</b>
<b>1.12 Heterogeneous catalysts</b>	<b>25</b>
<b>1.13 Supported Metal Catalysts</b>	<b>28</b>
<b>1.14 Catalysis in thermochemical research</b>	<b>29</b>
<b>1.15 Decomposition of HI on catalyst surfaces</b>	<b>30</b>
<b>1.16 Aim of our work in Hydriodic acid decomposition</b>	<b>33</b>
 <b>Chapter 2: Instrumentation and Experimental Methods</b>	 <b>35-67</b>
<b>2.1 Introduction</b>	<b>35</b>
<b>2.2 Sample Preparation</b>	<b>36</b>
<i>2.2.1 Wet Impregnation method</i>	<b>36</b>
<i>2.2.2 Hard Templating method / Nanocasting</i>	<b>37</b>
<i>2.2.3 Precipitation and Co-precipitation method</i>	<b>38</b>
<b>2.3 Characterization techniques</b>	<b>38</b>
<i>2.3.1 X-ray diffraction (XRD)</i>	<b>38</b>
<i>2.3.1.1 Instrumentation</i>	<b>41</b>
<i>2.3.1.2 Crystallite size estimation</i>	<b>44</b>
<i>2.3.2 Surface area analysis</i>	<b>45</b>
<i>2.3.2.1 Adsorption Desorption Isotherms and their types:</i>	<b>47</b>

2.3.2.2 Total Pore Volume and Average Pore Radius:	49
2.3.2.3 Pore Size Distribution	50
2.3.3 Electron Microscopy	52
2.3.3.1 Scanning Electron Microscopy	53
2.3.3.2 Energy Dispersive Analysis of X-rays (EDAX)	54
2.3.3.3 Field Emission - Scanning Electron Microscopy (FE-SEM)	54
2.3.3.4 Transmission Electron Microscopy (TEM)	55
2.3.4 X-Ray Photoelectron Spectroscopy (XPS)	56
2.3.5 Raman Spectroscopy	59
2.3.6 UV-Visible absorption Spectroscopy	61
2.3.7 Potentiometric Titration	63
2.3.8 ICP-Atomic Emission Spectroscopy	64
<b>2.4 Catalytic activity evaluation for Hydriodic acid decomposition</b>	<b>65</b>
2.4.1 Evaluation of Catalytic Activity of the catalysts	66
2.4.2 Evaluation of Stability of the catalysts	67
 <b>Chapter 3: HI Decomposition over Carbon Supported</b>	 <b>68-104</b>
<b>Platinum Catalysts</b>	
<b>3.1 Introduction</b>	68
<b>3.2 Platinum Graphite Catalyst</b>	69
3.2.1 Experimental	70
3.2.1.1 Preparation of Catalyst	70

3.2.1.2 <i>Characterization of Catalyst</i>	70
3.2.1.3 <i>Activity and Stability</i>	71
3.2.2 <i>Results and Discussion</i>	72
3.2.2.1 <i>XRD</i>	72
3.2.2.2 <i>SEM</i>	73
3.2.2.3 <i>Surface Area</i>	74
3.2.2.4 <i>Raman Spectroscopy</i>	75
3.2.2.5 <i>X-ray Photoelectron spectroscopy</i>	77
3.2.2.6 <i>Catalytic activity of the catalyst</i>	80
3.2.2.7 <i>Iodine Poisoning Studies</i>	84
3.2.2.8 <i>Stability of the Catalyst</i>	85
3.2.3 <i>Conclusion</i>	89
<b>3.3 Other Platinum Carbon Catalysts</b>	90
3.3.1 <i>Experimental</i>	90
3.3.1.1 <i>Preparation of Catalyst</i>	90
3.3.1.2 <i>Characterization of Catalyst</i>	91
3.3.1.3 <i>Activity and Stability</i>	91
3.3.2 <i>Results and Discussion</i>	92
3.3.2.1 <i>XRD</i>	92
3.3.2.2 <i>SEM</i>	92
3.3.2.3 <i>Surface Area</i>	94
3.3.2.4 <i>Raman Spectroscopy</i>	95

3.2.2.5 <i>X-ray Photoelectron spectroscopy</i>	96
3.2.2.6 <i>Catalytic activity of the catalyst</i>	100
3.3.2.7 <i>Stability of the Catalyst</i>	100
3.3.3 <i>Conclusion</i>	104
 <b>Chapter 4: HI Decomposition over Platinum Catalysts</b>	 <b>105-144</b>
<b>Supported on porous Carbon Supports</b>	
<b>4.1 Introduction</b>	105
<b>4.2 Platinum/ Porous Carbon Catalyst</b>	106
4.2.1 <i>Experimental</i>	107
4.2.1.1 <i>Preparation of Mesoporous silica</i>	107
4.2.1.2 <i>Preparation of Catalyst using hard templating Route</i>	108
4.2.1.3 <i>Characterization of Catalysts</i>	110
4.2.1.4 <i>Activity and Stability</i>	110
4.2.2 <i>Results and Discussion</i>	111
4.2.2.1 <i>XRD</i>	111
4.2.2.2 <i>SEM</i>	111
4.2.2.3 <i>Surface Area</i>	113
4.2.2.4 <i>Raman Spectroscopy</i>	116
4.2.2.5 <i>X-ray Photoelectron spectroscopy</i>	118
4.2.2.6 <i>Catalytic activity of the catalyst</i>	122
4.2.2.7 <i>Stability of the Catalyst</i>	123



4.2.3 Conclusion	128
<b>4.3 Platinum/Mesoporous Carbon Catalyst</b>	<b>129</b>
4.3.1 Experimental	129
4.3.1.1 Preparation of Mesoporous silica	129
4.3.1.2 Preparation of Catalyst using hard templating Route	130
4.3.1.3 Characterization of Catalysts	130
4.3.1.4 Activity and Stability	131
4.3.2 Results and Discussion	131
4.3.2.1 XRD	131
4.3.2.2 SEM	132
4.3.2.3 TEM	134
4.3.2.4 Surface Area	136
4.3.2.5 Raman Spectroscopy	137
4.3.2.6 X-ray Photoelectron spectroscopy	138
4.3.2.7 Catalytic activity of the catalyst	141
4.3.2.8 Stability of the Catalyst	142
4.3.3 Conclusion	144
 <b>Chapter 5: HI Decomposition over Oxide Supported</b>	 <b>145-180</b>
<b>Platinum Catalysts</b>	
<b>5.1 Introduction</b>	145
<b>5.2 Platinum/ Ceria and Platinum Titania Catalysts</b>	146

5.2.1 <i>Experimental</i>	146
5.2.1.1 <i>Preparation of Catalyst</i>	146
5.2.1.2 <i>Characterization of Catalysts</i>	146
5.2.1.3 <i>Activity and Stability</i>	147
5.2.2 <i>Results and Discussion</i>	147
5.2.2.1 <i>XRD</i>	147
5.2.2.2 <i>SEM</i>	150
5.2.2.3 <i>Surface Area</i>	152
5.2.2.4 <i>X-ray Photoelectron spectroscopy</i>	153
5.2.2.5 <i>Catalytic activity of the catalyst</i>	159
5.2.2.6 <i>Stability of the Catalyst</i>	160
5.2.3 <i>Conclusion</i>	162
<b>5.3 Platinum/ Zirconia Catalyst</b>	163
5.3.1 <i>Experimental</i>	163
5.3.1.1 <i>Preparation of catalyst</i>	163
5.3.1.3 <i>Characterization of Catalysts</i>	164
5.3.1.4 <i>Activity and Stability</i>	164
5.3.2 <i>Results and Discussion</i>	165
5.3.2.1 <i>XRD</i>	165
5.3.2.2 <i>SEM</i>	167
5.3.2.3 <i>TEM</i>	169
5.3.2.4 <i>Surface Area</i>	171

5.3.2.5 <i>X-ray Photoelectron spectroscopy</i>	173
5.3.2.6 <i>Catalytic activity of the catalyst</i>	176
5.3.2.7 <i>Stability of the Catalyst</i>	178
5.3.3 <i>Conclusion</i>	179
<b>Chapter 6: Iodine Speciation Studies</b>	<b>181-196</b>
<b>6.1 Introduction</b>	181
<b>6.2 Experimental</b>	184
6.2.1 <i>Preparation of solutions</i>	184
6.2.2 <i>Raman spectroscopy</i>	184
6.2.3 <i>UV-visible Spectroscopy</i>	184
<b>6.3 Results and discussion</b>	184
6.3.1 <i>Raman spectroscopy</i>	184
6.3.2 <i>UV-visible spectroscopy</i>	191
<b>6.4 Conclusion</b>	196
 <b>Chapter 7: Conclusions and Future Scope</b>	 <b>197-200</b>
<b>7.1 Conclusions</b>	197
<b>7.2 Future Scope</b>	200
<b>References</b>	<b>201-214</b>

## **Synopsis**



# **Homi Bhabha National Institute**

## **SYNOPSIS OF Ph. D. THESIS**

- 1. Name of the Student: DEEPAK TYAGI**
- 2. Name of the Constituent Institution: BARC**
- 3. Enrolment No. : CHEM01201004010**
- 4. Title of the Thesis: Development of Catalysts for Hydriodic Acid Decomposition Reaction for Hydrogen Generation from Thermochemical Cycles**
- 5. Board of Studies: CHEMICAL SCIENCES**

Hydrogen is an attractive energy carrier due to various reasons like cleanliness, sustainability etc. A lot of efforts are being made for hydrogen production from water worldwide by different methods like thermochemical cycles, electrolysis, photo-catalytic, photo-biological etc. Thermochemical cycles dissociate water into hydrogen and oxygen through a set of chemical reactions at a temperature much lower than that required for thermal decomposition of water. Sulfur Iodine cycle (S-I cycle) is one of the most studied thermochemical cycle as it has certain advantages over other competitors.

HI decomposition reaction is the hydrogen producing step in the S-I cycle as well as some other iodine based cycles. The main aim of this thesis is to find a suitable catalyst

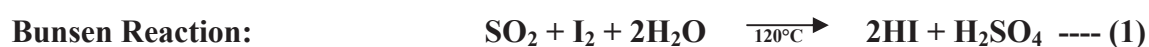
for this reaction and also to study polyiodide species present in the HI phase. In this thesis detailed investigations have been carried out on platinum based catalysts for liquid phase HI decomposition reaction. The thesis is divided into the following seven chapters:

## **Chapter 1: Introduction**

Hydrogen as future energy carrier is a scenario of high probability as well as necessity due to following various reasons like: the limited supply of currently used fossil fuels and their environmental impact [1,2]. Hydrogen is the most abundant element on earth, but it is not available freely. Most of the hydrogen on earth is available in molecular form either as water or organic compounds. Therefore water, being the most abundant molecule on earth's surface covering more than 70% of its area, can be a potential source of hydrogen. Production of hydrogen from water is highly energy intensive; therefore current production of hydrogen is mainly from fossil fuels only like steam reforming etc. But again these methods have the same limitations like limited supply and their environmental impacts. Therefore there is a need to develop methods for large scale production of hydrogen from water in an environment friendly manner.

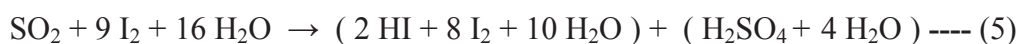
Hydrogen generation from water can be achieved by thermochemical cycles, electrolysis, photo-catalytic, photo-electrochemical, photo-biological or other means [3]. The two most important methods to generate hydrogen on a large scale are Thermochemical water splitting cycles and high temperature steam electrolysis. Thermochemical cycle dissociates water into hydrogen through a set of chemical reactions at a much lower temperature as compared to that required for direct thermal decomposition of water [4,5]. Thermochemical cycles have potential for better efficiency

because heat is directly being used in it. Hundreds of thermochemical cycles have been reported and studied worldwide like Sulfur Iodine thermochemical Cycle (S-I Cycle), Copper chlorine thermochemical cycle (Cu-Cl Cycle) etc. Sulfur-Iodine cycle is more developed than competitive thermochemical processes but still requiring significant development to be feasible on large scale [6,7]. This cycle comprises of the following three reactions:



S-I cycle has a few advantages over other thermochemical cycles such as only liquid/fluid handling, no electrolysis step etc. HI decomposition step is an integral part of not only this thermochemical cycle, but also for some other iodine based thermochemical cycles like magnesium iodide thermochemical cycle. HI decomposition reaction as such is thermodynamically limited with very low thermodynamic conversions and it requires a catalyst to achieve workable reaction rates.

In case of S-I Thermochemical cycle, the hydriodic acid coming from Bunsen reaction has excess of water and iodine, as required for an efficient phase separation of the two acids [8].





In this case production of Hydrogen from HI phase coming from Bunsen reaction is even more energy consuming due to the presence of pseudo azeotrope i.e. HI-H<sub>2</sub>O-I<sub>2</sub>.

Noble metal based catalysts are supposed to be the most useful catalyst for this reaction because of dissociative adsorption of Hydrogen Iodide over the noble metal surface. A number of noble metal based catalysts have been reported for HI decomposition reaction in gaseous phase at temperatures in excess of 400 °C [9].

HI can also be decomposed efficiently in liquid phase at much lower temperatures with the use of a suitable catalyst. Another advantage of liquid phase HI decomposition is that the iodine produced during the reaction gets dissolved in the liquid HI to form polyiodide species and does not poison the catalyst surface. Therefore liquid HI is still in contact with the catalyst surface. In order to find out suitable catalytic systems for liquid phase HI decomposition reaction, Pt based catalysts supported on different supports like oxides and carbons have been prepared, characterized and evaluated for liquid phase HI decomposition reaction. Effect of surface areas and pore structures of the support and platinum loading has also been evaluated. Formation of polyiodide species is an integral part of liquid phase HI decomposition reaction, therefore speciation studies of polyiodides have also been carried out and included in the thesis.

## **Chapter 2: Instrumentation and Experimental Methods**

Chapter 2 deals with the experimental techniques used for the synthesis, characterization and evaluation of the catalytic behavior of the supported platinum catalysts. Synthesis methods include wet impregnation method, hard templating methods employing hard

silica templates, precipitation combined with impregnation etc. Platinum loaded on the support was subsequently reduced by heating in flowing hydrogen and argon mixture.

Catalytic activity of a catalyst depend of its various properties like surface area and porosity of the support, particle size and dispersion of the noble metal over the support, surface morphology etc. These properties of the catalysts were found out using various techniques such as X-Ray Diffraction (XRD), N<sub>2</sub>-adsorption BET surface area, Chemisorption, Scanning Electron Microscopy (SEM), Transmission Electron Microscopy (TEM), and X-ray Photoelectron Spectroscopy (XPS). A brief account of all these techniques is presented in this chapter.

Also this chapter includes details of the methods used for activity and stability evaluation of the catalyst for HI decomposition reaction. Percentage conversion was calculated on basis of change in concentration of H<sup>+</sup>, I<sup>-</sup> and I<sub>2</sub> concentrations using acid-base, precipitation and iodometric titration respectively. One of the product hydrogen was monitored using Gas Chromatograph (GC) with Thermal Conductivity Detector (TCD). The stability of the catalyst against platinum leaching was evaluated by determining the presence of platinum in the solution after reaction by ICP-OES.

### **Chapter 3: HI Decomposition over Carbon Supported Pt Catalyst**

Chapter 3 includes the details of the preparation, characterization and catalytic activity of platinum catalyst supported on different carbon supports for hydriodic acid decomposition reaction. Carbon is widely used as support for noble metal based catalysts due to its various properties like high volume to weight ratio, tunability of support structure and stability of the support under the reaction conditions. 1% Pt/Carbon

catalysts were prepared by impregnation of support with hexachloroplatinic acid followed by reduction in flowing hydrogen argon mixture at 300 °C. Carbon supports used were (i) Activated carbon (ii) Colloidal Graphite and (iii) Carbon prepared by carbonization of rice at 600 °C. The samples were characterized by XRD, SEM, Raman and BET surface Area. Their activity for HI decomposition reaction in liquid phase at 120 °C was evaluated and it was found that the catalysts were stable under reaction conditions. Pt/Graphite catalyst showed higher conversion (17.8% in 2 hr) as compared to the other two catalysts (~13% in 2hr) in spite of having lower surface area.

Since Pt/Graphite catalyst was giving more conversion, it was selected for detailed study. Pt/Graphite catalysts with different platinum loading (0.5%, 1% and 2 %) were prepared and evaluated to see the effect of noble metal loading. The percentage conversion increase with increasing percentage loading, but in terms of per unit weight of noble metal 1% Pt/Graphite was giving maximum percentage conversion. 1% Pt/Graphite was evaluated for its detailed activity at different temperatures and for different time durations. Activation energy was calculated for 1% Pt/Graphite and it was found to be ~32kJ/mole, which is in the same range as reported for vapour phase HI phase decomposition reactions using Platinum catalysts.

#### **Chapter 4: HI Decomposition over Pt Catalysts supported on Porous Carbon supports**

Surface area and porosity of the support play important roles in catalysis. Therefore to increase the surface area of the carbon support, porous carbon support was prepared by hard templating route using silica templates like fumed silica, MCM-41 and SBA-15 [9].

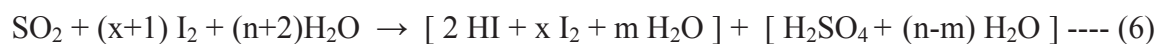
1 wt% platinum was loaded on these carbon supports and reduced under flowing hydrogen argon mixture at 300 °C. These catalysts were characterized by XRD, SEM, TEM, Raman and BET surface Area. All were having high surface area around 800m<sup>2</sup>/g. Fumed silica based catalyst was found to be microporous in nature while the other two were found to be mesoporous. While evaluating their activity for liquid phase HI decomposition reaction, it was observed that mesoporous catalysts give good conversion values which are almost comparable to that of Pt/Graphite catalyst. While the microporous carbon based catalyst give much lower conversion, in spite of having high surface area. Platinum leaching was evaluated and it was observed that the SBA based catalyst is the most stable among all carbon based catalysts.

#### **Chapter 5: HI Decomposition over Pt catalysts Supported on Oxides**

Oxides are also well known supports for noble metals in catalysis. In this chapter various supports for platinum like ceria, titania and zirconia have been explored for HI decomposition reaction. Different amount of platinum have been loaded over the oxide support. These catalysts are characterized by XRD, SEM, TEM, BET surface area, Chemisorption and XPS. Their activity is evaluated for HI decomposition reaction at 120 °C. It was observed that ceria based catalysts showed much higher conversions followed by zirconia and titania. But in terms of stability, the ceria based catalysts were least stable as most of the catalyst gets dissolved into HI itself. Among titania and zirconia, later was giving more conversion as well as it was more stable in terms of platinum leaching. Reasons for these observations are high noble metal dispersion and mesoporous nature of the zirconia support.

## Chapter 6: Iodine Speciation Studies

As discussed in the introduction, one of the advantages of liquid phase HI decomposition reaction is that iodine formed during the course of reaction gets dissolved in the liquid HI and forms polyiodides. Also in the Bunsen reaction, extra iodine is added to the reaction mixture to have more efficient phase separation as shown below[8].



The HI phase contains almost all the excess iodine and is known as  $\text{HI}_x$  phase. This iodine needs to be separated from HI before its decomposition. Even after separation of iodine, HI may have some iodine. Therefore it is important to study the presence and formation of these polyiodides species in the HI phase. Most of the polyiodide speciation studies reported in the literature are limited to solid phase in forms of salts and complexes of these ions [11,12] with very few reports on polyiodide species present in liquid phase [13,14]. Therefore it is important to study polyiodide species in liquid phase in connection to the  $\text{HI}_x$  phase of S-I thermochemical cycle.

For speciation studies, iodine and iodide solutions were mixed in different ratios and analyzed by various techniques like UV Visible spectrophotometry, Raman spectroscopy and electrochemical methods. It was observed from UV-Visible spectrophotometry, that the absorption band corresponding to  $\text{I}_3^-$  appears at 288 nm and 358 nm. The mixture showed maximum absorbance at 1:1 ratio of iodine and iodide. As the iodine concentration was increased, the absorbance corresponding to  $\text{I}_3^-$  decrease, which is indication of conversion of triiodide into higher polyiodides. Same trend was also observed from Raman spectroscopy where peak corresponding to  $\text{I}_3^-$  ( $113 \text{ cm}^{-1}$ ) is

maximum in intensity at 1:1 ratio of iodine and iodide and decrease on further addition of iodine. As shown in equation no. (6), small amount of  $\text{H}_2\text{SO}_4$  may also be present in HI phase. Therefore we studied the formation of triiodide species in presence of different amount of  $\text{H}_2\text{SO}_4$  also and we could find that there was no change in intensity of peak corresponding to  $\text{I}_3^-$  ( $113\text{ cm}^{-1}$ ) by presence of sulfuric acid.

To conclude in this chapter, presence of  $\text{I}_3^-$  and higher polyiodides in the  $\text{HI}_x$  phase of Bunsen reaction of sulfur Iodine thermochemical cycle was confirmed by UV-visible and Raman studies. Also indirect inference of formation of higher polyiodide species was also drawn in presence of higher concentrations of iodine.

## **Chapter 7: Conclusions and Future Scope**

The final chapter of the thesis includes the summary and the outcome of this thesis, and the scope for future work on hydriodic acid decomposition reaction. In this thesis various Pt/supported catalysts were explored for liquid phase hydriodic acid decomposition reaction. It was found that carbon is a suitable support for these catalysts which is stable in the reaction conditions and whose porosity and surface area can be tuned by different methods. It was also evident that the microporous support is ineffective in spite of its high surface area. The support should be either nonporous type or mesoporous in nature. In case of Pt supported on oxides,  $\text{ZrO}_2$  was found to be the best support in terms of both activity and stability. Here also mesoporosity of the support plays an important role. To summarize, among the studied catalyst systems Pt supported on graphitic carbon or mesoporous carbon or zirconia are suitable to be used in liquid phase HI decomposition reaction. Also formation of polyiodide species in the liquid phase was confirmed by

various techniques, which is important phenomenon in liquid phase HI decomposition reaction as well as in HI<sub>x</sub> phase of the Bunsen reaction. Future scope of this work includes use of these catalysts for vapor phase HI decomposition reaction and the comparison of the results with that of for liquid phase.

#### **References:**

- [1] I. Dincer, M.A. Rosen, *International Journal of Energy Research*, **1998**, 22, 1305-1321.
- [2] A. Midilli, M. Ay, I. Dincer, M.A. Rosen, *Renewable and Sustainable Energy Reviews*, **2005**, 9, 255-271.
- [3] I. Dincer, *International Journal of Hydrogen Energy*, **2012**, 37, 1954-1971.
- [4] C.E. Bamberger, D.M. Richardson, *Cryogenics*, **1976**, 16, 197-208.
- [5] J.E. Funk, *International Journal of Hydrogen Energy*, **2001**, 26, 185-190.
- [6] L.C. Brown, J.F. Funk, S.K. Showalter, *General Atomics Report GAA23373*, April 2000. Available on-line at <http://web.gat.com/pubs-ext/miscpubs/A23373.pdf> on March 21, **2006**.
- [7] D. O'Keefe, C. Allen, G. Besenbruch, L. Brown, J. Norman, R. Sharp et al., *International Journal of Hydrogen Energy*, **1982**, 7, 831-892.
- [8] M. Sakurai, H. Nakajima, K. Onuki, S. Shimizu, *International Journal of Hydrogen Energy*, **2000**, 25, 605-611.
- [9] D.R. O'Keefe, J.H. Norman, D.G. Williamson, *Catalysis Reviews Science and Engineering*, **1980**, 22, 325-369.

- [10] K. Scholz, J. Scholz, A.J. McQuillan, G. Wagner, O. Klepel., *Carbon*, **2010**, *48*, 1788-1798.
- [11] P.H. Svensson, L. Kloo, *Chem Rev*, **2003**, *103*, 1649-1684.
- [12] A.J. Blake, F.A. Devillanova, R.O. Gould, W.S. Li, V. Lippolis, S. Parsons et al., *Chem Soc Rev*, **1998**, *3*, 195-205.
- [13] D.A. Palmer, R.W. Ramette, R.E. Mesmer, *J Solution Chem*, **1984**, *13*, 673-83.
- [14] V.T. Calabrese, A. Khan, *J Phys Chem A*, **2000**, *104*, 1287-1292.



## **LIST OF FIGURES**

<b>Figure</b>	<b>Page No.</b>
<b>Fig. 1.1:</b> <i>Estimation of world energy demand and available energy form conventional sources. Adapted from <a href="http://www.plasma.inpe.br">http://www.plasma.inpe.br</a></i>	2
<b>Fig. 1.2:</b> <i>Increase in global average temperature with increase in the CO<sub>2</sub> emission. Adapted from <a href="http://www.ncdc.noaa.gov">http://www.ncdc.noaa.gov</a></i>	3
<b>Fig. 1.3:</b> <i>A schematic of the concept of thermochemical cycles</i>	9
<b>Fig. 1.4:</b> <i>Classification of thermochemical cycles</i>	10
<b>Fig. 1.5:</b> <i>Reaction paths for non-catalyzed and heterogeneously catalyzed reactions.</i>	23
<b>Fig. 2.1:</b> <i>Synthetic Strategy for the porous carbon support by Nanocasting</i>	37
<b>Fig. 2.2:</b> <i>Schematic diagram of X-ray Diffraction</i>	39
<b>Fig. 2.3:</b> <i>Ray diagram of a typical reflection mode diffractometer</i>	42
<b>Fig. 2.4:</b> <i>Different adsorption Isotherms (TYPE I to IV)</i>	48
<b>Fig. 2.5:</b> <i>Depiction of different phenomenon occurring on interaction of electron beam</i>	52
<b>Fig. 2.6:</b> <i>Schematic of a XPS instrument</i>	57
<b>Fig. 2.7:</b> <i>Schematic Presentation of the Raman Scattering</i>	60
<b>Fig. 2.8:</b> <i>A Schematic representation of UV-Visible spectrophotometer</i>	62

<b>Fig.2.9:</b> <i>Block diagram of ICP-AES instrument</i>	65
<b>Fig.2.10:</b> <i>Block diagram of the experimental set up used for Hydriodic acid decomposition studies</i>	67
<b>Fig. 3.1:</b> <i>XRD patterns of Pt/Graphite catalysts with different Pt loading</i>	72
<b>Fig. 3.2:</b> <i>SEM images of Pt/Graphite catalysts with different Pt loading (a) 0.5%, (b) 1% and (c) 2%</i>	73
<b>Fig. 3.3:</b> <i>High magnification SEM images of 1% Pt/Graphite catalyst</i>	74
<b>Fig. 3.4:</b> <i>Adsorption desorption isotherms and pore size distribution curve for 1 % Pt/graphite</i>	75
<b>Fig. 3.5:</b> <i>Raman spectra of different Pt/Graphite catalysts</i>	76
<b>Fig. 3.6:</b> <i>XPS survey scan of 1% Pt/Graphite catalysts</i>	77
<b>Fig. 3.7:</b> <i>XPS spectra of Pt 4f spectral region of different Pt/Graphite catalysts</i>	78
<b>Fig. 3.8:</b> <i>XPS spectra of Carbon 1s spectral region of different Pt/Graphite catalysts</i>	79
<b>Fig. 3.9:</b> <i>Increase in percentage conversion with time at different temperature</i>	81
<b>Fig. 3.10:</b> <i>Plots for calculation of rate constants at different temperatures.</i>	83
<b>Fig. 3.11:</b> <i>Plot for calculation of Activation energy</i>	83
<b>Fig 3.12:</b> <i>XRD for (a) fresh and (b) used 1% Pt/Graphite catalyst</i>	86

<b>Fig 3.13:</b> SEM for (a) fresh and (b) used 1% Pt/Graphite catalyst	87
<b>Fig. 3.14:</b> Raman spectra for different used Pt/Graphite catalysts	88
<b>Fig 3.15:</b> XRD for different 1% Pt/carbon catalysts	93
<b>Fig 3.16:</b> SEM micrographs of (a) Pt/AC, (b) Pt/RC and (c) RC/Pt	93
<b>Fig. 3.17:</b> Adsorption desorption isotherms and pore size distribution curve for Pt/AC	94
<b>Fig 3.18:</b> Raman spectra of different Pt/carbon catalysts	95
<b>Fig 3.19:</b> XPS survey scan of Pt/RC catalyst	96
<b>Fig 3.20:</b> XPS spectra of Pt-4f spectral region of different Pt/carbon catalysts	98
<b>Fig 3.21:</b> XPS spectra of C-1s spectral region of different Pt/carbon catalysts	99
<b>Fig 3.22:</b> XRD patterns of used Pt/carbon catalysts	101
<b>Fig 3.23:</b> SEM micrographs of fresh and used Pt/AC catalysts	102
<b>Fig 3.24:</b> Raman spectra of used Pt/Carbon catalysts	103
<b>Fig. 4.1:</b> XRD patterns for different catalyst	112
<b>Fig. 4.2:</b> SEM micrographs of different catalyst samples	112
<b>Fig. 4.3:</b> Adsorption desorption isotherms for mesoporous catalyst samples	114

<b>Fig. 4.4:</b> <i>Pore size distribution curve for mesoporous catalyst samples</i>	115
<b>Fig. 4.5:</b> <i>Raman spectra of different catalyst samples</i>	117
<b>Fig. 4.6:</b> <i>XPS survey scan for Pt/MCM-C</i>	119
<b>Fig. 4.7:</b> <i>XPS spectra of Pt-4f spectral region of all four catalysts</i>	120
<b>Fig. 4.8:</b> <i>XPS spectra of C-1s spectral region of all four catalysts</i>	121
<b>Fig. 4.9:</b> <i>XRD pattern of Used catalyst samples</i>	124
<b>Fig. 4.10:</b> <i>SEM micrographs of used catalyst samples</i>	125
<b>Fig. 4.11:</b> <i>Adsorption desorption isotherms of fresh and used MCM-C/Pt catalyst</i>	126
<b>Fig. 4.12:</b> <i>Raman spectra of Used catalyst samples</i>	127
<b>Fig. 4.13:</b> <i>XRD pattern of Pt/SBA-C catalyst</i>	132
<b>Fig. 4.14:</b> <i>SEM micrographs of Pt/SBA-C catalyst</i>	133
<b>Fig. 4.15:</b> <i>FEG-SEM images of Pt/SBA-C catalyst.</i>	133
<b>Fig. 4.16:</b> <i>TEM image of Pt/SBA-C catalyst</i>	134
<b>Fig. 4.17:</b> <i>Particle size distribution of Pt/SBA-C catalyst</i>	135
<b>Fig. 4.18:</b> <i>SAED pattern of Pt/SBA-C catalyst</i>	135
<b>Fig. 4.19:</b> <i>Adsorption isotherm of fresh and used Pt/SBA-C catalysts</i>	136

<b>Fig. 4.20:</b> <i>Pore size distribution of fresh and used Pt/SBA-C catalysts</i>	137
<b>Fig. 4.21:</b> <i>Raman spectrum of the Pt/SBA-C catalyst.</i>	138
<b>Fig. 4.22:</b> <i>XPS survey scan of the Pt/SBA-C sample</i>	139
<b>Fig. 4.23:</b> <i>XPS spectra of Pt/SBA-C in spectral region of Pt-4f</i>	140
<b>Fig. 4.24:</b> <i>XPS spectra of Pt/SBA-C in spectral region of C-1s</i>	140
<b>Fig. 4.25:</b> <i>XRD pattern of used Pt/SBA-C catalyst</i>	143
<b>Fig. 4.26:</b> <i>SEM micrographs of used Pt/SBA-C catalyst</i>	143
<b>Fig. 5.1:</b> <i>XRD patterns of different Pt/CeO<sub>2</sub> catalysts</i>	148
<b>Fig. 5.2:</b> <i>XRD patterns of different Pt/TiO<sub>2</sub> catalysts</i>	149
<b>Fig. 5.3:</b> <i>SEM images of Pt/CeO<sub>2</sub> catalyst with different platinum loading (a) 0.5%, (b) 1%, (c) 2%</i>	150
<b>Fig. 5.4:</b> <i>SEM images of Pt/TiO<sub>2</sub> catalyst with different platinum loading (a) 0.5%, (b) 1%, (c) 2%</i>	151
<b>Fig. 5.5:</b> <i>EDS spectra of Pt/TiO<sub>2</sub> catalyst with different platinum loading (a) 0.5%, (b) 1%, (c) 2%</i>	152
<b>Fig. 5.6:</b> <i>XPS spectra of Pt/CeO<sub>2</sub> catalysts in spectral region corresponding to Pt 4f</i>	155
<b>Fig. 5.7:</b> <i>XPS spectra of Pt/CeO<sub>2</sub> catalysts in spectral region corresponding to Ce 3d</i>	156

<b>Fig. 5.8:</b> <i>XPS spectra of Pt/TiO<sub>2</sub> catalysts in spectral region corresponding to Pt 4f</i>	157
<b>Fig. 5.9:</b> <i>XPS spectra of Pt/TiO<sub>2</sub> catalysts in spectral region corresponding to Ti 2p</i>	158
<b>Fig. 5.10:</b> <i>XRD pattern of used Pt/TiO<sub>2</sub> catalysts</i>	161
<b>Fig. 5.11:</b> <i>XRD Patterns for different Pt/ZrO<sub>2</sub> catalysts</i>	166
<b>Fig. 5.12:</b> <i>SEM images of Pt/ZrO<sub>2</sub> catalyst with different platinum loading (a)0.5%, (b)1%, (c)2%</i>	167
<b>Fig. 5.13:</b> <i>EDX spectra of Pt/ZrO<sub>2</sub> catalyst with different platinum loading (a)0.5%,(b) 1%,(c) 2%</i>	168
<b>Fig. 5.14:</b> <i>TEM images of Pt/ZrO<sub>2</sub> catalyst with different platinum loading (a) 0.5%,(b) 1% (c) 2%</i>	169
<b>Fig. 5.15:</b> <i>TEM images of 1% Pt/ZrO<sub>2</sub> catalyst</i>	170
<b>Fig. 5.16:</b> <i>Adsorption and Desorption isotherms for 1% Pt/ZrO<sub>2</sub> catalyst</i>	172
<b>Fig. 5.17:</b> <i>Pore size distribution for 1% Pt/ZrO<sub>2</sub> catalyst</i>	172
<b>Fig. 5.18:</b> <i>XPS spectrum of Pt/ZrO<sub>2</sub> catalysts in the spectral region corresponding to Pt-4f.</i>	174
<b>Fig. 5.19:</b> <i>XPS spectrum of Pt/ZrO<sub>2</sub> catalysts in the spectral region corresponding to Zr-3d</i>	175
<b>Fig. 5.20:</b> <i>Percentage conversion for 1 % Pt/ZrO<sub>2</sub> with time at 120 °C</i>	177

<b>Fig. 5.21:</b> <i>XRD patterns of used Pt/ZrO<sub>2</sub> catalysts</i>	178
<b>Fig. 6.1:</b> <i>Raman spectra of HI:I<sub>2</sub> 1:1 solution with deconvolutions showing <math>\nu_1</math>, <math>\nu_2</math> and <math>\nu_3</math> peaks</i>	185
<b>Fig. 6.2:</b> <i>Raman spectra for different HI:I<sub>2</sub> ratio solutions.</i>	186
<b>Fig. 6.3:</b> <i>Variation of intensity of <math>\nu_1</math>, <math>\nu_2</math> and <math>\nu_3</math> peaks for different HI:I<sub>2</sub> ratio solutions</i>	188
<b>Fig. 6.4:</b> <i>Multiple deconvolutions corresponding to HI:I<sub>2</sub> ratio of 1:3</i>	189
<b>Fig. 6.5:</b> <i>Raman spectra in presence of different concentrations of sulfuric acid, depicting no effect of its presence</i>	190
<b>Fig. 6.6:</b> <i>UV-visible spectra for different KI-I<sub>2</sub> solutions</i>	192
<b>Fig. 6. 7:</b> <i>Variation in absorbance value of 358 and 288 nm peaks with increasing iodine concentration in KI-I<sub>2</sub> solution.</i>	193
<b>Fig. 6.8:</b> <i>UV-visible spectra for different HI:I<sub>2</sub> ratio solutions</i>	194
<b>Fig. 6.9:</b> <i>UV-visible spectra for different HI:I<sub>2</sub> ratio solutions in range of 260-400 nm</i>	195
<b>Fig. 6.10:</b> <i>Variation in absorbance values of 193 nm and 223 nm peaks with respect to iodine-HI ratio</i>	196

## LIST OF TABLES

	Page No.
<b>Table 1.1:</b> <i>Present status of commercial hydrogen production from different sources</i>	6
<b>Table 3.1:</b> <i>Surface area and pore volume data for different Pt/graphite catalysts</i>	75
<b>Table 3.2:</b> <i>% Conversion in 2 hours at 120 °C for different catalysts</i>	80
<b>Table 3.3:</b> <i>% Conversion with time at different temperatures</i>	82
<b>Table 3.4:</b> <i>% Conversion in presence of iodine</i>	85
<b>Table 3.5:</b> <i>% Conversion in 2 hours at 120 °C for different catalysts</i>	100
<b>Table 4.1:</b> <i>Classification of porous materials on basis of their pore size</i>	105
<b>Table 4.2:</b> <i>Surface Area and Pore volume values of different catalyst samples</i>	113
<b>Table 4.3:</b> <i><math>I_G/I_D</math> and calculated <math>L_a</math> values of different catalyst samples</i>	118
<b>Table 4.4:</b> <i>Percentage conversion and platinum leaching values for different catalysts</i>	122
<b>Table 4.5:</b> <i>Raman data and calculated in-plane crystallite size for different samples</i>	128



<b>Table 5.1:</b> <i>BET surface area of different oxide supported catalysts</i>	153
<b>Table 5.2:</b> <i>% conversion values for different catalysts</i>	159
<b>Table 5.3:</b> <i>BET surface area, pore volume, pore size and noble metal dispersion</i>	171
<b>Table 5.4:</b> <i>Percentage conversion values for the different catalysts</i>	176

# Chapter 1

## Introduction

---

### 1.1 Introduction

Energy plays an important role in social, economic, industrial and technological development of any society. Due to increasing population and rising living standards, there is an increase in energy demand worldwide. In a developing country like India, energy sector is further more important owing to its large population. Hence there is a need for development of alternative energy sources both nationally as well as internationally. Lot of research is going on in this field; people are looking for new CO<sub>2</sub> free energy systems.

CO<sub>2</sub> free energy systems are important basically due to the following two reasons: Firstly, the gap between energy demand and available energy sources will increase in future because the demand will keep on increasing due to various reasons like increasing population, industrial growth etc but there will be decline in production of conventional fossil fuels. As per the BP Statistical Review of World Energy 2014, Oil remains the world's leading fuel with 32.9% of global energy consumption [1]. The same review also states that consumption as well as production of all types of fuels has increased in recent times but for each of the fossil fuel, rise in consumption was much more as compared to rise in production. These trends raise an alarm about possible energy crisis in near future.

## Chapter 1

---

There are various reports suggesting that global energy demand may increase so rapidly that it cannot be met by available fossil fuels, nuclear and hydrothermal energy as shown in graph below.

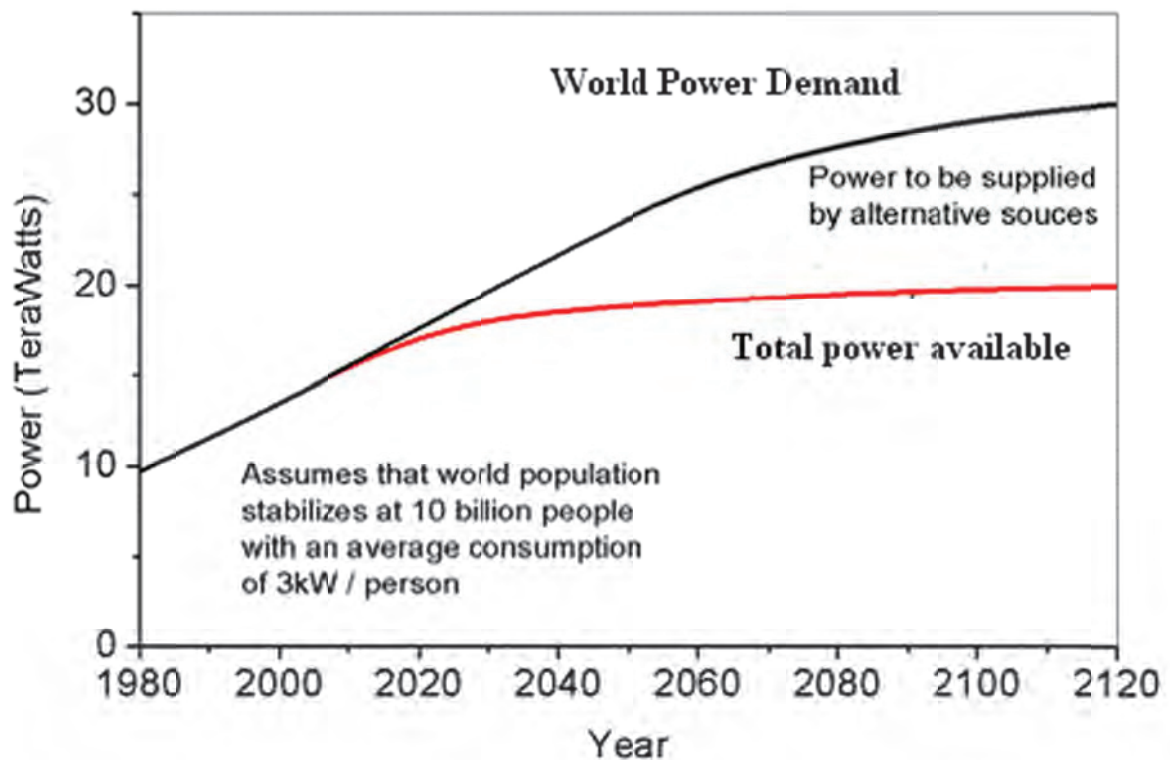


**Fig. 1.1:** Estimation of world energy demand and available energy form conventional sources. Adapted from <http://www.plasma.inpe.br>

Second reason for the increase in efforts and research for alternate energy sources is the environmental problems associated with the combustion of fossil fuels. Since fossil fuels are mainly hydrocarbons therefore their burning leads to  $\text{CO}_2$  emission. Hence an increase in usage of these fossil fuels leads to increase in  $\text{CO}_2$  emission. The concentration of  $\text{CO}_2$  in atmosphere in last 120 years is shown in figure below (Fig 1.2). It is clear that there is a continuous increase in  $\text{CO}_2$  levels in atmosphere over the last

## Chapter 1

---

century but the increase is much rapid in the last 50 years. These increased CO<sub>2</sub> levels have huge impact on environment and climate since CO<sub>2</sub> is a greenhouse gas. A greenhouse gas absorbs thermal radiation and reemits it back towards Earth's surface. Earth's natural greenhouse effect helps in maintaining the temperature of earth. But increased CO<sub>2</sub> levels, due to human activities like burning of fossil fuels, intensifies this greenhouse effect and lead to global warming. This trend of increasing global temperature with increase in CO<sub>2</sub> levels can be observed if Fig 1.2.

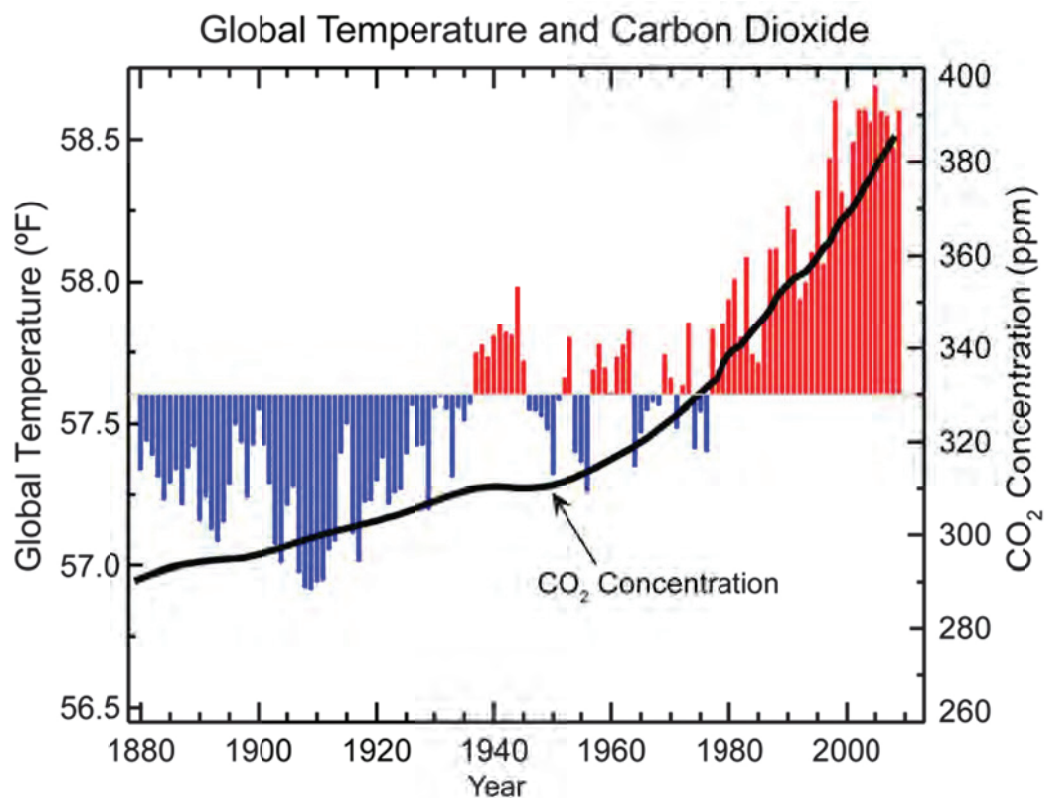


**Fig. 1.2:** Increase in global average temperature with increase in the CO<sub>2</sub> emission.

Adapted from <http://www.ncdc.noaa.gov>

It has been shown in recent investigations that global temperature will be increased by 2°C when the CO<sub>2</sub> concentrations cross the 450 ppm mark. But if the CO<sub>2</sub>

## ***Chapter 1***

---

concentrations increase in the same trend or rather more rapidly as required by growing energy demands, the temperature increase will be much more. Such a temperature increase will lead to melting of glaciers, increase in sea level and change in seasonal events [2].

### **1.2 Hydrogen as an Energy Carrier: Solution to the current energy and environmental problems**

As of now most of the world's energy requirement for electricity generation and transportation etc. are met by combustion of fossil fuels like oil, coal and natural gas. Due to their finite resources and the irreparable harm that they cause to environment, there is a need to look for cleaner alternate primary energy sources. Some of the promising non-polluting renewable energy sources are like nuclear, solar, wind, geothermal and biomass etc.

For some applications like transportation purpose where fossil fuels are extensively used, it is highly desirable to replace fossil fuels by a more environment friendly energy carrier. Hydrogen seems to be the most suitable option for this purpose due to its favorable properties.

- The only combustion product of hydrogen is water. Hence no pollutants or greenhouse gas is emitted.
- Hydrogen has the highest energy density (140 MJ/kg) among all fuels.
- Hydrogen can be stored over relatively long periods of time.
- Hydrogen can be used for all sorts of application like heat, electricity and transportation.

## ***Chapter 1***

---

- Hydrogen is highly abundant in nature.

### **1.3 Hydrogen Production**

In spite of being the most abundant element on Earth, hydrogen is not available freely. It is present in the form of big molecules in combination with other elements. It is present in form of water (with oxygen) or organic molecules (with carbon and other elements). Therefore hydrogen needs to be generated from its compounds using some primary energy source. Hydrogen therefore is an energy carrier rather than primary energy source. Many methods are being used or can be used for hydrogen production from fossil fuels as well as from water. From fossil fuels, hydrogen can be produced by methods like steam reforming of natural gas or other light hydrocarbons, gasification of coal and other heavy hydrocarbons etc. From water it produced by methods like electrolysis, thermochemical cycles, photochemical methods etc.

Hydrogen produced from fossil fuels or non-renewable energy sources is generally associated with emission of carbon and it is called as “Brown Hydrogen”. While Hydrogen produced from renewable energy sources such as water by using solar, wind, hydro or tidal power is known as “Green Hydrogen”. Hydrogen produced as a waste or industrial byproduct is sometimes called as “Grey Hydrogen”.

### **1.4 Hydrogen Production: Present Status**

Presently commercial hydrogen is mainly produced from fossil fuels based sources like coal, oil and natural gas (~96%) and only small fraction (~4%) comes from water electrolysis [3,4]. Main sources of hydrogen are shown below in table 1.1.

Source	% Hydrogen production
Coal	18
Oil	30
Natural gas	48
Water Electrolysis	4

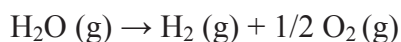
**Table 1.1:** *Present status of commercial hydrogen production from different sources.*

It can be seen from the above table that 96% of hydrogen is being produced from fossil fuels by using different methods like steam reforming of methane or natural gas, partial oxidation of methane, auto-thermal reforming and coal gasification etc. All these methods generate CO<sub>2</sub> as a byproduct which is not desirable, CO<sub>2</sub> being a greenhouse gas.

Therefore it is highly desirable to produce hydrogen from another abundant source i.e. water in an environment friendly manner using CO<sub>2</sub>-free primary sources of energy such as solar energy, wind energy, or nuclear energy.

### 1.5 Hydrogen Production from Water

Hydrogen generation from water can be depicted by the following equation:



But this reaction is highly endothermic ( $\Delta H = 243 \text{ kJmol}^{-1}$  at 298 K) and very high temperatures (>2500 °C) are required for direct thermal decomposition or thermolysis of water. Energy required for decomposition can be provided by solar, nuclear, wind,

## **Chapter 1**

---

electricity or combination of these. A large number of methods have been studied for producing hydrogen from water; some of them are listed below:

- Electrolysis
  - Alkaline electrolysis
  - PEM electrolysis
  - High temperature electrolysis
- Photo-electrolysis (Photolysis)
- Photobiological (Biophotolysis)
- Photocatalysis
- Thermal (Thermolysis)
- Thermochemical
- Radiolysis

Among these methods only electrolysis could be used at commercial level until now. But the cost of hydrogen production from electrolysis is high. Hence there is need as well as scope of improvement in efficiency and reduction of cost of hydrogen production. Thermochemical cycle is one such method which has potential for better efficiency. In this thesis use of heterogeneous catalyst for hydrogen production by thermochemical cycles has been investigated. Subsequently in this chapter thermochemical cycles, basics of catalysis and role of catalysis in thermochemical cycles is discussed.

### **1.6 Thermochemical Cycles for Hydrogen production**

As discussed earlier water can be directly decomposed into hydrogen and oxygen only at very high temperature ( $>2500\text{ }^{\circ}\text{C}$ ), but practically it is difficult to achieve such high temperatures for large scale production of hydrogen. One of the ways to achieve this



## ***Chapter 1***

---

at much lower temperatures is to break the reaction into a series of chemical reactions in such a way that sum of these works out to be decomposition of water into hydrogen and oxygen [5-7]. Thus thermochemical cycles can be defined as

“A thermochemical cycle decomposes water into hydrogen and oxygen through a set of thermally driven reactions at much lower temperatures than that required for direct thermolysis of water.”

Thus thermochemical cycles combine the heat source (Thermo) with chemical reactions (Chemical) to split water into hydrogen and oxygen. The term cycle is used here because all other chemical compounds except water, hydrogen and oxygen are recycled in the processes. Hence water and high temperature heat are the input and hydrogen, oxygen and low temperature heat are the output. If work is partially used as input along with the heat, the cycle is defined as hybrid thermochemical cycle.

The heat required for a thermochemical cycle can be obtained either from a nuclear reactor [8-10], solar concentrator [11,12] or by geothermal energy [13]. Nuclear reactors provide electricity with low or no carbon emissions, they can provide solution to the problems associated with future energy and environment related problems with further developments. Generation IV nuclear reactors such as very high temperature reactor (VHTR) can be used to generate hydrogen through thermochemical cycles or high temperature steam electrolysis. Solar radiation is another source of energy required for thermochemical cycles for generating hydrogen. Although Sun is source of enormous amount of energy, yet it is highly underutilized. One of the most effective methods to use solar radiation is photovoltaic cells but the problems associated is with the storage of

## Chapter 1

---

electricity produced. Hydrogen generated by thermochemical cycles using nuclear or solar can be stored and used for various applications. A thermochemical cycle can be schematically represented as shown in Fig 1.3.

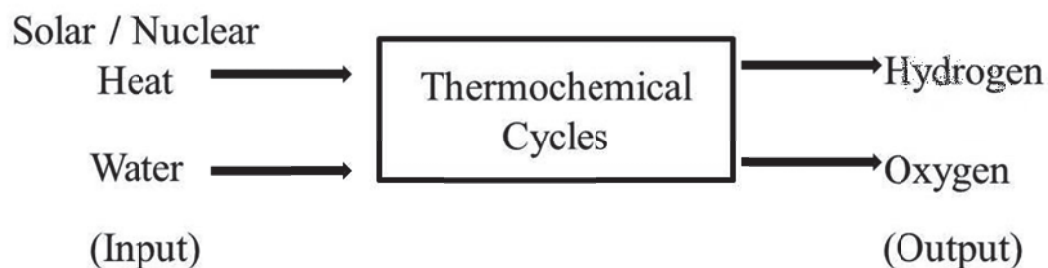


**Fig. 1.3:** *A schematic of the concept of thermochemical cycles*

The concept of thermochemical cycle was first given by Funk and Reinstrom (1966) for efficient production of fuels ( $H_2$ ,  $NH_3$ ) from stable and abundant species ( $H_2O$ ,  $N_2$ ) using heat sources [14]. Though it was not due to scarcity of fuels, it was for some special purposes like providing fuels to military vehicles in remote areas etc. However after the oil crisis era, several research groups around the world started to investigate the processes for energy independence. New energy crisis, growing concerns over global warming and recent advances in solar power technologies (whose high temperatures are ideal for thermochemical cycles) have given a new boost in the research in this field.

More than 350 thermochemical cycles have been proposed and investigated. Advanced computing facilities have facilitated the processes of screening of thermochemical cycles based on their thermodynamic database [15]. Thermochemical cycles can be classified on basis of no of steps involved, on basis of maximum

## Chapter 1

temperature or by the chemicals involved. An example of classification based on number of steps along with some examples is shown below in Fig 1.4

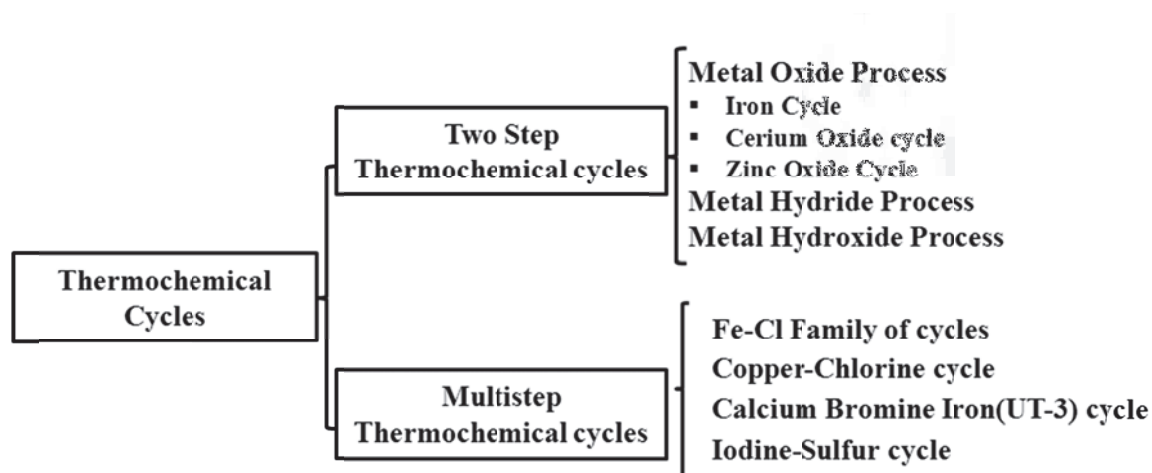


**Fig. 1.4:** *Classification of thermochemical cycles*

In terms of elements involved in thermochemical cycles, the main families are based on sulfur and halogens [16]. Brown et al [17] in their extensive literature survey has compared around 115 thermochemical cycles and shortlisted some potential candidates based on several criteria like number of steps involved, number of elements involved, cost, efficiency etc. Brief introduction of few cycles, reactions involved and the challenges associated with them is given in the following section:

### 1.6.1 Copper chlorine cycle

The copper–chlorine cycle (Cu–Cl cycle) is a four-step thermochemical cycle for the hydrogen production from water. This is a hybrid process because it involves electrolysis step along with thermochemical. Maximum temperature requirement for this cycle is

## Chapter 1

---

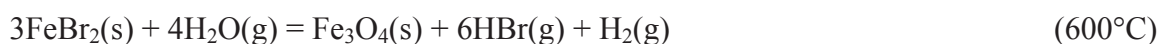
around 500 °C. It involves the following four reactions whose net result is decomposition of water into hydrogen and oxygen [18,19].



One of the main advantages of this cycle is low temperature requirements (500°C) as compared to other thermochemical cycles. Therefore low grade waste heat can be used and material cost is also low. Low temperature requirements make this cycle suitable to be used in combination with CANDU supercritical water reactor [20]. The challenges associated with this thermochemical cycle are solid handling and corrosive fluids. The overall efficiency of the Cu–Cl cycle has been estimated to be around 43%.

### 1.6.2 UT-3 (Ca-Br-Fe) Cycle

The UT-3 (University of Tokyo-3) process is a four-step thermochemical cycle for the hydrogen production from water, which was developed at University of Tokyo. It is also known as bromine-calcium-iron process. This cycle involves the following four reactions with maximum temperature requirement of around 750 °C [21-23].



## Chapter 1

---

The cycle shows promising energy efficiency of around 49% [24]. Lemort et al. have carried out detailed technological and chemical assessment of the UT-3 cycle along with physicochemical and thermodynamic investigation [25,26]. They have suggested that the physicochemical properties of the solid and gaseous reactants make the operation difficult at an industrial scale. Also corrosive nature of bromine and bromide compounds makes the process unsuitable for industrial scale. The process requires cost-effective corrosion-resistant materials for industrial large-scale applications. The toxicity of the reactants is also an important factor to be considered.

### 1.6.3 Ispra Mark cycles

An international round table on direct production of hydrogen with nuclear heat was held at Ispra, Italy in 1969. Beghi has published report on the research performed at the JRC, Ispra programme [27]. Around 24 version of Ispra mark cycles have been reported by Beghi. These thermochemical cycles are known as Ispra mark1, Ispra mark 2 etc. Few important cycles are described below

- **Ispra Mark 1 cycle**

The first phase of the research programme was focused on the Mark 1 cycle proposed by Marchetti and de Beni [28]. Mark 1 cycle is a four step cycle consisting of the following reactions:



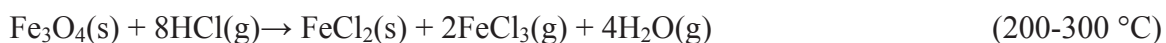
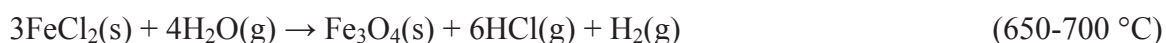
## Chapter 1

---

This process showed that thermochemical decomposition of water is a feasible concept, but presence of mercury makes it unsuitable for large scale production, due to toxicity of associated with use of mercury.

- **Ispra Mark 15 cycle**

The second phase of the programme dealt with the iron-chlorine family of cycles, which had been proposed in the early 1970s. An example of these cycles is Mark 15 which consists of following steps:



- **Ispra Mark 13 cycle (Sulfur-Bromine cycle)**

Ispra Mark 13 (Sulfur-Bromine cycle) is a hybrid thermochemical cycle involving the following three reactions, where decomposition of HBr is an electrolysis step.



Limiting factors in this case are electrolysis step as well as corrosive nature of the bromine and bromide compounds.

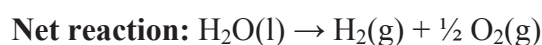
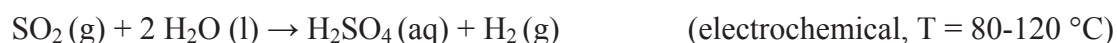
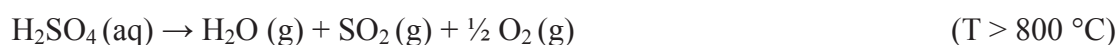
## Chapter 1

---

### 1.6.4 Hybrid Sulfur (Westinghouse) cycle

Hybrid sulfur cycle is a hybrid thermochemical cycle based on sulfur chemistry. This cycle was significantly developed by Westinghouse Electric Corp. in the 1970 [29], hence it is also known as known as the "Westinghouse" cycle. This cycle is also known as Ispra Mark 11 cycle.

It is a two-step cycle. Here sulfur dioxide  $\text{SO}_2$  and water are reacted electrolytically to produce hydrogen and sulfuric acid  $\text{H}_2\text{SO}_4$ . The resultant sulfuric acid is vaporized to produce steam and sulfur trioxide  $\text{SO}_3$ , with the latter being subsequently decomposed at high temperature into sulfur dioxide  $\text{SO}_2$  and oxygen  $\text{O}_2$ .



### 1.6.5 Sulfur-Iodine cycle

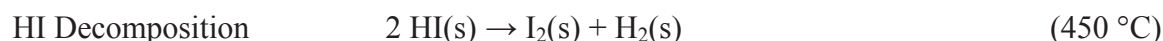
Sulfur iodine cycle (S-I or I-S cycle) is a three step thermochemical cycle involving sulfur and iodine. It is also known as Ispra Mark 16, which is variant of Ispra Mark 11 cycle, where hydrogen evolving step is purely thermochemical in nature. The cycle was proposed and pursued by General Atomics in the USA, which made significant contributions to the process engineering and scaling up of the cycle [30,31]. The cycle is also known as GA Sulfur Iodine cycle. It has potential for high efficiencies for hydrogen production [32]. Presently, Japan Atomic Energy Agency (JAEA) is continuing research in SI process [33-37]. They have conducted successful experiments with the S-I cycle using Helium cooled High Temperature Test Reactor as the heat source. JAEA has planned to use high

## Chapter 1

---

temperature generation IV nuclear reactor to produce industrial scale quantities of hydrogen. The French CEA, General Atomics and Sandia National Laboratories are jointly developing the sulfur-iodine under an International Nuclear Energy Research Initiative (INERI) agreement established by the U.S. Department of Energy. Lot of research is taking place in Canada, Korea, Italy, China and India.

The three reactions involved in S-I cycle are as follows:



The sulfur and iodine compounds are recovered and reused in the cycle. Bunsen reaction is exothermic in nature, while the two acid decomposition reactions are endothermic in nature. The S–I process works like a chemical heat engine, where heat enters the cycle in high-temperature endothermic reactions and heat exits the cycle in the low-temperature exothermic reaction. The balance heat leaves the cycle in form of heat of combustion of hydrogen produced during the course of reactions.

S-I cycle is the most studied and sought after cycle. It is due to the fact that it has certain advantages over other competitive thermochemical cycles. Some of them are listed below

- All fluid process hence suitable for continuous operation.
- All three reactions are thermochemical, no electrolysis steps involved.
- High efficiency due to high utilization of heat (about 50%),



## Chapter 1

---

- Abundance of elements involved is not a problem.
- Completely closed system without any byproducts or effluents.
- Suitable for application with solar and nuclear source of hydrogen.
- More developed than competitive thermochemical cycles.

S-I cycle has a few limitations also like corrosive nature of intermediates ( $I_2$ ,  $SO_2$ ,  $HI$ ,  $H_2SO_4$ ) which requires advanced materials for construction. Thus the economic viability of the process depends on availability of corrosion resistant materials. Some of the suggested materials include tantalum alloys, niobium alloys, noble metals, high-silicon steels, several nickel-based superalloys, mullite, silicon carbide ( $SiC$ ), glass, silicon nitride ( $Si_3N_4$ ) etc [38]. Recent research has suggested that new tantalum technologies may be a technically and economically feasible way for large scale applications in S-I cycle [39].

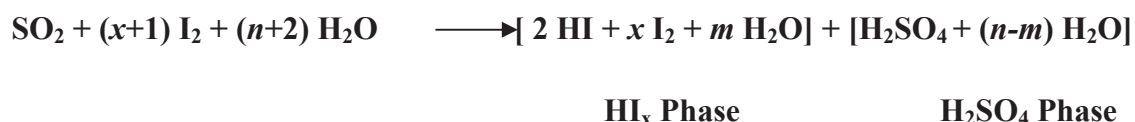
Thus sulfur-iodine cycle has been proposed as a way to supply hydrogen for a hydrogen-based economy. With an efficiency of around 50% it is more efficient than electrolysis, and it does not require hydrocarbons like current methods of steam reforming. The cost analysis shows that the cost of hydrogen produced by S-I cycle is lower as compared to that of steam-methane reforming, and conventional and high temperature electrolysis. The reason for low cost is due to less use of electricity, no carbon related charges and no methane requirement. Closed loop lab scale as well as bench scale testing of the process has already been demonstrated [40-42]. Designing, flow sheet proposal and evaluation is in progress for plant scale process which can be coupled to a nuclear reactor or a solar concentrator [43-49].

## Chapter 1

---

### 1.7 HI<sub>x</sub> Section of S-I Cycle

According to the reaction scheme of S-I thermochemical cycle, in Bunsen reaction one mole each of SO<sub>2</sub> and I<sub>2</sub> react in presence of two moles of water to produce two acids namely HI and H<sub>2</sub>SO<sub>4</sub>. But from operation point of view, the conditions for Bunsen reaction are optimized by adding extra iodine and water. The excess iodine enhance the phase separation of the two acids and shifts Bunsen reaction equilibrium forward to produce more acids. Excess of water makes the reaction spontaneous and also causes the equilibrium to shift forward to produce more acids. This modified Bunsen reaction with extra iodine ( $x$  moles) and extra water ( $n$  Moles) can be written as follows.



The lower is the water excess  $n$  the lower is the operating cost and higher is the efficiency. While on the other hand lower iodine excess  $x$  is advantageous for the management of HI section [50]. Norman et al [30] have reported the following optimum composition for the Bunsen reaction.



In case of S-I cycle, HI phase is containing excess iodine and water. Therefore production of hydrogen from this phase is highly energy consuming due the following two reasons:

- (i) The extraction of HI from the HI<sub>x</sub> mixture is difficult because of the presence of an azeotrope in the mixture, so simple distillation is not possible.

## Chapter 1

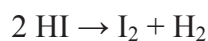
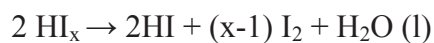
---

(ii) The extraction of HI from the  $\text{HI}_x$  mixture requires very large heat exchanges, due to the large heat capacity induced by the high water content of the mixture.

Hence various options have been tried to improve the overall efficiency of the process, like use of phosphoric acid for concentration of the HI solution [51], electro-electro dialysis concentration method [52,53], reactive distillation [54] and use of silica membrane reactor [55]. Reactive distillation has an advantage of combining reaction and separation in a single step leading to overall shift of equilibrium towards production of  $\text{I}_2$  and  $\text{H}_2$  [56].

### 1.8 HI Decomposition Reaction

HI decomposition reaction is the hydrogen producing step of the S-I cycle. Bamberger in his detailed report has shown that HI decomposition reaction is also integral part of some other iodine based cycles [57] for example Magnesium Iodine cycle [58], Magnesium-Sulfur-Iodine cycle [59]. The HI coming from Bunsen reaction of S-I cycle has iodine which is to be separated before HI decomposition, which can be achieved by various means as discussed in previous section. Therefore the reactions involved in the process can be written as:



HI decomposition reaction may take place in both vapor as well as liquid phase with both having their advantages and disadvantages. HI decomposition reaction has the following limitations:

- The decomposition reaction is incomplete (Equilibrium conversion is low).

## **Chapter 1**

---

- The decomposition reaction is slow.

Since hydrogen iodide (HI) decomposition is a thermodynamically limited reaction with low yields, therefore it requires considerable amount of energy for separation and recirculation of the unreacted species which in turn affects the overall efficiency of the thermochemical cycle. Therefore the efficiency of cycle depends on how efficiently HI is decomposed into hydrogen and iodine.

### **1.9 Catalyst requirement for HI Decomposition Reaction**

As mentioned in the previous section, HI reaction is a slow reaction with low yields. Hence it is very much required to use a suitable catalyst for HI decomposition to achieve workable reaction rates by increasing the decomposition rate. Also a catalyst with high performance and low cost will positively affect the overall efficiency of the thermochemical cycle.

The catalyst can be a heterogeneous catalyst on the surface of which HI molecules will get adsorbed and undergo decomposition via different mechanism than that of homogeneous gas phase reaction. This will decrease the activation energy barrier and increase the reaction rate

Now, we present a brief introduction and history of catalysis followed by the status on the development of the catalyst for hydriodic acid decomposition till date.

### **1.10 Brief history of catalysis**

Catalytic reactions play important roles in every aspect of our life. Most of the biological reactions that build the human body and control the functioning of the brain and other important organs are catalytic in nature. For example enzymatic catalysts

## Chapter 1

---

regulate the transformations within natural organisms. Catalyst play key role in in photosynthesis process in the plant kingdom in form of chlorophyll, a green pigment. Majority of industrial processes used for manufacturing of items of our day to day need like fuels, fertilizers, plastics, synthetic fibers, medicines etc. are supported by catalysts. As an estimate, about 90% of all chemical reactions in industries rely on catalysts of one kind or another. Thus, it can be said that the catalyst technology is in fact the backbone of the chemical industry.

Even though catalysts have been used in number of activities like making of bread, wine and cheese etc. since antiquity, the word “catalysis” was first used by Berzelius in a published report [60] in 1836. This report included observations of various catalytic substances by Berzelius, Faraday, Thenord, Dobernier and other scientists in the early nineteenth century. Berzelius suggested that reactions could occur at the surface of solids provided that the surface possessed a ‘*catalytic force*’ and used the collective title ‘*catalyzed process*’ taking place under the influence of a catalytic force.

The development of catalysts was found to be especially important for reactions which evolved heat. Although equilibrium constant, of one such reaction, may be favorable at room temperature, the rate may be so slow that the reaction cannot be used practically. When the temperature is raised the rate is increased, but the equilibrium constant might be unfavorable at this temperature, as is readily surmised from Le Châtelier’s principle. Thus, catalysis was said to be concerned with the control of the rate of a chemical reaction by introducing in the reaction path, transient states that as such do

## ***Chapter 1***

---

not appear in the chemical equation. They were supposed to provide an alternate route for the reaction by their own involvement, though they remain unchanged at the end.

Ostwald, in 1894 proposed that catalyst is a substance that alters the velocity of a chemical reaction without appearing in the end products. Second half of the 19<sup>th</sup> century and early 20<sup>th</sup> century witnessed discovery of significant number of catalytic processes for example Deacon Process for oxidation of HCl to water and chlorine gas (1860), oxidation of SO<sub>2</sub> to SO<sub>3</sub> by platinum (1875), Ostwald's process for ammonia oxidation to nitric oxides, a precursor of nitric acid manufacture (1902), Sebatier's process for the hydrogenation of carbon dioxide (1910) and Haber process for ammonia production which is marked as the most important invention of the 20th century [61] . A number of such historical accounts of the development of catalytic processes and related subjects may be found in literature [62-64].

The present day understanding of catalysts and catalytic processes is established over a period of time by efforts of various scientists like Langmuir (sticking probability, adsorption isotherm, dissociative adsorption, role of monolayer), Emmett (surface area measurements, kinetics of ammonia synthesis), Taylor (active sites, activated adsorption), Bonhoeffer, Rideal, Farkas (kinetics and molecular mechanisms of ethylene hydrogenation, ortho-para hydrogen conversion, isotope exchange, intermediate compound theories) and many others [63].

A more scientific definition of the catalyst has been coined on the basis of proper understanding of thermodynamics, reaction pathway, and kinetics of catalyzed reactions. According to which

## Chapter 1

---

*“Catalyst is a substance which increases the rate at which chemical reaction approaches equilibrium, without being consumed in the process and without causing any alteration in the free energy change involved”.*

It is generally accepted that catalysts function by forming chemical bonds with one or more reactants thereby opening up more favorable pathways (reduction in height of activation energy barrier) to their conversion into products as compared to those available for a non-catalyzed reaction.

Let us consider a gaseous reaction which can be represented by the following equation



The equilibrium constant of the reaction is given by,

$$K_p = \frac{P_C P_D}{P_A P_B} \quad \text{.....1.2}$$

where  $P_A$ ,  $P_B$ ,  $P_C$  and  $P_D$  are the partial pressures of the components A, B, C and D respectively.  $K_p$  is related to the standard state Gibbs free energy change  $\Delta G^0$  by the following equation

$$\Delta G^0 = -RT \ln K_p \quad \text{.....1.3}$$

Where R is the universal gas constant and T is the absolute temperature.

Therefore the value of equilibrium constant and thus the product yield is determined by the Gibbs free energy of the reaction. Since a catalyst cannot affect the Gibbs energy of the overall reaction and thus can't vary the equilibrium constant. The catalyst increases the rates of both the forward and backward reaction so that their ratio remains same as in

## Chapter 1

absence of catalyst. Thus a catalyst allows the equilibrium to be reached faster. Also a catalyst can only accelerate a reaction which is already thermodynamically feasible but it cannot initiate a reaction which is thermodynamically impossible [65]. So, another definition of a catalyst is “*A catalyst is a substance that allows a chemical reaction to attain equilibrium faster without itself being permanently involved.*”

The barriers for the above chemical reaction with, and without a catalyst are shown in Fig. 1.5.

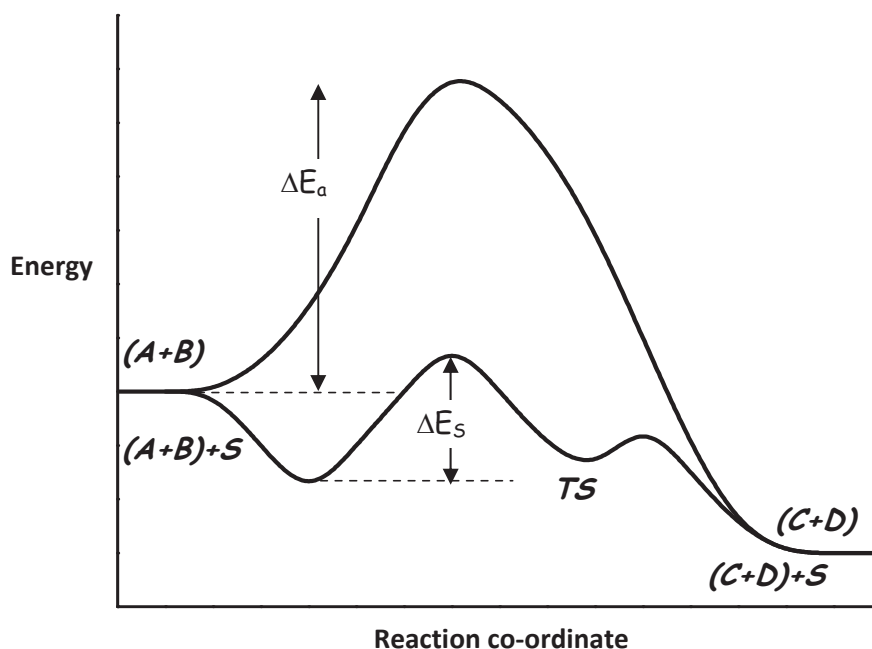


**Fig. 1.5:** Reaction paths for non-catalyzed and heterogeneously catalyzed reactions.

The velocity of such a reaction depends on its rate constant,  $k = A \exp(-\Delta E_a/RT)$ , where  $A$  and  $\Delta E_a$  are frequency factor and the activation energy respectively. Hence the rate of the reaction at a given temperature can be increased by increasing  $A$  or by reducing  $\Delta E_a$ . In the presence of a catalyst (say heterogeneous catalyst), which might



## Chapter 1

---

chemisorb either A or B, or both, the system may follow a new reaction path with a lower energy of activation,  $\Delta E_s$ . Here the system passes through a new chemisorbed transition state (TS). However, decrease in the value of the activation energy alone does not permit an evaluation of the catalytic activity, since the pre-exponential factor A also depends on the catalyst. Hence, attempt to understand the phenomenon of catalysis must include knowledge of the structure of the surfaces of catalysts, the state of chemisorbed molecules over these surfaces and their mode of interaction.

### 1.11 Classification of Catalysts

Catalysts can be categorized into three broad categories depending on catalyst-reactant phases and their nature of applications [66].

- (i) *Enzyme catalysis:* Enzymes are complex organometallic compounds generally occurring in nature and the reaction catalyzed by enzymes comes under the category Enzyme catalysis. Enzymes help carry out a reaction at low temperatures and generally yield a single product without any side reaction. But due to stringent requirement of conditions and environmental control, they find only limited applications in chemical industry e.g. the use of enzymes to obtain products such as alcohols, carboxylic acids, carboxylic esters etc by hydrolysis of esters.
- (ii) *Homogeneous catalysis:* Homogeneous catalysis refers to the catalytic processes where the catalyst and reactant(s) are present in the same phase (mostly liquid). These processes are also highly product selective and find application in production of many important chemicals, including many of

## Chapter 1

---

the vital drugs in pharmaceutical industry. A number of soluble organometallic complexes are used as catalysts for industrial processes such as hydroformylation, oxo-processes, hydrogenation, oxidation, polymerization etc. such as use of titanium complexes as homogenous catalysts in polymerization of olefins like propylene to polypropylene, a Ziegler-Natta Polymerization process.

- (iii) *Heterogeneous catalysis*: Heterogeneous catalysis includes those processes in which the reactant (mostly gaseous or liquid) and catalyst (generally solid) are present in different phases. The reaction in this case occurs at an interface. Most of the processes in chemical industry belong to this class e.g. use of Fe- $V_2O_5$  catalyst in synthesis  $NH_3$  from  $H_2$  and  $N_2$ , the famous Haber process.

### 1.12 Heterogeneous catalysts

Heterogeneous catalysts are the most used ones among the above classification. It is their important characteristics like ease of recovery from reaction system, higher stability and applicability in both continuous or batch mode of operation, which makes them suitable for wide range of applications. Several important industries viz. petroleum, petrochemicals, fine chemicals, pharmaceuticals, polymers etc. uses heterogeneous catalysts. On the basis of their chemical composition and physico-chemical properties, the heterogeneous catalysts can be broadly classified into the following categories:

- (a) Metals
- (b) Metal oxides
- (c) Supported metals

## ***Chapter 1***

---

- (d) Solid acids / super acids
- (e) Solid bases
- (f) Zeolites and molecular sieves
- (g) Clays and heteropoly acids.

Based on their nature and functionality, the above mentioned classes of catalysts, can be logically grouped into mere two types: (i) metals and (ii) non-metals. The former group consists of transition metals, especially Group VIII, and noble metals of Group IB, while the latter consists of metal oxides and sulfides, carbon materials, salts and acids.

Another classification of the catalysts can be done on the basis of conductivity of the catalysts. Thus it can be subdivided in three categories (i) Conductors (ii) Semiconductors and (iii) Insulators. The conductors (metals) are considered to be good catalysts for hydrogen addition or abstraction but are poor catalysts for addition or abstraction of oxygen. The semiconductors (metal oxides and sulfides) are good catalyst for oxidation – reduction processes and insulators work better as dehydration and isomerization catalysts.

All the catalytic reactions involve the same basic steps, irrespective of the class to which a heterogeneous catalyst belongs. The overall process can be broken down in the following five steps [67]:

- (i) Transport of reactants to the catalyst surface.
- (ii) Adsorption of reactants on the catalytic sites.
- (iii) Interaction of the adsorbed reactants (bond breaking, bond forming, molecular rearrangement) leading to the product formation.

## ***Chapter 1***

---

- (iv) Desorption of the products from the catalytic sites.
- (v) Transport of products away from the catalyst surface.

Therefore the activity as well as selectivity of catalyst depends on the bonding between the catalyst and reactant and the transformations that they undergo during the course of the reaction. As a thumb rule, the stronger the bond between adsorbate and the catalyst, the less will be the catalytic activity. On the other hand, a very weak bonding will not result in a catalytic activity.

Heterogeneous catalysis finds its use in a wide range of industrial and technological applications and it cannot be explained by any single theory. However there have been many attempts to a general theory for such processes. For example, one such theory is the electronic theory of catalysis. This theory correlates electronic energy levels of the solids (especially semiconductors) and the reactant molecules. In case of transition metals, the catalytic activity is related to vacant atomic d orbitals. Hence large numbers of vacant d-orbitals present are responsible for high chemisorption activity of the transition metals. This is further explained in terms of a parameter called as percent d-character of a transition metal [67-69]. According to another approach based on localized model, the reactant molecules form unstable complexes with the surface atoms of the catalyst and this complex decompose to give products.

Therefore in absence of a unique theory, attempts are being made around the world to correlate the catalytic activity of a catalyst to some of its specific properties. This can narrow down the search of a suitable catalyst for a given reaction. Therefore in spite of lot of progress in the field of catalysis, it is still regarded as an art rather than science.

## Chapter 1

---

Prof. Morrison quoted [70]: “ *The development of new catalysts to accelerate specific reactions is approximately 10% theory, 50% experience and intuition and 40% empirical optimization As our knowledge of surface science grows, we can hope that these percentages will shift to the left in that tabulation, but at present heterogeneous catalysis is so complex that detailed analysis of even the simplest reactions is almost impossible*”

### 1.13 Supported Metal Catalysts

Supported metal catalysts has an important role in the field of heterogeneous catalysis especially catalysis by metals. A supported metal catalyst has metal (0.1 to 20 % of the catalyst weight) in form of small particles dispersed over an inert and high surface area material called as support. Some typical examples of supports are alumina, silica, zeolite and carbon.

Supported metal catalysts have certain advantages over other forms of metal catalysts like powder, particles, wire or films. The use of high surface area support leads to high dispersion of metal in form of very small crystallites, which results in high surface area of metal and higher resistance against sintering. In case of noble metals, high dispersion of metal by using high surface area support significantly reduces the cost of catalyst. In some cases pore structure of the support may have advantage in terms of selectivity for a particular reaction. Support may affect the morphology and distribution pattern of metal particles also. In some cases, support may increase the catalytic activity of the metal through metal support interactions.

### **1.14 Catalysis in thermochemical research**

Catalyst plays important role in any industrial process by affecting product yield as well as selectivity of the process. Since thermochemical processes for hydrogen production are highly energy intensive and cyclic in nature, therefore these two factors of yield and specificity are not of that importance in this case. In case of thermochemical cycles, the catalyst plays some other important roles and most of the cycles mentioned in ref [57], can be considerably improved in terms of efficiency as well as cost by using suitable catalyst.

Following are few important areas of thermochemical cycle, where catalysis plays important role. In general a thermochemical cycle have at least one endothermic reaction which takes up heat from heat source and this reaction involve large increase in entropy by change from condensed phase of reactants to gaseous phase of the products. This type of reactions requires a catalyst to promote the reaction. Another use of catalyst in case of thermochemical cycle is by speeding of a reaction. Higher speed of reaction requires lower steady state inventory of chemicals and thus size equipment can be lowered. These factors affect the economic operation of thermochemical cycle. In case of hybrid thermochemical cycles, catalysis is used for production of large surface area electrodes which are used in intermediate electrochemical reactions of the cycle.

Till today most studied catalytic processes in thermochemical research are sulfuric acid decomposition and hydriodic acid decomposition reactions. A detailed account of catalytic decomposition of these two acids with respect to thermochemical cycles have been given by O'keefe et al [71]. Among these two reactions, sulfuric acid thermal

## **Chapter 1**

---

decomposition is the most endothermic reaction in the sulfur based thermochemical cycles and is normally carried out at above 800 °C in presence of supported platinum catalysts such as (Pt/Al<sub>2</sub>O<sub>3</sub>, Pt/TiO<sub>2</sub> and Pt/ZrO<sub>2</sub>) [72], (Pt/TiO<sub>2</sub> (rutile) [73], (Pt/BaSO<sub>4</sub>) [74] or several metal oxides [75]. Another reaction i.e. HI decomposition reaction is part of iodine based thermochemical cycles including S-I cycle. The catalysts reported for it are discussed in detail in the following section.

### **1.15 Decomposition of HI on Catalyst Surfaces**

This reaction involving HI, H<sub>2</sub> and I<sub>2</sub> is one of the most extensively studied reactions in gaseous phase. Homogeneous chemical equilibrium studies and reports are available as early as beginning of twentieth century [76-77]. Second half of the twentieth century has witnessed lot of work related to this reaction carried out by Suvillan [78-81]. The use of this reaction in thermochemical cycles has unleashed its practical use in addition to already existing fundamental interest. Therefore this reaction is of great importance from both fundamental and technical point of view due to the increasing interest in hydrogen generation by thermochemical cycles.

The biggest advantage of using catalyst for HI decomposition reaction with respect to thermochemical cycles is lowering of reaction temperature which is of advantage in terms of corrosivity issues related to HI and I<sub>2</sub>. A wide range of catalysts have been used and studied for HI decomposition reaction. We give a comprehensive account of the catalysts studied for this reaction globally.

Most of the catalysts proposed and used for HI decomposition reaction are noble metal based, predominately platinum based. NCLI (National Chemical Laboratory for

## ***Chapter 1***

---

Industry) Japan has carried out extensive work on HI decomposition reaction using various metals (Pt, Pd and Ni) and substrate (Alumina, silica, zeolite, carbon etc) combinations [71]. From their studies it was found that platinum was better as compared to other two metals. Platinum is known to be active for this type of reaction, where the reactant molecule gets dissociatively adsorbed over the platinum surface (active site). The adsorption and decomposition of HI on supported platinum surface has been studied by many researchers. Shindo et al [82] have proposed a reaction mechanism, where they suggest that reaction proceeds via adsorption and dissociation of HI at the surface active sites i.e. the active noble metal centres.

One of the earliest studies on HI decomposition reaction on catalyst surface are reported by Hinshelwood in 1925 on platinum and gold surface [83-84]. Another report of HI decomposition over activated carbon catalyst is available in British patent 796,049 of year 1958. A 1968 US patent 3,365,276 describes decomposition of HI over platinum surfaces that has been electrically deposited as a thin film on a high surface area membrane. Holmes et al [85] describes use of pyrolytic carbon as a catalyst. All of the above groups have reported substantial increase in reaction rate with use of a catalyst.

The interest in development of efficient catalyst for HI decomposition reaction still exists and it is evident from large number of publication in the first decade of 21<sup>st</sup> century. Numbers of research groups from around the globe are working in the field. Pt catalysts supported on different supports are the most studied systems like Pt/Carbon [86] , Pt/Alumina [87], Pt/Ceria [88-89] , Pt/Ceria-Zirconia [90] and bimetallic Pt-Ir catalysts [91] on carbon.



## Chapter 1

---

Since cost of the catalyst plays crucial role in determining the cost of hydrogen produced, therefore non platinum based catalysts have been also studied with equal vigor. These non-platinum catalysts can be categorized in two classes, different types of carbon [91-96] and nickel based systems [97-101]. Ni based systems have limited stability and low production capacity which is of disadvantage for industrial scale production.

All the catalysts mentioned above have been employed for HI decomposition reaction in vapor phase at higher temperatures ( $T > 450^\circ\text{C}$ ). Another approach which can be followed for HI decomposition is decomposition in liquid phase. This was first explored by GA in 1952 to get enhanced conversion. The equilibrium constant equation for decomposition of HI to  $\text{H}_2$  and  $\text{I}_2$  can be illustrated as given below:

$$K_p = \frac{P_{\text{I}_2}^{0.5} P_{\text{H}_2}^{0.5}}{P_{\text{HI}}} \quad \text{.....1.4}$$

It is evident from this equation that at a given pressure of HI, lowering of  $\text{I}_2$  partial pressure is required for higher yield of  $\text{H}_2$ . This means that a sink of iodine is required to drive the reaction in forward direction. This sink for iodine can be provided by the reactant HI itself because  $\text{I}^-$  forms polyiodide species in presence of iodine. Thus the iodine formed gets dissolved in HI in form of polyiodides and does not get deposited on the catalyst surface. Therefore the active sites of the catalyst surface remain free for the reaction. Therefore in case of liquid phase decomposition reaction, dissolution of the  $\text{I}_2$  formed at catalyst surface into the HI solution and continued intimate contact between HI and catalyst maintains high reactivity levels with generation of gaseous  $\text{H}_2$  even in presence of  $\text{I}_2$ . Very high conversion level as high as 50% is reported by O'Keefe et al [71]. The liquid phase HI decomposition studies are limited as compared to vapor phase.

## ***Chapter 1***

---

### **1.16 Aim of our work in Hydriodic acid decomposition**

Bhabha Atomic Research Centre (BARC), India is in process of developing high temperature reactors which are capable of supplying process heat at around 1000°C. These reactors will be able to provide heat for production of hydrogen along with electricity. The present efforts are for development of technology for small power (100 kWth) Compact High Temperature Reactor (CHTR) capable of supplying high temperature process heat at 1273 K [102]. Additionally conceptual details of a 600 MWth reactor supplying heat at 1273 K for commercial hydrogen production (IHTR-H), are also being worked out.

Therefore R&D work has been initiated in BARC in most of the related areas, including studies on hydrogen generation by sulfur-iodine thermochemical cycle and Cu-Cl cycle, hydrogen storage materials along with solid oxide fuel cell materials. For S-I cycle, initially the feasibility demonstration has been carried out in a closed loop glass set up in Chemical technology division, which will be followed by bench scale and pilot scale plants. Chemistry Division is involved in the development of catalysts for sulfuric acid decomposition which is the most energy intensive step of S-I cycle. Chromium doped iron oxide catalyst [103,104], ferrosinels [105] have been developed and used for the reaction at lab scale. Doped iron oxide based catalysts have also been used for pilot plant scale studies also.

The aim of present work in hydriodic acid decomposition is to synthesize suitable platinum based catalyst with different supports, characterize their physico-chemical properties, evaluate their potential for the HI decomposition reaction in terms of activity

## ***Chapter 1***

---

as well as stability and establish structure activity correlation. Optimization of platinum loading to reduce the cost of catalyst is another aspect covered in the present study. All these aspects have been dealt in details in the following chapters.

In Chapter 2 of the thesis, the experimental methodologies have been discussed. Apart from the different instrumental techniques used for characterization, this Chapter includes different methods used for synthesis of catalysts and the method used for evaluation of activity and stability of these catalysts for liquid phase HI decomposition reaction. In Chapter 3, platinum catalysts supported in different type of carbons were prepared, well characterized and evaluated for HI decomposition reaction. The effect of pore structure of carbon support has been further investigated and presented in Chapter 4. Chapter 5 has the details of different catalysts supported on oxides like ceria, zirconia and titania. Effect of platinum loading on activity has also been investigated and presented in this chapter. The catalytic activities were correlated with structural and morphological properties of the catalysts by proper characterization of the fresh and the spent catalysts. Chapter 6 includes the results of various experiments carried out to identify the poly iodide species present in the mixture of HI and I<sub>2</sub>, which forms the basis of liquid phase HI decomposition. The summary of the present work and future scopes have been included in Chapter 7.

# Chapter 2

## Instrumentation and Experimental Methods

---

### 2.1 Introduction

A brief overview of the experimental methods adopted for synthesis of the catalysts, different techniques employed for the characterization of these samples and methodology for evaluation of their catalytic activities for hydriodic acid decomposition is presented in this chapter. The catalyst samples were synthesised by various techniques e.g. wet impregnation of the supports, precipitation of supports followed by impregnation and preparation of support by hard templating route or nanocasting. These samples were well characterised for various properties like structural morphological and oxidation states by various instrumental techniques e.g. X-Ray Diffraction (XRD), Scanning Electron Microscopy (SEM), Energy Dispersive X-ray (EDX), Transmission Electron Microscopy (TEM), X-ray photoelectron spectroscopy (XPS), N<sub>2</sub> adsorption and chemisorption. An autotitrator was used to determine the concentrations of H<sup>+</sup> and I<sup>-</sup> ions which was eventually used to determine the percentage conversion. Gas chromatograph was used to quantify the reaction products like H<sub>2</sub> for HI decomposition reaction. This chapter contains brief descriptions on general principles of these techniques.

## **Chapter 2**

---

Experimental setup used for evaluating activity and stability of the catalysts for HI decomposition is also discussed in this chapter in detail.

### **2.2 Sample Preparation**

This section gives account of different precipitation methods used for preparation of various catalysts investigated in this thesis. Since this thesis deals with platinum based catalysts supported on different supports, any method will essentially involve preparation of support and loading of platinum on the support. In general preparation of heterogeneous catalyst can be divided in three basic steps [106]:

- (i) Formation of primary solid e.g. impregnation, co-precipitation etc.
- (ii) Processing of primary solid e.g. heat treatment etc.
- (iii) Activation to give active catalyst e.g. reduction of metal precursor to metal

This section presents the general principles of various methods used for preparation of catalysts. However, detailed description of each method is presented in the respective chapter where the catalyst is studied and reported.

#### **2.2.1 Wet Impregnation method**

Wet impregnation method is one of the most common methods used for synthesis of heterogeneous catalysts. In this method active metal precursor, dissolved in an aqueous or organic solvent, is added to catalyst support. The solution goes into the pores of the support by capillary action. The solution in excess to the pore volume of support is transported through diffusion process. After wetting of the support, the volatile component of the solution is removed by drying and calcination. This method was used to prepare Pt/carbon catalysts as discussed in Chapter 3.

## Chapter 2

---

### 2.2.2 Hard Templating method / Nanocasting

Porosity of the support plays important role in case of catalysis. Porous materials can be ordered or disordered depending upon the synthetic strategy. In addition to catalysis, ordered porous materials find their applications in wide range of applications like separation, bioreactors, drug delivery, HPLC separation and fuel cell electrode membrane [107,108]. But these porous materials are difficult to synthesize due to tendency of solids to minimize void spaces within their structures.

Cooperative surfactant templating is one of the most studied method to prepare ordered mesoporous materials eg. OMS (Ordered Mesoporous Silica). But it is difficult to use this method for synthesis of mesoporous carbon materials because of the complexity of carbon structure evolution. One of the methods for preparation of porous carbon supports is hard templating methods using porous silica templates [108], this synthetic strategy is also known as Nanocasting. In this method hard silica templates are infiltrated by carbon precursors e.g. sucrose solution followed by solidification of carbon within the pores after which silica template is removed by HF leaching. This process is presented in the Fig.2.1

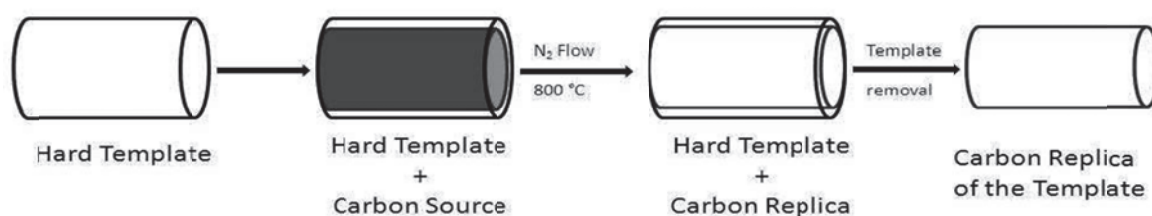


**Figure 2.1:** Synthetic Strategy for the porous carbon support by Nanocasting

## ***Chapter 2***

---

Silica templates used for this method were also prepared in-house using hydrothermal synthesis. Two types of mesoporous silica templates were prepared by using ionic (CTAB) and nonionic (P123) surfactants. Detailed procedure of preparation of the mesoporous silica followed by their use as template for synthesis of mesoporous carbon is given in Chapter 4.

### **2.2.3 Precipitation and Co-precipitation method**

The precipitation method is one of the commonly used methods for the preparation of ceramic materials. We have used this method for preparation of oxide supports. In this method an aqueous solution of the desired cation (s) is prepared and drop wise added to the solution containing the precipitating agent (Ammonia solution, alkali hydroxides, oxalic acid etc.) or vice versa. The precipitate (metal hydroxide or oxalate) is separated from the solution by filtration. The filtered product is heated to thermally decompose it to get the desired compound. The final product depends on several parameters like pH, temperature, rate and order of mixing of one solution into another. Oxide supports like zirconia, ceria and titania was prepared by this method and discussed in Chapter 5.

## **2.3 Characterization techniques**

### **2.3.1 X-ray diffraction (XRD)**

XRD is the most extensively used technique for the identification of crystalline phases of a solid and also to determine its crystal structure [109]. The principle of XRD technique is based on scattering of X-rays by a crystal consisting of well-defined array of

## Chapter 2

atoms, ions and molecules. The coherent scattering of X-rays results into constructive interference (bright fringes) or destructive interference (dark fringes). The condition for constructive interference is that the path difference between the two rays should be equal to an integral multiple of wavelength. This phenomenon is broadly termed as X-ray Diffraction. The crystal lattice consists of parallel rows of atoms which are equivalent to the parallel lines of the diffraction grating; therefore the inter-planar spacing ( $d$ ) could be successfully determined from the separations of bright fringes of the diffraction pattern. These interplanar spacings are of the same magnitude as the wavelength of X-rays (0.5 to 2 Å).

Interaction of X-rays reflected by a set of parallel planes satisfying Bragg's condition lead to constructive interference only at a particular angle ( $\theta$ ).

$$n\lambda = 2d \sin\theta \quad \dots 2.1$$

where,  $\lambda$  is wavelength of X-rays,  $\theta$  is the glancing angle (called as Bragg's angle),  $d$  is inter-planar separations, and  $n$  is the order of diffraction. A schematic representation of the X-ray Diffraction is illustrated in Fig. 2.2.

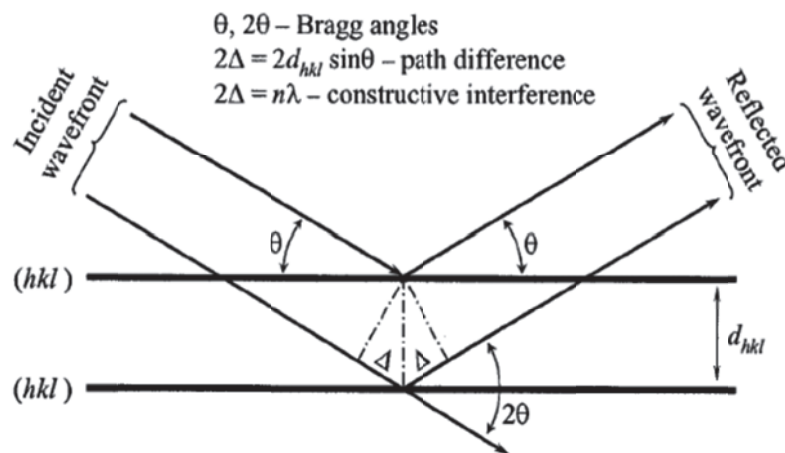


**Figure 2.2:** Schematic diagram of X-ray Diffraction



## Chapter 2

---

X-rays are electromagnetic waves, therefore electrons of the atoms vibrate when electric field of X-ray interact with the electron cloud of the atom. These vibrating electrons act as a source of radiation and thereby emit radiation of the same frequency as the incident radiation. Hence, the incident radiation appears to be scattered by the atoms. The intensity of radiation scattered by an electron is given by classical Thomson equation and called scattering power of an electron. Higher the number of electrons (equal to atomic number  $Z$  of the atoms), higher is the scattering power. Atom consist of many electrons and thus the overall scattering factor of an atom is given by,

$$f = f_0 e^{\frac{-B \sin^2 \theta}{\lambda^2}} \quad \dots 2.2$$

where  $f_0$  is the scattering factor of an atom when it is rest and at  $0^\circ$ ,  $\lambda$  is the wavelength of x-ray,  $\theta$  is the angle of diffraction,  $B$  is a constant (called isotropic temperature factor, which is related to the amplitude of vibration of the atom and is given as  $B = 8\pi^2 u^2$ , where  $u^2$  = mean of square displacement of the atom from the mean position). The exponential term is called Debye-Waller factor. A crystal lattice consists of 3D atomic planes, which in turn are made of numerous electrons. The scattering power of a particular plane in the lattice is called structure factor of that plane. The structure factor of a plane  $hkl$  is given as:

$$F_{hkl} = \sum_{j=1}^{j \rightarrow N} f_j e^{2\pi i (hx_j + ky_j + lz_j)} \quad \dots 2.3$$

where  $F_{hkl}$  is the amplitude of scattered radiation from the  $hkl$  plane,  $f_j$  is the scattering factor of the atom  $j$  at a diffracting angle  $\theta$ ,  $(x,y,z)$  are the position coordinates

## Chapter 2

---

of the atom  $j$ ,  $N$  is the number of atoms in the unit cell. The exponential factor is called the phase of the wave. This structure factor is related to the electron density distribution in the unit cell of the crystal, which in turn represents the atomic distribution in the crystal.

### 2.3.1.1 Instrumentation

A typical classical powder X-ray diffractometer consists of a source of X-ray and the detector for the detection of diffracted X-rays. Fig. 2.3 shows the block diagram of typical powder diffractometer. X-ray source in these diffractometer is generally a sealed X-ray tube, where X-rays are produced by bombarding high-speed electrons on a metal target. A fraction of electron energy is used in the production of X-ray beam the rest is lost by heating of the target elements. Thus, a continuous cooling of the target element is essential. The X-ray beam hence generated consists of a combination of continuous radiation with wavelength ranging from a particular shortest value and several intense spikes. These intense peaks are characteristic of the target elements (called characteristic radiation). The X-rays are produced in all the direction and it is allowed to escape from a particular direction (usually through a Be window) in a diffractometer. The background and  $\beta$ -radiations are filtered using  $\beta$ -filters (if  $Z$  is the atomic no. of the target metal then generally  $(Z-1)$  is generally the filter used). The details of the X-ray production and the typical X-ray spectra are explained in several monographs [110,111]. The beam of X-rays is passed through the soller and divergence slits and then allowed to fall on the sample, as shown in Fig 2.3.

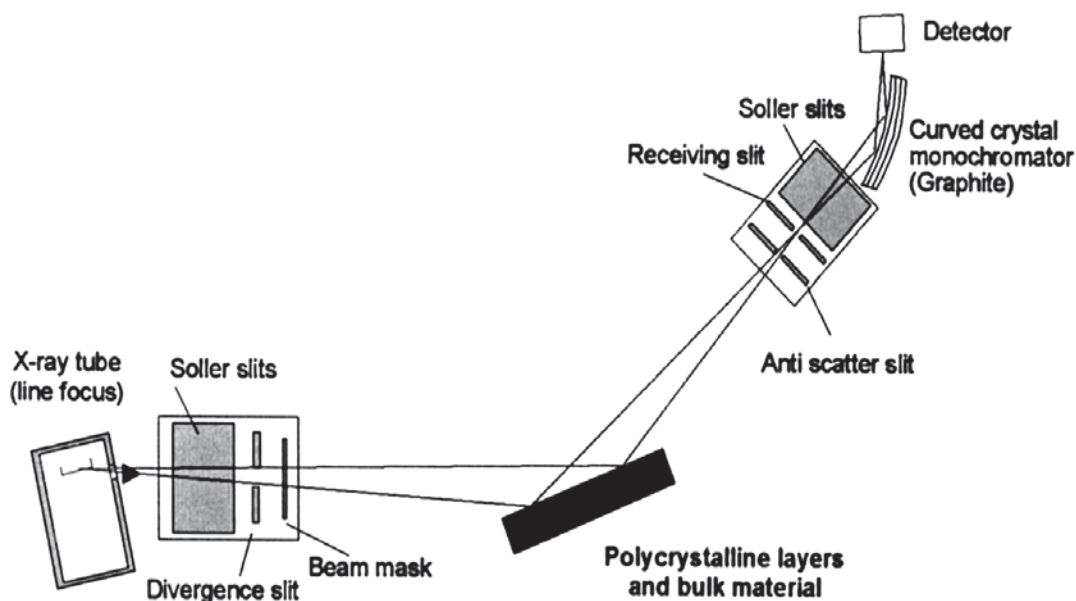


**Fig. 2.3:** Ray diagram of a typical reflection mode diffractometer

Sample in form of fine grains is uniformly spread over a glass slide. For adhesion of sample to the slide certain binders like collodion, grease or wax is used. The amounts of the sample exposed generally depend on the scattering power of the elements, absorption coefficient and of course on availability of the sample. The crystalline sample usually shows good scattering and sharp diffraction lines. The X-rays scattered (diffracted) from the sample are collected either by a film or counters. In the diffractometer, the diffracted beams are passed through the Soller slits and divergence and receiving slits. Then it is usually allowed to fall on a monochromator before detection.

For detection of the X-rays, scintillation counters or gas filled tube are commonly used. The gas filled tubes can either be a proportional counter or Geiger-Muller counter. The gas filled tube is usually filled with a gas, which gets ionized with the impact of the radiation. The ions are collected by applying a potential difference between the two electrodes. The typical current obtained is proportional to the number of photons reaching

## Chapter 2

---

the detector. Diffracted X-rays are detected by sweeping the detector from one angle to another. A sharp peak in the intensity is obtained when the detector angle is such that the Bragg's law is satisfied. Thus the output is obtained as plot of the intensity of diffracted X-rays versus angle ( $2\theta$ ). This plot is generally termed as XRD pattern of the sample.

The peaks (also called as reflections) in the XRD pattern correspond to a set of parallel planes with inter-planar spacing  $d_{hkl}$ . The position of the peaks is used to calculate  $d$  values. A particular sample gives a characteristic set of  $d$ -values. Thus, these values generally act as the fingerprint for the crystalline materials and they can be used for identification of the material. The intensity distribution of the reflections is governed by the nature and kind of distribution of atoms in the unit cell. The absolute intensities of the reflections depend on several factors like the intensity of the source, counting time and the nature and kind of distribution of atoms in the unit cell.

In the present work, X-ray diffraction experiments were carried out in the angle dispersive mode using Ni filtered Cu  $K_{\alpha}$  radiation (wavelength = 1.5418 Å) on a computer controlled Philips PW 1710 X-ray diffractometer, with X-ray generator operated at 30 kV and 20 mA and a proportional counter (Argon filled) as X-rays detector. The diffracted beam is monochromatized with a curved graphite single crystal. The sample was spread on a glass slide in form of fine powder and fixed with collodion binder. The samples were scanned in the  $2\theta$  range from 10 to 70° at a scanning speed of 1 °min<sup>-1</sup>. After data collection, the observed diffraction patterns were compared with JCPDS (Joint Committee on Powder Diffraction Standards) data available for reported crystalline samples.

## Chapter 2

---

### 2.3.1.2 Crystallite size estimation

The broadening of an X-ray peak can occur due to smaller crystallite size or strains in the lattice. The approximate size of a crystal can be estimated from broadening of the X-ray peak by the Scherrer formula, if the crystal thickness is less than  $\sim 2000 \text{ \AA}$ . Thus for all the compounds that were prepared, the approximate crystallite sizes were estimated using the Scherrer's formula given as follows:

$$\tau = \frac{0.9\lambda}{\beta \cos \theta} \quad \text{.....2.4}$$

where,

$\tau$  is the thickness of the crystal (in angstroms),

$\lambda$  is the X-ray wavelength measured in angstrom ( $\text{\AA}$ ) units

$\theta$  is the Bragg angle(in radians)

$\beta$  is the line broadening

The line broadening ( $\beta$ ) is measured from the full width at half maxima (FWHM) of the peak. Its square is obtained from the difference between the square of the measured peak width of the sample and the square of the measured peak width of a peak of a standard material as given in the Warren formula given below:

$$\beta^2 = \beta_M^2 - \beta_S^2$$

where,

$\beta_M$  is the measured peak width (in radians) at half peak height and

$\beta_S$  is the measured peak width (in radians) at half peak height (for a standard material.)

## Chapter 2

---

There may be some other factors like microstrain etc. also contributing to the peak broadening but these factors have not been considered here. Based on this concept of broadening of the XRD peak for the nanocrystalline sample, the approximate crystallite size of all the catalysts were estimated. The actual sizes in a number of nanocrystalline samples were also investigated by means of TEM, as explained in another section.

### 2.3.2 Surface area analysis

Surface area is one of the most important properties of a catalyst because it directly defines the adsorption process in the catalyst surface which in turn affects the catalytic activity. For measuring surface area and pore size distribution of solid materials gas adsorption-desorption techniques are generally used. BET method [112], which is the most commonly used procedure for determination of surface area, involves the following equation:

$$\frac{p}{v(p_o - p)} = \frac{1}{v_m C} + \frac{C-1}{v_m C} \left( \frac{p}{p_o} \right) \quad \dots\dots 2.5$$

Where,

$p$  = Adsorption equilibrium pressure

$p_o$  = Saturation vapour pressure of adsorbate at the adsorption temperature

$v_m$  = Volume of adsorbate required for mono layer coverage

$v$  = Volume of adsorbate adsorbed at equilibrium pressure  $p$

$C$  = Constant related exponentially to the heat of adsorption in the first layer ( $q_1$ ) and heat of liquefaction of adsorbate ( $q_L$ ) ;  $C = e^{(q_1 - q_L)/RT}$

The constant  $C$  determines the shape of the isotherm. The higher the value of  $C$ , the more the isotherm tends to type-II, which is desirable for accurate determination of

## Chapter 2

---

surface area. A plot of  $p/(p_0-p)v$  against relative pressure  $p/p_0$  yields a straight line and from the slope  $S = C-1/v_m C$  and intercept  $I = 1/v_m C$ ,  $v_m$  can be calculated as follows.

$$v_m = \frac{1}{S + I} \quad \text{.....2.6}$$

Thus the values of the specific surface area of sample can be derived by knowing the monolayer cross sectional area of adsorbate molecule and from slope and intercept, as described above. Thus,

$$\text{Specific Surface Area} = \frac{v_m N_A A_m}{W \times 22414} \times 10^{-20} \text{ m}^2/\text{g} \quad \text{.....2.7}$$

Where

$N_A$  = Avogadro's number

$v_m$  = Monolayer volume in ml at STP

$W$  = Weight of the catalyst sample (g).

$A_m$  = Mean crosssectional area occupied by adsorbate molecule which is  $16.2 \text{ \AA}^2$  for nitrogen at 77 K.

For many practical purposes the BET equation (2.4) is generally fitted to the data over a range  $p/p_0 = 0.05 - 0.35$  as at higher  $p/p_0$  values complexity associated with multilayer adsorption and/or pore condensation may arise. In our study, Quantachrome Autosorb - 1 surface area analyser was employed. Prior to surface area determination, samples were subjected to a pre-treatment at  $300^\circ\text{C}$  for  $\sim 5$  h under vacuum so as to remove impurities such as moisture.

## **Chapter 2**

---

### **2.3.2.1 Adsorption Desorption Isotherms and their types**

An understanding of the surface area and porosity of an adsorbent can be achieved by the construction of an adsorption desorption isotherms. When the quantity of adsorbate on a surface is measured over a wide range of relative pressures at constant temperature, the result is an adsorption isotherm. It is obtained point-by-point by admitting successive known volumes of adsorbate to the adsorbent and by measuring the equilibrium pressure. Similarly, desorption isotherms can be obtained by measuring the quantities of gas removed from the sample as the relative pressure is lowered.

All adsorption isotherms can be grouped into six types; Type I to type VI. Type I or Langmuir isotherms are concave to the  $P/P_0$  axis. The amount of adsorbate approaches a limiting value (plateau) rapidly as  $P/P_0$  increases, which is indication of filling of all pores with adsorbate. These types of isotherms are generally obtained in case of microporous solids having relatively small external surfaces like activated carbons and molecular sieve zeolites.

Type II and Type III isotherms are obtained in case of a nonporous or macroporous adsorbent. Monolayer multilayer adsorption occurs in both the cases. The beginning of the isotherms in case of these types of solids may be concave (Type II) or convex (Type III) depending upon the surface properties of a given adsorbent. Type II has a distinct point B (as shown in fig. 2.4) as the start of the linear central section of the isotherm and it is usually taken to indicate the relative pressure at which monolayer coverage is complete. This point is not present in case of Type III due to stronger



## Chapter 2

adsorbate-adsorbate interactions than adsorbate-adsorbent interactions. Type II is the most commonly obtained while type III is rarely obtained.

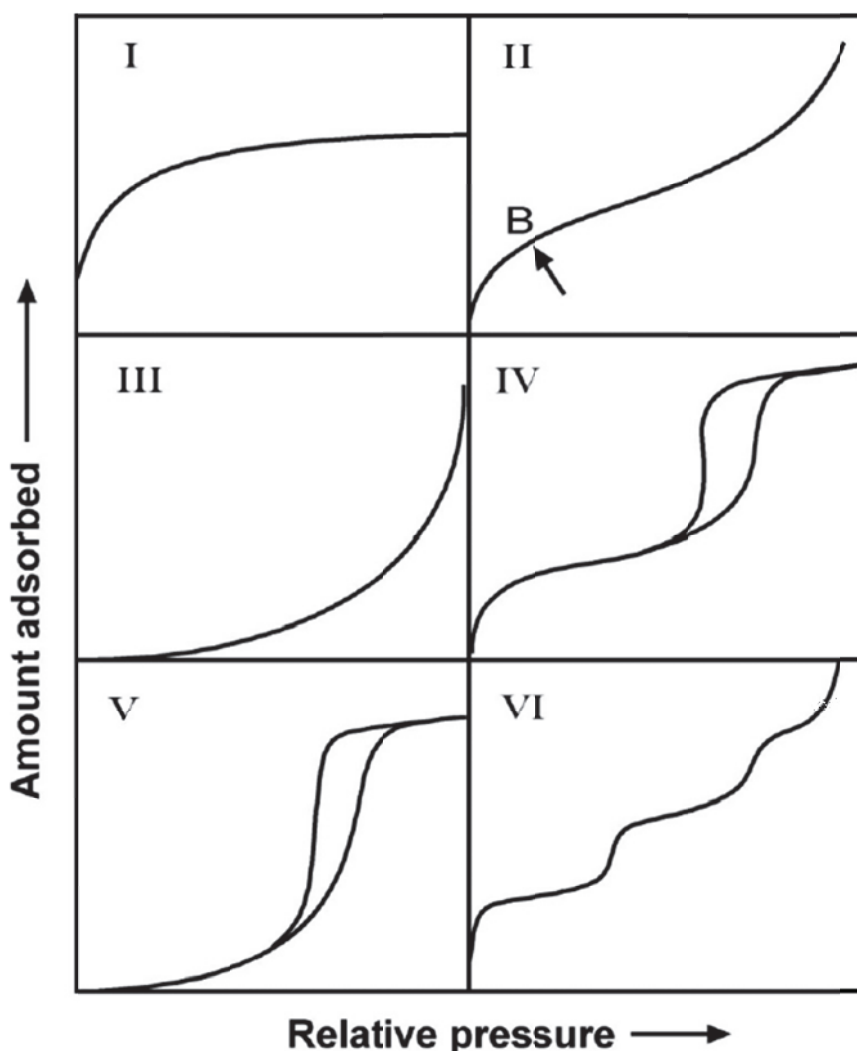


**Fig. 2.4:** *Different adsorption Isotherms (TYPE I to VI)*

Types IV and V of adsorption isotherms are obtained for mesoporous materials. They contain a hysteresis loop which is due to capillary condensation in mesopores. The initial part of the type IV isotherm follows the same path as the type II and corresponds to the formation of a mono- and multilayer of adsorbate on a surface, followed by capillary condensation in the mesopores. Type V isotherms corresponds to type III and like type III

## Chapter 2

---

these isotherms are also uncommon. The only difference between type III and V is the presence of mesopores in case of type V. Type VI isotherms corresponds to layer by layer adsorption or energetically highly homogeneous surfaces, either nonporous or macroporous.

The adsorption branch of isotherm is used to determine all adsorption properties of the porous materials while desorption branch is used to get information about the pore geometry. N<sub>2</sub> is extensively used adsorbate for gas adsorption studies; it has been well-characterized and serves as the most common adsorbate for pore size distribution measurements.

### 2.3.2.2 Total Pore Volume and Average Pore Radius

The total pore volume for a porous solid is calculated from the amount of vapour adsorbed at a relative pressure close to unity. It is based on the assumption that at this point the pores are completely filled with the liquid adsorbate. In absence of macropores, the isotherm is nearly horizontal (Type I) over a wide range of  $P/P_0$  approaching unity and in this case the pore volume is well defined. While in presence of macropores the isotherms rises rapidly near  $P/P_0 = 1$ . It may exhibit a vertical rise in case of large macropores. Generally nitrogen is used as an adsorbate for these measurements. The adsorbed volume ( $V_{ads}$ ) can be converted to the volume of liquid nitrogen ( $V_{liq}$ ) contained in the pores using equation

$$V_{liq} = \frac{P_a V_{ads} V_m}{RT} \quad \dots\dots 2.8$$

Where  $P_a$  and  $T$  are ambient pressure and temperature respectively, and  $V_m$  is the molar volume of the liquid adsorbate ( $34.7 \text{ cm}^3/\text{mol}$  for nitrogen).

## Chapter 2

---

The pores that would not be filled below a relative pressure of 1 have negligible contribution to the total pore volume and surface area. The average pore size can be calculated from the pore volume. Assuming cylindrical pore geometry, the average pore radius  $r_p$  can be calculated from pore volume ( $V_{liq}$ ) and surface area (S) by using the following equation,

$$r_p = \frac{2 V_{liq}}{S} \quad \text{.....2.9}$$

### 2.3.2.3 Pore Size Distribution

The distribution of pore volume with respect to pore size is termed as pore size distribution. The pore size distribution of an adsorbent can be calculated from either adsorption or desorption isotherm. But in general, desorption branch of the isotherms is considered to be more appropriate than the adsorption isotherm for calculating the pore size distribution. For the same volume of gas, the desorption isotherm corresponds to a lower relative pressure resulting in a lower free energy state. Therefore the desorption isotherm is closer to true thermodynamic stability as compared to adsorption isotherm. Size of mesopores can be calculated by using Kelvin equation, assuming cylindrical pore geometry.

$$r_K = \frac{-2\gamma V_m}{RT \ln(P/P_0)} \quad \text{.....2.10}$$

Where

$r_K$  = the Kelvin radius of the pore (in meters)

$\gamma$  = the surface tension of nitrogen at its boiling point ( $8.85 \times 10^{-3} \text{ Jm}^{-2}$  at 77 K).

## Chapter 2

---

$V_m$  = the molar volume of liquid nitrogen ( $3.47 \times 10^{-5} \text{ m}^3 \text{ mol}^{-1}$ ).

$R$  = gas constant ( $8.314 \text{ JK}^{-1} \text{ mol}^{-1}$ ).

$T$  = boiling point of nitrogen (77 K).

$P/P_0$  = relative pressure of nitrogen.

Using the appropriate constants for nitrogen, equation (16) reduces to

$$r_K (\text{\AA}) = \frac{4.15}{\log (P_0/P)} \quad \text{.....2.11}$$

The Kelvin radius ( $r_k$ ) is the radius of the pore in which condensation occurs at a relative pressure of  $P/P_0$ . Since some adsorption has already taken place on the walls of the pore prior to condensation,  $r_k$  does not represent the actual pore radius. Also during desorption an adsorbed layer remains on the walls of pores when evaporation occurs. Therefore the actual pore radius  $r_p$  is given by the following equation

$$r_p = r_k + t \quad \text{.....2.12}$$

Where  $t$  is the thickness of the adsorbed layer, whose value is given by

$$t = 3.54 (V_{\text{ads}}/V_m) \quad \text{.....2.13}$$

Where  $3.54 \text{ \AA}$  is the thickness of one nitrogen molecular layer,

$V_{\text{ads}}$  is the volume of nitrogen adsorbed at a given relative pressure,

$V_m$  is the volume adsorbed at the completion of a monolayer for a nonporous solid of the same composition as the porous sample.

Another way of finding  $t$  was given by de Boer [113] in form of the following equation

$$t(\text{\AA}) = \left[ \frac{13.99}{\log (P_0/P)} \right]^{1/2} \quad \text{.....2.14}$$

## Chapter 2

---

The pore size distribution can be calculated by many methods like BJH method [114], DH method [115] etc. Among then BJH method is the most commonly used one.

### 2.3.3 Electron Microscopy

Electron microscopy techniques of material characterization are based on the interaction of a focused electron beam with matter. This interaction may result into several phenomena like (i) emission of secondary electrons (SE) (ii) back-scattering electrons (BSE) and (iii) transmission of electrons etc. Emissions of characteristic X-rays, Cathode luminescence and absorption of electrons also occur during the interaction of primary electrons with the matter. All these are shown below in Fig 2.5.

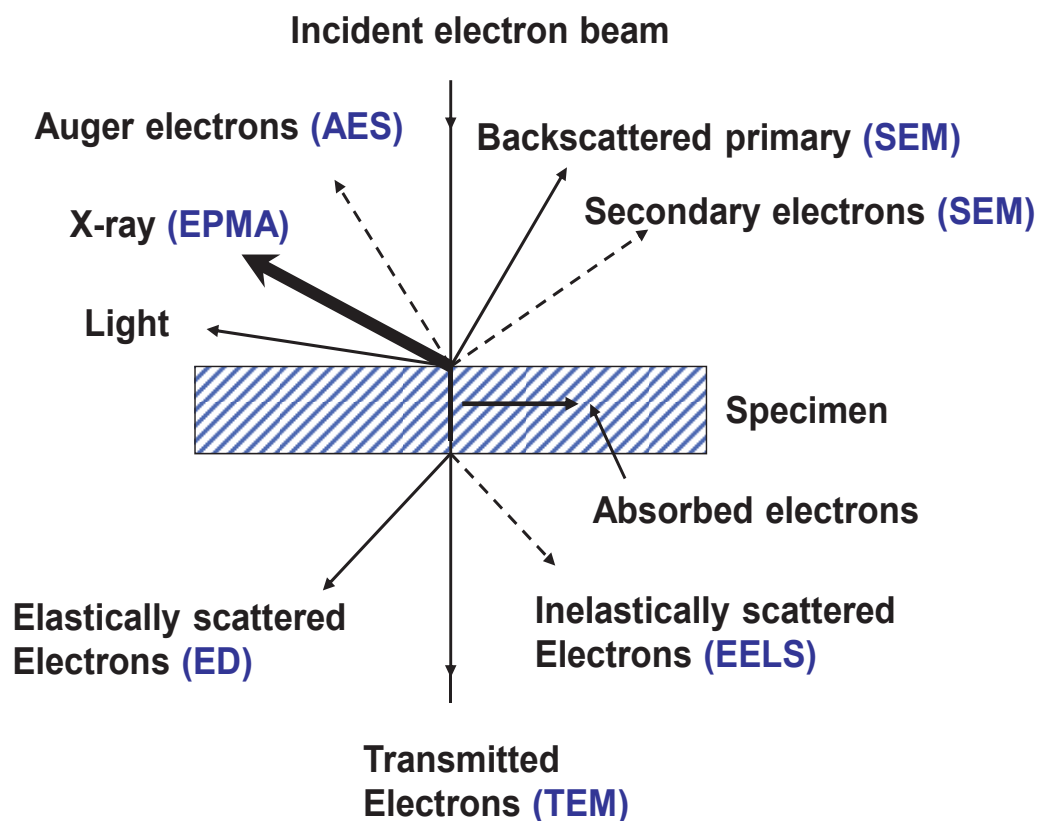


**Fig. 2.5:** Depiction of different phenomenon occurring on interaction of electron beam

## ***Chapter 2***

---

### **2.3.3.1 Scanning Electron Microscopy**

Scanning electron microscopy is a technique based on the detection of the secondary electrons and back-scattered electrons. The signals corresponding to these two are detected and fed to a synchronously scanned CRT as an intensity-modulating signal and thus display a specimen image on the CRT screen [116]. In general an SEM system comprises of the following four parts (i) electron optical system, (ii) specimen stage, (iii) display and recording system and (iv) vacuum system.

In scanning electron microscope technique, a finely focused electron beam is rastered across the surface of the sample by two pairs of electro-magnetic deflection coils [116]. The signals generated from the surface by secondary and back-scattered electrons are detected and fed to a synchronously scanned cathode ray tube (CRT) as intensity modulating signals. Thus, the specimen image is displayed on the CRT screen, which gives a map of the surface topography of the sample. Changes in the brightness represent changes of a particular property within the scanned area of the specimen. This technique can be used for finding out particle size, crystal morphology, surface defects etc. It can be used in wide range of magnifications. The best reported resolution is around 2 nm.

For carrying out SEM analysis the sample should be (i) vacuum compatible, since electrons, being charged particles, require vacuum environment for traversing without change in their number and density. (ii) Electrically conducting, to avoid the charge build up due to coming electrons. The non-conducting samples are coated with gold, platinum or graphite to stop charge build up on their surface.

## ***Chapter 2***

---

### **2.3.3.2 Energy Dispersive Analysis of X-rays (EDAX)**

During SEM measurements, the elements present in the sample also emit characteristic X-rays. These X-rays can be separately detected using a silicon-lithium detector. These X-rays give qualitative and quantitative analysis of the elements present in the sample. This technique is known as energy dispersive analysis of X-rays (EDAX or EDX).

This technique of Scanning Electron Microscopy (along with EDX) was used to study the microstructure evolution (grain size, porosity, etc.) The instrument used was a Scanning Electron Microscope, Mirero, Korea, model- AIS2100.

### **2.3.3.3 Field Emission - Scanning Electron Microscopy (FE-SEM)**

Field emission scanning electron microscopy (FE-SEM) is a variation of SEM, where field emitter source is used as electron source while conventional SEM have thermo ionic source. FE-SEM is also used to obtain topographical and elemental information but at higher magnifications (upto 300Kx) as compared to conventional SEM. As compared to conventional SEM, Field emission SEM (FESEM) produces clearer, less electrostatically distorted images with spatial resolution down to 2 nanometers.

Working of FESEM is similar to that of conventional SEM, only difference being source of electron. In an FESEM is electrons are produced by a field emission source, where an extremely thin and sharp tungsten needle (tip diameter  $10^{-7}$  –  $10^{-8}$  m) functions as a cathode in front of a primary and secondary anode. In this case, the field-emission cathode is able to produce narrower probing beams at low as well as high electron energy,

## ***Chapter 2***

---

which results in improved spatial resolution as well as minimized sample charging and damage. As field emission necessitates an extreme vacuum ( $10^{-8}$  Torr) in the column of the microscope, a device is present that regularly decontaminates the electron source by a current flash. In contrast to a conventional tungsten filament, a FE tip last theoretically for a lifetime, provided the vacuum is maintained stable. Also need for placing conducting coatings on insulating materials is virtually eliminated.

### **2.3.3.4 Transmission Electron Microscopy (TEM)**

Transmission Electron Microscopy (TEM) is another technique based on interaction of electrons with matter, which gives information about microstructural as well as crystallographic features of the sample. In TEM, a highly focused beam of electrons is directed towards a thin sample. These highly energetic electrons interact with the atoms in the sample, producing characteristic radiation and particles which provide the necessary information for characterization of various materials. Information is obtained from both transmitted electrons (i.e. image mode) and diffracted electrons (i.e. diffraction mode). The image mode provides the information regarding micro-structural features whereas the diffraction mode is used for crystallographic information. The transmission electron microscopes operated at the voltage as high as 200 kV with a magnification of 3,00Kx is routinely used at present.

Another variation of this technique is High resolution TEM (HR-TEM), which is used to investigate the finest possible details in specially prepared specimens. For such requirements, it is advantageous to use the shortest possible wavelength illumination (i.e., high voltage), an objective lens with very low aberrations and a microscope with



## Chapter 2

---

extremely high mechanical and electrical stabilities. High resolution requires both high instrumental resolving power and high image contrast [117].

JEOL-2000FX transmission electron microscope operating at accelerating voltages up to 200 kV was used for TEM studies. The samples for TEM were prepared by dispersing the sample in acetone by sonication and placing a drop of the dispersed sample on to a carbon coated copper grid.

### 2.3.4 X-Ray Photoelectron Spectroscopy (XPS)

X-ray photoelectron spectroscopy (XPS) is a spectroscopic technique that gives information about the elemental composition, empirical formula, chemical state and electronic state (oxidation state) of the elements present in the sample. This technique is also known as Electron Spectroscopy for Chemical Analysis (ESCA). In XPS, sample is irradiated with X-rays (generally Al or Mg X-rays) and the number and kinetic energy of electrons emitted from the sample is detected. Since XPS involves detection of electrons emitted from the sample, it requires ultra-high vacuum (UHV) conditions. XPS can detect all elements with an atomic number ( $Z$ ) of 3 (lithium) and above. This limitation means that it cannot detect hydrogen ( $Z=1$ ) or helium ( $Z=2$ ).

Since the energy of a particular X-ray wavelength is fixed, therefore by measuring the kinetic energy of emitted electron one can calculate the binding energy of the electron (BE) using the following equation

$$E_{\text{binding}} = E_{\text{photon}} - E_{\text{kinetic}} - \Phi \quad \dots\dots 2.15$$

Where  $E_{\text{binding}}$  is the binding energy of the electron

$E_{\text{photon}}$  is the energy of the X-ray photons being used

## Chapter 2

$E_{\text{kinetic}}$  is the kinetic energy of the emitted electron as measured by the instrument

$\Phi$  is the work function of the spectrometer (not the material).

A simple schematic of an XPS instrument is given in fig 2.6. It has an X-ray source for production of X-rays, a hemispherical analyser for analysing the emitted electrons and data recording system.

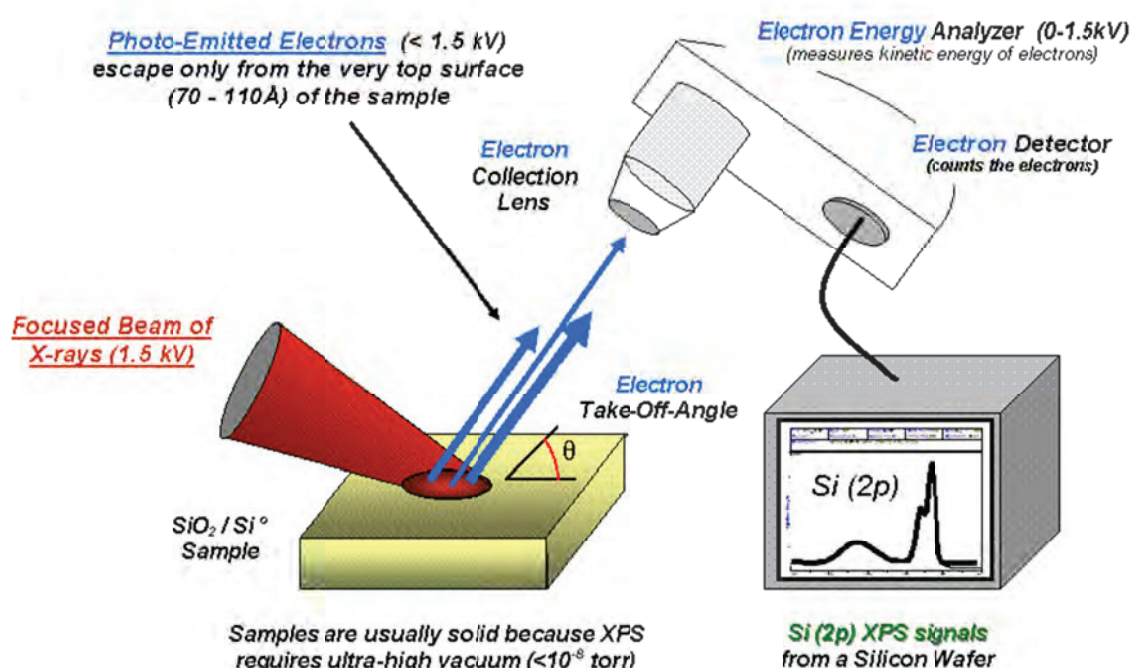


Fig. 2.6: Schematic representation of a XPS instrument

In general, Al or Mg anodes are used for producing X-rays. Al  $K\alpha$  has energy of 1486.7 eV, while Mg  $K\alpha$  has energy of 1253 eV. The energy width of the non-monochromatic X-ray is roughly around 0.9 eV and 0.8 eV for Al and Mg respectively. The ultimate energy resolution of the common electron energy analyser (spectrometer) is in the order of 0.25 eV. Thus the ultimate energy resolution of a system using non-

## *Chapter 2*

---

monochromatic X-rays is governed by the energy width of the source. To improve the energy resolution of the XPS system monochromatic Al  $K\alpha$  X-rays are used. These monochromatic Al  $K\alpha$  X-rays are produced by diffracting and focusing a beam of non-monochromatic X-rays off of a thin disc of natural, crystalline quartz. The energy width of the monochromatic X-rays is 0.16 eV. Thus the ultimate energy resolution should be 0.25 eV, which is the resolution of detector. Under practical conditions, high energy resolution settings will produce peak widths (FWHM) between 0.4-0.6 eV for various pure elements and some compounds.

A typical XPS spectrum is a plot of the number of electrons detected (Y-axis) versus the binding energy of the electrons detected (X-axis). Each element has a characteristic set of XPS peaks at characteristic binding energy values, these peaks are directly used to identify each element that exist on the surface of the sample being analysed. These characteristic peaks correspond to the electron configuration of the electrons within the atoms, e.g., 1s, 2s, 2p, 3s, etc. The area of the characteristic peak can be correlated to the amount of element present in the surface of area irradiated. XPS detects only those electrons that escape from the sample into the vacuum and reach the detector. During this escape the photoelectron travel through the sample also and hence it can undergo inelastic collisions, recombination, excitation of the sample, recapture or trapping in various excited states within the material. All these phenomena reduce the number of escaping photoelectrons. These effects increase as the depth increases. Therefore the signals detected from the surface are much stronger than the signals

## ***Chapter 2***

---

detected from deeper below the sample surface. Thus XPS is mostly used as a surface characterization technique.

The XPS studies of the samples were carried out on SPECS surface analysis system which is equipped with Al-Mg dual anode source as well as Ag-Al monochromatic source. Non monochromatic Al K-Alpha radiation (1486.6 eV) with operating power of 280 W employed as source for most of the studies. The spectra were calibrated with Au 4f<sup>7/2</sup> line at 84.0 eV from a specimen of Au film. For sample preparation a few milligram of well-ground sample powder was pressed to make a pellet. The pellet was attached to a stainless steel stub using a carbon tape.

XPS spectra were obtained with pass energy 50 eV for survey scan and 20 eV for individual scan. The XPS positions were referenced using Carbon (1S) peak at 284.6 eV.

### **2.3.5 Raman Spectroscopy**

Raman Spectroscopy is a vibrational spectroscopic technique used for characterization of materials. It is widely used to study vibrational, rotational, and other low-frequency modes in a system. It is based on inelastic scattering or Raman scattering (Fig. 2.7) of monochromatic light and it is named after Sir C. V. Raman, who discovered the Raman scattering. The source of light is usually a laser in the visible, near infrared, or near ultraviolet range. The laser light interacts with phonons or other excitations in the system, resulting in the energy of the laser photons being shifted up or down. The shift in energy gives information about the phonon modes in the system. Therefore in Raman spectroscopy, a monochromatic incident radiation is scattered inelastically from different vibrational states of the sample and the spectrum of the scattered radiation contains

## Chapter 2

information about the vibrational energy levels in terms of energy differences between the incident and the scattered radiation [118-121]. Infrared spectroscopy yields similar, but complementary, information.

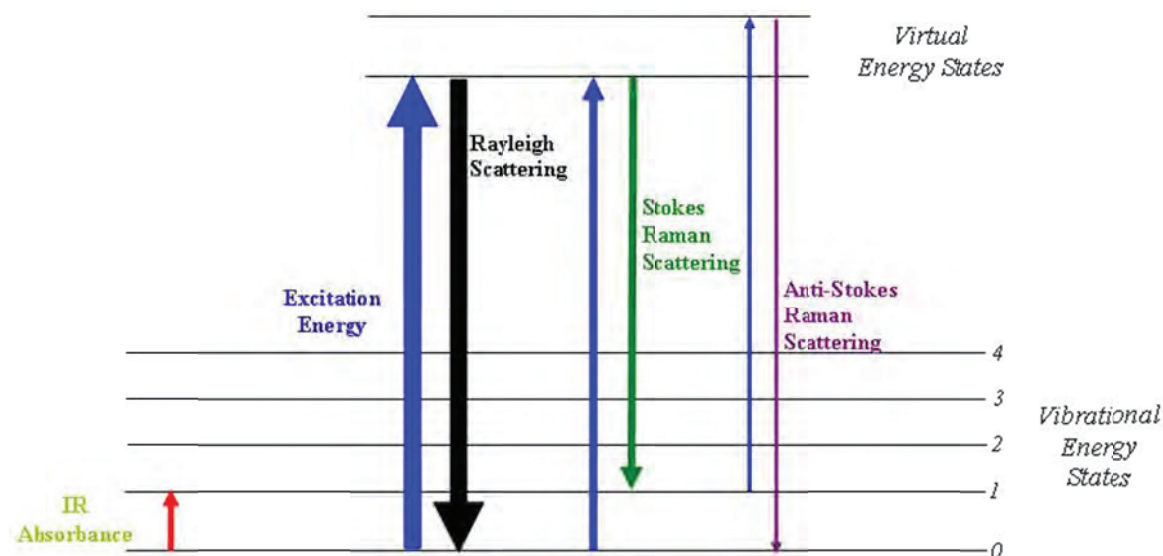


**Figure 2.7:** *Schematic Presentation of the Raman Scattering*

The Raman spectrometer necessarily consists of the following components:

- 1) An excitation source: He-Ne or Ar-ion laser.
- 2) A lens system to illuminate, collect and direct the incident and scattered light.
- 3) A dispersive element (single, double or a triple monochromator).
- 4) A detector: photomultiplier tube or a cooled CCD.

Typically, a sample is illuminated with a laser beam. Light from the illuminated spot is collected with a lens and sent through a monochromator. Wavelengths close to the laser line, due to elastic Rayleigh scattering, are filtered out while the rest of the collected light is dispersed onto a detector.

## Chapter 2

---

Raman spectroscopy is one of the most used techniques for characterization of carbon based materials. In present study Raman was used to study the structure of carbon support also it was used for studying the speciation of iodine. In house developed micro-Raman set up was used for these studies. 532 nm line of a diode laser was used for excitation and the scattered light was analyzed using a 0.9 nm single stage monochromator coupled with CCD detector. Laser Raman spectra were taken on LABRAM - 1 spectrometer (back-scattering geometry, excitation source Ar<sup>+</sup> ion laser, spectral resolution of 2 cm<sup>-1</sup>).

### 2.3.5 UV-Visible absorption Spectroscopy

Optical absorption spectroscopy is one of the simplest and most widely used techniques for studying the absorption properties of material. These techniques are generally categorized into two groups. First is the absorption and emission spectroscopy and the other is the vibrational spectroscopy. The former determines the electronic structures of atoms, ions, molecules or crystals through exciting electrons of atoms, ions, molecules (absorption) and relaxing from the excited to ground states (emission). The vibrational spectroscopy involves the interactions of photons with species in a sample that results in energy transfer to or from the sample via vibrational excitation or de-excitation. The vibrational frequencies provide the information of chemical bonds in the compound.

According to Lambert-Beer law attenuation in the intensity of photons  $I_0$  upon passing through a material is given by

$$I = I_0 e^{-\alpha c l} \quad \dots 2.16$$

## Chapter 2

Where,  $\alpha$  is the absorption coefficient,  $c$  is the concentration of material in mole/liter and  $l$  is the path length in centimeters.

Thus absorption of photons after passing through a material can be expressed as

$$A = \log\left(\frac{I_0}{I}\right) = \alpha c l \quad \dots 2.17$$

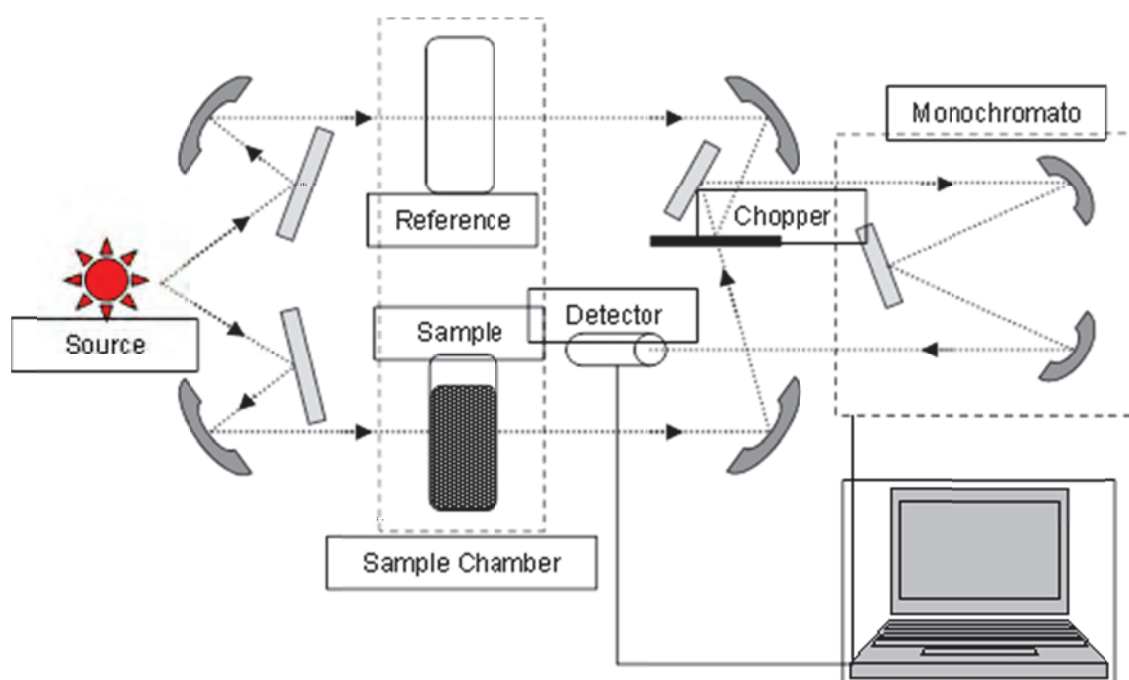


**Fig. 2.8:** Schematic representation of UV-Visible spectrophotometer

In the present work, UV visible absorption spectroscopy was used for studying the polyiodide species present in the solution (Chapter 6). The absorption spectra were recorded using a double beam UV-Visible spectrophotometer (Make-Jasco, V670). Schematic diagram for a typical absorption set-up is shown in Fig. 2.8.

## ***Chapter 2***

---

It consists of a source of electromagnetic radiation from 185 to 900 nm [Deuterium lamp (UV light Source) and a tungsten halide lamp (visible light source)]. Deuterium lamp is operated under low pressure (~ 0.2 to 0.5 torr) and low voltage (~ 40 VDC). Tungsten iodide lamp consists of a tungsten filament, which is heated to incandescence by passing electric current. The filament is enclosed in a sealed bulb filled with a small amount of iodine. This iodine helps in redepositing of tungsten back on the filament by halogen cycle thus increase life of the lamp. Filters and monochromators are used to isolate narrow band of wavelengths.

The advantage of using a double beam spectrometer is minimization of the error in the measurement. Here a single beam from the source is divided into two beams of equal intensities which fall on sample as well as reference. This nullifies the signal from the solvent and signal from the sample only is recorded. A photomultiplier tube is used for recording the output signal, this signal is passed to computer which records the spectrum.

### **2.3.6 Potentiometric Titration:**

Potentiometric titration is generally used for characterizing an acid. It is similar to direct titration of a redox reaction, but an indicator is not required. In this case potential is measured across the analyte. For measuring the potential two electrodes are used an indicator electrode (the glass electrode and metal ion indicator electrode) and a reference electrode. Reference electrodes generally used are hydrogen electrodes, calomel electrodes, and silver chloride electrodes. The indicator electrode forms an



## Chapter 2

---

electrochemical half-cell with the interested ions in the test solution. The reference electrode forms the other half cell.

The overall electric potential is calculated as  $E_{\text{cell}} = E_{\text{ind}} - E_{\text{ref}} + E_{\text{sol}}$ .  $E_{\text{sol}}$  is the potential drop over the test solution between the two electrodes. A fixed amount of titrant is added at regular intervals and  $E_{\text{cell}}$  is measured.  $E_{\text{cell}}$  is plotted against the volume added and end point is calculated by half way between the jump in voltage. Thus the potentiometric titration involves measurement of  $E_{\text{cell}}$  with the addition of titrant. Different type of potentiometric titrations are used for various analysis, like acid-base titration (For determination of acidity and alkalinity), redox titration, precipitation titration (For determination of halides) and complexometric titrations (for determination of EDTA).

In present study LABINDIA autotitrator was used for determination of concentrations of  $\text{H}^+$  and  $\text{I}^-$  ions by titrating them against NaOH and  $\text{AgNO}_3$  solutions. Glass electrode and silver-silver chloride potentiometric electrodes were used for these titrations.

### 2.3.6 ICP-Atomic Emission Spectroscopy

Atomic emission spectroscopy (AES) is an analytical method used for the determination of elemental composition of the sample. It involves detection of visible or ultraviolet emission following the thermal excitation. Each element emits at a particular wavelength, therefore wavelength of the atomic spectral line gives the identity of the element while the intensity of the emitted light gives the concentration of the element. Atoms present in the sample can be excited by a flame, arc, spark or plasma.

## Chapter 2

---

If inductively coupled plasma is used for production of excited atoms, the technique is known as inductively coupled plasma atomic emission spectroscopy (ICP-AES). It is also known as inductively coupled plasma optical emission spectrometry (ICP-OES). ICP-AES have certain advantages over flame AES like excellent limit of detection, multi-element capability, low chemical interference and a stable and reproducible signal. The disadvantages are spectral interferences (many emission lines), cost and requirement of samples in solution form only. A block diagram of ICP-AES can be represented as shown in Fig 2.9,

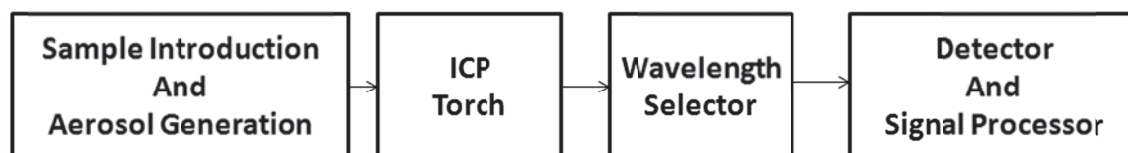


**Fig.2.9:** *Block diagram of ICP-AES instrument*

In present study ICP-AES instrument Model Activa, Horiba Jobin Vyon was used for the determination of the amount of platinum present in the HI solution after carrying out the HI decomposition reaction.

### 2.4 Catalytic activity evaluation for Hydriodic acid decomposition

The process for evaluation of catalytic activity and stability of various catalysts for hydriodic acid decomposition are discussed here in details. A block diagram of the setup used for the decomposition of HI is shown in Fig. 2.10. Hydriodic acid along with the catalyst was kept in a two neck round bottom flask. The mixture is heated under reflux conditions using a heater. A thermometer is kept in the solution for monitoring the temperature of the study. The top of the flask has a water condenser along with an air

## **Chapter 2**

---

condenser. The objective to choosing this type of reaction setup is that the unreacted HI as well as iodine is condensed back into the flask and only hydrogen can escape. The outlet of the upper condenser is passed through two traps containing starch solution and silver nitrate solution. These two traps were to ensure that HI and iodine are not coming out. If there is no colour change in the traps, it confirms that the gas coming out is neither iodine nor HI vapours. This gas was collected in an inverted column and taken out by a syringe through a septum at the top of the column. It was analysed using a gas chromatograph (Chromatography and Instruments company, GC 2011) equipped with molecular sieve 5A column and thermal conductivity detector and found to be hydrogen.

In addition to the time dependent and temperature dependent catalytic activity, effect of presence of iodine on the catalytic activity was also investigated.

### **2.4.1 Evaluation of Catalytic Activity of the catalysts:**

After carrying out the reaction for desired interval, the resulting solution was filtered and the filtrate was analysed for concentrations of  $\text{H}^+$  and  $\text{I}^-$  ions. The decrease in concentrations of  $\text{H}^+$  and  $\text{I}^-$  ions was used to calculate the percentage conversion. The conversion was also calculated by increase in iodine concentration. In general, these values were found to be in good agreement.

The concentrations of  $\text{H}^+$  and  $\text{I}^-$  ions were determined by titrating them against 0.1N NaOH and 0.1N  $\text{AgNO}_3$  solutions. The  $\text{H}^+$  and  $\text{I}^-$  titrations were carried out using an auto titrator, Model Titra from Lab India with glass electrode and silver-silver chloride potentiometric electrodes respectively. Iodine concentration was determined by titrating the solution against thiosulphate using starch as an indicator.

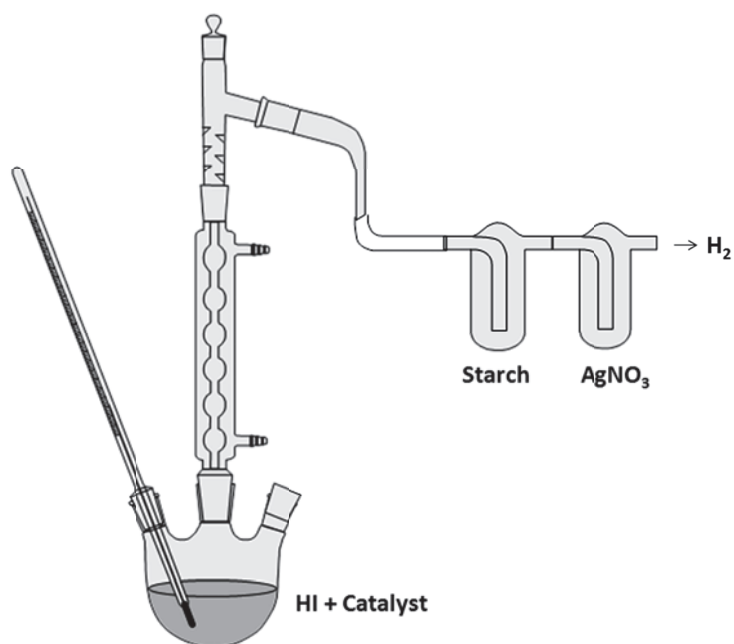


**Fig.2.10:** Block diagram of the experimental set up used for Hydriodic acid decomposition studies

### 2.4.1 Evaluation of Stability of the catalysts:

After carrying out the reaction, the used catalyst was washed thoroughly and dried. Then a thorough ex-situ characterization of the spent catalyst was carried out using various techniques like XRD, SEM and Raman spectroscopy to see if any structural and morphological changes have taken place after HI decomposition reaction. Leaching of noble metal from the supported noble metal catalyst is a problem in case of harsh reaction conditions. The stability of these catalysts against noble metal leaching was determined by analysing platinum content in the HI phase using ICP-AES.

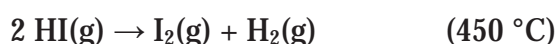
# Chapter 3

## HI Decomposition over Carbon Supported Platinum Catalysts

---

### 3.1 Introduction

Catalytic decomposition of Hydriodic Acid to produce hydrogen and iodine is a reaction of great importance with respect to thermochemical cycles, since it is the hydrogen producing step of sulfur iodine (S-I) cycle as well as some other iodine based cycles. This aspect has been discussed in detail in Chapter 1. Therefore, in Chapter 1 we have given a brief overview of the activities related to development of the catalysts for this reaction. Hydriodic acid decomposition can be written as follows:



This reaction is thermodynamically limited with low thermodynamic yields and requires a catalyst for achieving workable reaction rates. A large number of catalysts are reported for this reaction. Most of these catalysts are noble metal based (predominately platinum). Dissociative adsorption of the reactant on the platinum surface is the reason behind its activity as a catalyst for the reaction. As discussed in Chapter 1, platinum being a costly metal needs to be dispersed over a support. Use of the support reduces the

## ***Chapter 3***

---

cost of the catalyst as well as increase the number of active sites of platinum in form of fine particles. Various supports like alumina, silica, zeolite and carbon can be used for preparation of supported platinum catalyst.

Carbon is widely used as a support for noble metal based catalysts because it can have very high surface area, varying porosity according to the requirement of the reaction and it is inert in most of the reaction environments [122-123]. Platinum catalysts supported on carbons can have wide range of applications like low temperature fuel cells [124], energy conversion [125], hydrogenation reactions [126] and biomass conversion [127] to name a few. Carbon can be used in various forms as a catalyst support like activated carbon [128], carbon black [129], carbon nanotubes [130], graphite [131] and various types of porous carbons [132].

In addition to the above mentioned applications, Pt supported on carbon catalyst is widely used for HI decomposition reaction also. There are various reports on use of platinum-carbon catalyst for HI decomposition reaction [86, 91]. All these reports for HI decomposition are for vapor phase at temperatures in excess to 450°C. As discussed in Chapter 1, we have chosen liquid phase HI decomposition reaction due to various reasons. In this chapter, synthesis and characterization of different carbon supported platinum catalysts and their application for HI decomposition reaction, are reported.

### **3.2 Platinum Graphite Catalyst**

This section contains details of Pt catalysts supported on graphitic carbon with different platinum loading. It includes synthesis and characterization of these catalysts and evaluation of their catalytic activity and stability for liquid phase HI decomposition

## ***Chapter 3***

---

reaction. The effect of noble metal loading has also been studied. We have carried out kinetic studies using one of these catalysts as well as poisoning effects of iodine on the activity of these catalysts.

### **3.2.1 Experimental**

#### **3.2.1.1 Preparation of Catalyst**

The catalysts were prepared by wet impregnation method which includes impregnation of the support with a noble metal precursor followed by its reduction. For getting different loading of platinum (0.5 , 1 and 2 ) different amount of hexachloroplatinic acid (Hindustan Platinum) solution was added drop wise into colloidal graphite (Aquadag Acheson Colloids Company) with continuous stirring. The resulting mixtures were dried at 100 °C for 6 h followed by drying at 160 °C for another 6 h. Then these mixtures were reduced by heating at 300 °C for 3 h under flowing H<sub>2</sub>-N<sub>2</sub> mixture (8 hydrogen in nitrogen). Then the resulting samples were thoroughly washed with distilled water and dried.

#### **3.2.1.2 Characterization of Catalyst**

The powder X-ray diffraction patterns of all the catalysts were recorded on Philips analytical diffractometer using Ni-filtered Cu K $\alpha$  radiation. The surface morphology was studied using JEOL JSM-6360 and Zeiss scanning electron microscope. The BET surface area of the catalyst was obtained from physical adsorption of N<sub>2</sub> at -196°C, on a Quantachrome Autosorb - 1 instrument. The prepared sample was characterized for carbon structure and hybridization, by spatially resolved Raman scattering (Bruker Model

## Chapter 3

---

MultiRAM) using 150 mW at laser head and 4 mW on the sample of 1064 nm line of Nd:YAG laser, detected with a liquid-nitrogen cooled high resolution charge coupled device (CCD) detector at  $4\text{ cm}^{-1}$  resolution. Oxidation state of platinum along with the nature of carbon supports was studied by X-ray photoelectron spectroscopy using SPECS instrument.

### 3.2.1.3 Activity and Stability

Pt/Graphite catalysts were evaluated for their catalytic activity for liquid phase HI decomposition and noble metal leaching employing a reflux type batch reactor. The details of this reactor are as given in Chapter 1. For this 250 mg of catalyst was added to 50 ml of 27% hydriodic acid solution in 250 ml round bottom flask. This flask was heated and the gas bubbling out through the two traps was collected in an inverted column and was analyzed using a gas chromatograph. After reaction, the HI decomposition was measured by means of titrating  $\text{H}^+$  and  $\text{I}^-$  ions using acid-base and iodometric titrations, respectively. The solution was filtered to separate the used catalyst and the eluent. The spent catalyst was characterized by XRD, Raman and SEM for their physical integrity and the eluent was analyzed using ICP-OES for the leached out platinum.

As mentioned earlier, the hydriodic acid coming from Bunsen reaction may have excess iodine even after separation, which can affect the activity of the catalyst since iodine can act as poison. Therefore, we have tested the catalyst for its activity in presence of iodine. For this extra iodine was added in the HI solution ( $\text{I}_2$ :HI ratio 1:1 and 1:2) and conversion was measured after two hours of reaction.



## Chapter 3

### 3.2.2 Results and Discussion

#### 3.2.2.1 XRD

The X-ray diffraction measurements were recorded in  $10\text{--}60^\circ$   $2\theta$  range. Fig. 3.1 shows XRD patterns recorded for the catalysts. XRD patterns shows sharp peak at  $26.4^\circ$  matching with JCPDS No. 26-1079, corresponding to the graphitic carbon. Another small peak at  $43.5^\circ$  also corresponds to graphitic carbon. No distinct peak was observed at  $39.7^\circ$ , pertaining to platinum metal, which implies that platinum nanoparticles are in highly dispersed state.

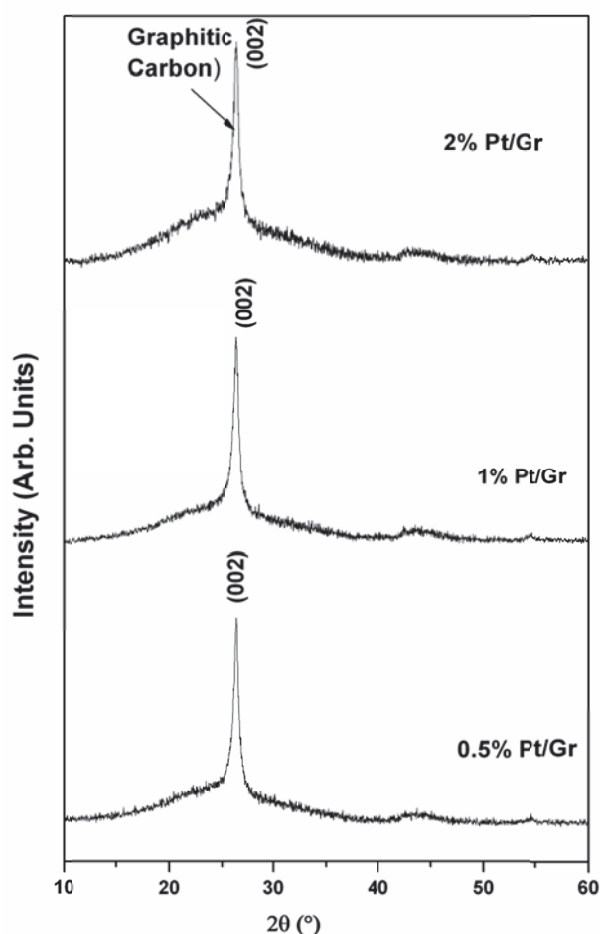


**Fig. 3.1:** XRD patterns of Pt/Graphite catalysts with different Pt loading

## Chapter 3

### 3.2.2.2 SEM

Scanning electron microscopy was used to study the surface morphology of the platinum on carbon catalysts and the change in their morphology after using them for the HI decomposition reaction. SEM images of the Pt/Graphite catalysts with different Pt loading are shown in Fig. 3.2. These images show a rough surface with few open pores and loose particles over it. The SEM images (for 1 Pt/Graphite) recorded, at higher magnification, in both secondary electron (Fig. 3.3a) and backscattered electron (Fig. 3.3b) mode depicts the presence of noble metal particles of  $\sim 20$  nm dimensions. In general, the particles are well separated, without much of agglomeration.

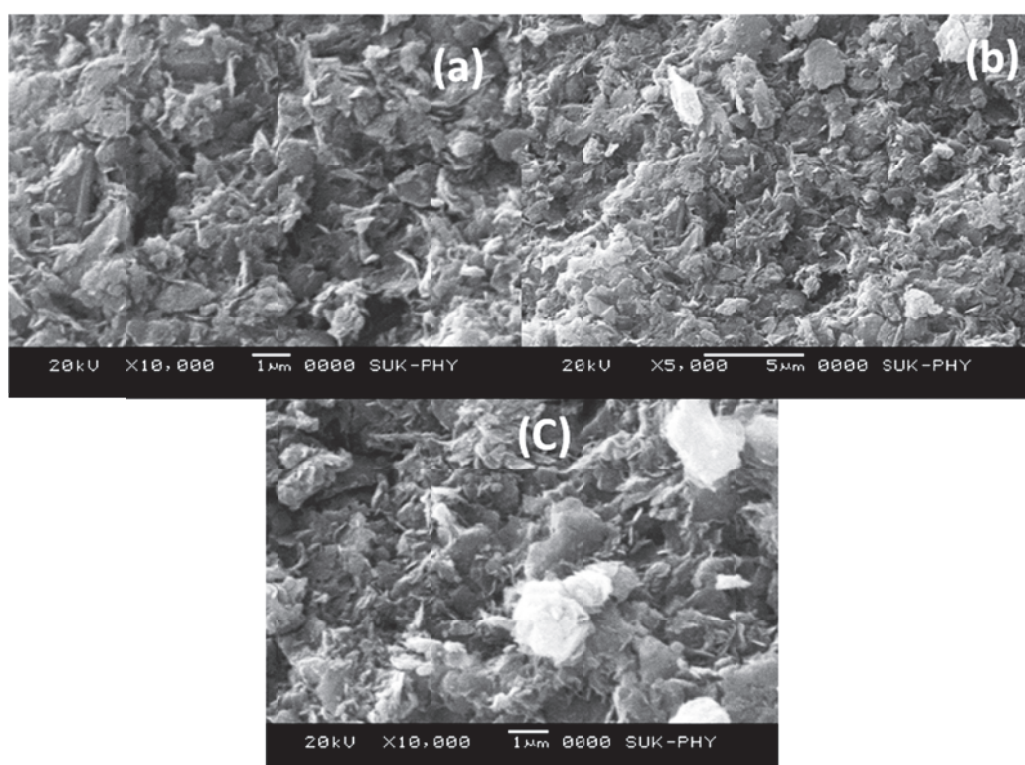


**Fig. 3.2:** SEM images of Pt/Graphite catalysts with different Pt loading (a) 0.5%, (b) 1% and (c) 2%

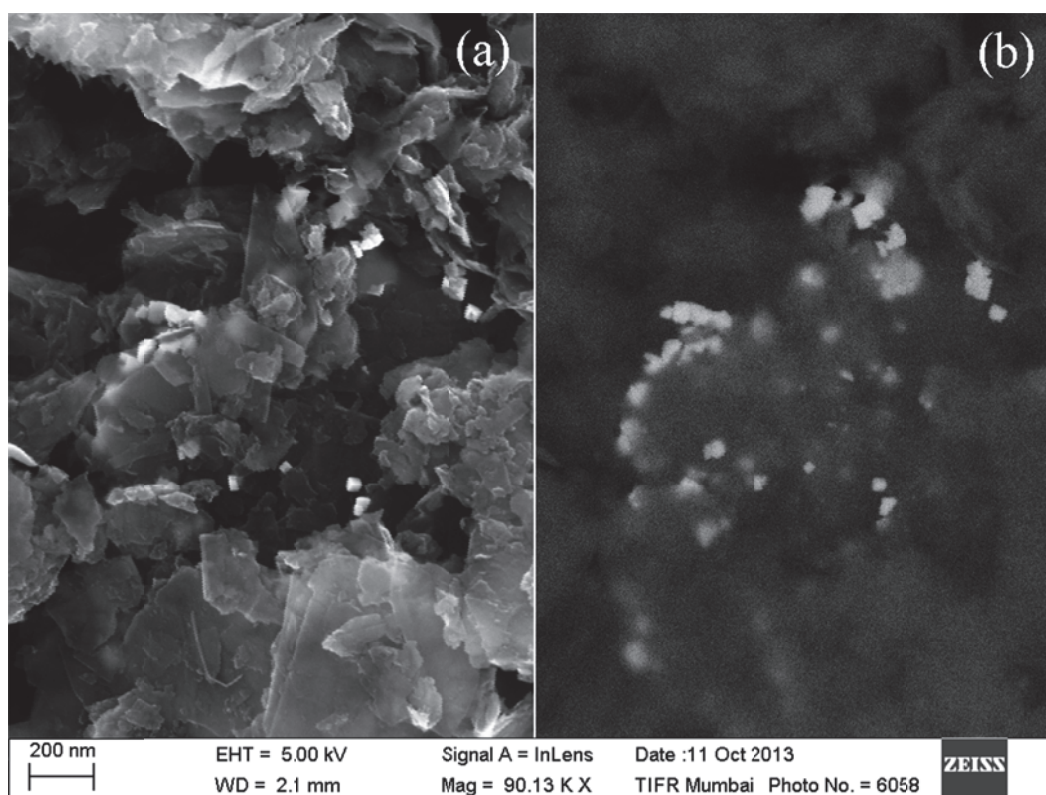


**Fig. 3.3:** High magnification SEM images of 1% Pt/Graphite catalyst

### 3.2.2.3 Surface Area

BET Surface area of the Pt/Gr catalysts were evaluated using N<sub>2</sub> adsorption technique, all the samples were found to exhibit very little porosity with major contribution from intra-particle pores. A typical adsorption isotherm along with generated pore size distribution is shown in Fig 3.4. The surface area and pore volume data for all the samples are given in Table 3.1. The surface area of all the three catalysts is in the range of 65-80 m<sup>2</sup>g<sup>-1</sup>, while pore volume is in the range of 0.34-0.39 m<sup>3</sup>g<sup>-1</sup>. These values also corroborate with the low porosity of the support.

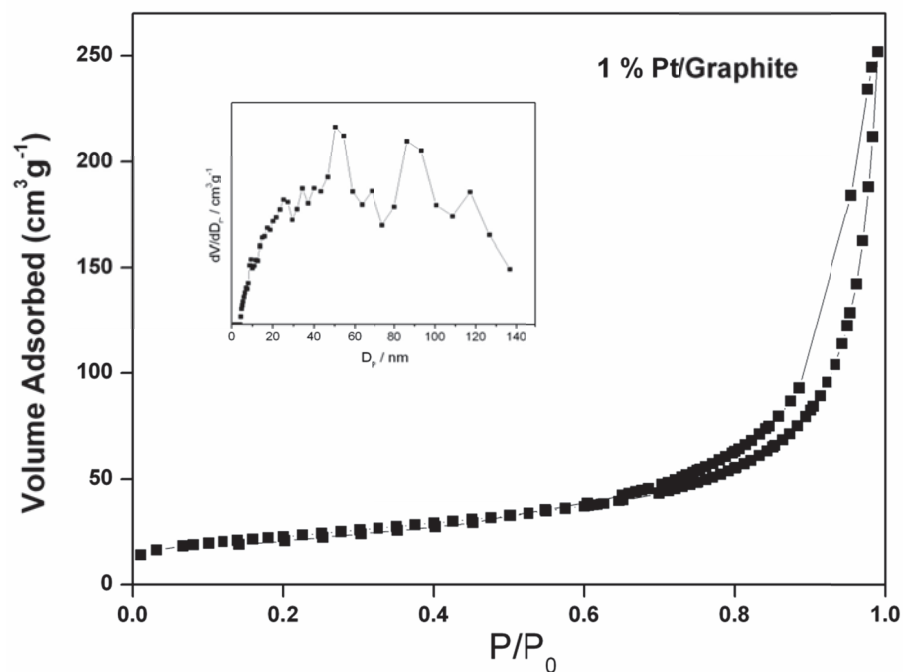


**Fig. 3.4:** Adsorption-desorption isotherms and pore size distribution curve  
for 1 % Pt/graphite catalyst

S. No.	Catalyst	Surface Area (m² g⁻¹)	Pore Volume (cm³ g⁻¹)
1	0.5 Pt/Graphite	73.3	0.34
2	1 Pt/Graphite	80.0	0.39
3	2 Pt/Graphite	67.5	0.38

**Table 3.1:** Surface area and pore volume data for different Pt/graphite catalysts

### 3.2.2.4 Raman Spectroscopy

Raman spectroscopy is most powerful tool to characterize carbon systems. The Raman spectra of graphite carbon exhibit a single peak at  $\sim 1580 \text{ cm}^{-1}$  corresponding to

## Chapter 3

the  $E_{2g}$  mode of vibration of  $sp^2$  hybridized carbon (G band). Appearance of another peak at  $\sim 1350\text{ cm}^{-1}$  is inevitably observed for  $sp^3$  hybridized carbon and some defects present in the carbon texture. This peak is known as D band [133]. The Raman spectra for the catalysts are shown in Fig. 3.5. It clearly shows that Pt/Graphite catalysts exhibit a sharp G band corresponding to the  $sp^2$  hybridized carbon. Appearance of a broad D-band at  $1350\text{ cm}^{-1}$ , suggests for the presence of  $sp^3$  hybridized carbon and some defects in the graphite structure.

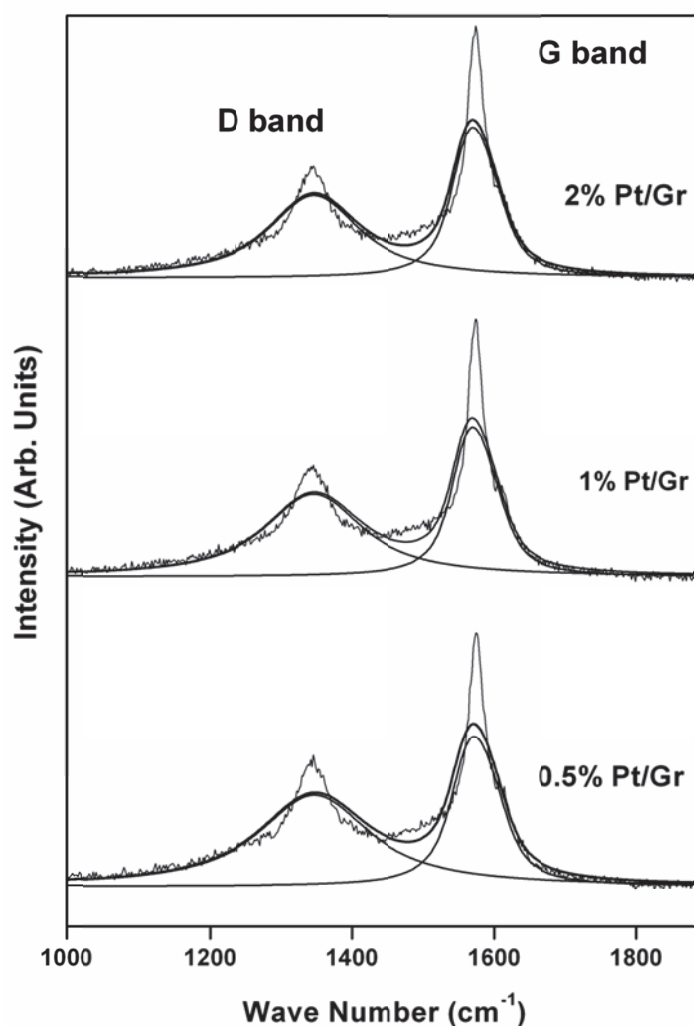


Fig. 3.5: Raman spectra of different Pt/Graphite catalysts

## Chapter 3

### 3.2.2.5 X-ray Photoelectron spectroscopy

Surface compositions of the catalysts were analyzed using X-ray photoelectron spectroscopy. The XPS measurements for Pt/C were carried out in constant analyzer energy mode using Al  $K_{\alpha}$  radiation (1486.6 eV). The survey scans of all three showed peaks in the spectral regions corresponding to carbon, platinum and oxygen only. Survey scan of one of the catalyst (1 Pt/Graphite) is shown below in Fig 3.6.

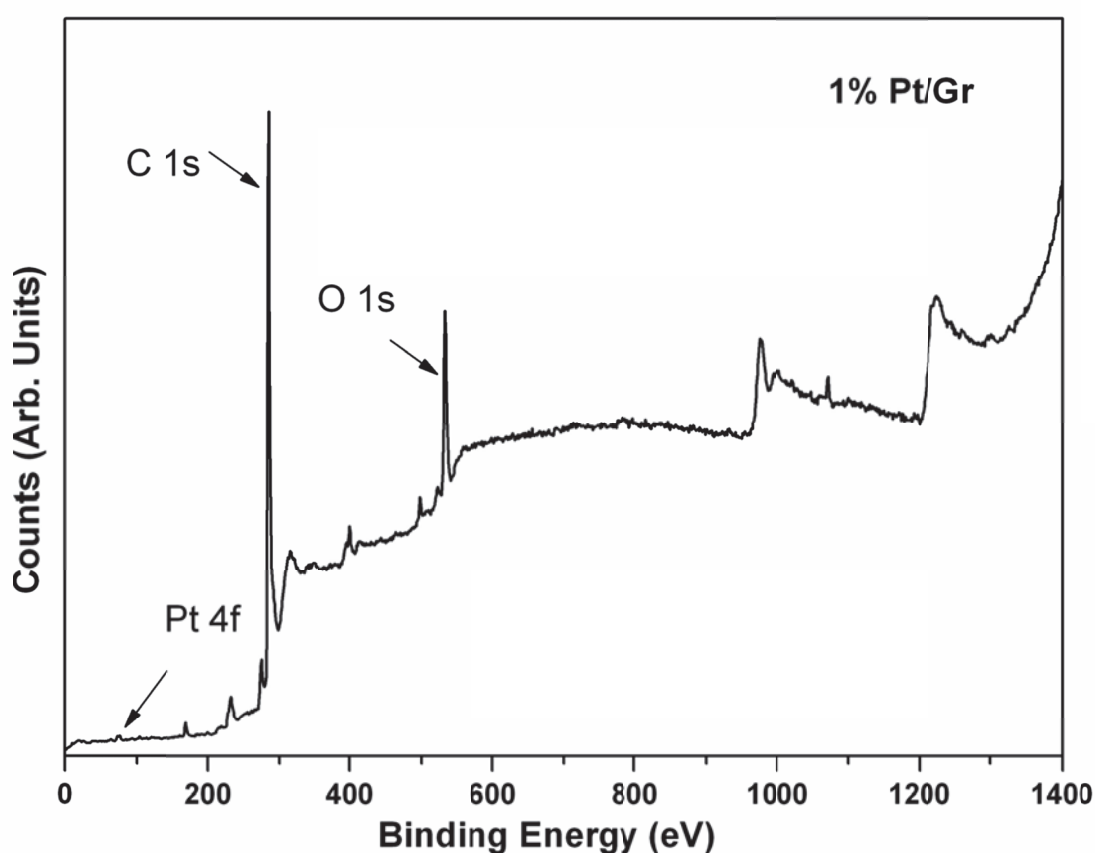
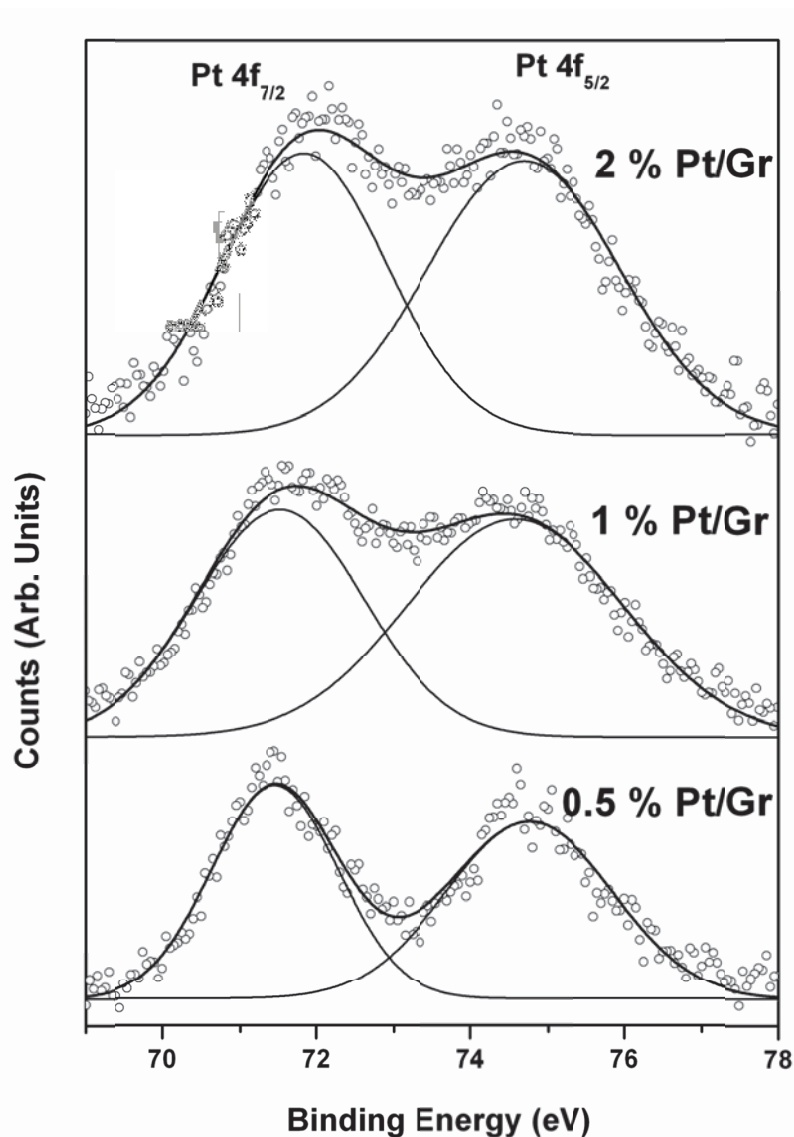


Fig. 3.6: XPS survey scan of 1% Pt/Graphite catalysts

Fig 3.7 shows the intensity versus binding energy data obtained for spectral region corresponding to Pt 4f of the three catalysts. It can be deconvoluted into only one doublet ( $4f_{5/2}$  and  $4f_{7/2}$ ) with respective binding energies of around 71.3 eV and 74.5 eV. These

## Chapter 3

binding energy values correspond to metallic state of platinum [134-135]. Thus XPS study reveals that platinum present here is in zero oxidation state which is essential for its catalytic activity.



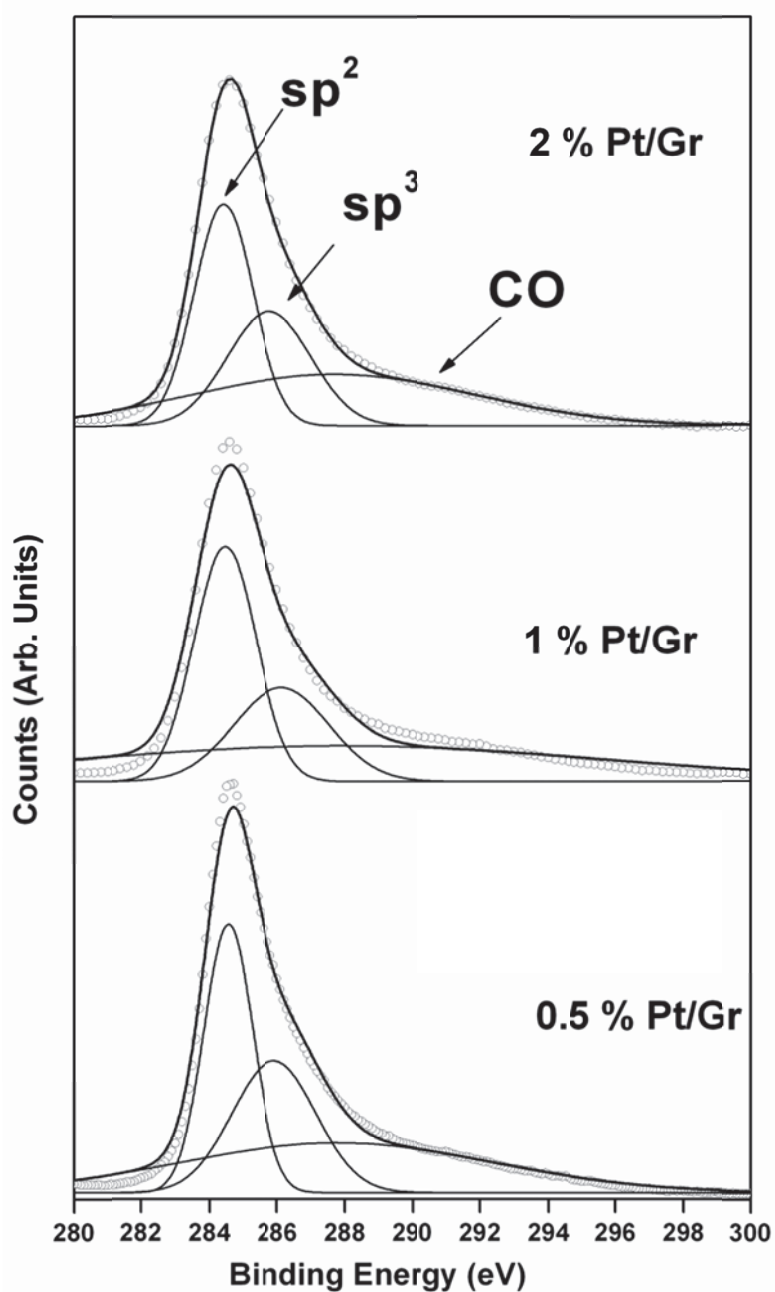
**Fig. 3.7:** XPS spectra of Pt 4f spectral region of different catalysts

Fig 3.8 shows the XPS spectra of all three catalysts in the C-1s spectral region. It can be fitted to three peaks with binding energies around 284.5, 285.9 and 287.7 eV. These peaks correspond to  $sp^2$  hybridized carbon,  $sp^3$  hybridized carbon and CO (Carbon



## Chapter 3

bonded to oxygen, C-O or C=O) types of carbon [134]. Therefore the oxygen present (observed in the survey scan of the samples) is associated with carbon and not platinum. Also presence of  $sp^2$  hybridized carbon is in confirmation with the results of Raman.



**Fig. 3.8:** XPS spectra of Carbon 1s spectral region of different Pt/Graphite catalysts



## Chapter 3

### 3.2.2.6 Catalytic activity of the catalyst

All the three catalysts were employed for liquid phase HI decomposition reaction. The percentage conversions values were calculated from change in  $\text{H}^+$ ,  $\text{I}^-$  and  $\text{I}_2$  concentrations. All three gave similar level of conversions. The average conversion values obtained for a typical 2 hour study at 120 °C are shown in Table 3.2.

From the Table, it can be seen that the conversion increases significantly on using a catalyst (blank run gives only 2.9 conversion), also conversion increase with the noble metal loading. However the percentage conversion doesn't increase linearly with the noble metal loading, it increases sub linearly. If we calculate for per unit weight of the noble metal 1 catalyst gives maximum conversion among the three loadings.

S. No.	Catalyst	% Conversion
1.	Blank	2.9
2.	0.5 Pt/Graphite	8.4
3.	1 Pt/Graphite	17.5
4.	2 Pt/Graphite	23.4

**Table 3.2:** % Conversion in 2 hours at 120 °C for different catalysts

Based on above results 1 platinum graphite was chosen for detailed study. Using 1 Pt/Graphite catalyst liquid phase HI decomposition reaction was carried out for three different reaction temperatures, 50 °C, 80 °C and 120 °C, for reaction times ranging from 1 h to 5 h. The per cent conversion obtained with time for different temperatures is as shown in Fig. 3.9.

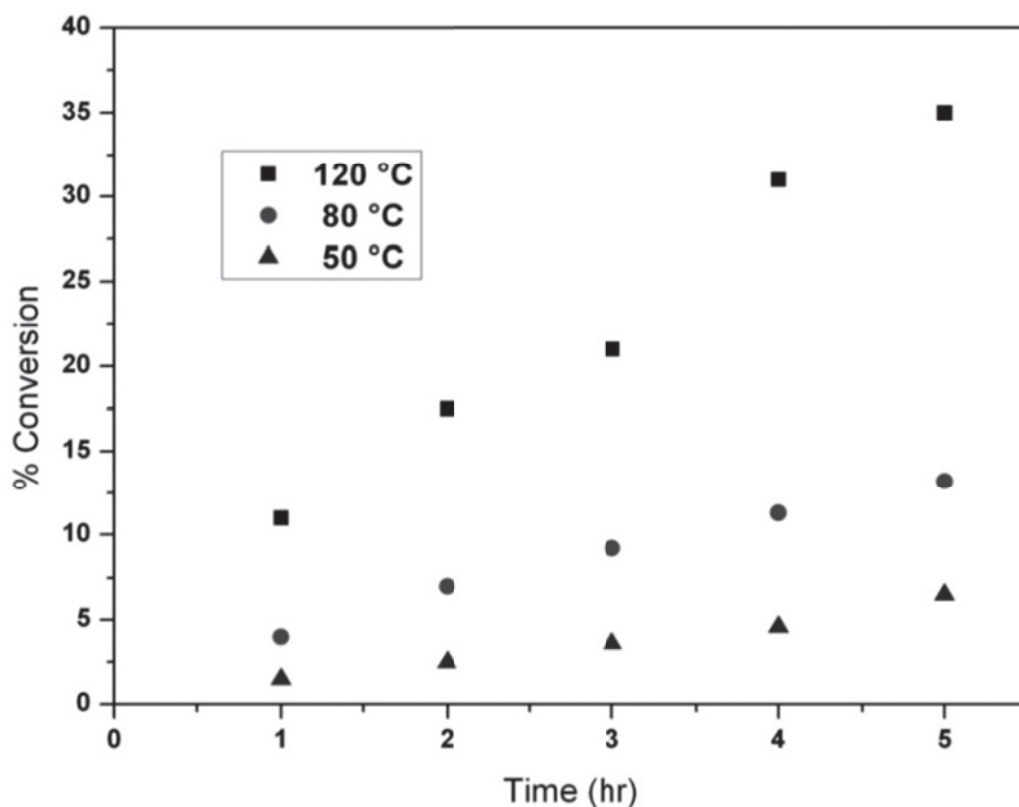


**Fig. 3.9:** Increase in percentage conversion with time at different temperatures

The conversion is found to increase with time for all the three temperature conditions. For 50 °C temperature, the per cent conversion is found to increase from 1.5 at 1 h to 6.5 for 5 h, as given in Table 3.3. The same increasing trend is observed in amount of hydrogen produced at each temperature, which is analyzed by the gas chromatograph. As the temperature is increased the conversion is found to increase by many folds, e.g. for reaction time of four hours, the per cent conversion is found to be 4.6, 11.3 and 31.0 for 50, 80 and 120 °C temperature, respectively.

## Chapter 3

---

Time (h.)	% Conversion At 50 °C	% Conversion At 80 °C	% Conversion At 120 °C
1	1.5	4	11
2	2.5	7	17.5
3	3.6	9.2	21
4	4.6	11.3	31
5	6.5	13.2	35
Rate Constant (s <sup>-1</sup> )	3.52 x 10 <sup>-6</sup>	7.69 x 10 <sup>-6</sup>	2.37 x 10 <sup>-5</sup>

**Table 3.3:** % Conversion with time at different temperatures

Considering, the remarkably higher conversion for 120 °C temperature, it is prudent to calculate the activation energy for this reaction. Taking change in HI concentration with time from reaction data and order of reaction as one, rate constant can be calculated for different temperatures (Fig. 3.10). Plotting rate constant versus reciprocal of temperature as shown in Fig 3.11, the activation energy could be obtained and is found to be 32 kJ/mole. Low activation energy explains for sharp increase in reaction rate at a low temperature of 120 °C.

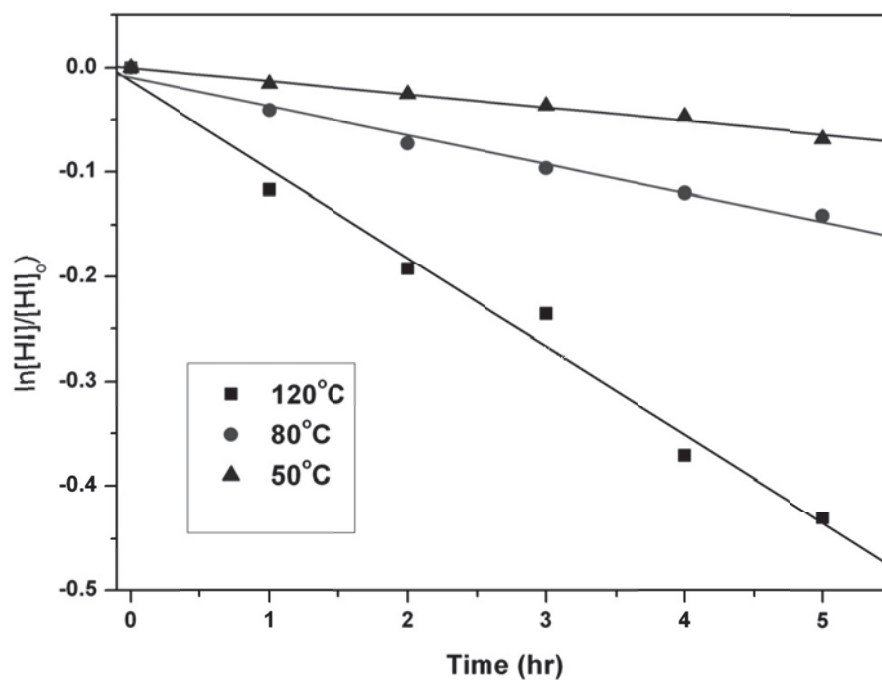


**Fig. 3.10:** Plots for calculation of rate constants at different temperatures

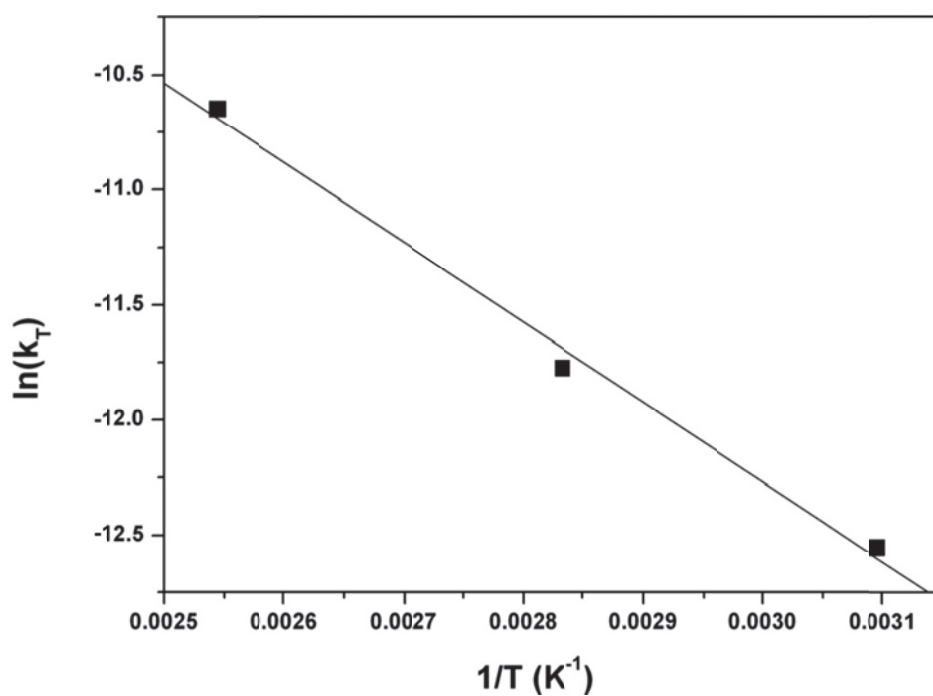


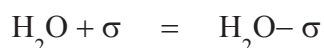
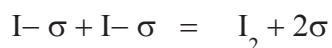
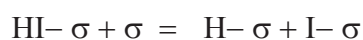
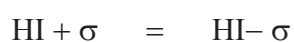
**Fig. 3.11:** Plot for calculation of Activation energy

## Chapter 3

---

The activation energy calculated from present studies is 32 kJ/mole. This is in the same range as of that obtained by various researchers for gas phase HI decomposition reaction. Shindo et al. [82] obtained 27.6 kJ/Mole over Pt/  $\gamma$ -Alumina catalyst. Also Oosawa *et al* [136] obtained 53.2 kJ mole over Pt/active-carbon catalyst and Hinshelwood et al [84] obtained 58.6 kJ mole over the Pt wire.

Shindo *et al* [82] has proposed the following mechanism for the reaction as follows



The rate determining step according to them is decomposition of HI over catalyst surface ( $\sigma$ ). This mechanism corroborates with our observation of first order of the reaction. Thus it can be assumed that the above reaction mechanism holds valid for the liquid phase HI decomposition reaction also.

### 3.2.2.7 Iodine Poisoning Studies

Iodine is a known poison for many catalytic reactions. In case of HI decomposition iodine is one of the products; therefore it is necessary to find out its effect on the catalytic activity of the catalysts. The reaction when carried out in presence of extra iodine only shows a slight reduction in percentage conversion values. The

## Chapter 3

percentage conversion value for a two hour study at 120 °C with HI and I<sub>2</sub> ratios 2:1 and 1:1 is shown below in Table 3.4.

S. No.	Reactant	% Conversion
1.	HI	17.5
2.	HI+I <sub>2</sub> ( 2:1)	16.8
3.	HI+I <sub>2</sub> ( 1:1)	16.0

**Table 3.4:** % Conversion in presence of iodine

We can see from the table that even for equimolar amount of iodine added to HI the percentage conversion drops from 17.5 to 16.0. It can be attributed to the fact that the iodine gets dissolved in HI, forming polyiodide species and therefore it does not get deposited on the surface of catalyst and hence does not affect the performance of the catalyst.

### 3.2.2.8 Stability of the Catalyst

Stability of a catalyst is an important aspect especially in case of harsh reaction conditions. We have evaluated two aspects of the stability of the catalysts viz., (i) stability with respect to any change in structure and morphology and (ii) stability against noble metal leaching. For stability against structural and morphological changes, the used catalysts were analysed by XRD, SEM and Raman spectroscopy etc. Fig 3.12 shows the XRD pattern of different used Pt/Graphite catalyst. The XRD pattern for the used catalysts remain similar to original sample, with peak at ~26.4° 2θ value which corresponds to the graphitic carbon. There is no apparent difference in the XRD pattern of

## Chapter 3

used catalyst as compared to the fresh one and also peak corresponding to platinum is not observed, which indicates that the Pt nanoparticles are not getting sintered.

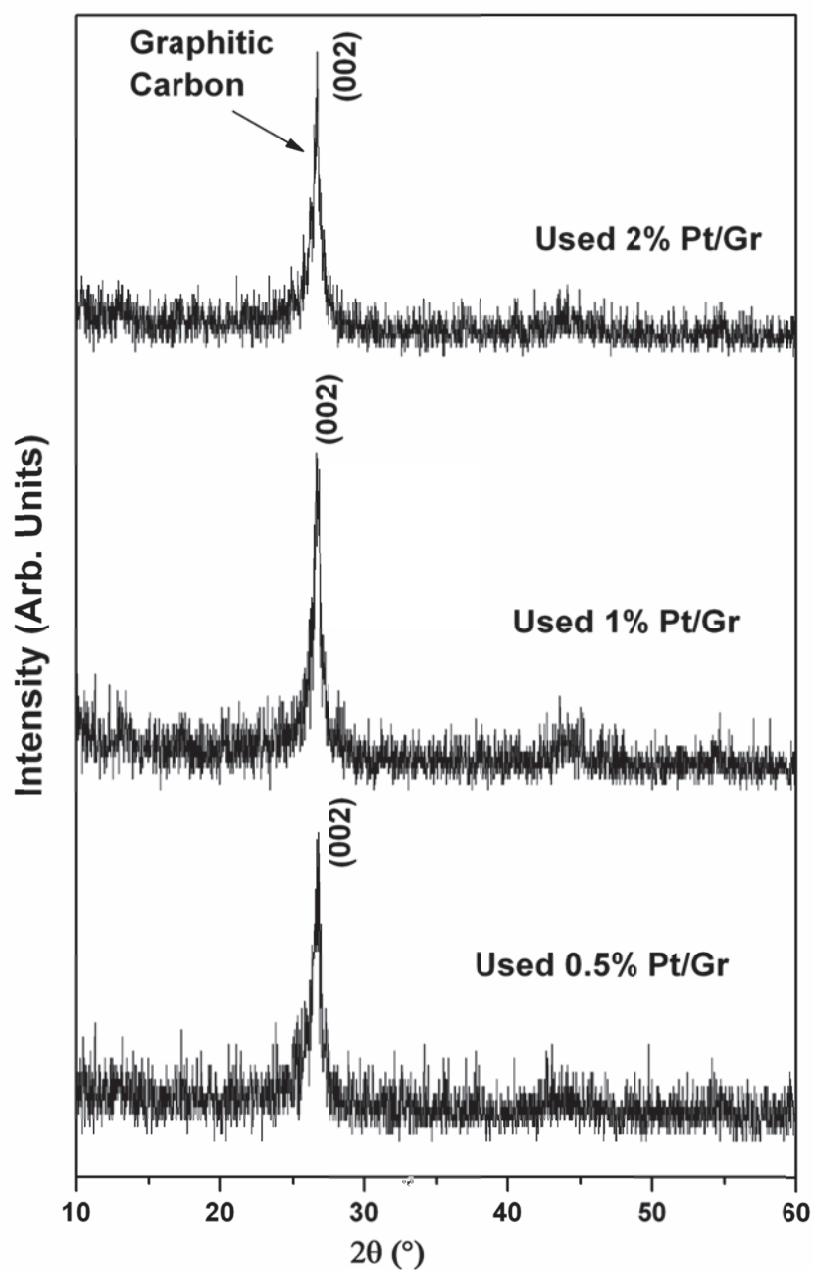


**Fig 3.12:** XRD for different used Pt/Graphite catalyst

## Chapter 3

Fig 3.13 shows the SEM image of fresh and used 1% Pt/Graphite catalyst (after 2 hrs of usage). It can be observed from the two images that the overall features of used catalysts are similar to the fresh one. Therefore there is no remarkable change in the morphology of the catalyst after being used for HI decomposition reaction.

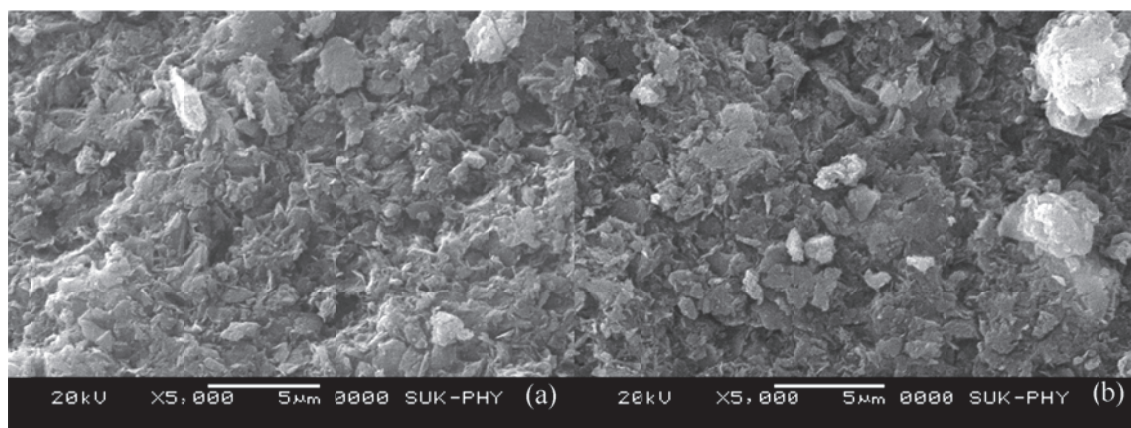


**Fig 3.13:** SEM for (a) fresh and (b) used (2 hrs use) 1% Pt/Graphite catalyst

Raman spectra for the used samples (used for 2 hrs) as shown in Fig. 3.14 do not show much variation as compared to original samples. The presence of both G band and D band are retained after HI decomposition. Also  $I_G/I_D$  ratio does not change for fresh and used catalyst which means that there are not much structural changes in the catalyst.



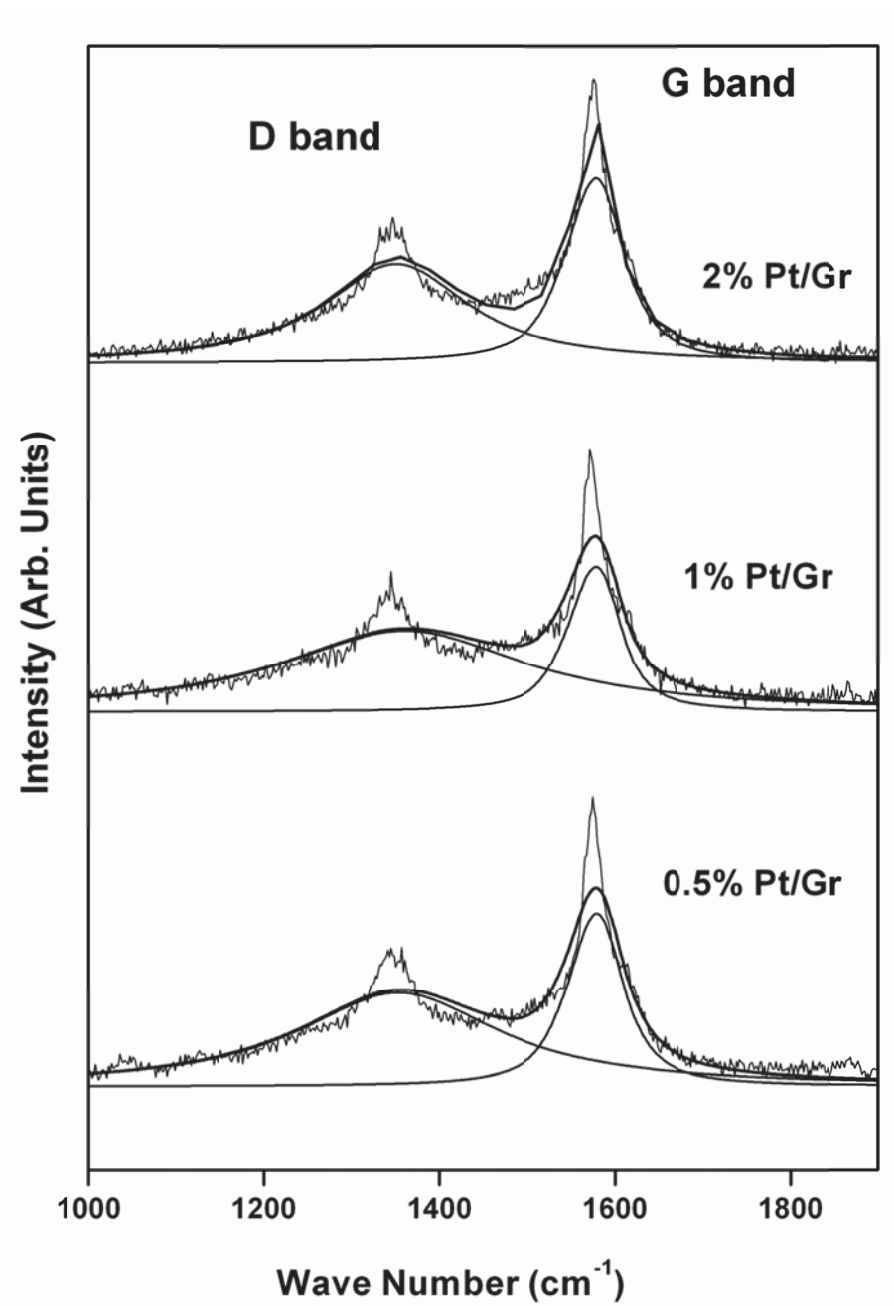


**Fig. 3.14:** Raman spectra for different used Pt/Graphite(2 hrs use) catalysts

The stability of the catalysts against noble metal leaching was studied by analyzing the eluent after a typical two hour reaction. The ICP AES analysis of the eluents showed presence of only few ppm of platinum (23, 39 and 68 ppm for 0.5 , 1

## Chapter 3

---

and 2 Pt/Graphite catalyst). Therefore 0.23 , 0.39 and 0.68 of the original platinum loading is getting eluted out into the solution, indicating that the catalysts are having good stability against noble metal leaching in the harsh reaction environment. All these finding leads to the conclusion that the Pt/Gr catalyst thus prepared is stable for liquid phase HI decomposition reaction.

### 3.2.3 Conclusion

The supported noble metal catalysts with graphite as support prepared by impregnation route are found to be active for liquid phase decomposition of hydriodic acid. The percentage conversion increase with increasing noble metal loading and 1 Pt/Graphite shows maximum percentage conversion per unit weight of platinum. 1 Pt/Graphite catalysts has a small activation energy barrier of 32 kJ/mole and also its activity is not affected by the presence of iodine in the reaction mixture. Also these catalysts are also found to be stable in terms of structure of the support, noble metal elution, surface morphology and catalytic activity.

## ***Chapter 3***

---

### **3.3 Other Platinum Carbon Catalysts**

This section contains details of catalysts supported on carbon supports. Two types of carbon supports have been used. First is commercially available activated carbon and another is prepared by carbonization of carbohydrate source (we have used rice). These catalysts have been discussed in this section with respect to their characterization, catalytic activity and stability for liquid phase HI decomposition reaction.

#### **3.3.1 Experimental**

##### **3.3.1.1 Preparation of Catalyst**

Three different Pt/carbon catalysts with 1 wt% platinum loading were prepared. First catalyst was prepared by impregnation of activated carbon (commercial) which include impregnation of activated carbon with hexachloroplatinic acid followed by its reduction by heating at 300 °C for 3 h under flowing H<sub>2</sub>-N<sub>2</sub> mixture (8 wt% hydrogen in nitrogen). This catalyst is called as Pt/AC in this thesis.

Other catalysts were prepared by using carbon produced by carbonization of rice at 600 °C [137]. In this case platinum can be added at two stages: either before carbonization of rice or after carbonization of rice. Thus in one case, rice was soaked in hexachloroplatinic acid solution followed by drying at 100 °C. Next step was to carbonize the rice by heating upto 600 °C under N<sub>2</sub> atmosphere. Finally the product was reduced by heating at 300 °C for 3 h under flowing H<sub>2</sub>-N<sub>2</sub> mixture (8 wt% hydrogen in nitrogen). This catalyst is named as Pt/RC. In another case rice was carbonized first by heating upto 600

## **Chapter 3**

---

°C under N<sub>2</sub> atmosphere followed by addition of hexachloroplatinic acid and subsequent reduction. This catalyst will be called at RC/Pt in subsequent discussion.

### **3.3.1.2 Characterization of Catalyst**

The powder X-ray diffraction patterns of all the catalysts were recorded on Philips analytical diffractometer (using Ni-filtered Cu K $\alpha$  radiation. The surface morphology was studied using JEOL JSM-6360 and Zeiss scanning electron microscope. The BET surface area of the catalyst was obtained from physical adsorption of N<sub>2</sub> at -196°C, on a Quantachrome Autosorb - 1 instrument. The prepared sample was characterized for carbon structure and hybridization, by spatially resolved Raman scattering (Bruker Model MultiRAM) using 150 mW at laser head and 4 mW on the sample of 1064 nm line of Nd:YAG laser, detected with a liquid-nitrogen cooled high resolution charge coupled device (CCD) detector at 4 cm<sup>-1</sup> resolution. Oxidation state of platinum was studied by XPS using SPECS instrument.

### **3.3.1.3 Activity and Stability**

These three catalysts were employed for liquid phase HI decomposition reaction for evaluating their activity for the reaction as well as their stability in the reaction medium using the reactor (details given in Chapter 2). For this 250 mg of catalyst was added to 50 ml of 27% hydriodic acid solution in 250 ml round bottom flask. The reaction was carried out for 2 hours at 120 °C. After reaction, the HI decomposition was measured by means of titrating H<sup>+</sup> and I<sup>-</sup> ions using potentiometric titration. The solution was filtered to separate the used catalyst and the eluent. The spent catalyst was

## ***Chapter 3***

---

characterized by XRD and SEM for their physical integrity and the eluent was analyzed using ICP-OES for the leached out platinum.

### **3.3.2 Results and Discussion**

#### **3.3.2.1 XRD**

The XRD patterns of the three catalysts are shown in Fig. 3.15. These shows a broad hump at around  $23^\circ$  which is for the amorphous carbon. Pt/RC shows peak corresponding to platinum at around  $39.7^\circ$  (JCPDS No. 04-0802). The other two do not show peak corresponding to platinum inspite of having the same percentage loading (1 %). It may be due the fact that platinum in these two sample sees a maximum temperature of  $300^\circ\text{C}$  (during reduction step) therefore remains dispersed. While in case of Pt/RC, the maximum temperature seen by platinum is  $600^\circ\text{C}$  (during carbonization step). It may lead to agglomeration of platinum.

#### **3.3.2.2 SEM**

Fig 3.16 shows the SEM micrographs of the three catalysts. The SEM image of Pt/AC shows a smooth surface with large pores and few loose particles over it. In case of Pt/RC similar features (large pores and loose particles) are observed only difference is that the surface is little rough. In case of RC/Pt, the SEM image shows well dispersed particles over a smooth surface with few pores present over it.

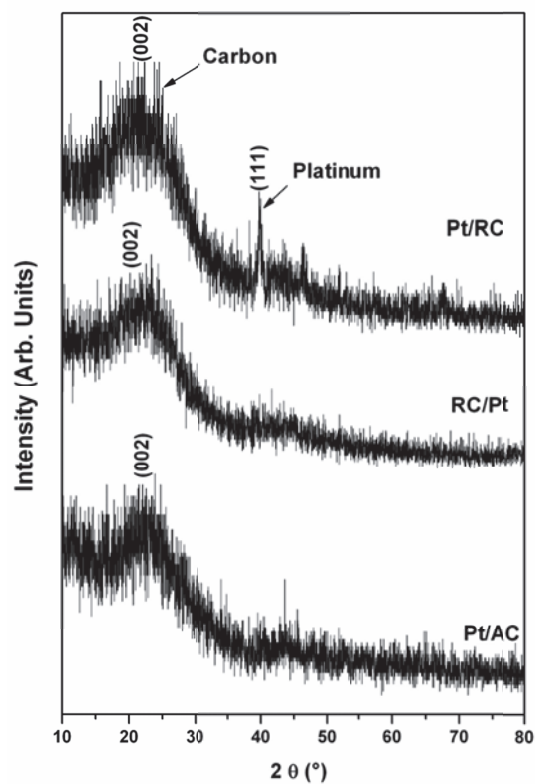


Fig. 3.15: XRD for different Pt/carbon catalysts

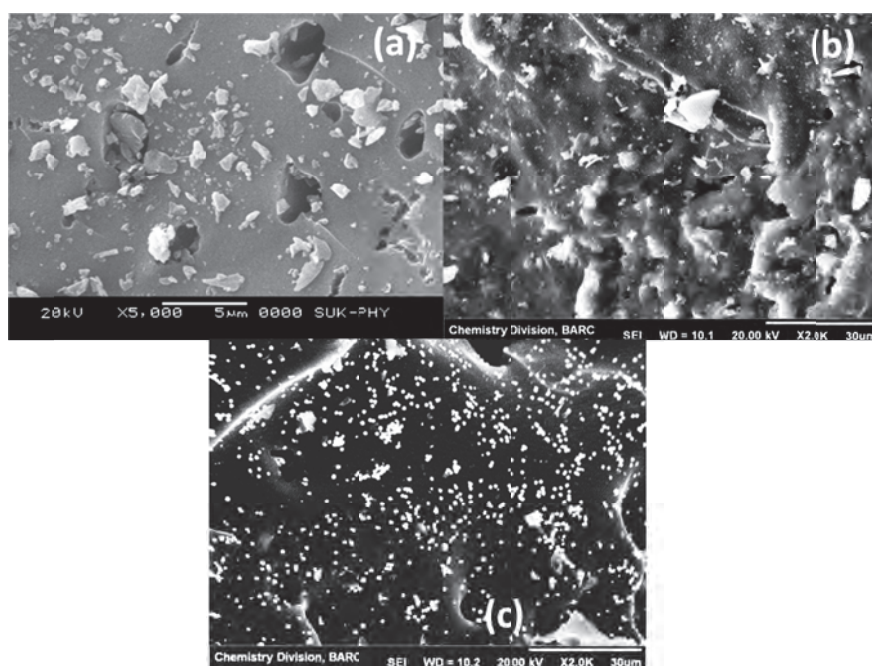
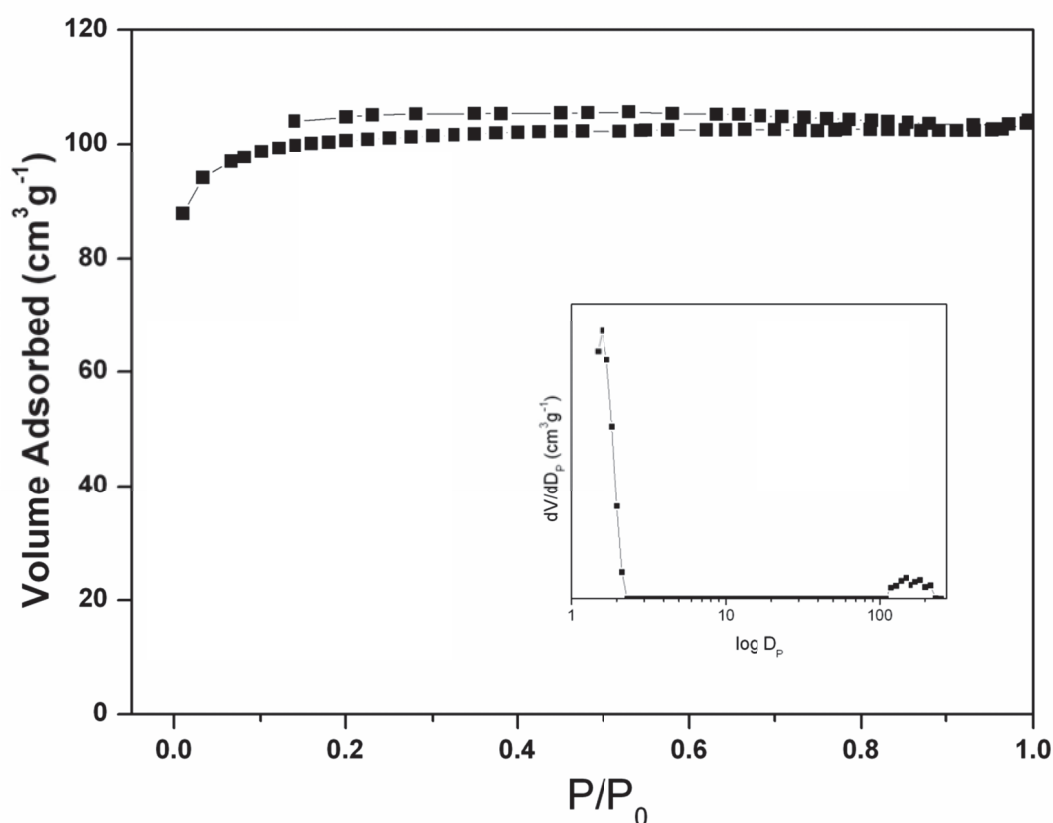


Fig. 3.16: SEM micrographs of (a) Pt/AC, (b) Pt/RC and (c) RC/Pt

## Chapter 3

### 3.3.2.3 Surface Area

BET Surface area of the Pt/AC catalysts evaluated using  $N_2$  adsorption technique exhibit presence of microporous morphology leading to high surface area. A typical adsorption isotherm along with generated pore size distribution for Pt/AC is shown in Fig 3.17. The isotherms belong to a mixed type in the IUPAC classification, type I at low relative pressures ( $p/p^0$ ) and type IV at intermediate and high relative pressures. There is high uptake at low  $p/p^0$  values which is characteristic microporous materials and a certain hysteresis slope can be observed at intermediate and high  $p/p^0$  values, indicating the presence of bigger pores. The surface area and pore volume values for Pt/AC were found to be  $338 \text{ m}^2 \text{ g}^{-1}$  and  $0.16 \text{ m}^3 \text{ g}^{-1}$  respectively.



**Fig. 3.17:** Adsorption-desorption isotherms and pore size distribution curve for Pt/AC

## Chapter 3

### 3.3.2.4 Raman Spectroscopy

Raman spectroscopy is used for characterization of carbon support of all the three catalysts. The Raman spectra for the catalysts in the range of 1000 to 1800  $\text{cm}^{-1}$  are shown in Fig. 3.18. It clearly shows that all three catalyst exhibits two peaks at around 1350 and 1580  $\text{cm}^{-1}$ , which corresponds to the D band and G bands, respectively. In this case the G band is less intense as compared to graphite based catalysts and the presence of a strong D-band suggests the presence of  $\text{sp}^3$  hybridized carbon as well as lot of defects and edge sites [138].

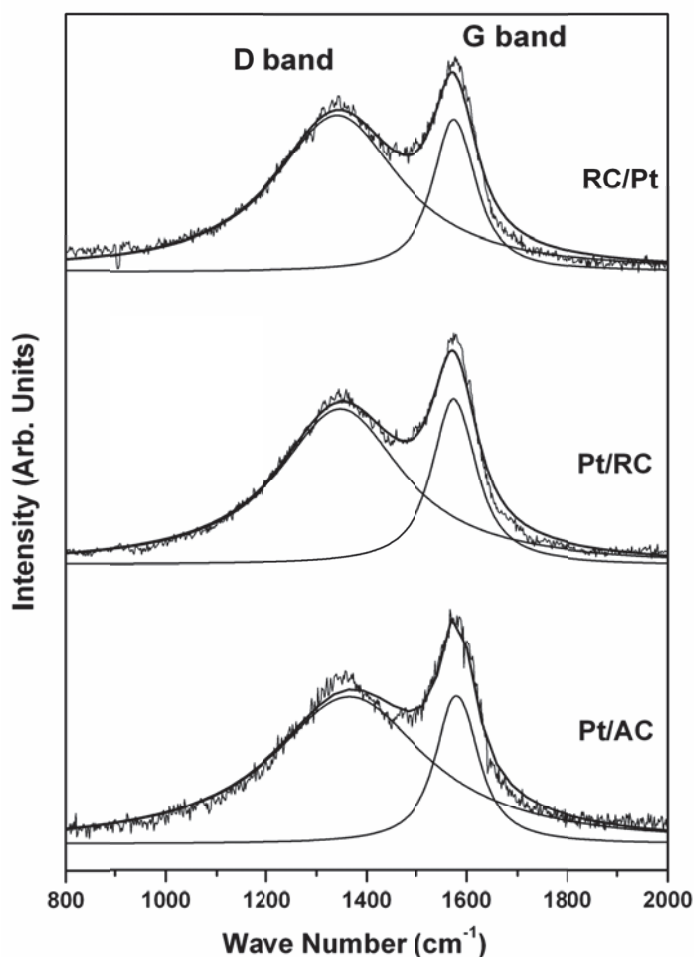


Fig. 3.18: Raman spectra of different Pt/carbon catalysts



## Chapter 3

### 3.2.2.5 X-ray Photoelectron spectroscopy

Surface compositions of the catalysts were analyzed using X-ray photoelectron spectroscopy. The XPS measurements for all three were carried out in constant analyzer energy mode using Al  $K_{\alpha}$  radiation (1486.6 eV). The survey scans of all three catalysts shows peaks in the spectral regions that correspond to carbon, platinum and oxygen only. One of the survey scan (for Pt/RC catalyst) is shown below in Fig 3.19.

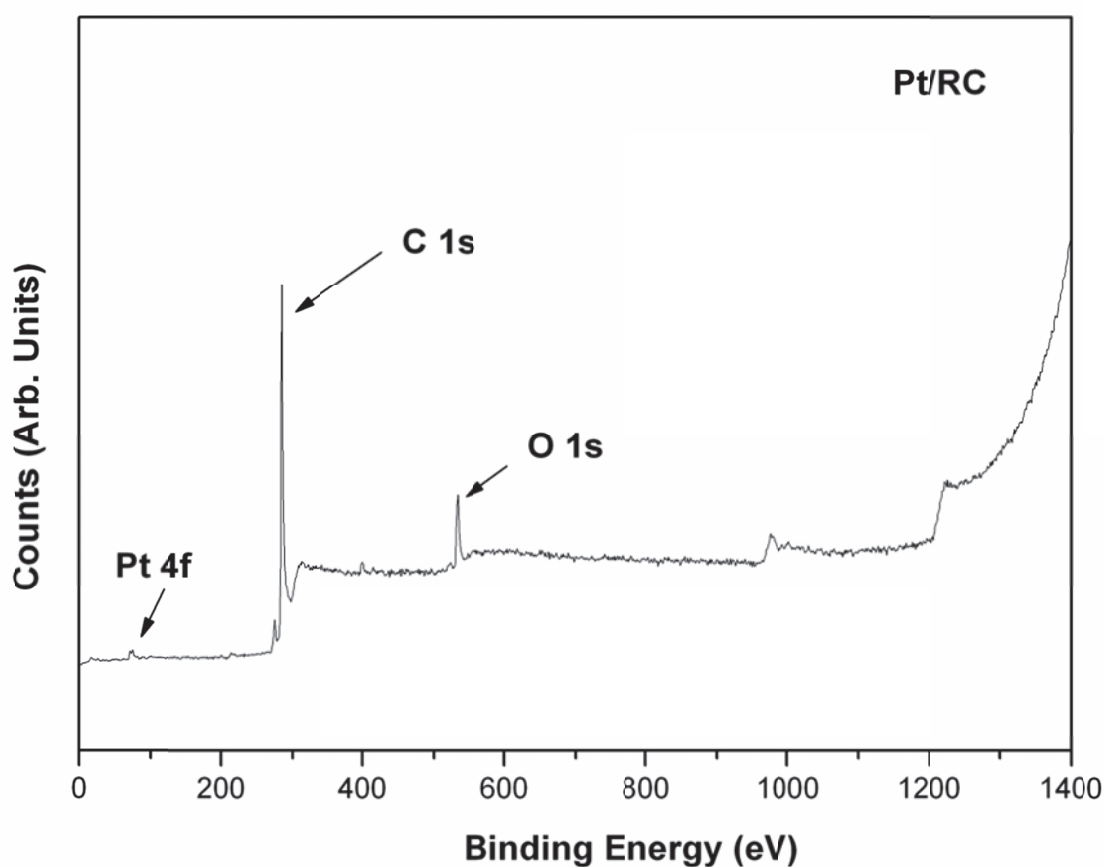


**Fig. 3.19:** XPS survey scan of Pt/RC catalyst

## Chapter 3

---

Fig 3.20 shows the intensity versus binding energy data obtained for spectral region corresponding to Pt 4f of the three catalysts. Spectra corresponding to each catalyst can be deconvoluted into a doublet ( $4f_{5/2}$  and  $4f_{7/2}$ ) with respective binding energies of around 71.5 and 74.8 eV. These values of binding energy correspond to metallic state of platinum [134-135]. Therefore XPS study confirms that platinum present here is in zero oxidation state which is essential for its catalytic activity.

Fig 3.21 shows the spectral region corresponding to C-1s spectral region; it can be fitted to three peaks with binding energy 284.7, 286.0 and 287.7 eV. These peaks correspond to  $sp^2$ ,  $sp^3$  and CO (Carbon bonded to oxygen, C-O or C=O) types of carbon [134]. Therefore the oxygen present is associated with carbon and not platinum. Presence of  $sp^2$  as well as  $sp^3$  hybridized carbon is in confirmation with the results of Raman spectroscopy.

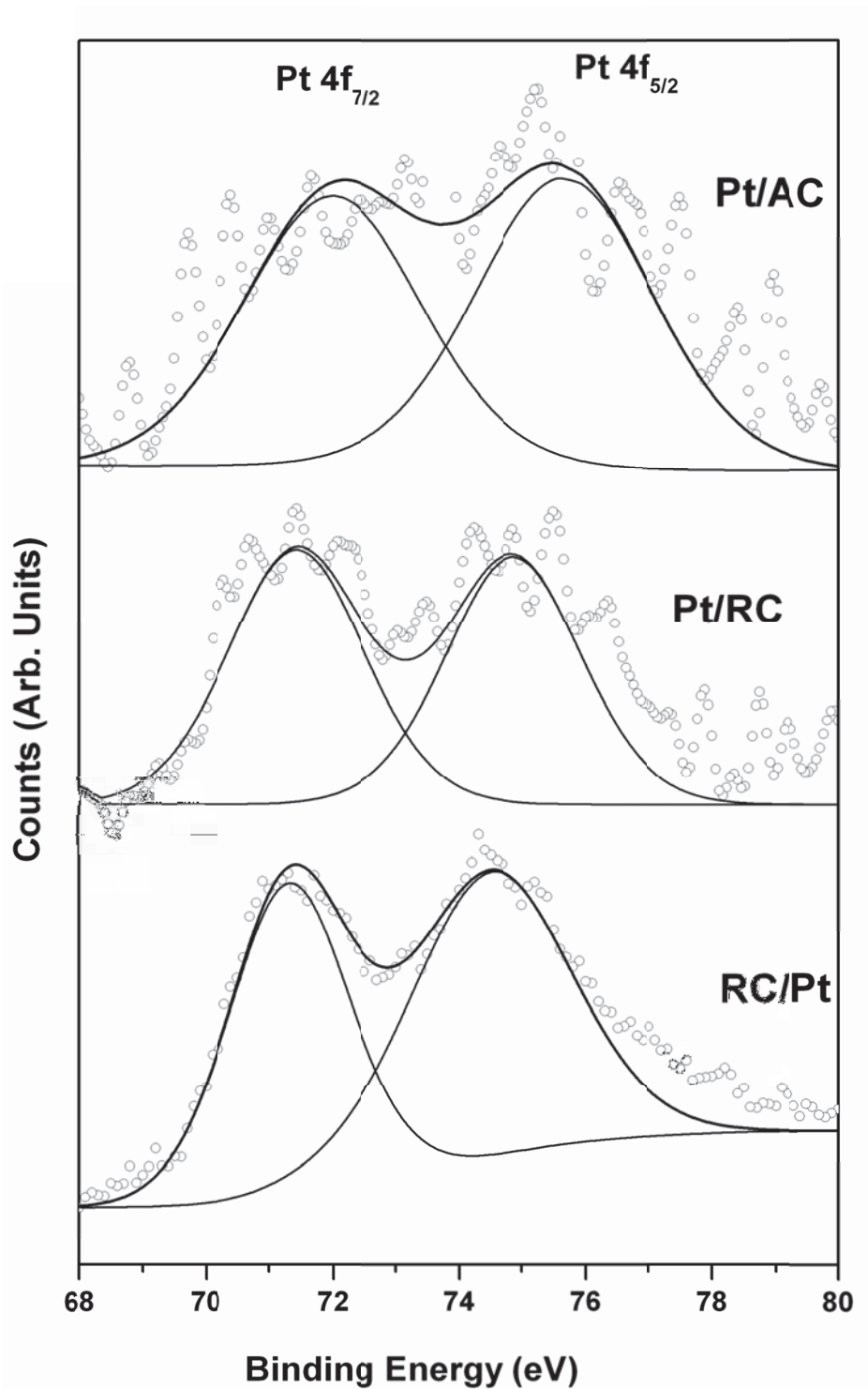


Fig 3.20: XPS spectra of Pt-4f spectral region of different Pt/carbon catalysts

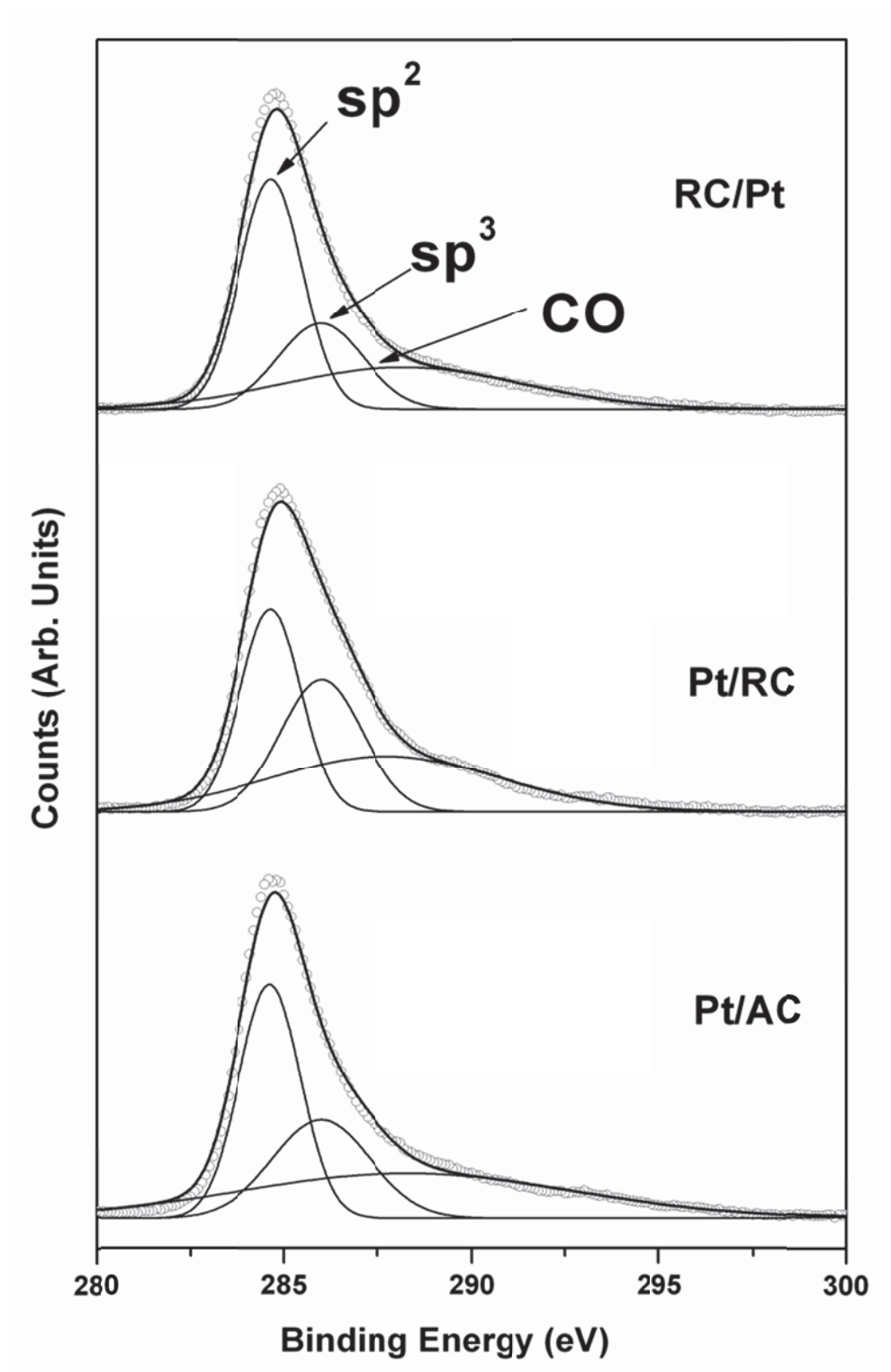


Fig 3.21: XPS spectra of C-1s spectral region of different Pt/carbon catalysts

## Chapter 3

### 3.2.2.6 Catalytic activity of the catalyst

All the three catalysts were employed for liquid phase HI decomposition reaction. The percentage conversions values were calculated from change in  $H^+$ ,  $I^-$  and  $I_2$  concentrations. All three gave similar level of conversions. The average conversion values obtained for a typical 2 hour study at 120 °C are shown in table 3.6. It can be seen that all the three catalysts are comparable in terms of catalytic activity, which is little less than that of Pt/Graphite catalyst with 1 loading of platinum.

S. No.	Catalyst	% Conversion
1.	Blank	2.9
2.	Pt/AC	13.2
3.	Pt/RC	13.2
4.	RC/Pt	13.4

**Table 3.5:** % Conversion in 2 hours at 120 °C for different catalysts

### 3.3.2.7 Stability of the Catalyst

The stability of these catalysts was evaluated with respect to change in structure and platinum leaching. For stability against structural and morphological changes, the used catalysts were analysed by XRD and SEM. Fig 3.22 shows the XRD pattern of fresh and used catalysts. There is no apparent change in the XRD patterns of all the three catalysts. Broad peak at  $\sim 23^\circ$   $2\theta$  value which corresponds to the amorphous carbon remains same for all the three catalysts. Also there is no appearance of platinum peak in

## Chapter 3

the Pt/AC and Pt/RC catalysts, which suggests that the catalysts are stable against the sintering of platinum particles. Also the platinum peak present in the Pt/RC catalyst is present in the used catalyst as well.

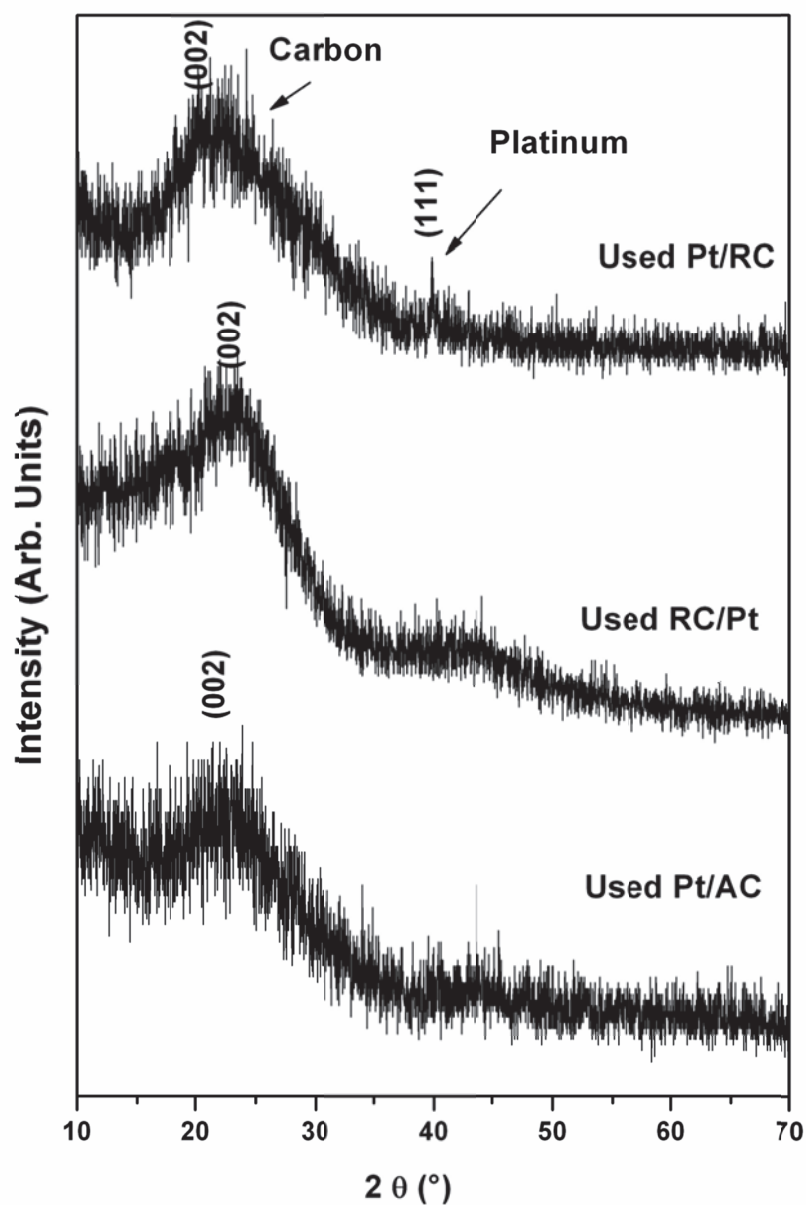
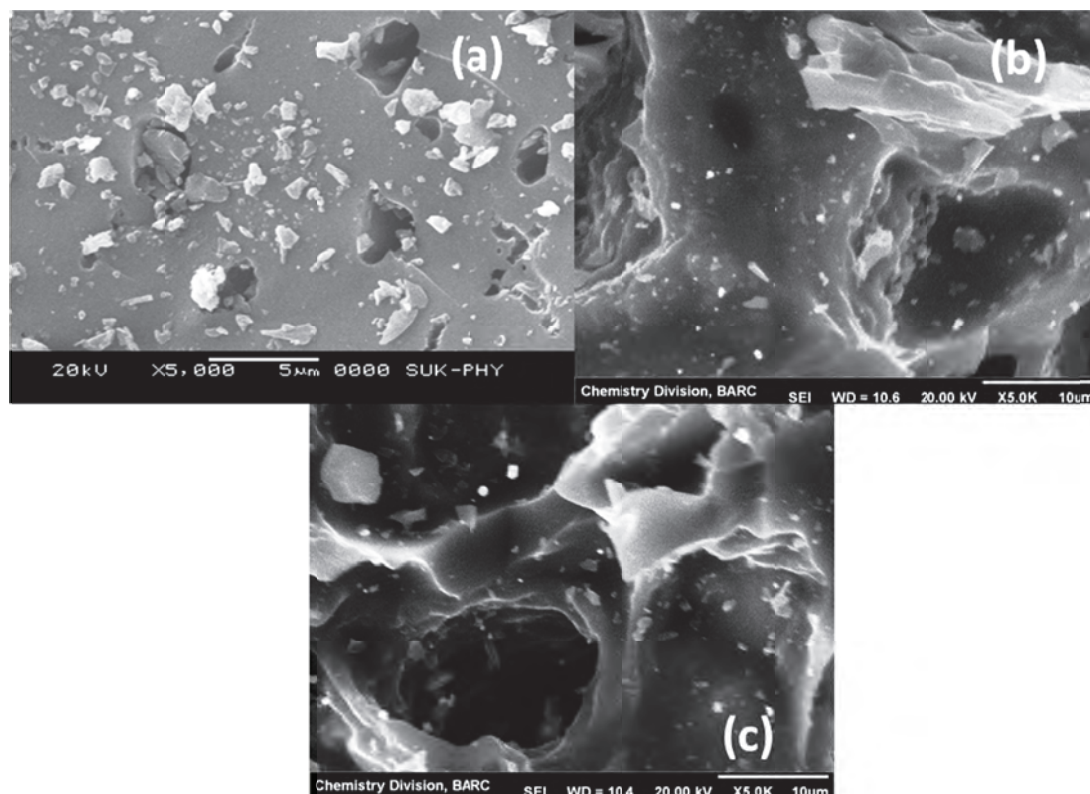


Fig. 3.22: XRD patterns of used Pt/Carbon catalysts

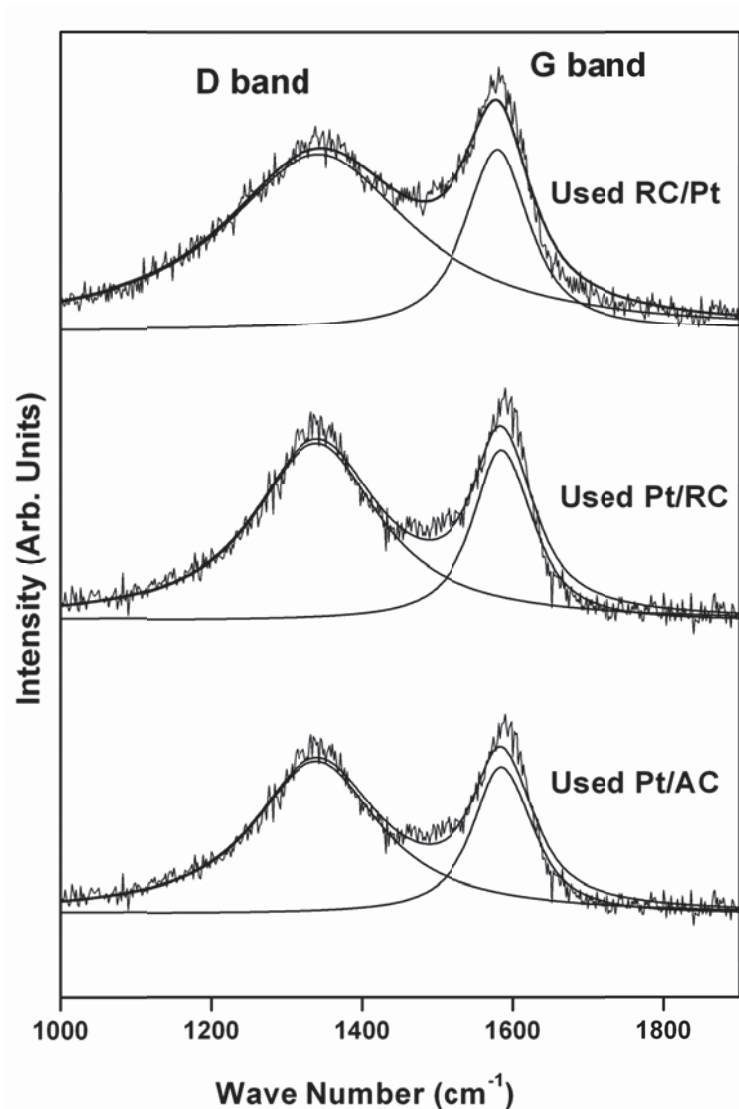
## Chapter 3

Fig 3.23 shows the SEM of used catalysts. Surface of each catalyst appears to be little smoothened and loose particles are still present on the surface. In case of Pt/AC and Pt/RC there is no remarkable change in the morphology. While in case of RC/Pt, some large pores appear to be formed.



**Fig. 3.23:** SEM micrographs of used (a) Pt/AC, (b) Pt/RC and (c) RC/Pt

Raman spectra of used catalysts are shown above in Fig. 3.24. These also do not shown any change when compared to that of fresh catalysts. Presence as well as intensity of G band and D band is not affected by the reaction environment. All these facts support the stability of catalysts in the harsh reaction conditions.



**Fig. 3.24:** Raman spectra of used Pt/Carbon catalysts

The stability of the catalysts against noble metal leaching was studied by analyzing the eluent after a typical two hour reaction. The ICP AES analysis of the eluents showed that only 0.39 , 0.48 and 0.60 of the original platinum loading is getting eluted out into the solution for Pt/AC, Pt/RC and RC/Pt catalyst respectively. These numbers indicate that the catalysts are quite stable against noble metal leaching



## ***Chapter 3***

---

### **3.3.3 Conclusion**

The supported noble metal catalysts with carbon as support prepared by impregnation route are found to be active for liquid phase decomposition of hydriodic acid. The catalysts were found to be stable in terms of structure of the support, noble metal elution, surface morphology and catalytic activity. Although the surface area of the catalyst (Pt/AC) is significantly higher than the Pt/Graphite catalyst with same metal loading (1 %), percentage conversion is lower. It indicates that the surface area of the support is not the only factor determining the activity of the catalyst. There may be several other factors which affect the activity of the catalysts along with the surface area of the support. One such factor is pore structure of the support, which will be explored in the next chapter.

# Chapter 4

## HI Decomposition over Platinum Catalysts Supported on porous Carbon Supports

### 4.1 Introduction

Surface area and porosity of the support used for dispersing the metal plays important role in the activity and stability of the catalyst. Also surface area of any material is directly associated with the porosity present. In this chapter we present carbon with varying porosity and surface area as support for platinum. Porous materials are classified as macroporous, mesoporous and microporous based on their pore size [139,140]. (Table 4.1)

S. No.	Type of Porosity	Pore Size (nm)	Example
1.	Macroporous	50	Porous Glasses
2.	Mesoporous	2-50	MCM-41, MCM-48
3.	Microporous	2	Zeolites, ZSM-5

**Table 4.1:** *Classification of porous materials on basis of their pore size*

## ***Chapter 4***

---

There are a number of methods that can be used for synthesis of porous materials like hydrothermal synthesis of zeolites, template synthesis of mesoporous silica materials etc. Porous silica with varying porosity is the most commonly prepared material by various methods. The reason for this is that silica structure can grow easily over various templates. The porosity of these structures can be varied by varying silica source, structure directing agent, pH of the medium, temperature etc.

Porous carbon is difficult to prepare as compared to silica because the structure evolution in carbon is more complicated as compared to silica. Therefore soft templating methods that are used for preparation of porous silica cannot be used for preparation of porous carbon. For carbon hard templating route or nanocasting route is employed where hard templates like silica are used as structure directing agents for formation of porous carbon [107,108].

In this chapter, synthesis of different platinum on porous carbon catalysts is reported, where the porous carbon supports are generated using hard template route. Platinum incorporation has also been carried out either at carbonization stage or by impregnation after complete preparation of carbon support. These catalysts were characterized and evaluated for liquid phase HI decomposition reaction.

### **4.2 Platinum/ Porous Carbon Catalyst**

This section contains details of Pt catalysts supported on mesoporous and microporous carbons. Mesoporous and microporous carbon support were prepared by hard templating route using mesoporous and microporous silica templates. Mesoporous silica was prepared by soft templating route while commercial microporous silica was

## ***Chapter 4***

---

used. These catalysts were characterized and evaluated for their catalytic activity and stability for liquid phase HI decomposition reaction.

### **4.2.1 Experimental**

#### **4.2.1.1 Preparation of Mesoporous silica**

**Materials Required:** Cetyl trimethyl ammonium bromide (CTAB) 29.52 g, Fumed Silica 18g, NaOH 3.096 g in 10 ml water, Tetra methyl ammonium hydroxide (TMAOH) 27ml, Nanopure water 360 ml.

**Procedure:** The hydrothermal synthesis of mesoporous MCM-41 molecular sieves was carried out as per the procedure described in literature [141]. CTAB was used as the structure directing or templating agent and fumed silica was used as silica source. The reaction gel was prepared by mixing the starting materials in stoichiometric proportion followed by vigorous stirring at room temperature. First of all CTAB solution was prepared by mixing CTAB in 87 ml of water with constant stirring. Then half of the fumed silica (9 g) was added to TMAOH along with 5 ml of NaOH solution. This solution was added drop by drop to CATB solution. Rest of the fumed silica was added to this mixture along with remaining water. The mixture was given a stirring of 1 hr. After which pH of the mixture was adjusted to 11.6 after which again 1 hr stirring was given. Then the gel was transferred into Teflon-lined stainless steel autoclaves with a typical filling level of ~ 30-50 and then allowed to crystallize under autogeneous pressure at 150 °C for 24 hours. The crystallized product was recovered by washing repeatedly with distilled water followed by filtration. The solid product was dried in an air oven at 180-

## **Chapter 4**

---

200 °C for 12 h. The sample thus prepared was subjected to calcination for removal of surfactant (template) water and other gaseous molecules. The heating was carried out in a tubular furnace under flowing nitrogen and/or oxygen atmosphere (60 ml min<sup>-1</sup>). The heating was carried out from room temperature to 550 °C with a heating rate of 2°min<sup>-1</sup>, with intermediate holding at 300 °C for 1 hour under N<sub>2</sub> flow. The sample was kept at 550 °C for seven hours (1 hours under N<sub>2</sub> flow and 5 hours under O<sub>2</sub> flow) followed by cooling under N<sub>2</sub> flow.

### **4.2.1.2 Preparation of Catalyst using hard templating Route**

During preparation of catalysts using mesoporous and microporous silica, two approaches for addition of platinum was followed, first where platinum was added along with the carbon source to the porous silica and another where platinum was loaded after the preparation of porous carbon.

For first approach of synthesis, 3 g of porous silica template (MCM-42 or Fumes Silica) was mixed with 3g Sucrose, 6.3 ml chloroplatinic acid (1% solution) and 8.7 ml of water, in a round bottom flask and stirred for 6h and then left standing overnight. The paste obtained was dried at 100 °C for 6h and then carbonized at 160 °C for another 6 h. The powder obtained was added to 2.4g sucrose and 15 ml water and whole process of stirring, drying and carbonisation was repeated. The powder obtained was calcined at 800 °C (heat rate 2 °C/min) in nitrogen flow for 3 h, and reduced in hydrogen flow at 300 °C for 3h. Subsequently, the resulting silica-platinum-carbon material was suspended in 25 ml of 40% hydrofluoric acid and stirred overnight at room temperature. Finally, the product was then filtered, thoroughly washed, and dried at 80 °C overnight. The sample

## ***Chapter 4***

---

prepared by this route using MCM-41 and fumed silica as template will be called as Pt/MCM-C and Pt/FS-C in further discussion.

For another approach of synthesis, 3g of porous silica template (MCM-41 or Fumed silica) was mixed with 3.75g Sucrose, 0.42g sulfuric acid and 15 ml of water, in a round bottom flask and stirred for 6 h and then left standing overnight. The paste obtained was dried at 100 °C for 6 h and then carbonized at 160 °C for another 6 h. The powder obtained was again mixed with 2.4g sucrose, 0.27g sulfuric acid and 15 ml water and whole process of stirring, drying and carbonization was repeated. The powder obtained was calcined at 800 °C (heat rate 2 °C/min) in nitrogen flow for 3 h. Subsequently, the resulting silica-carbon material was suspended in 25 ml of 40% hydrofluoric acid and stirred overnight at room temperature. Finally, the pure porous carbon was then filtered, thoroughly washed, and dried at 80 °C overnight and weighed. The yield of porous carbon prepared from MCM-41 (MCM-C) and Fumed silica (FS-C) is found to be 2.15g and 3.72g, respectively. The carbon support obtained was mixed with appropriate quantity of 1 wt% chloroplatinic acid solution (for final platinum loading in catalyst to be of 1 wt%) and stirred for 6 h and left standing overnight. The paste obtained is dried at 100 °C for 8h. The platinum loaded carbon samples hence obtained were reduced in hydrogen flow at 300 °C for 3 h. The samples prepared by this route using MCM-41 and fumed silica as template are referred as MCM-C/Pt and FS-C/Pt in further discussion

## ***Chapter 4***

---

### **4.2.1.3 Characterization of Catalysts**

The powder X-ray diffraction patterns of all the catalysts were recorded on Philips analytical diffractometer (using Ni-filtered Cu K $\alpha$  radiation). The surface morphology of the catalysts was studied using JEOL JSM-6360 scanning electron microscope. The BET surface area of the catalyst was obtained from physical adsorption of N<sub>2</sub> at -196°C, on a Quantachrome Autosorb - 1 instrument. These catalysts were also characterized for carbon structure by spatially resolved Raman scattering (Bruker Model MultiRAM) using 150 mW at laser head and 4 mW on the sample of 1064 nm line of Nd:YAG laser, detected with a liquid-nitrogen cooled high resolution charge coupled device (CCD) detector at 4 cm<sup>-1</sup> resolution. The catalysts were studied by XPS using SPECS surface analysis system to examine the oxidation state of platinum.

### **4.2.1.4 Activity and Stability**

All the four catalysts were evaluated for their catalytic activity for liquid phase HI decomposition and noble metal leaching employing a reflux type batch reactor. The details of this reactor are as given in Chapter 2. For this 250 mg of catalyst was added to 50 ml of 27% hydriodic acid solution in 250 ml round bottom flask. This flask was heated and the gas bubbling out through the two traps was collected in an inverted column and was analyzed using a gas chromatograph. After reaction, the HI decomposition was measured by means of titrating H<sup>+</sup> and I<sup>-</sup> ions using acid-base and iodometric titrations, respectively. The solution was filtered to separate the used catalyst and the eluent. The spent catalyst was characterized by XRD, Raman and SEM for their physical integrity and the eluent was analyzed using ICP-OES for the leached out platinum.

## **Chapter 4**

---

### **4.2.2 Results and Discussion**

#### **4.2.2.1 XRD**

The X-ray diffraction measurements were recorded in 10-80° 2 $\theta$  range. Fig. 4.1 shows XRD patterns recorded for different samples. All the XRD patterns show a broad peak centring on ~23° value. This is matching with that for the amorphous carbon materials. Pt/MCM-C and Pt/FS-C samples exhibit distinct peak at 39.7° conforming to platinum metal (JCPDS No. 04-0802). All other samples do not show any peak corresponding to platinum. This implies that during the first approach of synthesis by hard template route, the platinum particles get sintered during high temperature carbonization step, whereas they remain uniformly distributed in all other samples. The crystallite size as calculated by Scherrer equation indicate for 33 and 42 nm dimensions for platinum particles in Pt/MCM-C and Pt/FS-C samples, respectively.

#### **4.2.2.2 SEM**

Scanning electron microscopy was employed to compare morphology of the catalyst particles. SEM micrographs obtained for all the four catalysts samples are shown below in fig. 4.2 Pt/MCM-C (a) and MCM-C/Pt (b) catalysts show rough surface with lot of trough and crest like features but very few pore openings or particles. Surface morphology of these catalysts is quite different from the samples prepared using fumed silica as template, Pt/FS-C (c) and FS-C/Pt (d). Fumed silica based catalysts presents rough surface morphology with some loose particles. There are no visible macro pore openings for Pt/FS-C catalyst.



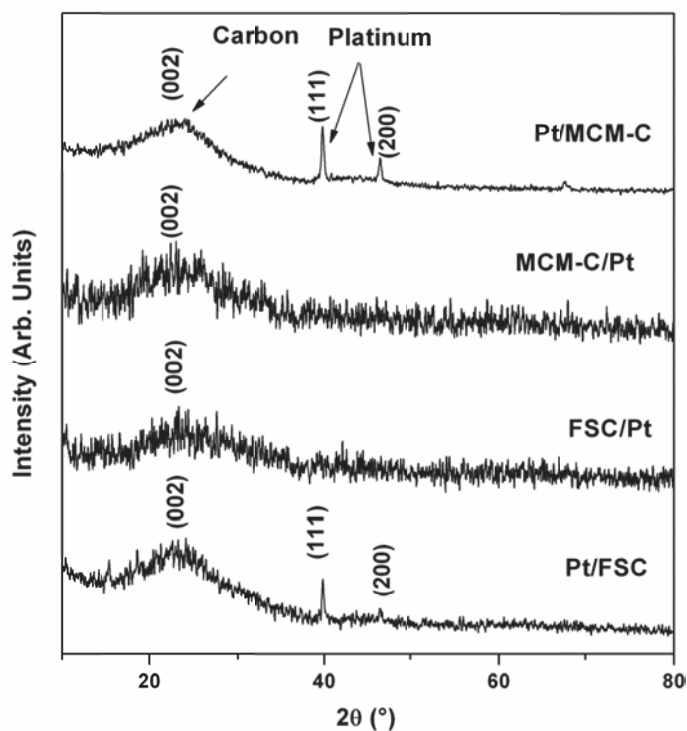


**Fig. 4.1:** XRD patterns for different catalysts

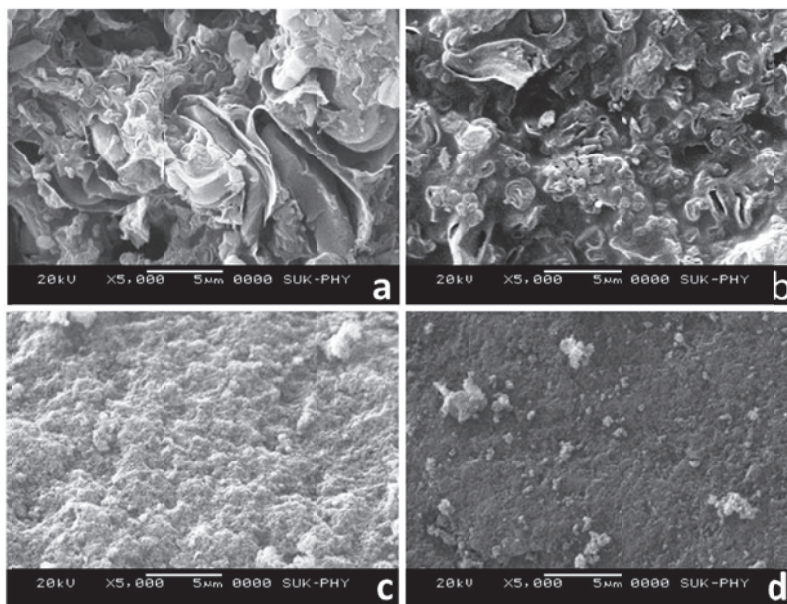


**Fig. 4.2:** SEM micrographs of different catalyst samples (a) Pt/MCM-C, (b) MCM-C/Pt (c) Pt/FS-C and (d) FS-C/Pt

## Chapter 4

### 4.2.2.3 Surface Area

Nitrogen adsorption isotherms were recorded at  $-196^{\circ}\text{C}$  temperature. The samples prior to recording of the isotherm were subjected to insitu evacuation at  $300^{\circ}\text{C}$  temperature for 12 h. The data obtained for different samples is compiled in Table 4.2. All four catalysts were found exhibit high surface area ranging from 700 to  $900\text{ m}^2/\text{g}$ . The catalysts prepared by using MCM-41 as the template showed a remarkable decrease in their surface area and pore volume as compared to the parent MCM-41 itself. This indicates towards infusion of carbon inside the MCM-41 pore but at the same time the porous nature is retained as indicated by the adsorption isotherm. Among Pt/MCM-C and MCM-C/Pt, catalysts first one shows lower surface area and pore volume.

Sample	Surface Area ( $\text{m}^2\text{g}^{-1}$ )	Pore Volume ( $\text{cm}^3\text{g}^{-1}$ )	Porosity
Pt/MCM-C	720	0.395	Meso
MCM-C/Pt-C	850	0.511	Meso
Pt/FS-C	800	2.658	Micro
FS-C/Pt	901	2.617	Micro

**Table 4.2:** Surface Area and Pore volume values of different catalyst samples

Fig 4.3 shows the adsorption desorption isotherms for both samples which has a hysteresis loop (type IV) which is indication of mesoporous nature of the sample. The pore size distribution for both the samples is shown in Fig 4.4 which shows the presence of pores around 3 nm size.

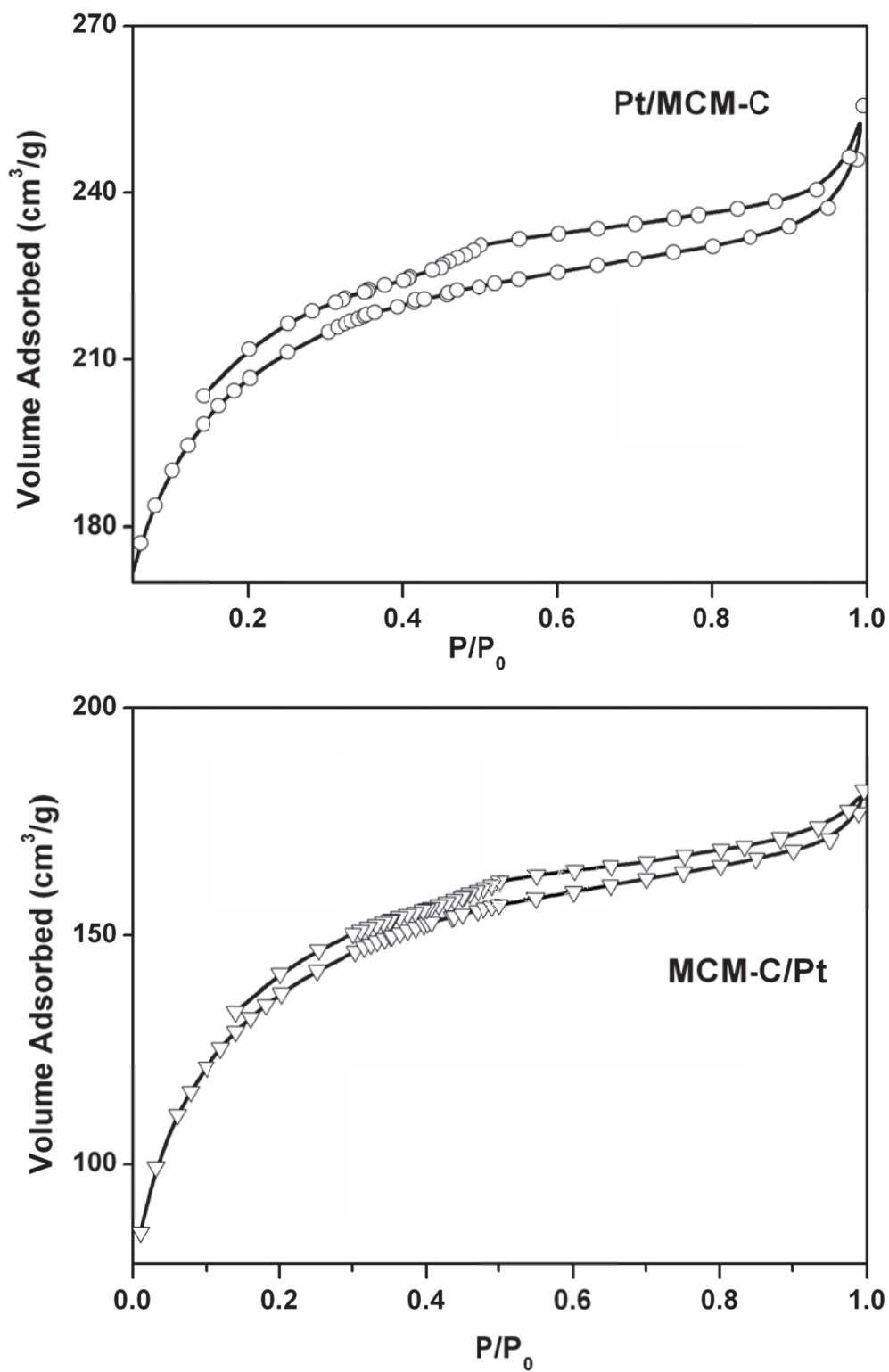


Fig. 4.3: Adsorption desorption isotherms for mesoporous catalyst samples

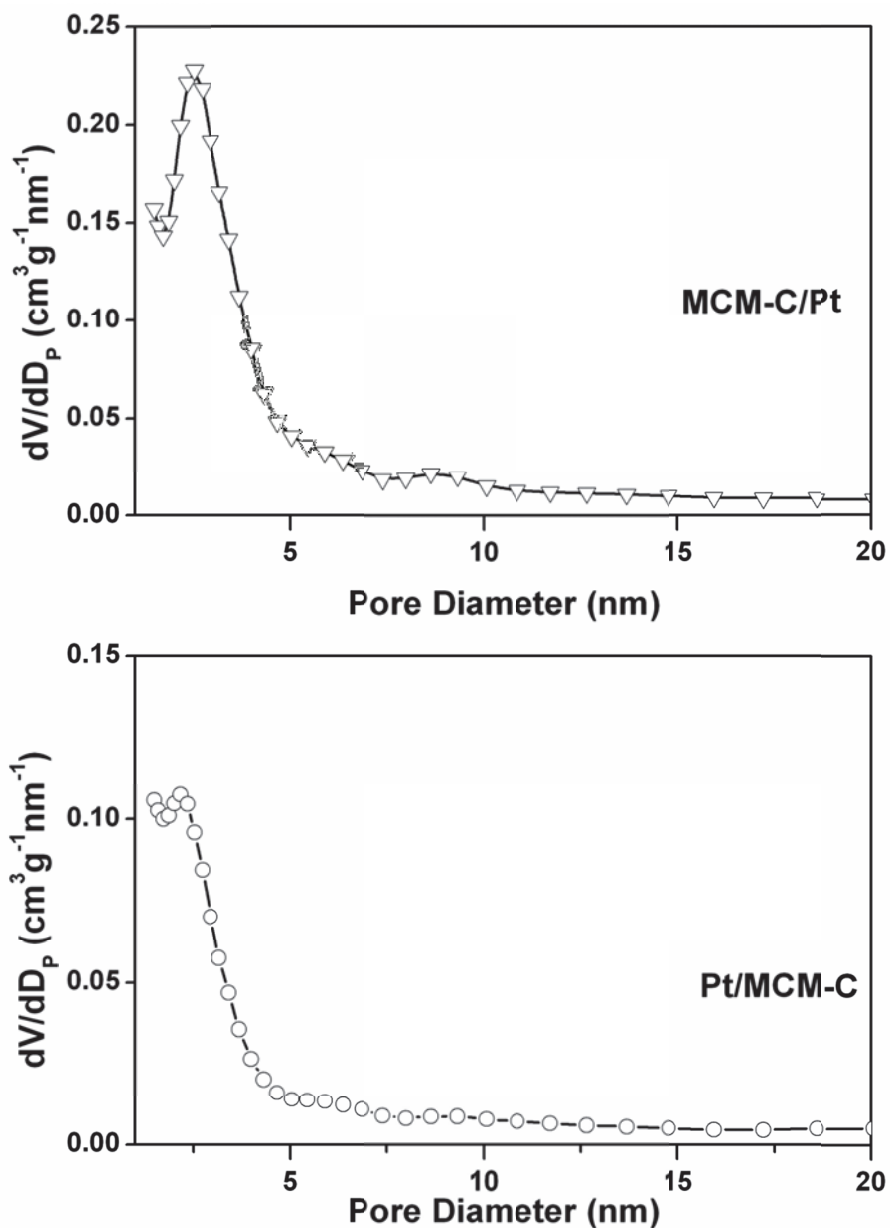


Fig. 4.4: Pore size distribution curve for mesoporous catalyst samples

Sample prepared using fumed silica as template (Pt/FS-C) exhibits both high surface area and also high pore volume. The nature of the isotherm indicates for presence of micropores in these samples. Also Pt/FS-C is having lower surface area as compared to FS-C/Pt, similar to that of the case of MCM-C based catalysts.

## Chapter 4

---

### 4.2.2.4 Raman Spectroscopy

Raman spectroscopy was used for studying the nature of carbon supports. Fig 4.5 shows the Raman spectra of all four porous carbon catalysts (Pt/MCM-C, MCM-C/Pt, Pt/FS-C and FS-C/Pt). The spectra show that the catalysts show well defined G-band along with a very broad D-band. The presence of narrow peak around  $1580\text{ cm}^{-1}$ , signifies presence of  $\text{sp}^2$ -bonded carbon atoms in a two dimensional hexagonal lattice, similar to graphitic carbon species. Broad D-band is the result of defects within the carbon textures and suggests for existence of disordered graphitized domains.  $I_G / I_D$  ratios for all four catalysts, as given in Table-4.2, are observed to be close to 1 and found to be in good agreement with similar mesoporous carbon materials as reported in literature [142,143].  $I_G / I_D$  ratios obtained here are almost double of the values reported for mesoporous carbons with semi graphitized walls synthesized by Wu et al [144] using methane as carbon precursor at  $1000^\circ\text{C}$ . Also, the in-plane crystallite size ( $L_a$ ) is calculated from  $I_G / I_D$  ratio using equation shown below, as reported by Pimenta et al [145] and the calculated values are given in Table 4.3. The  $L_a$  values obtained are found to be in multiple of hundreds of nm. Though there is no direct evidence of incorporation of Pt into the carbon chain from tell tale shift in G-band value, the crystallite size of Pt (30-40 nm obtained from XRD) may be the contributing factor for such high  $L_a$  values.

$$L_a (nm) = (2.4 \times 10^{-10}) \lambda_{laser}^4 \left( \frac{I_G}{I_D} \right) \quad \dots\dots 4.1$$

These data indicate for long range ordering of the graphitized carbon with co-existence of defects. The long range ordering and defects both can be attributed to presence of noble metal incorporated on the carbon support.

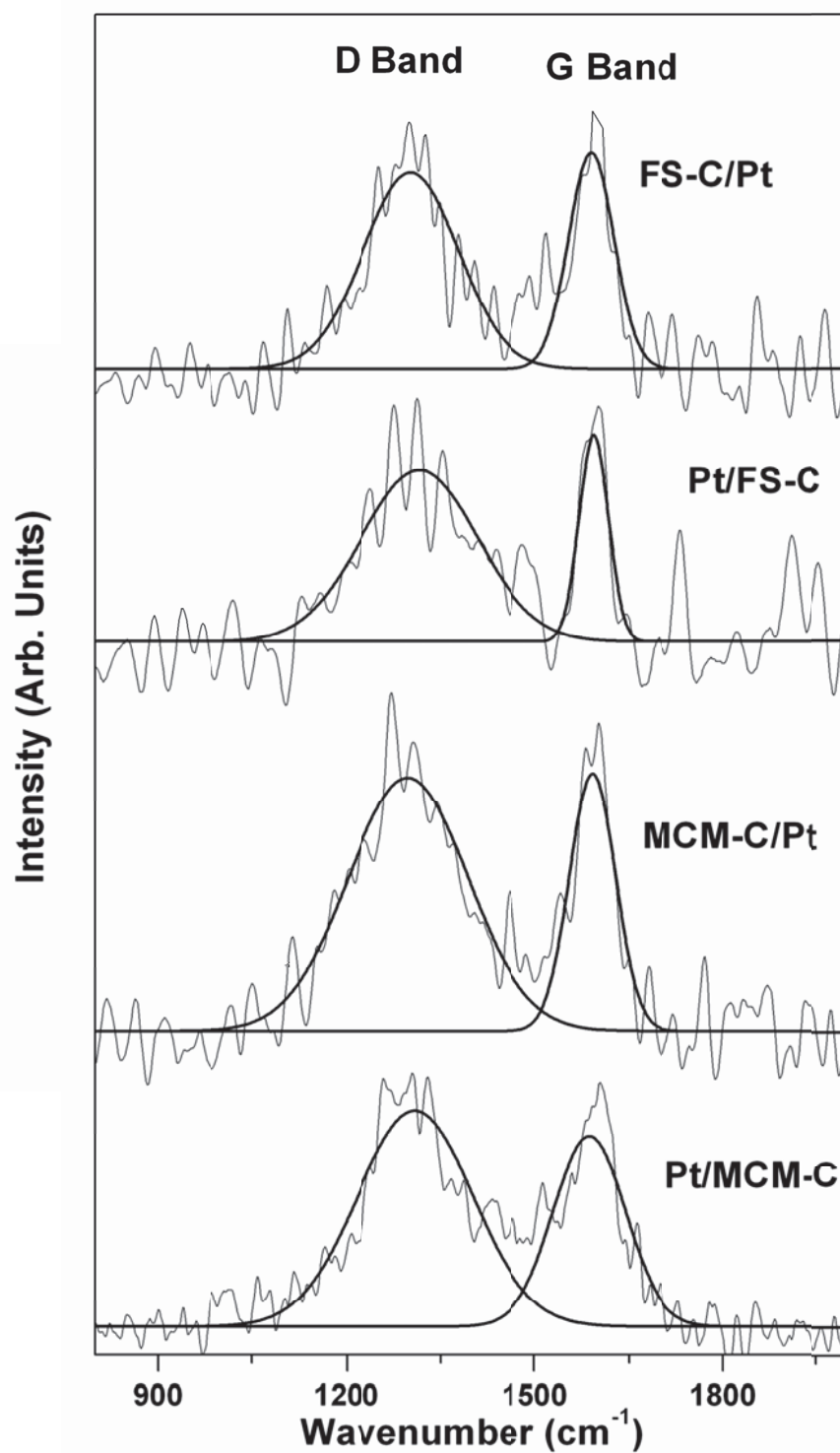


**Fig. 4.5:** Raman spectra of different catalyst samples

S. No.	Sample	$I_G/I_D$	$L_a$ (nm)
1	Pt/MCM-C	0.89	274
2	MCM-C/Pt	1.06	326
3	Pt/FS-C	1.39	427
4	FS-C/Pt	1.15	354

**Table 4.3:**  $I_G/I_D$  and calculated  $L_a$  values of different catalyst samples

#### 4.2.2.5 X-ray Photoelectron spectroscopy

Surface compositions of the catalysts were analyzed using X-ray photoelectron spectroscopy. The XPS measurements for all four samples were carried out in constant analyzer energy mode using Al  $K_\alpha$  radiation (1486.6 eV). The survey scans of all catalysts shows peaks in the spectral regions that correspond to carbon, platinum and oxygen only. Survey scan for one of the catalyst (Pt/MCMC) is given below in Fig 4.6. Here no peak is observed in the spectral region of Si which confirms that silica is removed completely by HF treatment during synthesis.

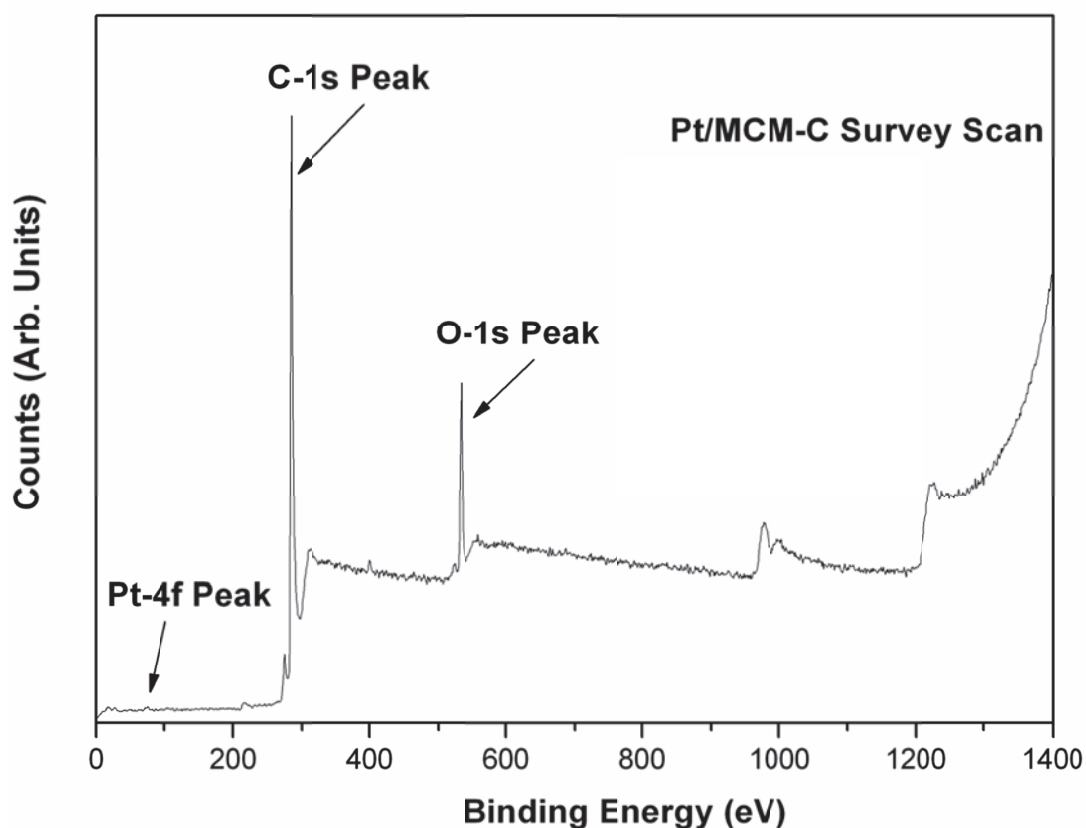


**Fig. 4.6:** XPS survey scan for Pt/MCM-C catalyst

Fig 4.7 shows the 4f region of Pt for all the four catalysts. Peaks can be deconvoluted into doublet ( $4f_{7/2}$  and  $4f_{5/2}$ ) with respective binding energies of around 71.4 eV and 74.6 eV. These binding energy values correspond to metallic state of platinum [134-135]. The peaks obtained were symmetric in nature, hence indicating for the presence of single platinum species ( $\text{Pt}^0$ ). Broadening of the peak may be due to either the presence of platinum in amorphous phase or due the platinum-support interaction. Thus XPS study confirms the complete reduction of Platinum to  $\text{Pt}(0)$  state which is essential for its catalytic activity.



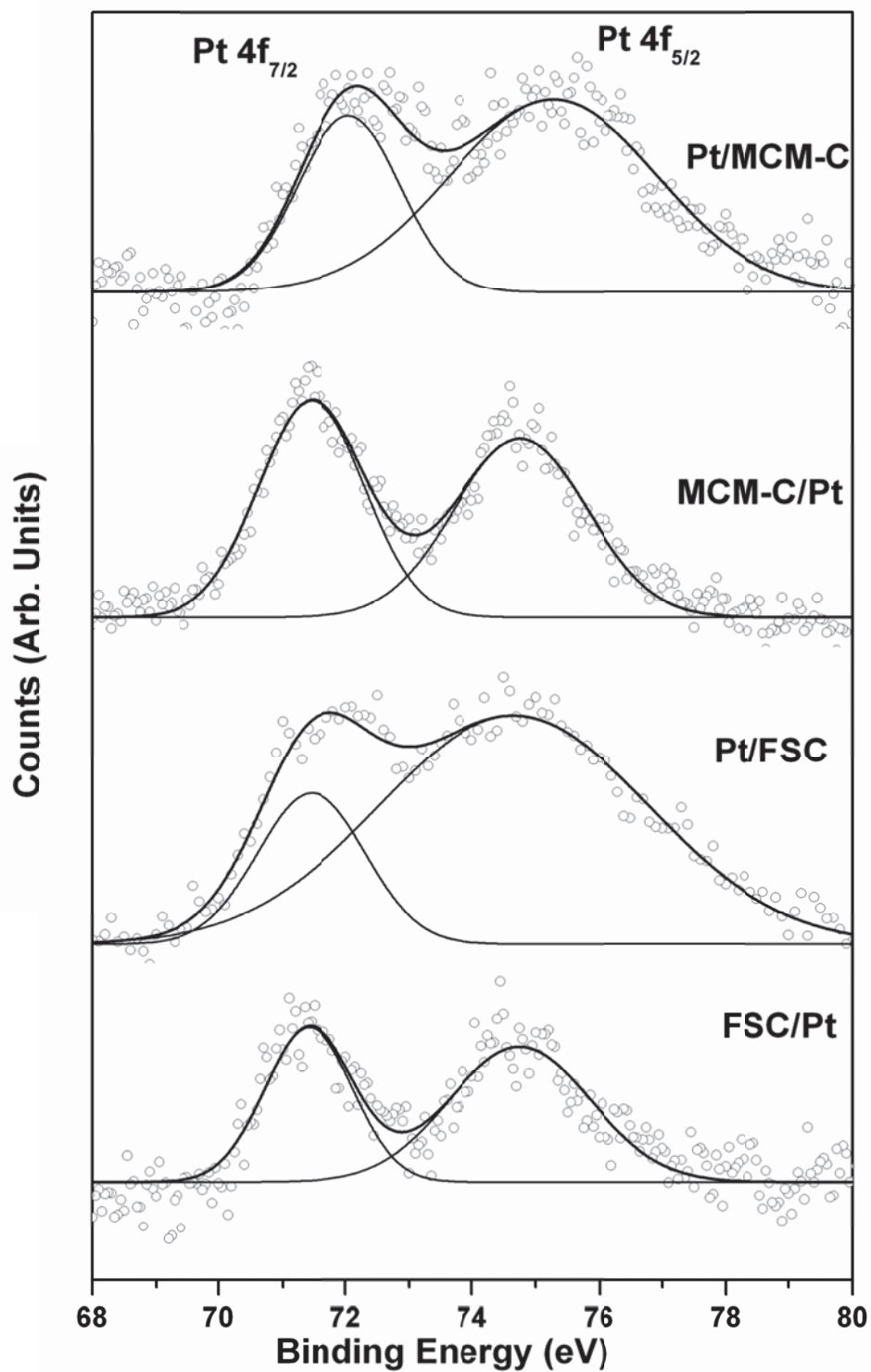
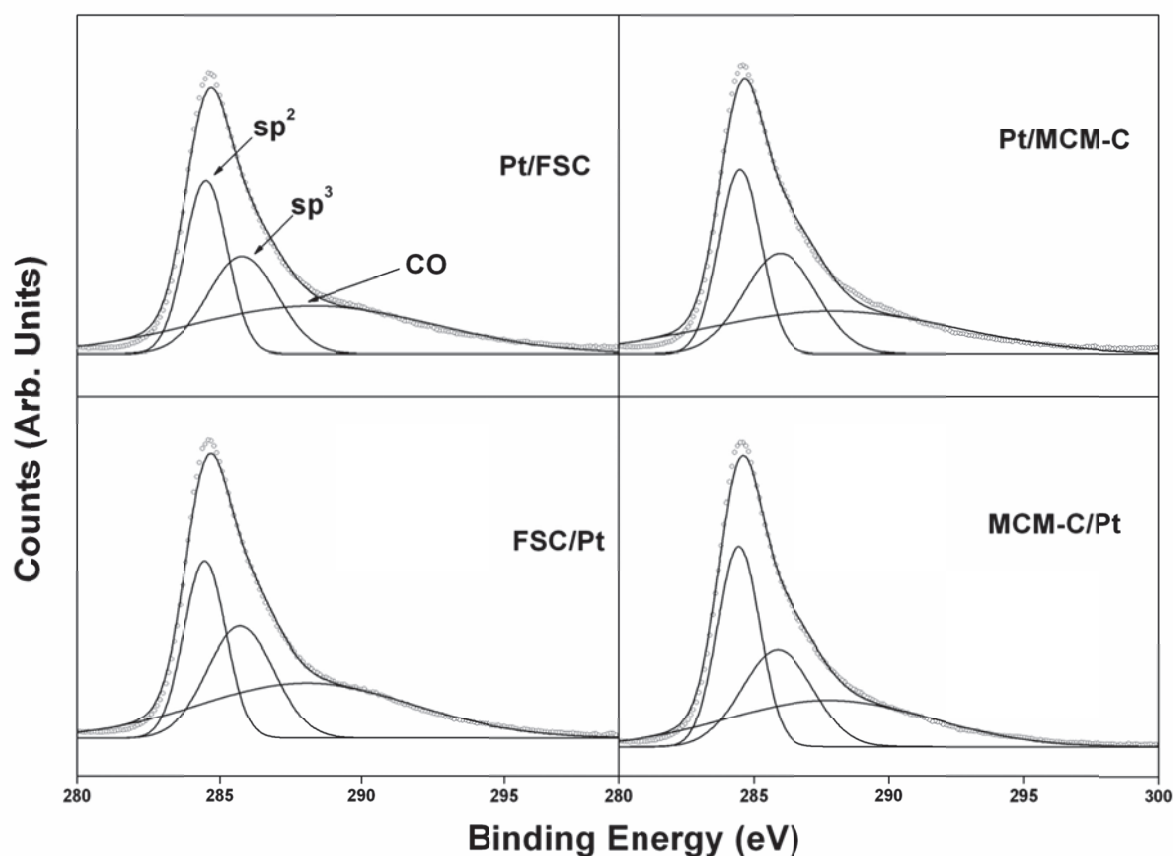


Fig. 4.7: XPS spectra of Pt-4f spectral region of all four catalysts

## Chapter 4

Fig 4.8 shows the spectral region corresponding to C-1s spectral region; it can be fitted to three peaks with binding energy 284.3, 285.4 and 287.9 eV. These peaks correspond to  $sp^2$ ,  $sp^3$  and CO (Carbon bonded to oxygen, C-O or C=O) types of carbon [134]. Therefore the oxygen present is associated with carbon and not platinum. Also presence of  $sp^2$  hybridized carbon is in confirmation with the results of Raman. Carbon must be present in  $sp^2$  hybridized state for formation of this type of porous structure.



**Fig. 4.8:** XPS spectra of C-1s spectral region of all four catalysts

## Chapter 4

### 4.2.2.6 Catalytic activity of the catalyst

The catalytic activity of all the catalysts used in this study for HI decomposition using the setup as given in Chapter 2 is as given in Table 4.4. Percentage conversions as calculated using  $H^+$  titration and  $I^-$  titration are found to be in good agreement. The blank solution without catalysts yields HI conversion of ~2.8% after 2 h of refluxing. Compared to this, Pt/FS-C and FS-C/Pt catalysts yielded a conversion in 6-7% range. The platinum/carbon catalysts based on MCM-41 hard template (Pt/MCM-C and MCM-C/Pt) exhibit best catalytic activity with HI conversion over 17%.

S. No.	Catalyst	% Conversion	Pt in eluant	
			Concentration ( $\mu g/l$ )	% of original Pt loading
1.	Blank	2.8	---	---
2.	Pt/MCM-C	17.0	39.8	0.398
3.	MCM-C/Pt	17.7	59.1	0.591
4.	Pt/FS-C	6.5	65.7	0.657
5.	FS-C/Pt	6.5	80.7	0.807

**Table 4.4:** Percentage conversion and platinum leaching values for different catalysts

Although Pt/FS-C catalyst has surface area and platinum particle size similar to Pt/MCM-C catalyst its catalytic activity is still very low. Among, Pt/MCM-C and MCM-C/Pt catalysts the activity remains similar despite of difference in their surface area, pore volume and platinum particle size. Only similarity between these two catalysts is their surface morphology and mesoporous nature of the pores. This indicates for the vital

## Chapter 4

---

impact of surface morphology and pore dimensions on the catalytic activity for HI decomposition reaction. This is expected due to large size of iodine moiety, which has to be removed for smooth functioning of the catalyst.

### 4.2.2.7 Stability of the Catalyst

The analysis of the eluent obtained after two hour refluxing was carried out using ICP-OES technique for leaching of noble metal from the platinum carbon catalysts prepared in this study. The data obtained is presented in Table 4.4. It is obvious that platinum leaching is very limited. In general all the catalysts have good retention of the noble metal within the carbon matrix and Pt/MCM-C catalyst is found to be the most stable. Also it was observed that the catalyst prepared through first approach shows less platinum leaching (both in case of MCM-C as well as FS-C). It may be due the fact that platinum becomes part of carbon structure during carbonization step.

XRD pattern recorded for the samples after the stability studies are shown in Fig. 4.9. The XRD pattern for remain similar to original samples with broad peak at  $\sim 23^\circ$  2theta value corresponding to the amorphous carbon. XRD pattern for used MCM-C/Pt catalyst remain exactly same as for the original samples. For Pt/MCM-C and Pt/FS-C, change is observed in the peak corresponding to platinum at  $\sim 39.6^\circ$  value for other samples. This peak is drastically reduced for Pt/MCM-C and Pt/FS-C catalysts. Since platinum leaching is very low, therefore this reduction in peak intensity must be due to disintegration of larger particles into smaller entities and their redistribution over the carbon support. FS-C/Pt catalyst shows a different kind of behaviour with appearance of a peak at  $39.6^\circ$ , indicating for the growth of noble metal particle in this particular catalyst.

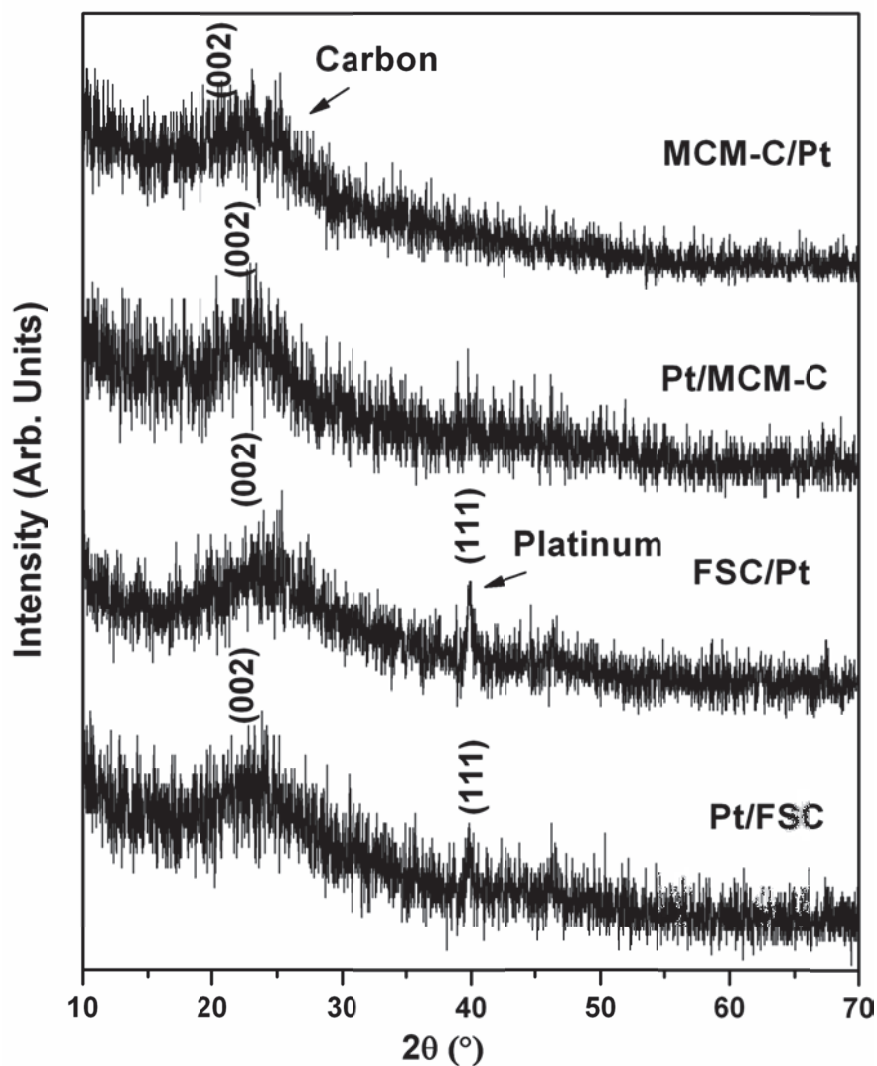


**Fig. 4.9:** XRD pattern of used catalyst samples

Surface morphology of the used samples was analyzed using scanning electron microscopy and is shown in Fig. 4.10. Catalysts prepared using fumed silica as template (Fig. 4.10a and 4.10b) are found to retain morphological features similar to the fresh catalysts. The catalysts prepared using MCM-41 as template, Pt/MCM-C (Fig. 4.10 c) and MCM-C/Pt (Fig. 4.10d), show slight change in surface morphology with over all smoothening of the features.

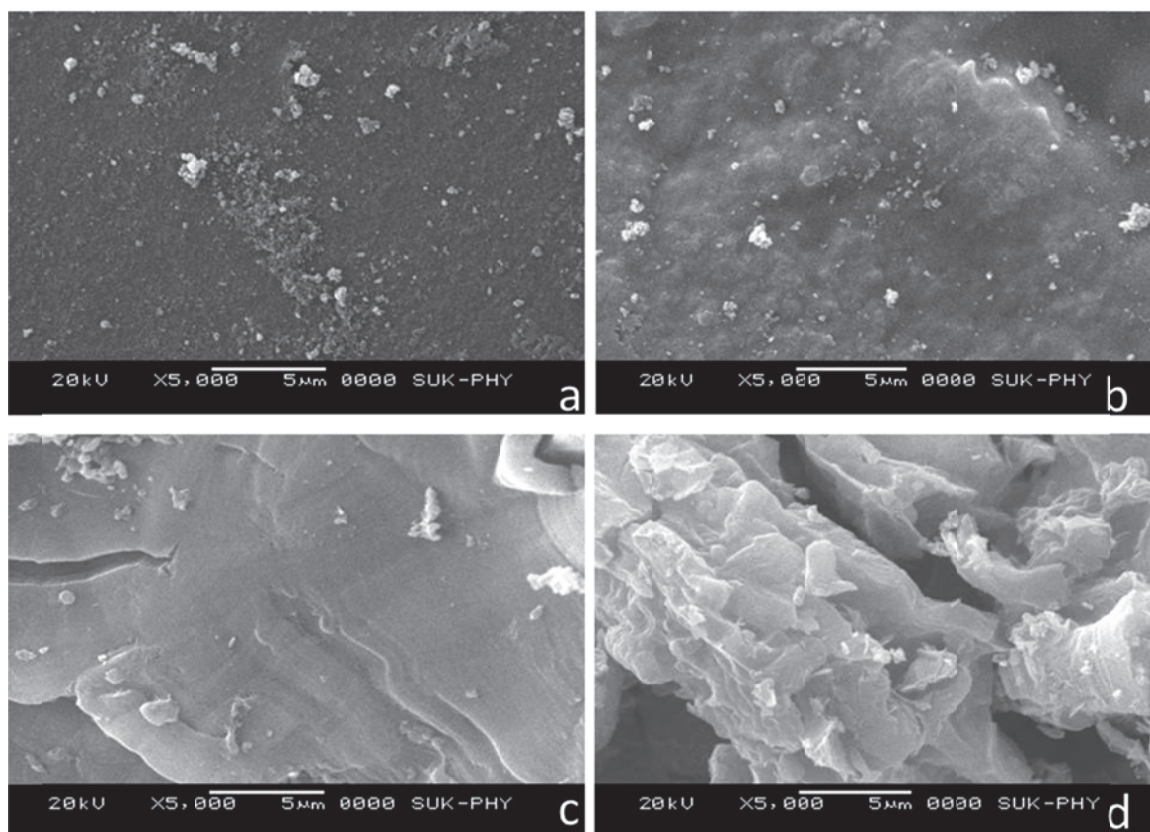


**Fig. 4.10:** SEM micrographs of used catalyst samples (a) Pt/MCM-C, (b) MCM-C/Pt (c) Pt/FS-C and (d) FS-C/Pt

Used mesoporous carbon based catalysts were also characterized by N<sub>2</sub> adsorption. Fig. 4.11 shows the adsorption desorption isotherm for one of the catalyst (MCM-C/Pt) both in fresh as well as used form. There was no change in the nature of isotherm as well as the hysteresis loop, which indicate that the catalyst retain mesoporous nature even after being used in the harsh reaction conditions.

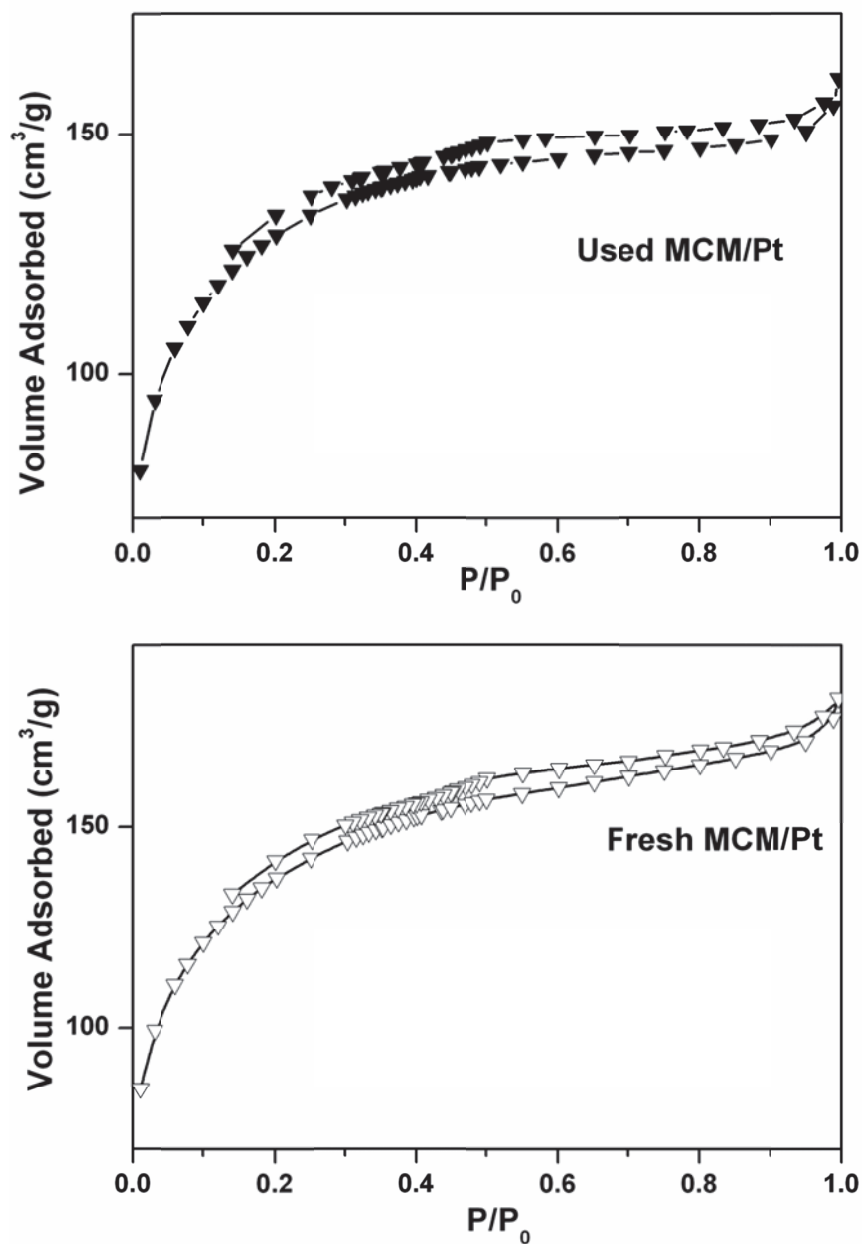


**Fig. 4.11:** Adsorption-desorption isotherms of fresh and used MCM-C/Pt catalyst

Raman spectra for the used samples as shown in Fig. 4.12 do not show much variation as compared to original samples. The presences of graphene like basic units are retained after HI decomposition. In general  $I_G/I_D$  ratio shows only marginal decrease for all the samples. (Table 4.5). Only Pt/FS-C catalyst with high degree of ordering ( $I_G/I_D =$

1.39) for original sample has a dramatic decrease in  $I_G/I_D$  ratio (0.95). Still the ratios remain around 1 for all samples for retention of graphene like carbon framework.

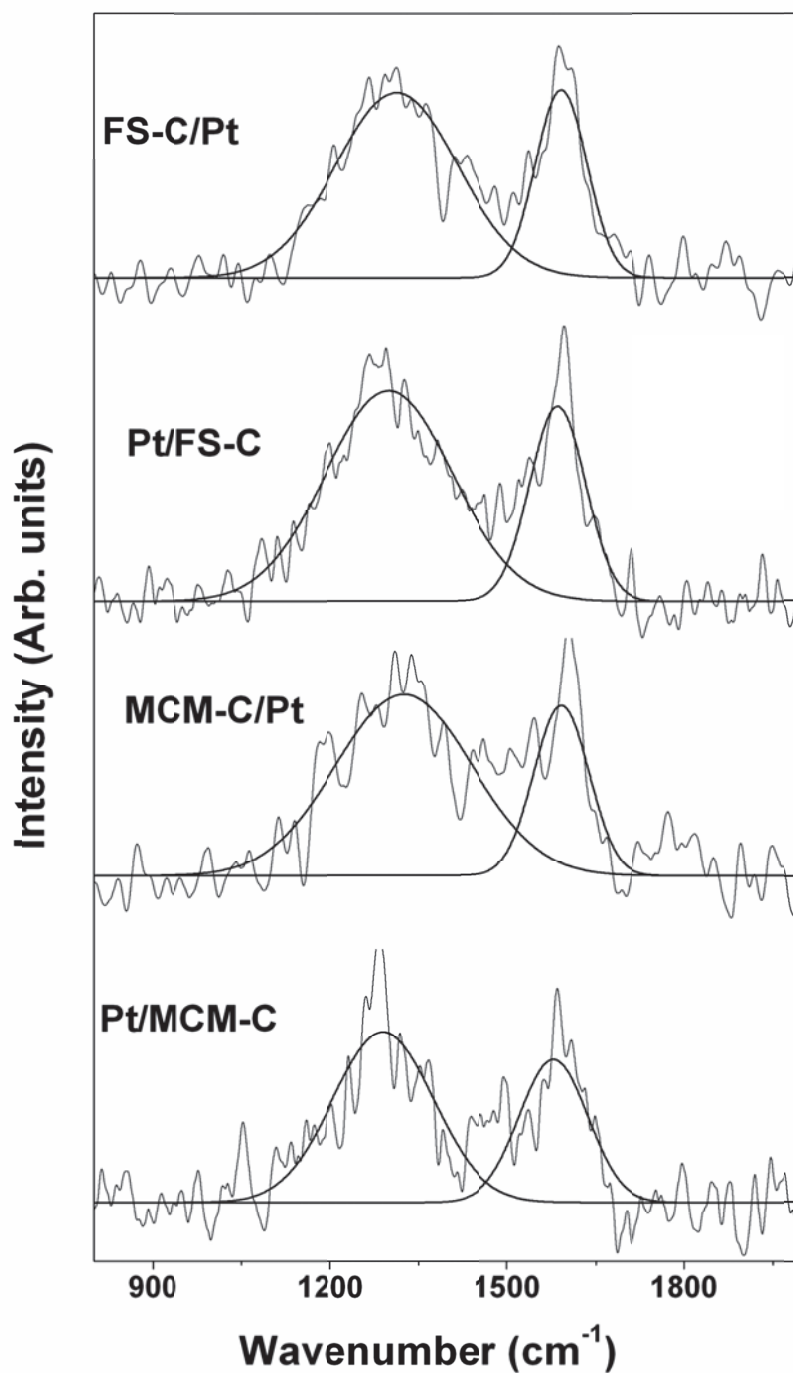


**Fig. 4.12:** Raman spectra of Used catalyst samples



S. No.	Catalyst	Fresh Sample		Used Sample	
		I <sub>G</sub> /I <sub>D</sub> ratio	L <sub>a</sub> (nm)	I <sub>G</sub> /I <sub>D</sub> ratio	L <sub>a</sub> (nm)
1.	Pt/MCM-C	0.89	274	0.85	262
2.	Pt/FS-C	1.39	427	0.95	292
3.	MCM-C/Pt	1.06	326	0.97	298
4.	FS-C/Pt	1.15	354	1.05	323

**Table 4.5:** Raman data and calculated in-plane crystallite size for different samples.

### 4.2.3 Conclusion:

Porous carbon supports were prepared using MCM-41 and fumed silica based hard templates and catalysts supported on these supports were found to be stable under liquid phase HI decomposition conditions. The efficiencies of these materials for HI decomposition reaction were found to be dependent on the structural nature of the porous carbon and their surface morphologies. Both the catalysts prepared using MCM-41 as template with platinum incorporation before and after carbonization stage are found to be effective catalysts for HI decomposition reaction and are found to be stable under the reported reaction conditions. Catalysts prepared by using fumed silica as template are less active as compared to other catalysts in spite of having high surface area. This difference in activity is attributed to the type of porosity, micropores in this case. Also step at which platinum is added plays role in stability against platinum leaching, catalysts where platinum precursor is added before carbonization are more stable against platinum leaching.

## ***Chapter 4***

---

### **4.3 Platinum/ Mesoporous Carbon Catalyst**

Mesoporous carbon support is found to be having advantage over micropores in terms of activity as well as stability as discussed in previous section of this chapter. In this section we will further explore the effect of size of mesopores. For this purpose mesoporous silica with larger pore sizes (SBA-15 type material) was used for synthesis of mesoporous carbon support.

#### **4.3.1 Experimental**

##### **4.3.1.1 Preparation of Mesoporous silica**

Synthesis of template i.e. mesoporous silica was carried out by using following chemicals Pluronic P123, Cetyl trimethylammonium bromide (CTAB) and Tetra ethyl ortho silicate (TEOS) using a method as described in literature[146]. For synthesis of mesoporous silica Poly-(ethylene glycol)–poly-(propylene glycol)–poly-(ethylene glycol) block copolymer (P123, average molecular mass 5800, Aldrich) was used as the structure directing or templating agent and tetra ethyl ortho silicate (TEOS) was used as silica source. Four grams of P123 was dissolved in in a mixture of 30 g of water and 90 g of 2M HCl with continuous stirring. After which 1.4 g of 25 % aqueous solution of Cetyl trimethylammonium bromide (CTAB) and 11.84 g of TEOS was added to the mixture. This mixture as stirred for 20 h at room temperature after which it was transferred to a polypropylene bottle, sealed and kept at 100 °C for 24 h followed by cooling to room temperature. After cooling the mixture was filtered, washed several times with deionized water and ethanol to remove excess template. For calcination the mixture was heated up

## **Chapter 4**

---

to 540°C at a heating rate of 3°C/min under N<sub>2</sub> atmosphere. After which the sample was kept at this temperature for 3 hours under N<sub>2</sub> flow and 2.5 hours under N<sub>2</sub>+O<sub>2</sub> mixture (4:1) followed by cooling under N<sub>2</sub> flow.

### **4.3.1.2 Preparation of Catalyst using hard templating Route**

For the synthesis of catalyst 2 g of the prepared silica template was mixed with 2 g of sucrose and 4.2 ml chloroplatinic acid (1% solution) in 5.8 ml of water in a round bottom flask and stirred for 6 h and left overnight. The paste obtained in this process was first dried at 100°C for 6 h and then carbonized at 160°C for another 6 h. The powder thus obtained was added to 1.6 g sucrose in 10 ml of water. After which the process of stirring and drying was repeated. The powder so obtained was heated at 800 °C under Nitrogen flow for 3 h. Subsequently noble metal was reduced by heating under hydrogen flow at 300 °C for 3 h. After reduction of noble metal, removal of silica was carried out by suspending the mixture in 20 ml of 40% hydrofluoric acid and stirring overnight at room temperature. The final product was filtered, washed thoroughly several times and dried at 80 °C and it is called as Pt/SBA-C in subsequent discussion.

### **4.3.1.3 Characterization of Catalysts**

The powder X-ray diffraction patterns of fresh as well as used catalysts were recorded on Philips Analytical Diffractometer in the range 20 to 70 °(Using Ni filtered Cu K $\alpha$  radiation). The surface morphologies and particle size were studied using Siron AIS 2100 and Zeiss Scanning electron microscope and Transmission Electron Microscope. The BET surface area of the catalysts by N<sub>2</sub> adsorption method and noble metal dispersion by CO chemisorption was determined by using Micromeritics ASAP 2010 Surface Area and

## Chapter 4

---

Porosity Analyser. XPS measurements were carried out using XPS system by SPECS, Germany using Al X-ray. The amount of noble metal in the reflux was determined by using Horiba Jobin Vyon JY 2000 ICP-AES.

### 4.3.1.4 Activity and Stability

Pt/SBA-C catalyst was evaluated for its activity and stability using the same reactor as given in Chapter 2. For a typical study 250 mg of catalyst was heated with 50 ml of 27% hydriodic acid solution in 250 ml round bottom flask up to 120°C. After the reaction the HI decomposition was measured by change in H<sup>+</sup> and I<sup>-</sup> ions concentration using titration. After the reaction the catalyst was filtered, washed, dried and used for its characterization by XRD, surface area and SEM etc. The solution was analyzed using ICP-OES for the leached out platinum.

### 4.3.2 Results and Discussion

#### 4.3.2.1 XRD

The X-ray diffraction patterns were recorded in 10 to 70° 2θ range on Philips Analytical Diffractometer (using Ni-filtered Cu-Kα radiation). Fig 4.13 shows the XRD pattern of the catalyst which has a broad peak centring at 23°, which is characteristic of amorphous carbon. The XRD pattern also exhibit a peak at 39.7° conforming to platinum metal (JCPDS No. 04-0802).

Crystallite size  $\tau$  of platinum was calculated from the Scherrer formula

$$\tau = \frac{0.9\lambda}{\beta \cos \theta} \quad \dots\dots 5.2$$

## Chapter 4

where,  $\lambda$  is the X-ray wavelength,  $\theta$  is the Bragg angle(in radians) and  $\beta$  is the full width at half maximum of the diffraction peak (in radian).

Crystallite size calculated from above equation was found to be around 6 nm.

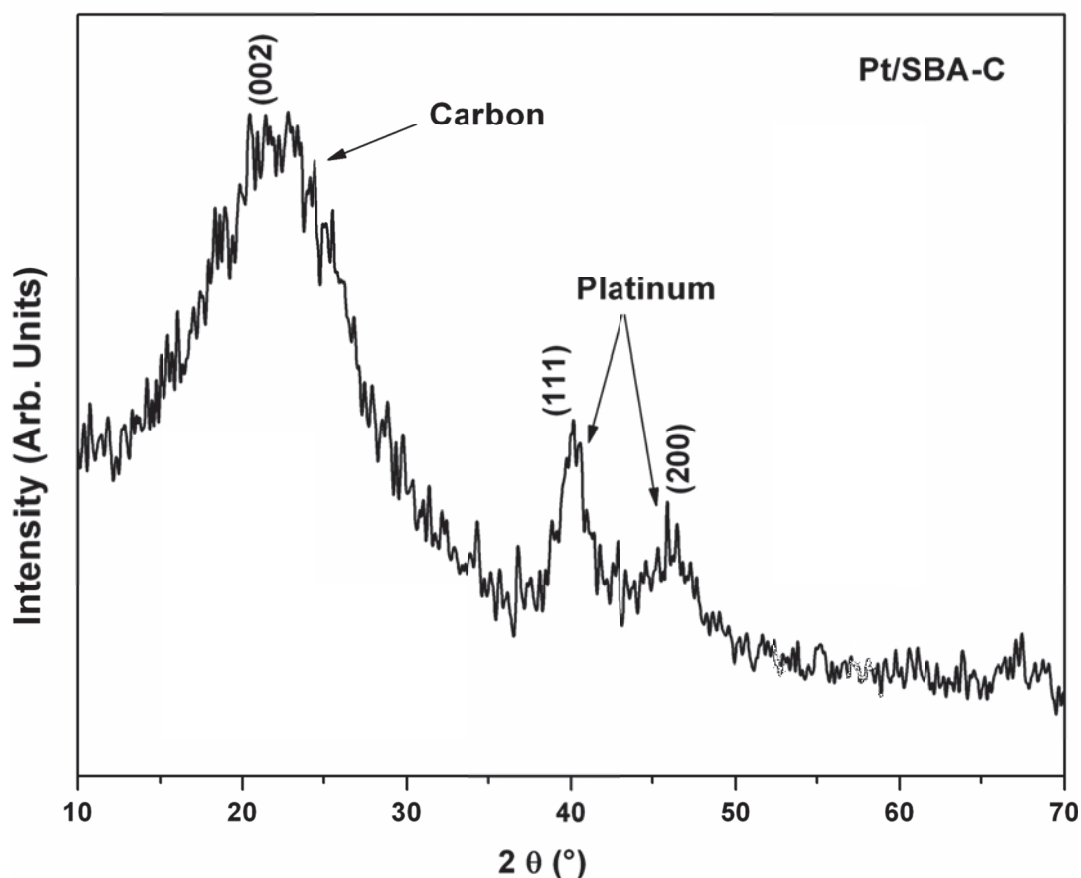


**Fig. 4.13:** XRD pattern of Pt/SBA-C catalyst

### 4.3.2.2 SEM

Surface morphology of the catalyst was observed using Scanning Electron Microscopy (SEM). Fig. 4.14 shows the SEM images of Pt/ SBA-C (at two different magnifications) catalyst which show rough surface with open pores all over the surface of the catalyst.

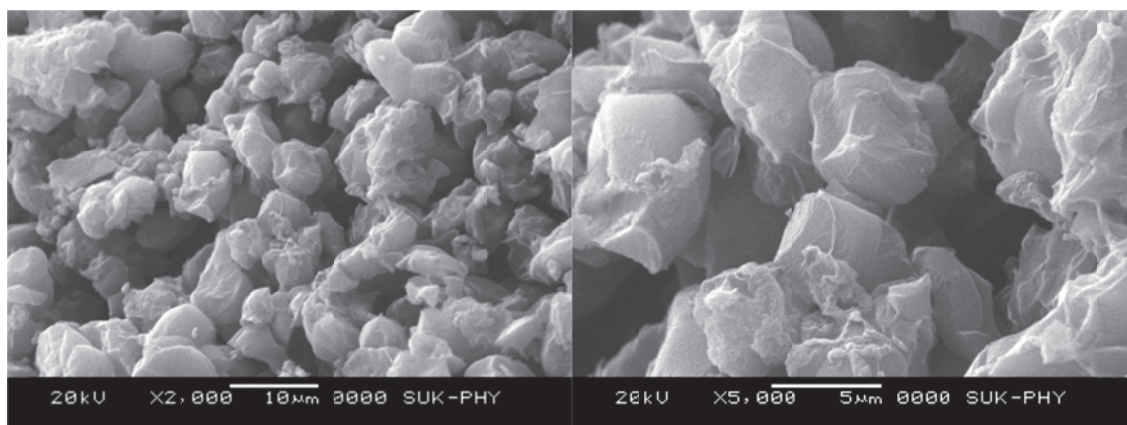


**Fig. 4.14:** SEM micrographs of Pt/SBA-C catalyst

Fig 4.15 shows high resolution FEG-SEM micrograph, it clearly showed well dispersed particles of platinum (white dots) over the support.

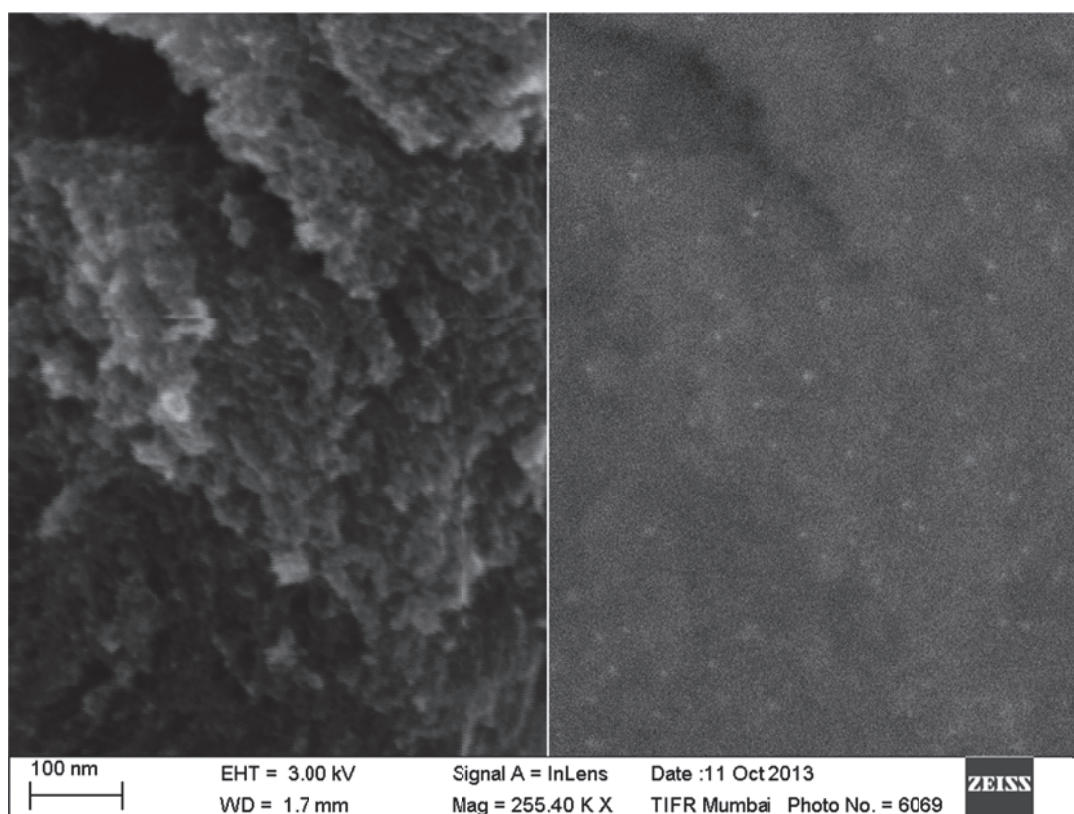


**Fig. 4.15:** FEG-SEM images of Pt/SBA-C catalyst.



## Chapter 4

---

### 4.3.2.3 TEM

Platinum particles can be easily seen in TEM images. Fig. 4.16 shows the TEM image of the Pt/SBA-C sample, which clearly shows highly dispersed platinum particles over the support.

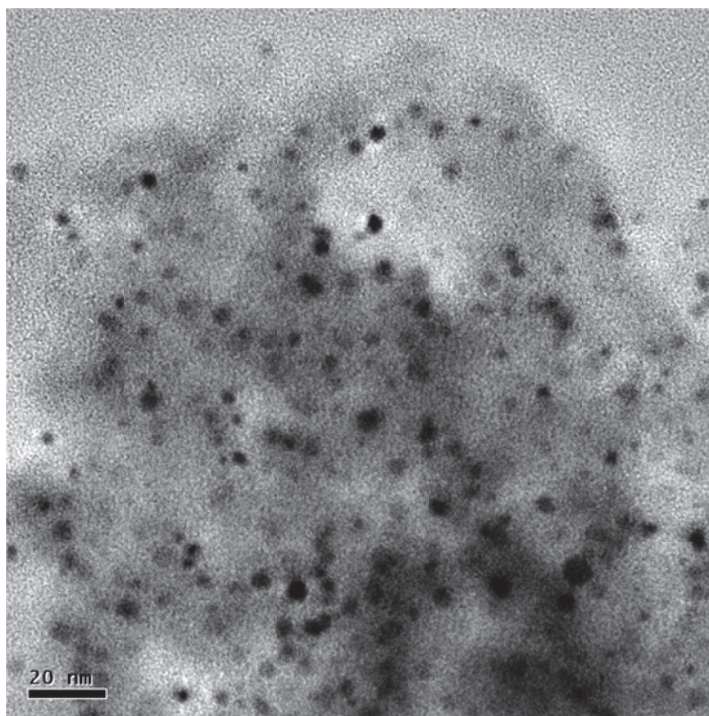


**Fig. 4.16:** *TEM image of Pt/SBA-C catalyst*

The analysis of TEM micrographs suggests that the Platinum particles are almost spherical. Fig. 4.17 shows the particle size distribution where diameter was measured for than 150 randomly selected particles in enlarged TEM images. It shows that most of the particles ( 80 ) are in the range of 4 to 7 nm with an average of around 6 nm which is in very good agreement with the size calculated from XRD. Fig 4.18 shows the SAED pattern of platinum particle which is indexed as (111), (200) reflections of fcc structure of platinum.

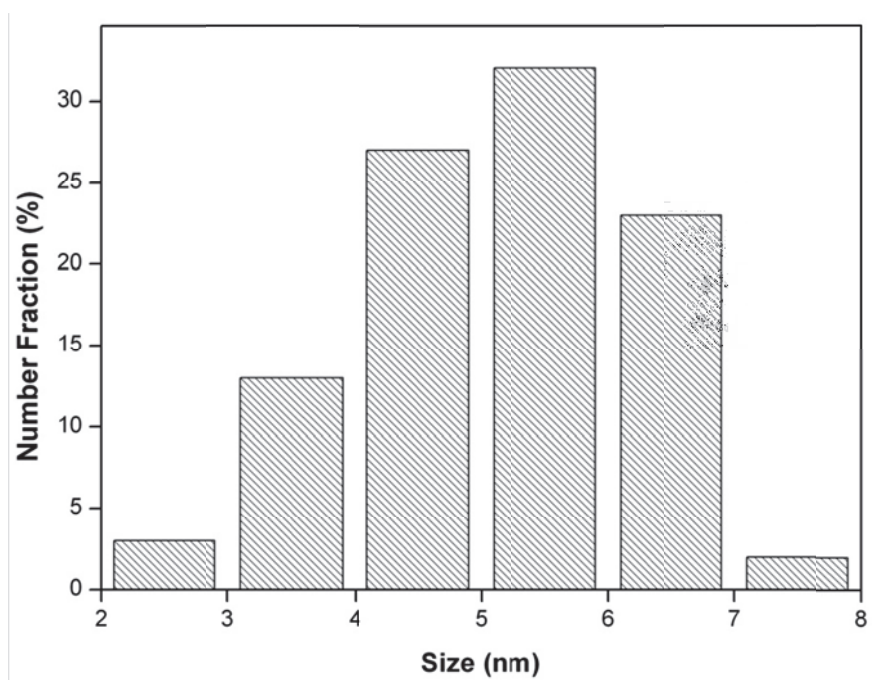


**Fig. 4.17:** Particle size distribution of Pt/SBA-C catalyst

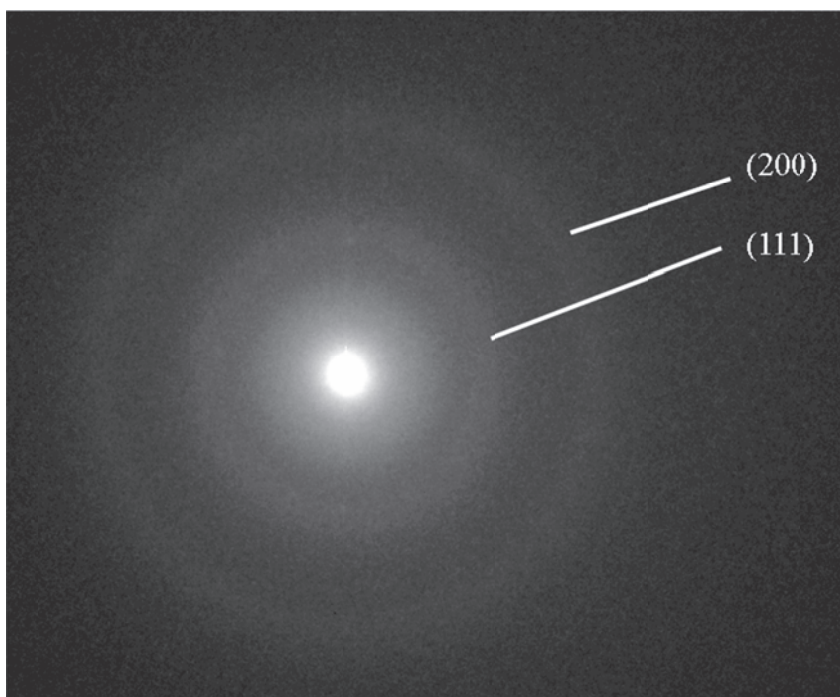


**Fig. 4.18:** SAED pattern of Pt/SBA-C catalyst



## Chapter 4

### 4.3.2.4 Surface Area

Nitrogen adsorption isotherms for fresh as well as used samples were recorded at -196 °C temperature. Before recording of the isotherm, both the samples were subjected to *in situ* evacuation at 300 °C temperature. The BET surface area of the catalyst was found to be as high as 1122 m<sup>2</sup>g<sup>-1</sup> and pore volume was 0.893 cm<sup>3</sup>g<sup>-1</sup>. Fig 4.19 and Fig 4.20 shows the adsorption desorption isotherm and pore size distribution curve for both the samples respectively. Fig. 4.19 shows a hysteresis loop (Type- IV) which is a characteristic of mesoporous materials. Pore size distribution curves also indicate the presence of pores around 4 nm, which again corresponds to presence of mesopores.

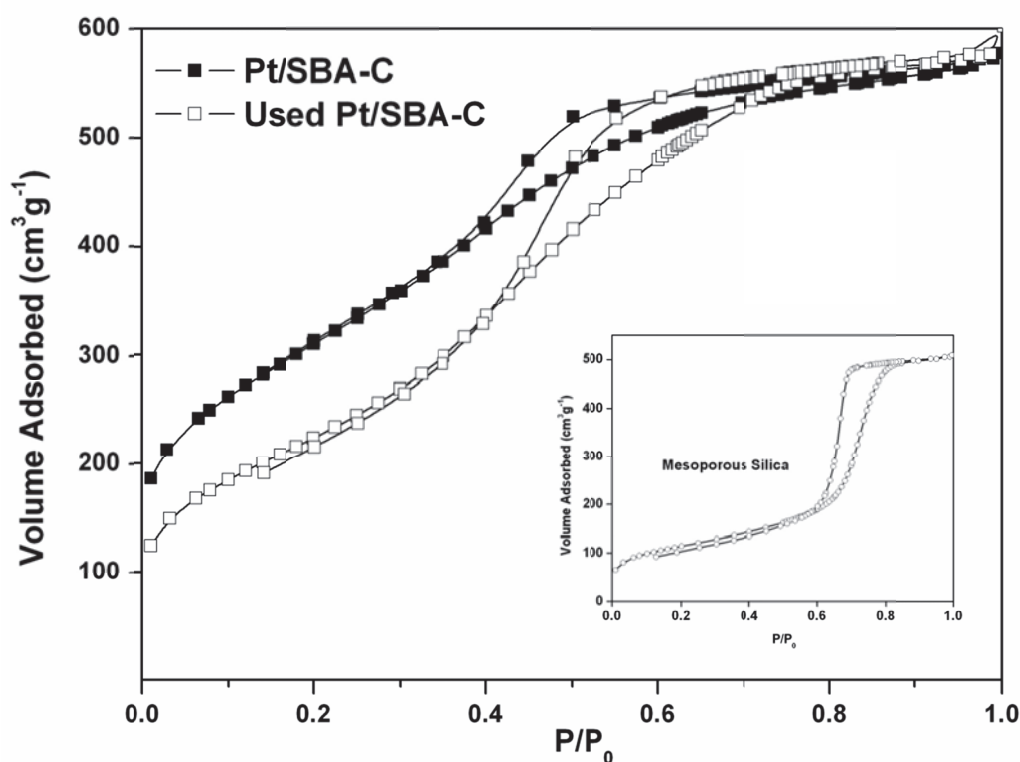


Fig. 4.19: Adsorption isotherm of fresh and used Pt/SBA-C catalysts

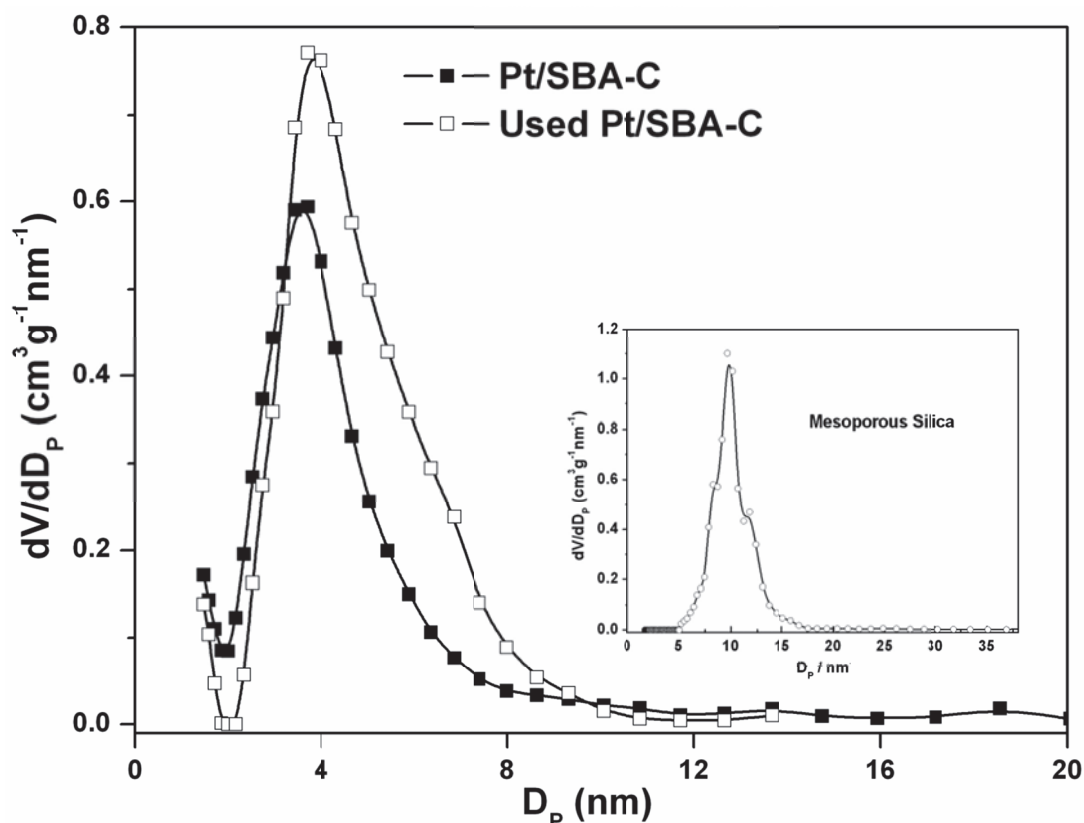


Fig. 4.20: Pore size distribution of fresh and used Pt/SBA-C catalysts.

### 4.3.2.5 Raman Spectroscopy

Fig. 4.21 shows the Raman spectra of the Pt/SBA-C catalyst, which shows two peaks at around  $1310$  and  $1590 \text{ cm}^{-1}$ . These two peaks are assigned as D band and G band respectively. D band here is very broad and it contains contributions from both  $\text{sp}^3$  hybridized carbon as well as disordered carbon structure. Thus Raman spectroscopy results indicate that the carbon contains disordered carbon in addition to graphitized carbon. The width and relative intensities of both G and D lines ( $I_G/I_D$ ) is also used for characterization of carbon materials.  $I_G/I_D$  ratio for the Pt/SBA-C catalyst is 1.15, which is in good agreement with similar mesoporous carbon materials as reported in literature.

## Chapter 4

These results and IG/ID ratio are in good corroboration with the XPS results and  $sp^2/sp^3$  ratio as reported by Tai et al [147].

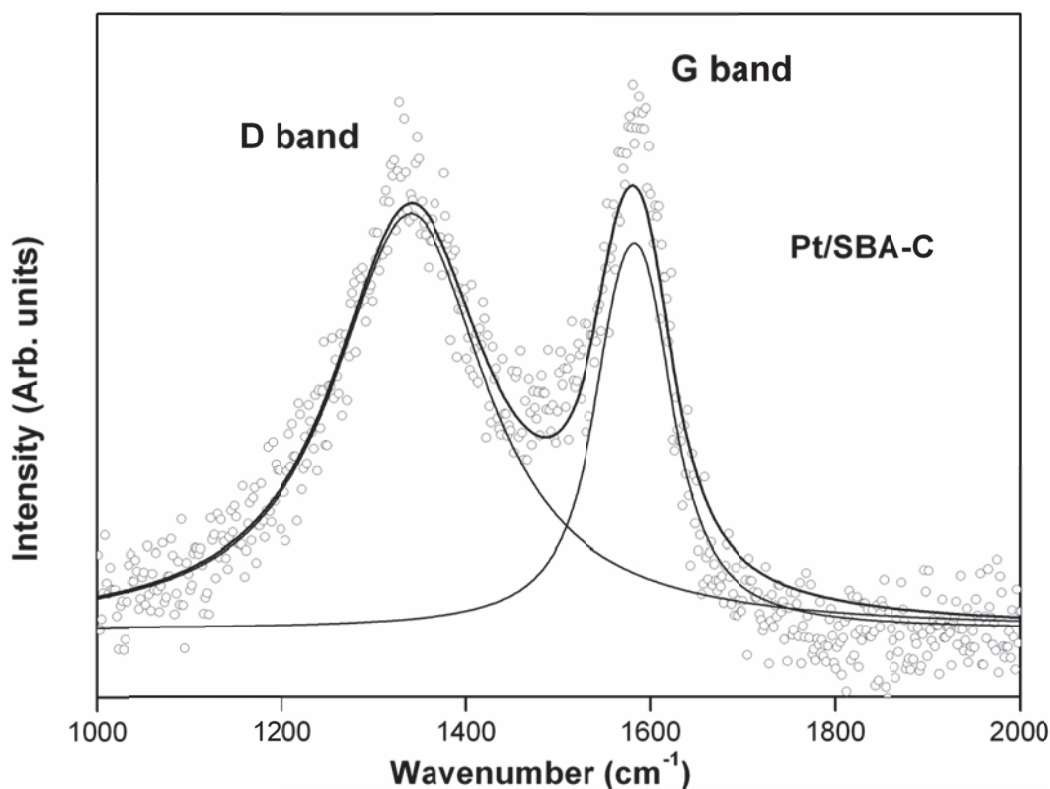


**Fig. 4.21:** Raman spectrum of the Pt/SBA-C catalyst.

### 4.3.2.6 X-ray Photoelectron spectroscopy

Surface composition of the catalyst was analyzed using X-ray photoelectron spectroscopy. The XPS measurements for Pt/SBA-C were carried out in constant analyzer energy mode using Al K $\alpha$  radiation (1486.6 eV). The survey scan (Fig. 4.22) of the sample shows peaks only in the spectral regions corresponding to carbon, platinum and oxygen. It doesn't show any peaks in the spectral regions of Si, thus we can say that silica is removed completely after HF washing step of the synthesis.

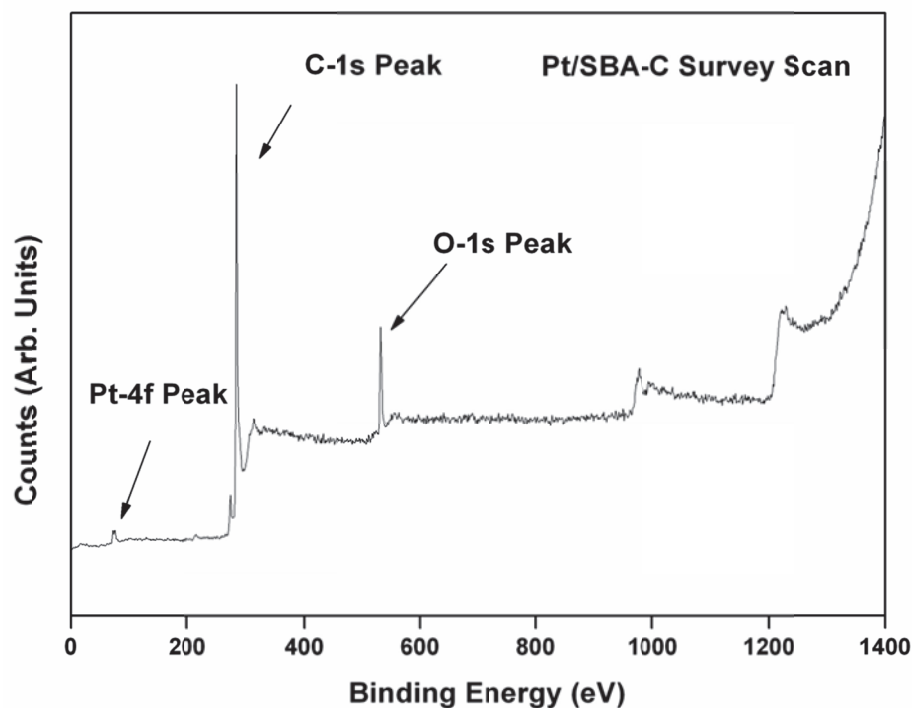


**Fig. 4.22:** XPS survey scan of the Pt/SBA-C sample

Fig 4.23 shows the intensity versus binding energy data obtained for spectral region corresponding to Pt 4f. It can be deconvoluted into only one doublet ( $4f_{5/2}$  and  $4f_{7/2}$ ) with respective binding energies of 71.3 and 74.6 eV. These binding energy values correspond to metallic state of platinum [134,135]. Thus XPS study reveals that platinum present here is in zero oxidation state which is essential for its catalytic activity.

Fig 4.24 shows the spectral region corresponding to C-1s spectral region; it can be fitted to three peaks with binding energy 284.3, 285.4 and 287.9 eV. These peaks correspond to  $sp^2$ ,  $sp^3$  and CO (Carbon bonded to oxygen, C-O or C=O) types of carbon [134]. Therefore the oxygen present is associated with carbon and not platinum. Also presence of  $sp^2$  hybridized carbon confirms the presence of rolled graphene like structure which is very much required for formation of mesoporous structures of carbon.

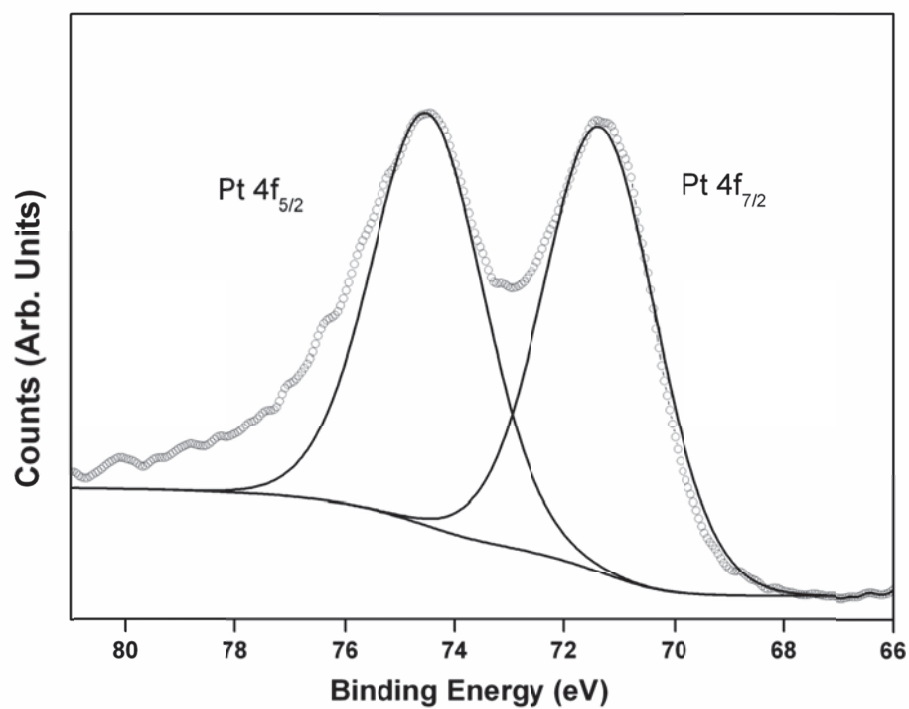


Fig. 4.23: XPS spectra of Pt/SBA-C in spectral region of Pt-4f

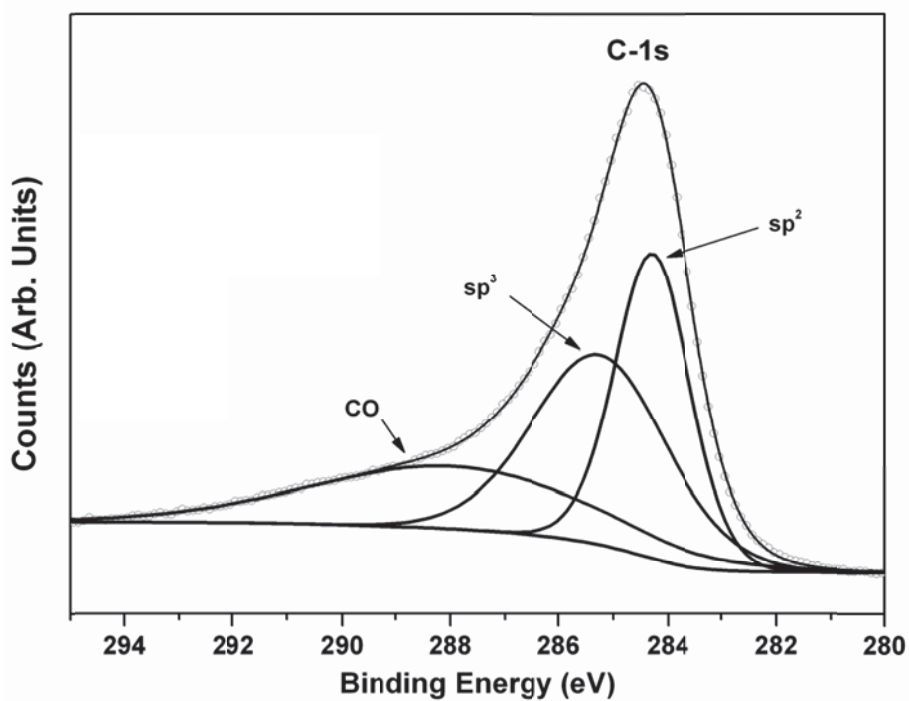


Fig. 4.24: XPS spectra of Pt/SBA-C in spectral region of C-1s

## Chapter 4

### 4.3.2.7 Catalytic activity of the catalyst

The catalyst was evaluated for its activity for liquid phase HI decomposition reaction. Reaction was carried out at 120 °C for different time intervals. After the reaction the solution was filtered and the eluent was analysed for concentrations of  $H^+$ ,  $I^-$  and  $I_2$  present in it. The concentrations of  $H^+$  and  $I^-$  ions was determined by titrating this eluent solution against 0.1 N NaOH and 0.1 N  $AgNO_3$  respectively using an autotitrator. The titrants NaOH and  $AgNO_3$  were standardized by their titration against Potassium Hydrogen Phthalate (KHP) and NaCl respectively. The decrease in  $H^+$  and  $I^-$  ions with respect to their concentrations in original solutions was used to calculate the percentage conversion. These two values were found to be in good agreement. The concentration of iodine in the solution was determined by titrating it against Sodium thiosulfate using starch as an indicator. There was increase in the concentration of iodine after the reaction which was also used to calculate the percentage conversion of HI. This value was in agreement with that of calculated by the ion concentrations. The conversion values thus obtained are shown below in Table 4.5.

S. No.	Reaction Time (h)	% Conversion
1.	1	9.6
2.	2	15.2
3.	3	21.4
4.	4	28.2

**Table 4.5:** Catalytic activity of Pt/SBA-C catalyst for HI decomposition reaction

## Chapter 4

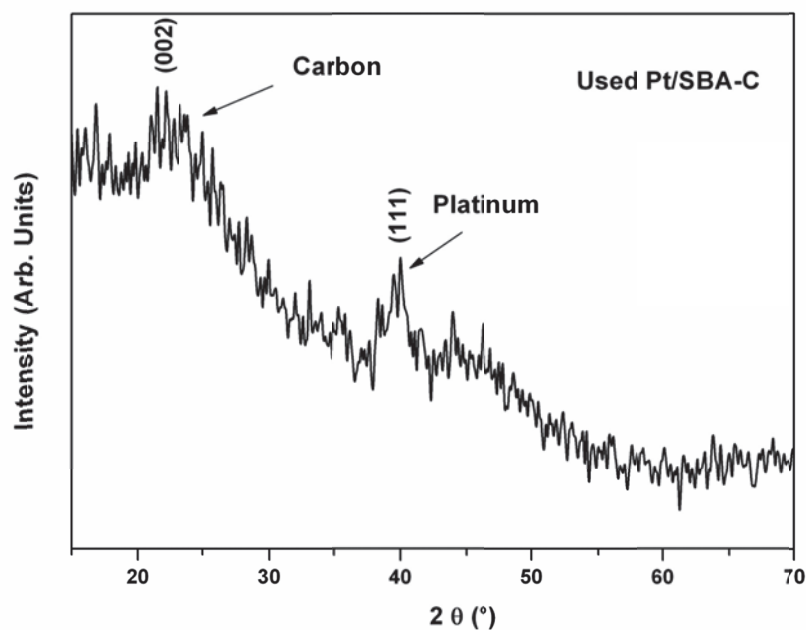
---

### 4.3.2.8 Stability of the Catalyst

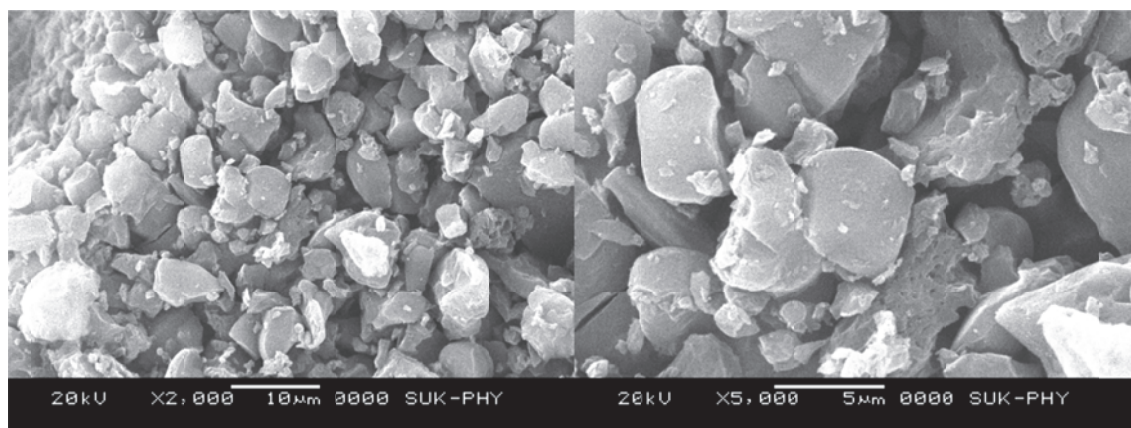
The stability of the catalyst in terms of its structural integrity and platinum leaching was studied after a typical study of 2 hours. After 2 hour run of the reaction, the used catalyst was removed from the solution by filtering. It was washed thoroughly and dried. This catalyst was analysed by several techniques like XRD, SEM, N<sub>2</sub> sorption etc.

Fig 4.25 shows the XRD pattern of the used catalyst. Here, there is no shift in peaks corresponding to carbon as well as platinum, which means there is no major change in the structure of catalyst during the course of the reaction. Fig 4.26 shows the SEM images of the used catalyst, these also indicate that there are no major morphological changes when compared with the fresh catalyst SEM images.

The adsorption desorption isotherm and the pores size distribution curve for the used catalyst are given in Fig 4.19 and Fig. 4.20 along with the fresh catalyst. These two also indicate that the mesoporous structure of the catalyst remain stable after the reaction. All these facts imply that the catalyst was stable the harsh conditions of liquid phase HI decomposition reaction.



**Fig. 4.25:** XRD pattern of used Pt/SBA-C catalyst



**Fig. 4.26:** SEM micrographs of used Pt/SBA-C catalyst

The eluent solution was analysed for presence of platinum by ICP-AES to evaluate how much platinum is being leached out into the solution. The ICP-AES analysis of the solution shows that the concentration of platinum in the solution is 18 ppm (0.18 of initial platinum loading). This number indicates that the platinum has good retention in the mesoporous carbon matrix.



### **4.3.3 Conclusion**

Mesoporous carbon supported platinum nano catalyst was successfully synthesized by hard templating route with bigger pore size silica. Platinum was found to be present in the form of uniformly distributed particles of 4-7 nm size over the mesoporous carbon support. This catalyst was used the liquid phase HI decomposition reaction of the Sulfur-Iodine process. The catalyst was found to be stable in terms of structure of supports as well as in terms of noble metal retention under the reaction conditions. When compared to previously studied MCM-C based mesoporous catalyst, Pt/SBA-C catalyst was comparable in terms of activity while more stable in terms of noble metal leaching. This type of material has a potential to be used in HI decomposition reaction of Sulfur-Iodine cycle for hydrogen production as well as other applications which requires highly dispersed Pt nanocatalyst on a carbon support.

# Chapter 5

## HI Decomposition over Platinum Catalysts Supported on Oxides

---

### 5.1 Introduction

Oxides are another class of materials which is heavily used as support for noble metal catalysts. Different oxides like silica ( $\text{SiO}_2$ ), titania ( $\text{TiO}_2$ ), zirconia ( $\text{ZrO}_2$ ), ceria ( $\text{CeO}_2$ ), different forms of alumina ( $\text{Al}_2\text{O}_3$ ), and others are used as catalyst supports [65]. These oxides serve the purpose of support in terms of their stability, surface area tunability and their activity in some cases. Silica for example can be prepared with very large surface area [148,149], ceria can be non-stoichiometric in oxygen [150], alumina can have acidic or basic characteristics [151] and titania have semiconductor properties [152], and so on. Therefore oxides form a large class of support for noble metals due to their properties. In this chapter we present few oxide supported platinum catalysts for HI decomposition reaction.

## ***Chapter 5***

---

### **5.2 Platinum/ Ceria and Platinum/Titania Catalysts**

This section contains details of Pt catalysts supported on ceria and titania with different platinum loading, including synthesis and characterization of these catalysts and evaluation of their catalytic activity and stability for liquid phase HI decomposition reaction.

#### **5.2.1 Experimental**

##### **5.2.1.1 Preparation of Catalyst**

A series of Pt/Ceria and Pt/Titania catalyst with three different Pt loading (0.5, 1.0 and 2.0 by weight) was synthesized. Catalyst synthesis was carried out by wet impregnation followed by chemical reduction. Ceria powder was synthesized by calcination of cerium hydroxide, obtained by addition of ammonium hydroxide to ceric nitrate solutions. In case of titania, commercial titania powder was used as support. For different loading of Platinum, stoichiometric amount of hexachloroplatinic acid was added to the support. The dried mixture was then heated at 350 °C to achieve the decomposition of hexachloroplatinic acid from its highly water soluble form to water insoluble  $\text{PtCl}_4$  form. The Hydrazine was added drop wise with constant stirring for chemical reduction of platinum from 4+ oxidation state to 0 oxidation state. The final product was filtered and washed several times with distilled water and dried.

##### **5.2.1.2 Characterization of Catalysts**

The powder X-ray diffraction patterns of all catalysts were recorded on Philips Analytical Diffractometer in the range 20 to 70° (Using Ni filtered  $\text{Cu K}\alpha$  radiation). The

## **Chapter 5**

---

surface morphologies and particle size were studied using Seron AIS 2100 Scanning electron microscope. The BET surface area of the catalysts was determined by N<sub>2</sub> adsorption method using Micromeritics ASAP 2020 Surface Area and Porosity Analyser. The oxidation state of Pt in the catalyst was found out by X-ray Photoelectron Spectroscopy measurements using multitechnique surface characterization system by SPECS. The amount of noble metal in the reflux was determined by using Horiba Jobin Vyon JY 2000 ICP-AES.

### **5.2.1.3 Activity and Stability**

All the catalysts were evaluated for their catalytic activity for liquid phase HI decomposition and noble metal leaching employing a reflux type batch reactor. The details of this reactor are as given in Chapter 2. For this 250 mg of catalyst was added to 50 ml of 27% hydriodic acid solution in 250 ml round bottom flask. This flask was heated and the gas bubbling out through the two traps was collected in an inverted column and was analyzed using a gas chromatograph. After reaction, the HI decomposition was measured by means of titrating H<sup>+</sup> and I<sup>-</sup> ions using acid-base and iodometric titrations, respectively. The solution was filtered to separate the used catalyst and the eluent. The spent catalyst was characterized by XRD, Raman and SEM for their physical integrity and the eluent was analyzed using ICP-OES for the leached out platinum.

### **5.2.2 Results and Discussion**

#### **5.2.2.1 XRD**

The X-ray diffraction measurements were recorded in 20 to 70° 2θ range on Philips Analytical Diffractometer (using Ni-filtered Cu-Kα radiation). Fig.5.1 shows the

## Chapter 5

XRD patterns of different Pt/CeO<sub>2</sub> catalysts. The XRD pattern of all three catalyst samples corresponds to that of cubic structure of ceria. There is no peak corresponding to platinum metal (JCPDS No. 04-0802). This indicates that the platinum is present in form of highly dispersed particles.

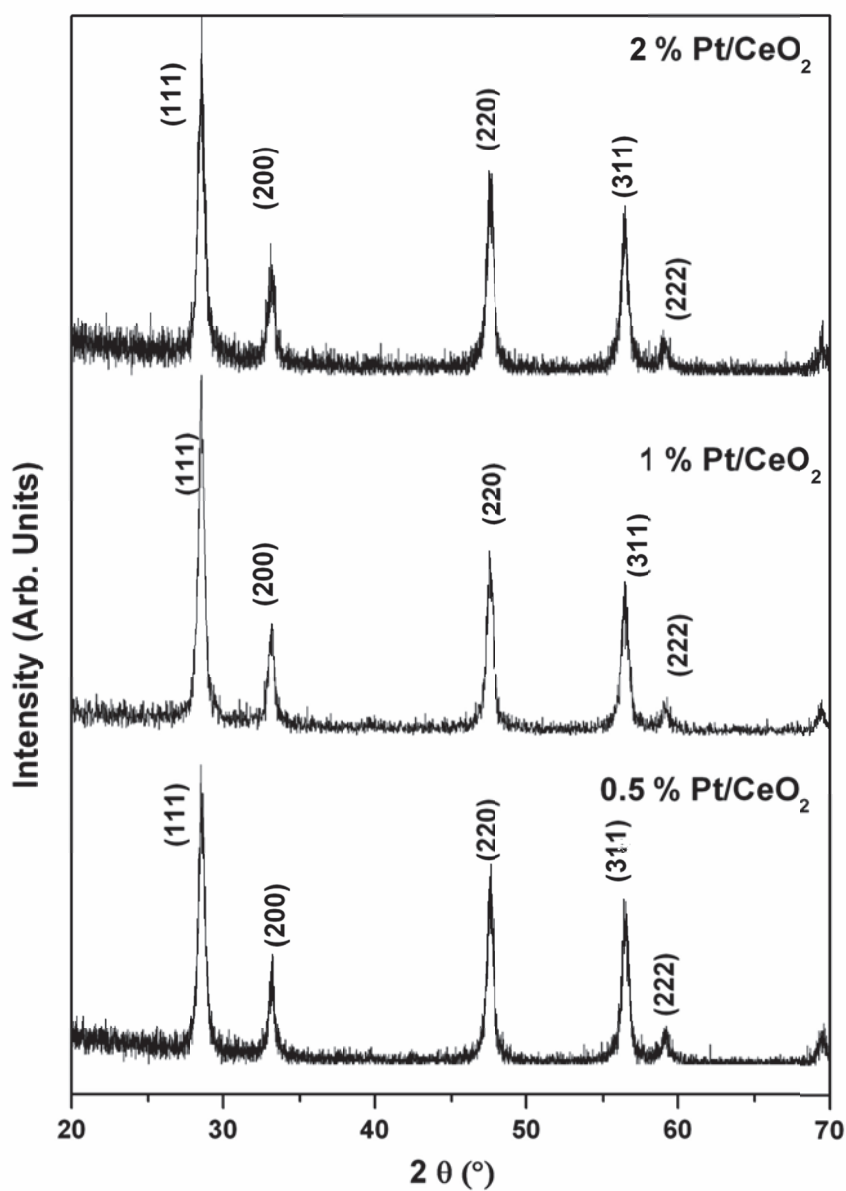


**Fig 5.1:** XRD patterns of different Pt/CeO<sub>2</sub> catalysts

Similarly XRD patterns of different Pt/TiO<sub>2</sub> catalysts are shown in Fig. 5.2. The TiO<sub>2</sub> peaks here correspond to its anatase form. The Platinum peak is not visible in case of Pt/TiO<sub>2</sub> catalysts also.

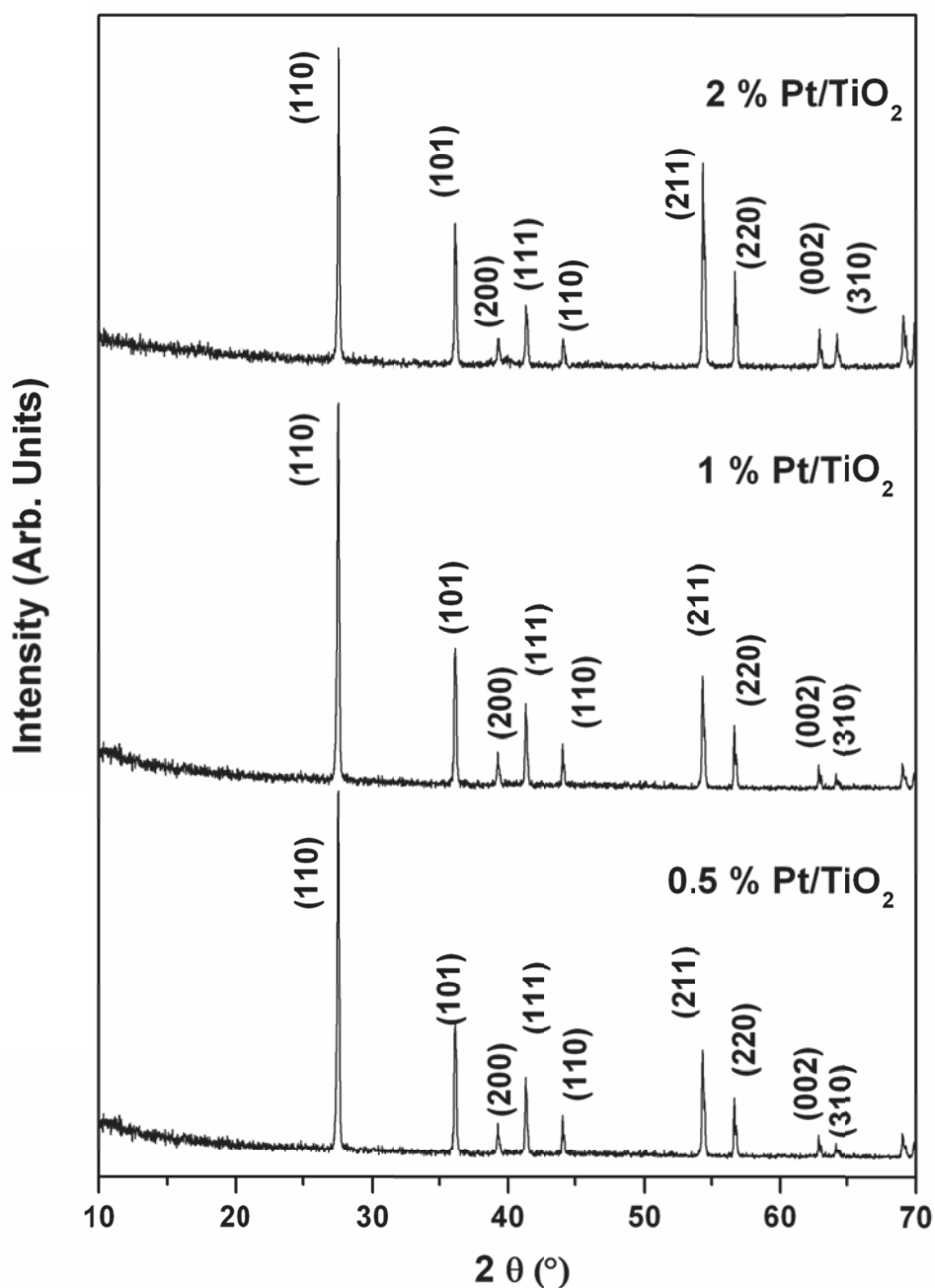


**Fig 5.2:** XRD patterns of different Pt/TiO<sub>2</sub> catalysts

## Chapter 5

### 5.2.2.2 SEM

Surface morphology of all the catalysts was studied using scanning electron microscopy. Fig 5.3 presents the SEM micrographs of different Pt/CeO<sub>2</sub> catalysts. All the three catalysts have similar morphology. It can be seen that there are few openings on the surface with few loose particles.

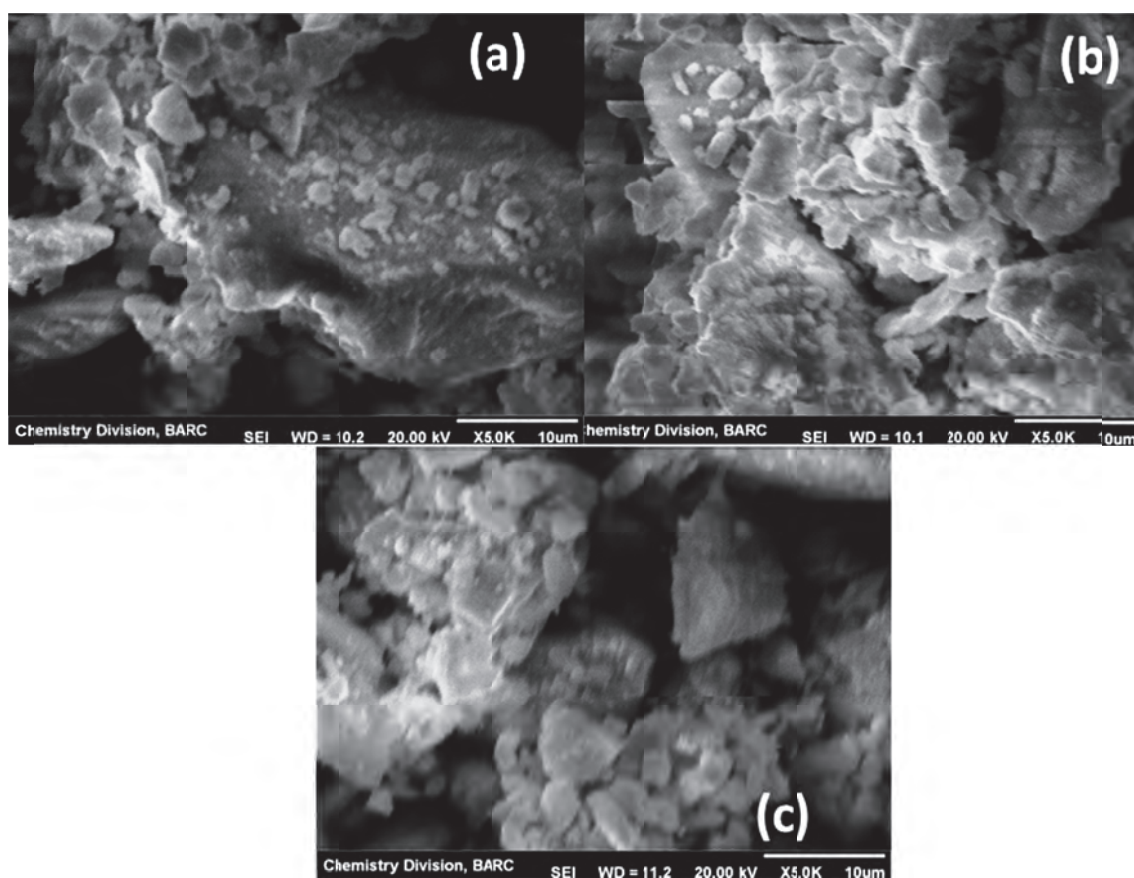


**Fig 5.3:** SEM images of Pt/CeO<sub>2</sub> catalyst with different platinum loading (a) 0.5%, (b) 1%, (c) 2%



## Chapter 5

SEM micrographs of Pt/TiO<sub>2</sub> with different platinum loading are shown in Fig. 5.4. All the three catalysts have similar morphology with few pore openings on the surface and few loose particles.

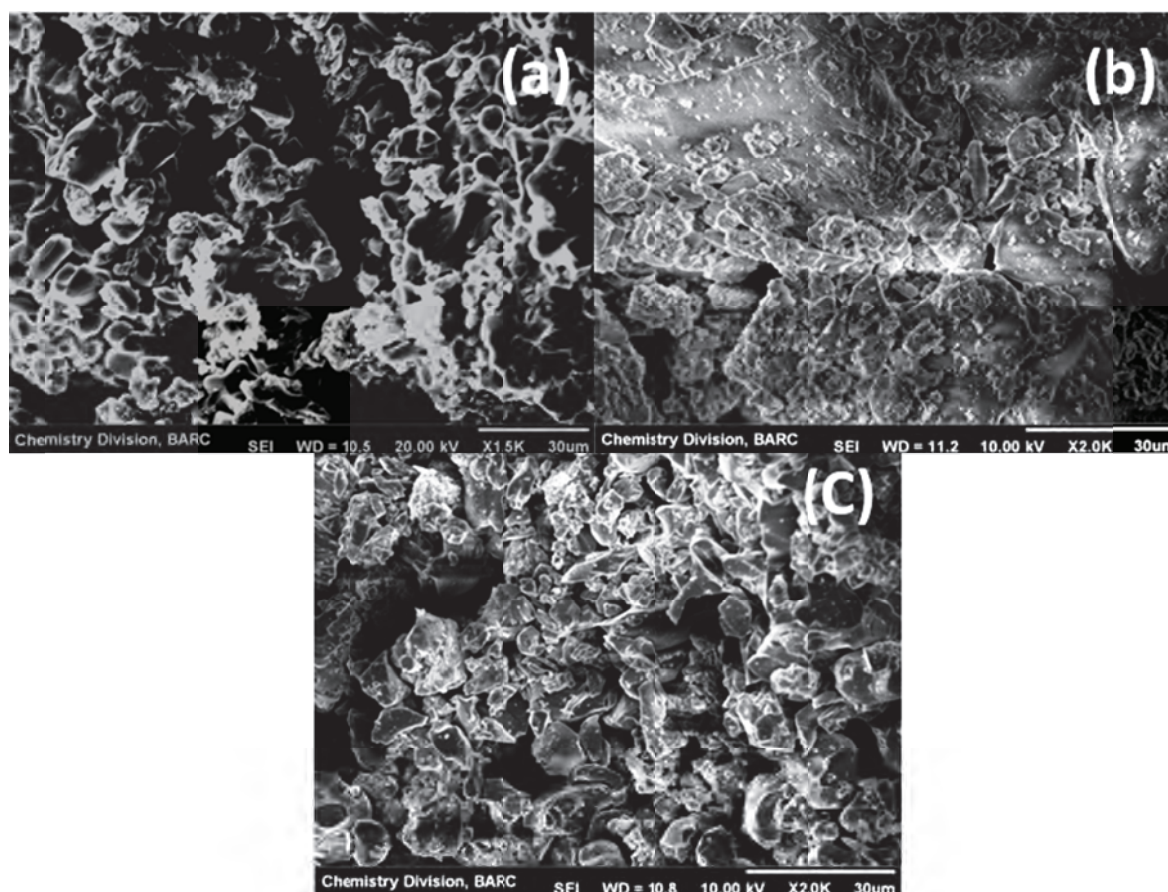


**Fig 5.4:** SEM images of Pt/TiO<sub>2</sub> catalyst with different platinum loading (a) 0.5%, (b) 1%, (c) 2%

EDX spectra of the Pt/TiO<sub>2</sub> samples are shown below in Fig. 5.5. Here peaks corresponding to Ti, O and Pt are observed (except for 0.5 Pt/TiO<sub>2</sub> where Pt peak is not observed). The weight percentage values obtained by EDS measurements here are in accordance with our initial percentage loading for 1 and 2 catalysts.



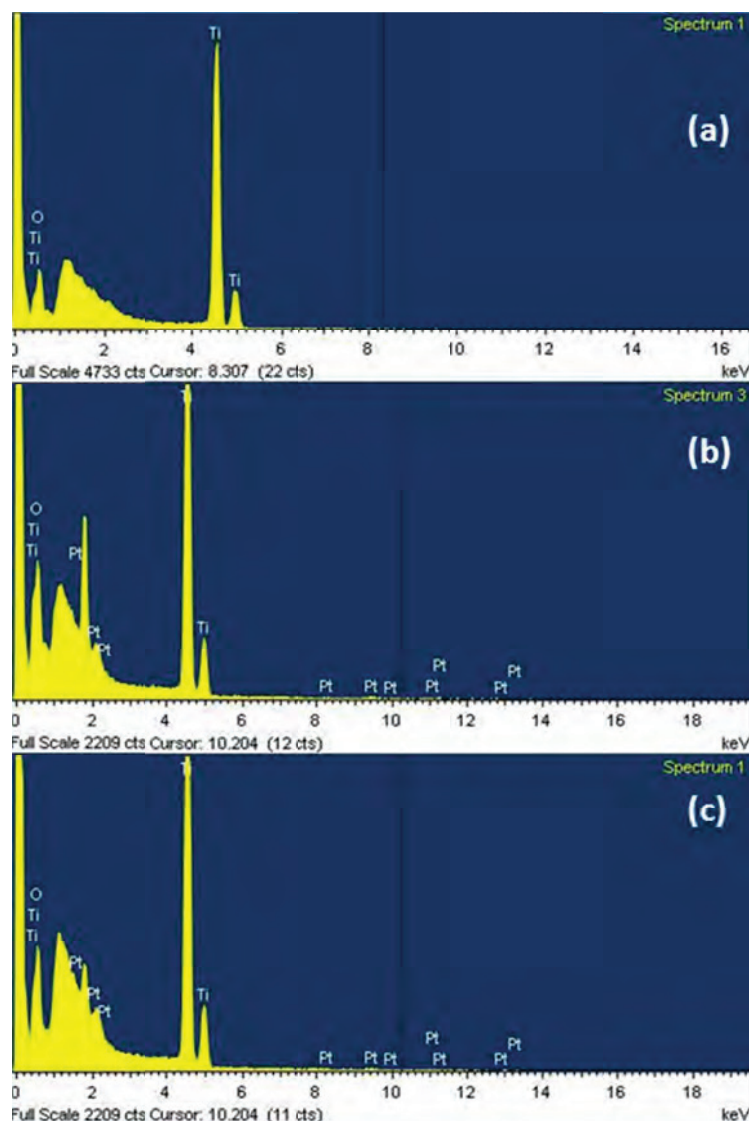


**Fig 5.5:** EDS spectra of Pt/TiO<sub>2</sub> catalyst with different platinum loading (a) 0.5%, (b) 1%, (c) 2%

### 5.2.2.3 Surface Area

Surface area of the catalysts is shown in Table 5.1. Ceria based catalyst have little higher surface area in the range of 40-50 m<sup>2</sup>/g, while titania based catalysts have surface area around 30-40 m<sup>2</sup>/g.

Catalyst	Surface Area (m <sup>2</sup> /g)	Catalyst	Surface Area (m <sup>2</sup> /g)
0.5 Pt/CeO <sub>2</sub>	44.6	0.5 Pt/TiO <sub>2</sub>	28.8
1 Pt/CeO <sub>2</sub>	39.9	1 Pt/TiO <sub>2</sub>	31.9
2 Pt/CeO <sub>2</sub>	48.5	2 Pt/TiO <sub>2</sub>	33.2

**Table 5.1:** BET surface area for different oxide supported catalysts

### 5.2.2.4 X-ray Photoelectron spectroscopy

XPS measurements for all the catalysts were carried in constant analyzer energy mode. Survey scans of Pt/CeO<sub>2</sub> catalysts show peaks corresponding to cerium, oxygen, platinum and carbon (adventitious aliphatic carbon). The charging effect due to insulating nature of the samples was compensated by correction using C-1s (284.5 eV) as internal reference. The XPS spectra for different Pt/CeO<sub>2</sub> catalyst corresponding to Ce 3d and Pt 4f spectral region are shown in Fig. 5.6 and 5.7 respectively. Spectra corresponding to Pt-4f can be deconvoluted into 4f<sub>5/2</sub> and 4f<sub>7/2</sub> bands with respective binding energies of about 71.1 and 74.4 eV ( $\pm 0.1$ eV) as shown in Fig. 5.6. These binding energy values correspond to metallic state of platinum. Hence platinum is present in zero oxidation state [134,153], which is required for its catalytic activity. Fig 5.7 shows the XPS spectra of all three catalysts in the spectral region corresponding to Ce-3d region. Six peaks marked in the Fig. 5.8 correspond to three pairs of spin-orbit doublets and they are characteristic of Ce<sup>4+</sup> 3d states [154,155].

## Chapter 5

---

Similarly survey scans of Pt/TiO<sub>2</sub> catalysts show peaks corresponding to titanium, oxygen, platinum and carbon. Here also charging effect was compensated by correction using C-1s (284.5 eV). The XPS spectra for different Pt/TiO<sub>2</sub> catalyst corresponding to Ti 2p and Pt 4f spectral region are shown in Fig. 5.8 and 5.9 respectively. As shown in Fig. 5.8, spectra corresponding to Pt-4f can be deconvoluted into 4f<sub>5/2</sub> and 4f<sub>7/2</sub> bands with binding energies corresponding to Pt zero oxidation state [134,153]. The binding energy values of the Ti 2p peaks (Ti 2p<sub>3/2</sub> at 458.eV) as shown in Fig. 5.9 indicate that the samples consist only of Ti<sup>4+</sup> surface species [156,157].

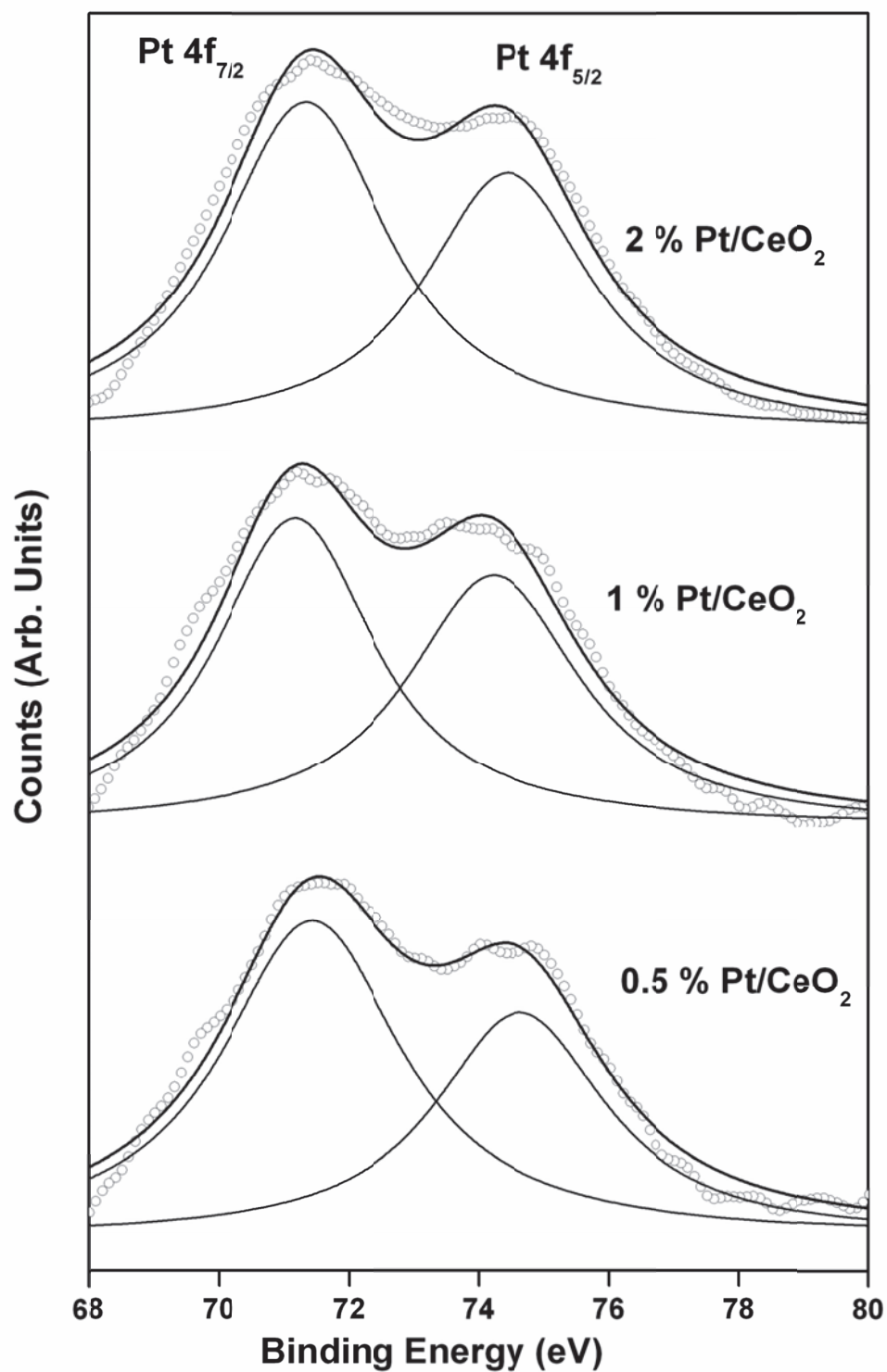


**Fig 5.6:** XPS spectra of Pt/CeO<sub>2</sub> catalysts in spectral region corresponding to Pt 4f

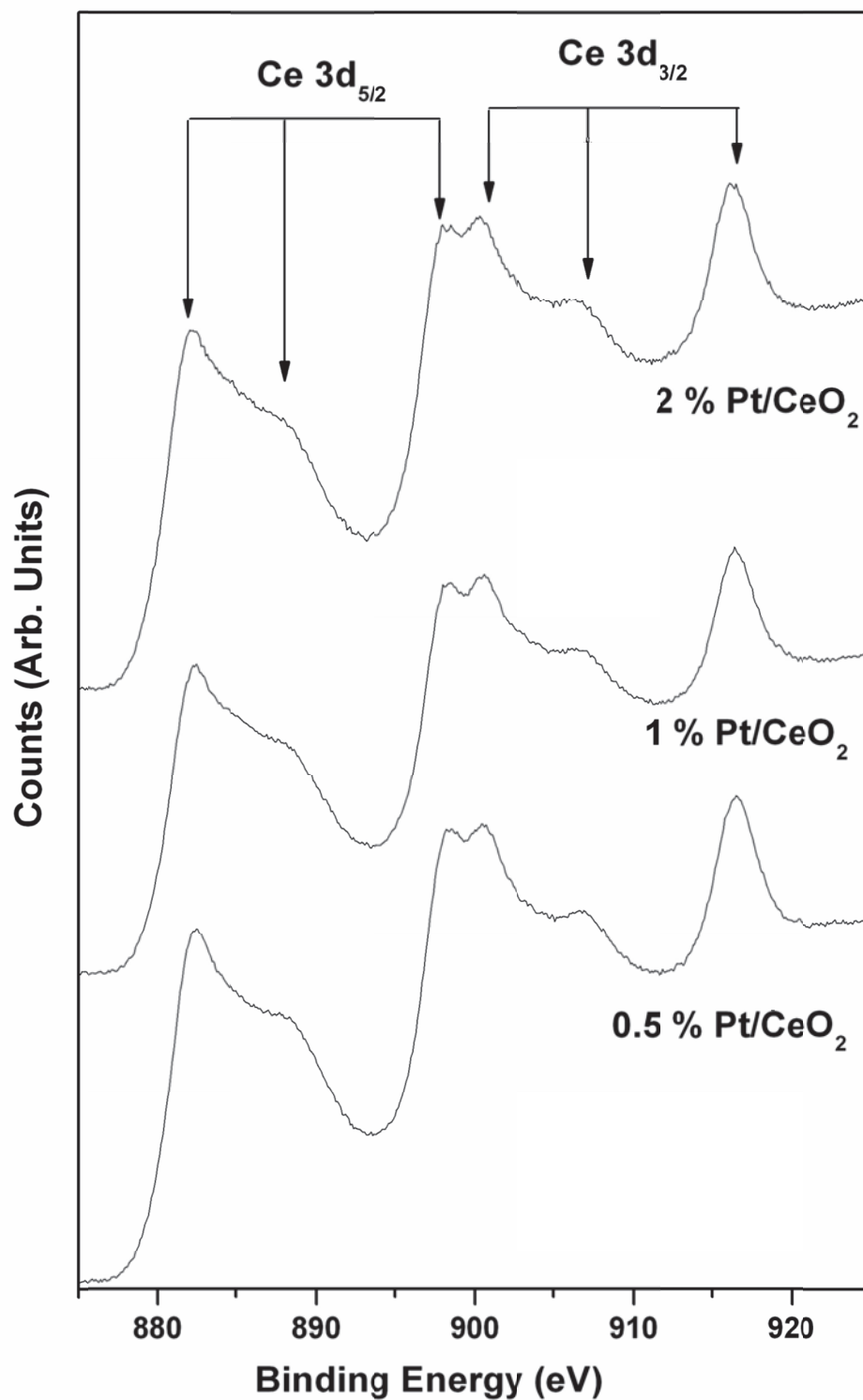


**Fig 5.7:** XPS spectra of Pt/CeO<sub>2</sub> catalysts in spectral region corresponding to Ce 3d

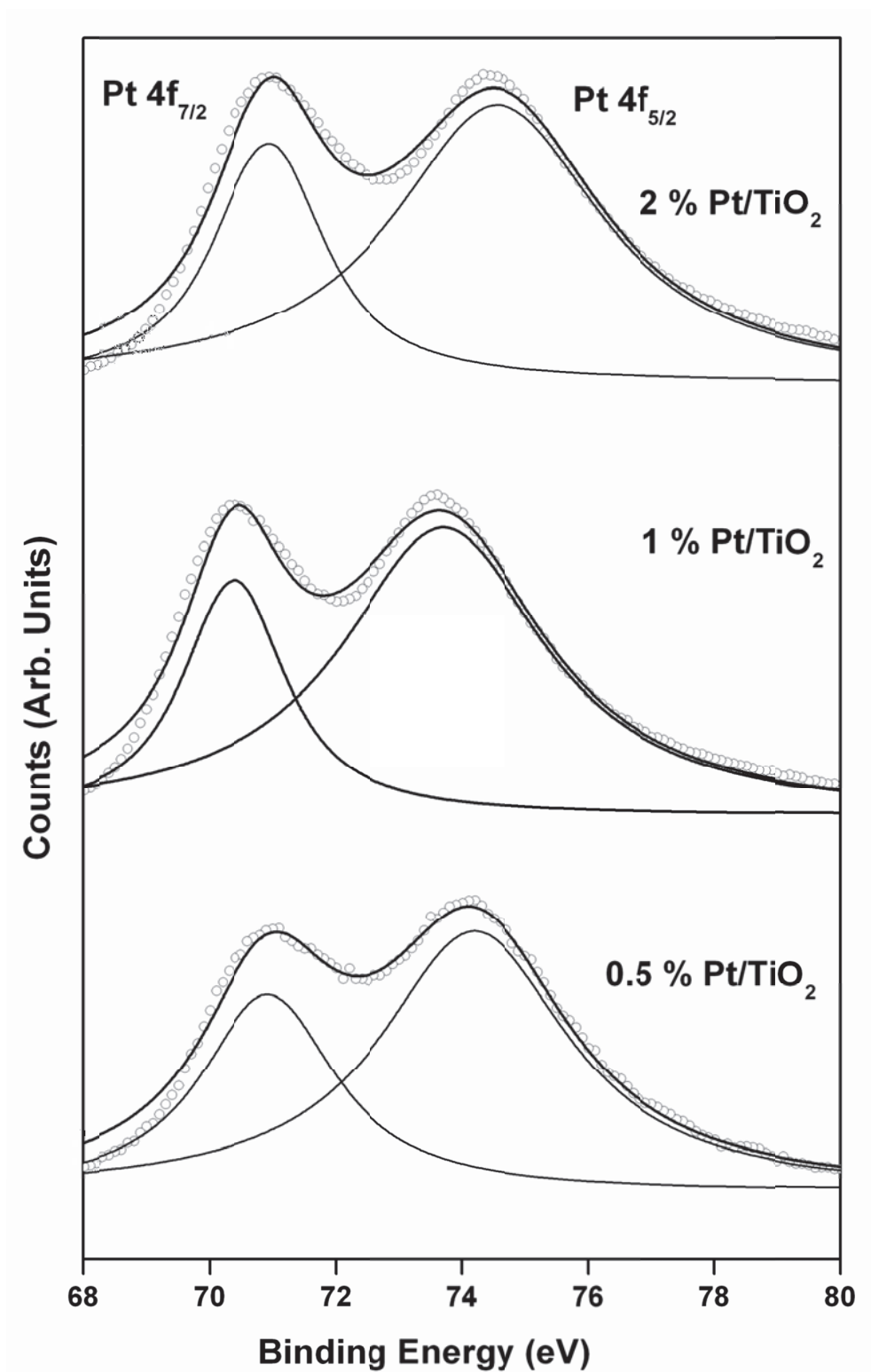


**Fig 5.8:** XPS spectra of Pt/TiO<sub>2</sub> catalysts in spectral region corresponding to Pt 4f

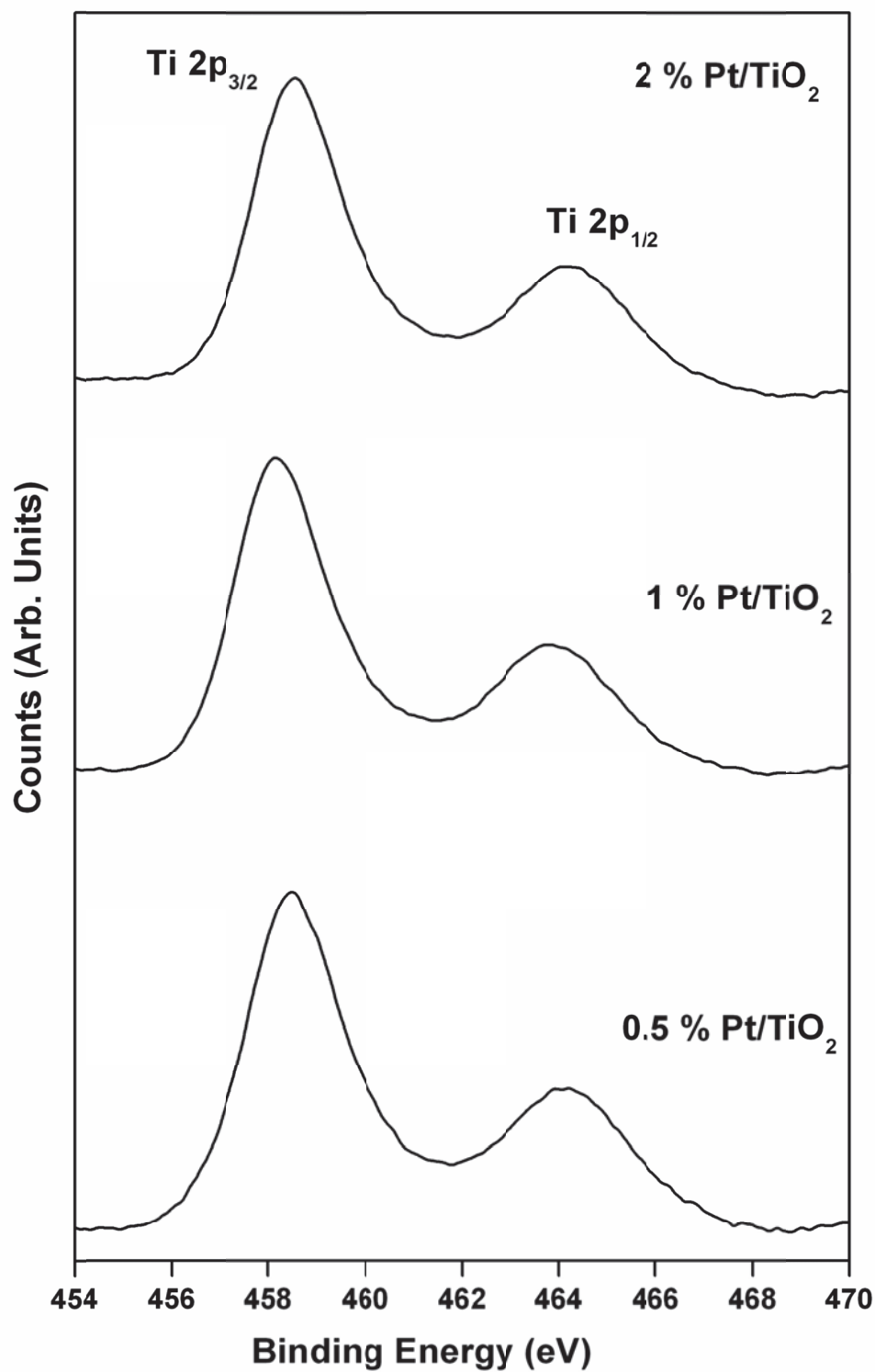


**Fig 5.9:** XPS spectra of Pt/TiO<sub>2</sub> catalysts in spectral region corresponding to Ti 2p

## Chapter 5

### 5.2.2.5 Catalytic activity of the catalyst

All the catalysts prepared were evaluated for their activity for liquid phase HI decomposition reaction. The percentage conversion was calculated for a typical 2h and 120 °C study by change in concentrations of  $H^+$ ,  $I^-$  and  $I_2$ . The conversion values thus obtained are shown below in Table 5.2.

From Table 5.2, it can be seen that for both ceria as well as titania based catalysts, the percentage conversion increase with noble metal loading. Also conversion values for ceria based catalysts are much higher when compared with the titania based catalysts.

S. No.	Catalyst	% Conversion (2 hr, 120 °C)
1.	0.5 Pt/CeO <sub>2</sub>	17.1
2.	1 Pt/CeO <sub>2</sub>	20.2
3.	2 Pt/CeO <sub>2</sub>	24.6
4.	0.5 Pt/TiO <sub>2</sub>	6.3
5.	1 Pt/TiO <sub>2</sub>	11.8
6.	2 Pt/TiO <sub>2</sub>	14.3

**Table 5.2:** % conversion values for different catalysts



## Chapter 5

---

The above results show that the percentage conversion increases on increasing the loading percentage of the noble metal. Also, ceria supported catalysts are found to be better than titania supported ones in terms of catalytic activity.

### 5.2.2.6 Stability of the Catalyst

To evaluate the stability of the catalysts, the reaction mixture was filtered. In case of CeO<sub>2</sub> based catalysts, it was observed that most of the catalyst gets dissolved in the HI solution itself i.e. we get very small amount of catalyst (less than 50 mg out of 250 mg initially used) upon filtering the reaction mixture. The solution after filtration was analysed for presence of Pt by ICP-OES and it showed high amount of platinum in it.

While this was not the case with titania based catalyst, the used titania based catalysts were XRD and SEM. Fig 5.10 shows the XRD patterns of different used Pt/TiO<sub>2</sub> catalysts. The XRD patterns for the used catalyst remain similar to original sample. Neither there is any change in peaks corresponding to titania nor there is appearance of peak corresponding to platinum. Both these fact confirms that the catalysts is quite stable in terms of support structure as well against platinum sintering.

The stability of the titania based catalysts against platinum leaching was studied by analysing the filtrate by ICP-AES. The amount leached out for the 0.5 , 1 and 2 loaded catalysts comes out to be 0.2 , 0.38 and 0.25 of the original loading. These numbers indicate that the catalyst is quite stable against noble metal leaching.

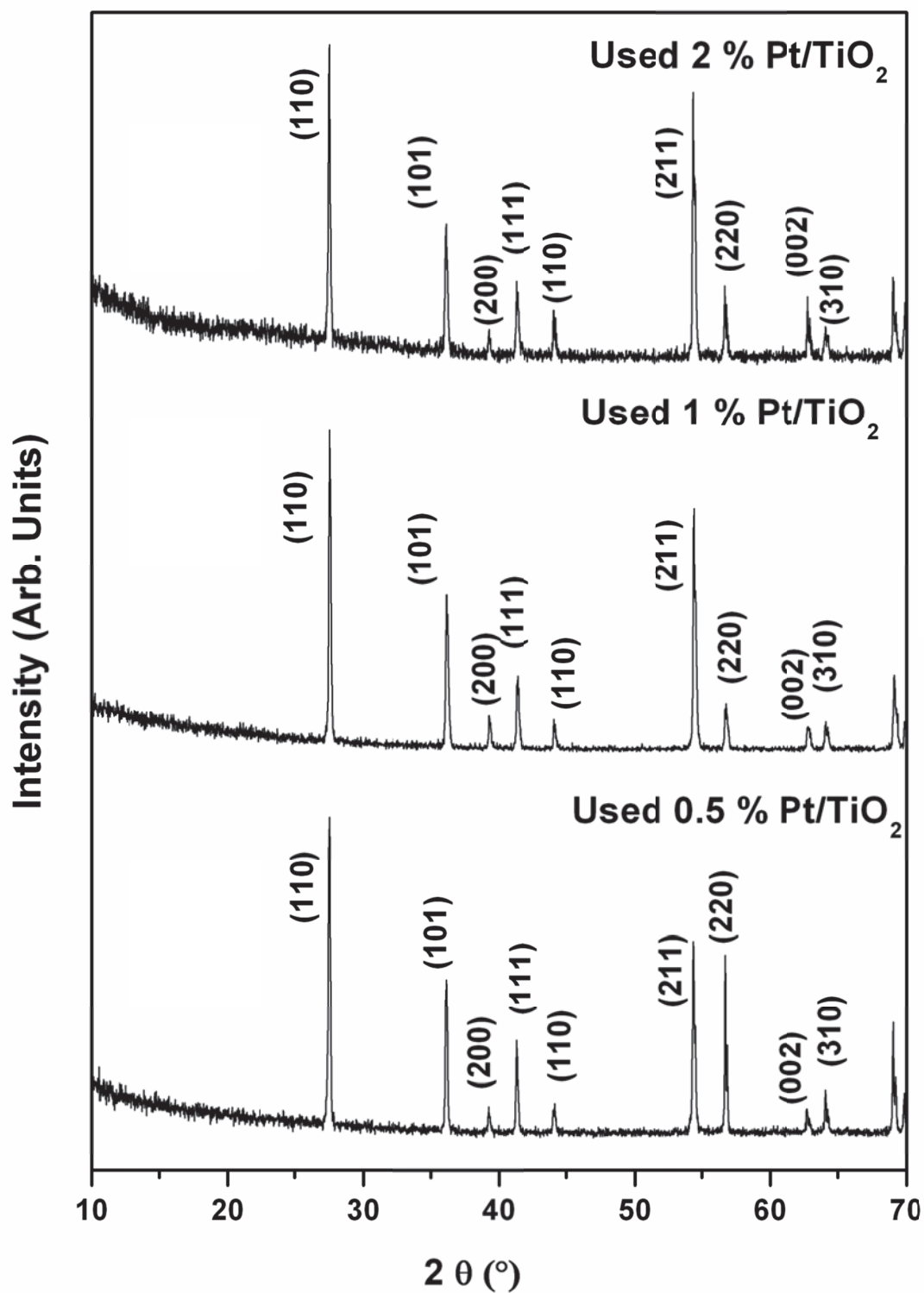


Fig 5.10: XRD pattern of used Pt/TiO<sub>2</sub> catalysts

### 5.2.3 Conclusion

Ceria and titania were explored as support for supported platinum catalysts for HI decomposition reaction. Catalysts with different platinum loading were prepared by wet impregnation followed by chemical reduction method. Chemical reduction method was effective for reduction of platinum as confirmed by XPS studies in both the cases. These catalysts were employed for the liquid phase HI decomposition reaction of the Sulphur-Iodine cycle. For both the systems, the conversion is found to increase with the increasing noble metal loading, a trends similar to what we observed in case of graphitic carbon based catalysts. It reconfirms the role of platinum in the catalytic decomposition of HI over these supported noble metal catalysts. The higher conversion levels were obtained for the Pt/CeO<sub>2</sub> catalysts as compared to Pt/TiO<sub>2</sub> catalysts. Stability wise, Pt/TiO<sub>2</sub> catalysts were found to be stable under the liquid phase HI decomposition reaction conditions, while Pt/CeO<sub>2</sub> catalysts were not stable under reaction conditions.

## ***Chapter 5***

---

### **5.3 Platinum/ Zirconia Catalyst**

In this section Pt catalysts supported on zirconia is reported. It includes synthesis and characterization of these catalysts and evaluation of their catalytic activity and stability for liquid phase HI decomposition reaction.

#### **5.3.1 Experimental**

##### **5.3.1.1 Preparation of Catalyst**

A series of Pt/Zirconia catalyst with three different Pt loading (0.5, 1.0 and 2.0 by weight) was synthesized. Zirconia was chosen as support for metal catalysts because of its inertness and stability under the highly acidic reaction environments. Catalyst synthesis was carried out by wet impregnation followed by chemical reduction. Zirconia powder was synthesized by calcination of zirconium hydroxide, obtained by addition of ammonium hydroxide to zirconyl oxy nitrate solutions. For different loading of Platinum, stoichiometric amount of hexachloroplatinic acid was added to the zirconia powder. The dried mixture was then heated at 350 °C to achieve the decomposition of hexachloroplatinic acid from its highly water soluble form to water insoluble  $\text{PtCl}_4$  form. The Hydrazine was added drop wise with constant stirring for chemical reduction of platinum from 4+ oxidation state to 0 oxidation state. The final product was filtered and washed several times with distilled water and dried. The percentage loading of the noble metal in the catalysts sample was confirmed by Neutron Activation Analysis (NAA).

## ***Chapter 5***

---

### **5.3.1.3 Characterization of Catalysts**

The powder X-ray diffraction patterns of fresh as well as used catalysts were recorded on Philips Analytical Diffractometer in the range 20 to 70 °(Using Ni filtered Cu K $\alpha$  radiation). The surface morphologies and particle size were studied using Seron AIS 2100 and Zeiss Scanning electron microscope and Transmission Electron Microscope. The BET surface area of the catalysts by N<sub>2</sub> adsorption method and noble metal dispersion by CO chemisorption was determined by using Micromeritics ASAP 2020 Surface Area and Porosity Analyser. The oxidation state of Pt in the catalyst was found out X-ray Photoelectron Spectroscopy measurements using multitechnique surface characterization system by SPECS. The amount of noble metal in the reflux was determined by using Horiba Jobin Vyon JY 2000 ICP-AES.

### **5.3.1.4 Activity and Stability**

The catalysts prepared were evaluated for their activity for HI decomposition reaction using setup as given in Chapter 2. For this, 250 mg of catalyst was added to 50 ml of 27 % hydriodic acid solution in 250 ml round bottom flask. The solution was heated at 120°C temperature for 2 h duration. This two hours of refluxing shows evolution of gas bubbles at regular intervals. This evolving gas was passed through two traps containing starch solution and silver nitrate solutions, respectively. There was no colour change in the traps, from which it could be inferred that Iodine and HI vapours are not escaping out from the system. The gas coming out, was collected in an inverted column and was analysed using a gas chromatograph (Chromatography and Instruments company, GC

## Chapter 5

---

2011) equipped with molecular sieve 5A column and thermal conductivity detector and was found to be hydrogen.

### 5.3.2 Results and Discussion

#### 5.3.2.1 XRD

The X-ray diffraction patterns were recorded in  $10$  to  $70^\circ$   $2\theta$  range on Philips Analytical Diffractometer (using Ni-filtered  $\text{Cu-K}\alpha$  radiation). Fig.5.11 shows the XRD patterns for zirconia based catalysts with different loading of platinum (i.e.  $0.5 \text{ Pt/ZrO}_2$ ,  $1 \text{ Pt/ZrO}_2$  and  $2 \text{ Pt/ZrO}_2$ ). The XRD pattern shows that Zirconia here is biphasic with the tetragonal phase (JCPDs No. 17-0923) being the major component and monoclinic phase (marked by  $\square$ ) being the minor component for all catalysts. Crystallite size  $D$  of these catalyst samples were calculated from the Scherrer formula. The calculated crystallite sizes of all the catalyst samples were found to be in  $6\text{-}8 \text{ nm}$  range, indicating nanocrystalline nature of the samples. Also, after loading the support with platinum, there is no appearance of peak corresponding to platinum metal (JCPDS No. 04-0802). This indicates that the platinum is present in form of highly dispersed particles.

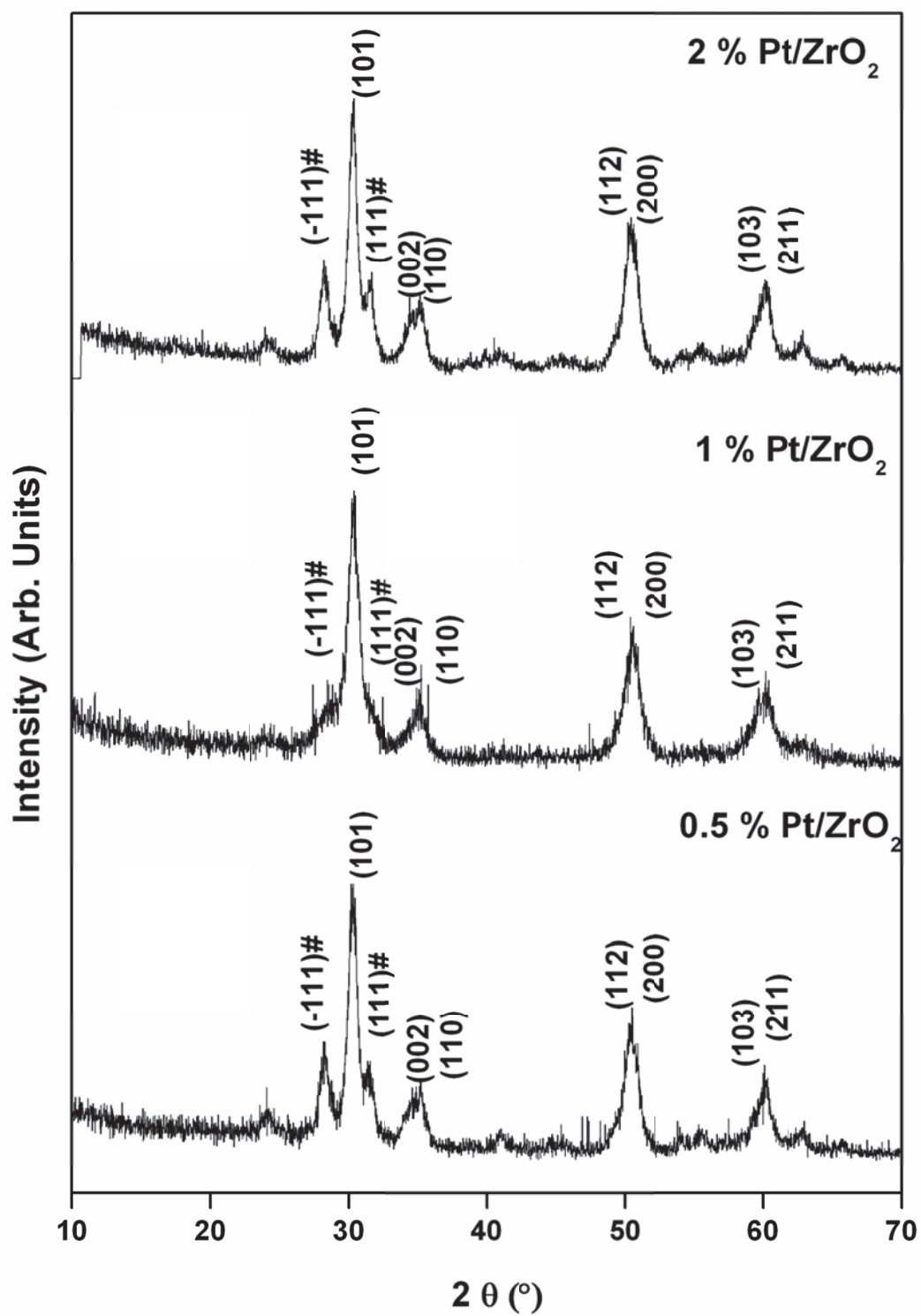


Fig 5.11: XRD Patterns of different Pt/ZrO<sub>2</sub> catalysts

## Chapter 5

### 5.3.2.2 SEM

Scanning Electron Microscopy was employed to observe morphology of the catalyst samples. All the catalysts show rough surface with open pores and a few loose particles over it. Fig. 5.12 shows the SEM images of 0.5 Pt/ZrO<sub>2</sub>, 1 Pt/ZrO<sub>2</sub> and 2 Pt/ZrO<sub>2</sub>. As one can see from the SEM images that overall morphology of the three catalysts with different noble metal loading is same.

EDX spectra of the Pt/ZrO<sub>2</sub> samples are shown below in Fig. 5.13. Here peaks corresponding to Zr, O and Pt are observed. The weight percentage values obtained here are in accordance with our initial percentage loading. Also, when EDX measurement was carried out over various areas, weight percentage of Pt was found to be almost similar. Therefore Pt is uniformly distributed over the surface of catalyst particles.

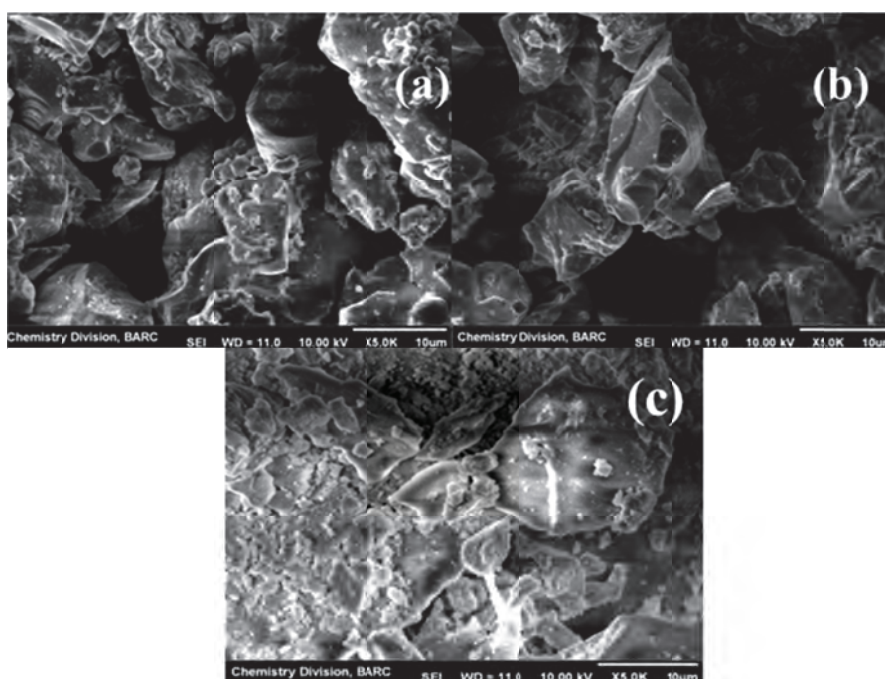


**Fig 5.12:** SEM images of Pt/ZrO<sub>2</sub> catalyst with different platinum loading (a) 0.5%, (b) 1%, (c) 2%



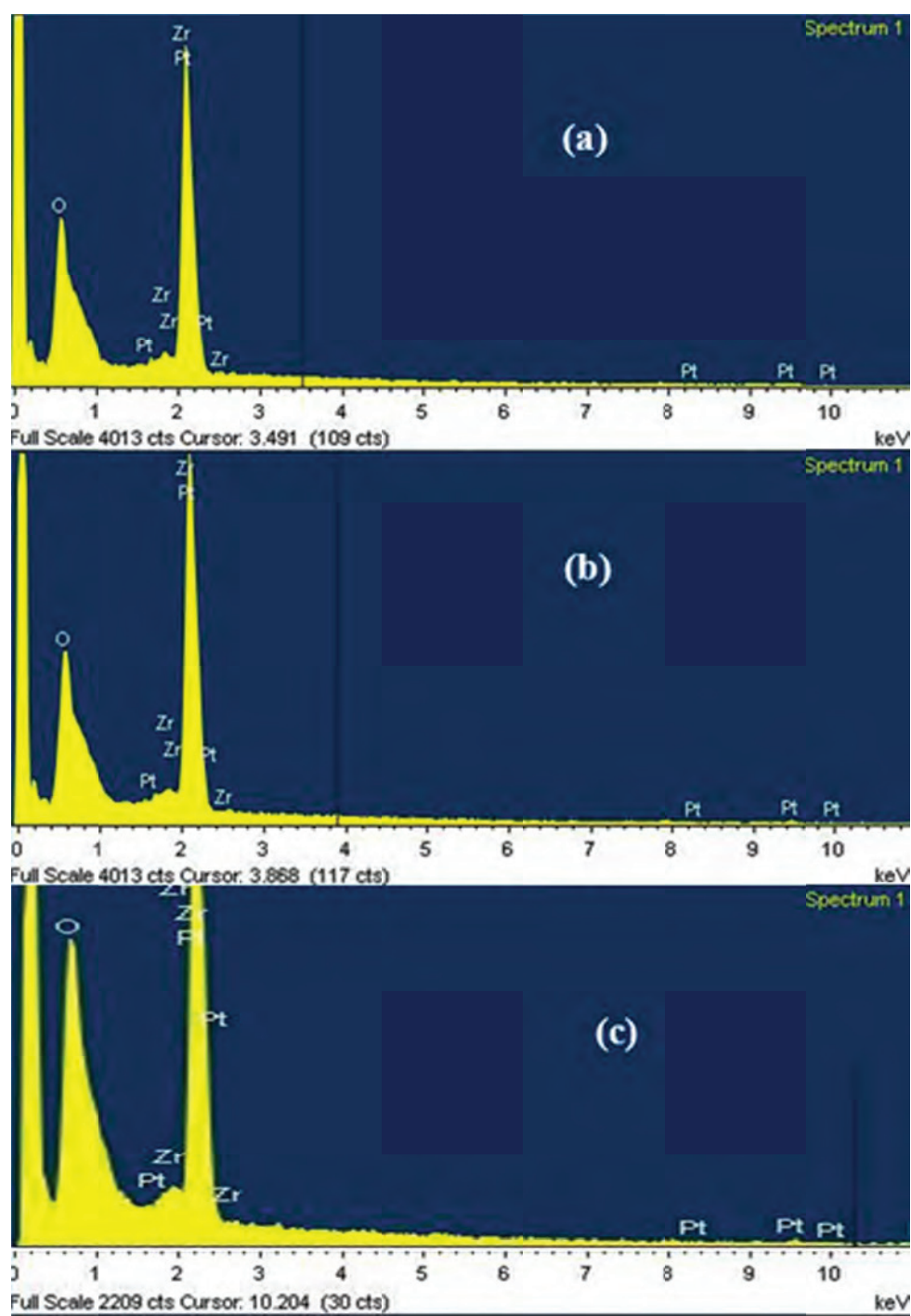
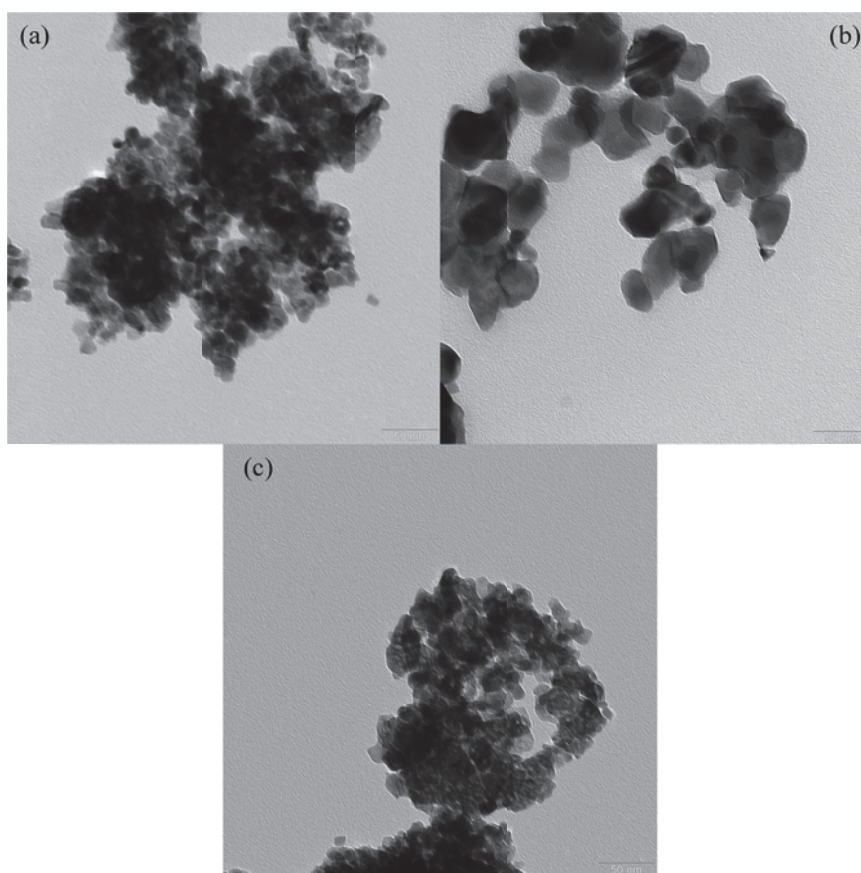


**Fig 5.13:** EDX spectra of Pt/ZrO<sub>2</sub> catalyst with different platinum loading (a) 0.5%, (b) 1%, (c) 2%

## Chapter 5

### 5.3.2.3 TEM

Transmission Electron Microscopy was used to evaluate particle size of Pt/ZrO<sub>2</sub> catalysts. Fig 5.14 shows the TEM images of the 0.5 Pt/ZrO<sub>2</sub>, 1 Pt/ZrO<sub>2</sub> and 2 Pt/ZrO<sub>2</sub> samples. TEM images exhibit Zirconia support particles of 5-8 nm dimensions which is in close agreement with the crystallite size data generated from XRD.



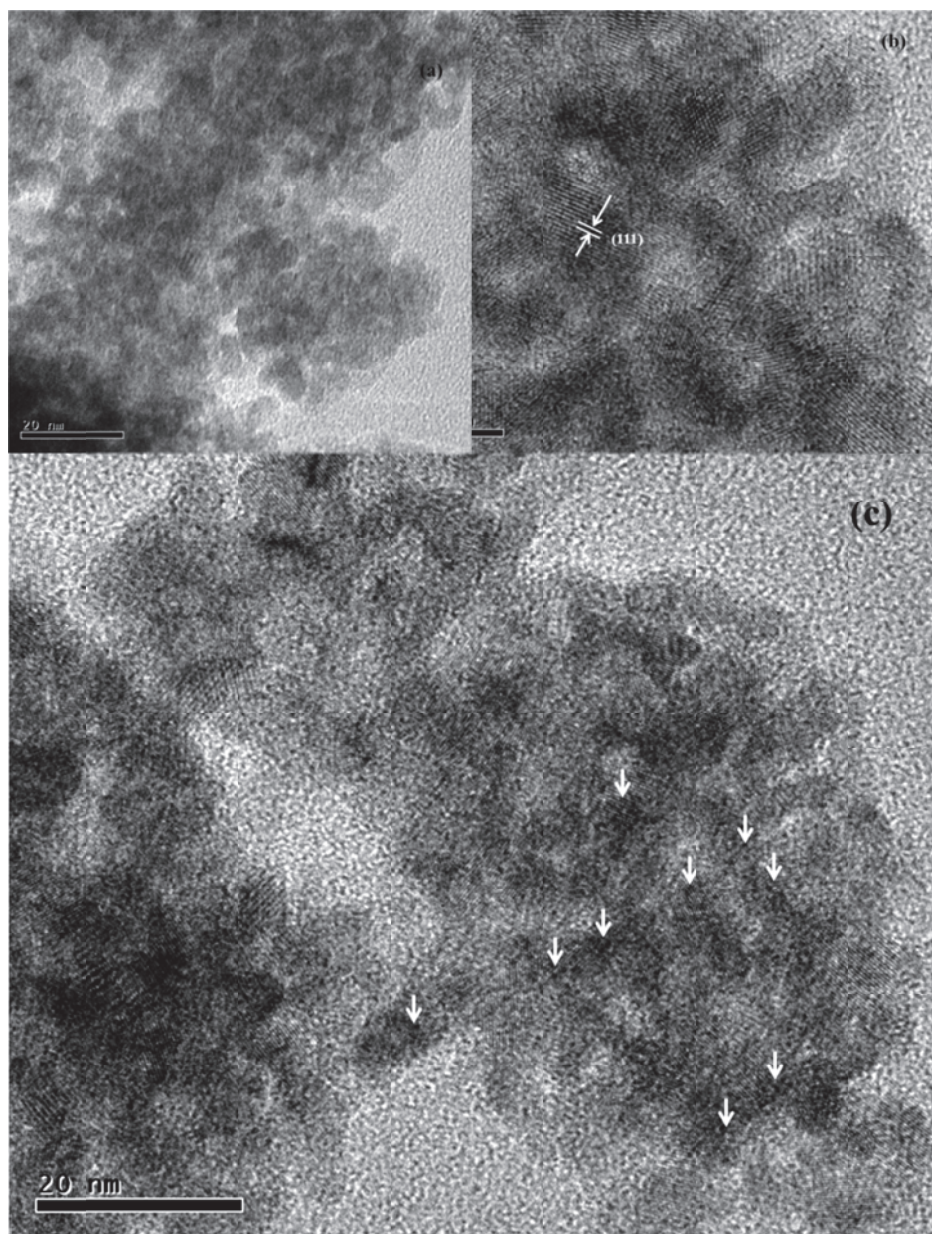
**Fig 5.14:** TEM images of Pt/ZrO<sub>2</sub> catalyst with different platinum loading (a) 0.5%, (b) 1%, (c) 2%

Fig. 5.15 shows the TEM images of the 1 Pt/ZrO<sub>2</sub> sample. Fig. 5.15(a) exhibits Zirconia support particles of 5-8 nm size. Identity of these particles as zirconia support was established by measuring the d-spacings from the lattice lines as shown in Fig

## Chapter 5

---

5.15(b). The d-spacing is found to be of 2.96 Å, pertaining to (111) plane of tetragonal zirconia. In addition to this, small dark spots of about 1 nm dimension, as marked by white arrows, in Fig. 5.15(c), can be observed in various TEM micrographs. These can be assigned to the noble metal supported on the zirconia particles.



**Fig 5.15:** TEM images of 1% Pt/ZrO<sub>2</sub> catalyst

## Chapter 5

### 5.3.2.4 Surface Area

Nitrogen adsorption isotherms were recorded at -196 °C temperature. The samples were subjected to *in situ* evacuation at 300 °C temperature for 3 h prior to recording of the isotherm. The BET surface area, pore volume and pore size data obtained for the samples is compiled in Table 5.3.

The adsorption desorption isotherm and pore size distribution curve for one of the sample (1 Pt/ZrO<sub>2</sub>) are shown in Fig. 5.16 and Fig. 5.17 respectively. Fig. 5.16 shows a hysteresis loop (Type- IV) for 1 Pt/ZrO<sub>2</sub> catalyst sample which is characteristic of mesoporous materials. Pore size distribution corresponds to median for ~4 nm pore opening, again corresponding to the mesoporous materials. Also, the noble metal dispersion of the catalysts was determined by H<sub>2</sub> chemisorption taking 2:1 stoichiometry of metal and adsorbate gas.

Catalyst	Surface Area ( m <sup>2</sup> /g )	Pore Volume ( cm <sup>3</sup> /g )	Pore Size ( nm )	Noble Metal Dispersion (%)
ZrO <sub>2</sub>	108.64	0.11	3.61	---
0.5 Pt/ZrO <sub>2</sub>	126.67	0.14	3.68	44.50
1 Pt/ZrO <sub>2</sub>	140.26	0.16	3.75	31.39
2 Pt/ZrO <sub>2</sub>	158.69	0.15	3.74	24.49

**Table 5.3:** BET surface area, pore volume, pore size and noble metal dispersion



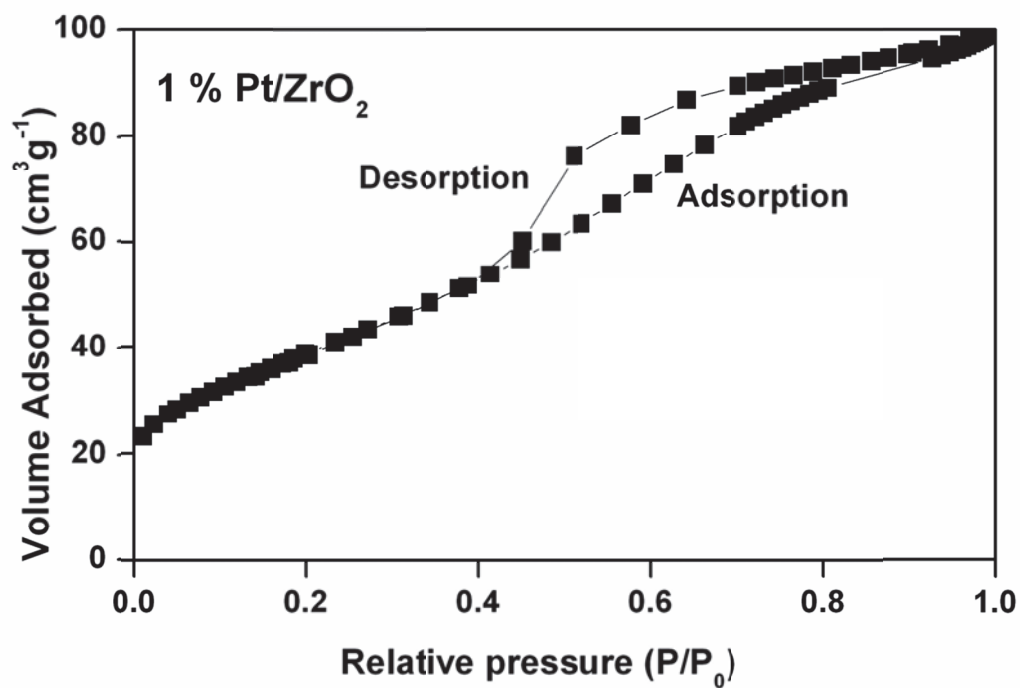


Fig 5.16: Adsorption and Desorption isotherms for 1% Pt/ZrO<sub>2</sub> catalyst

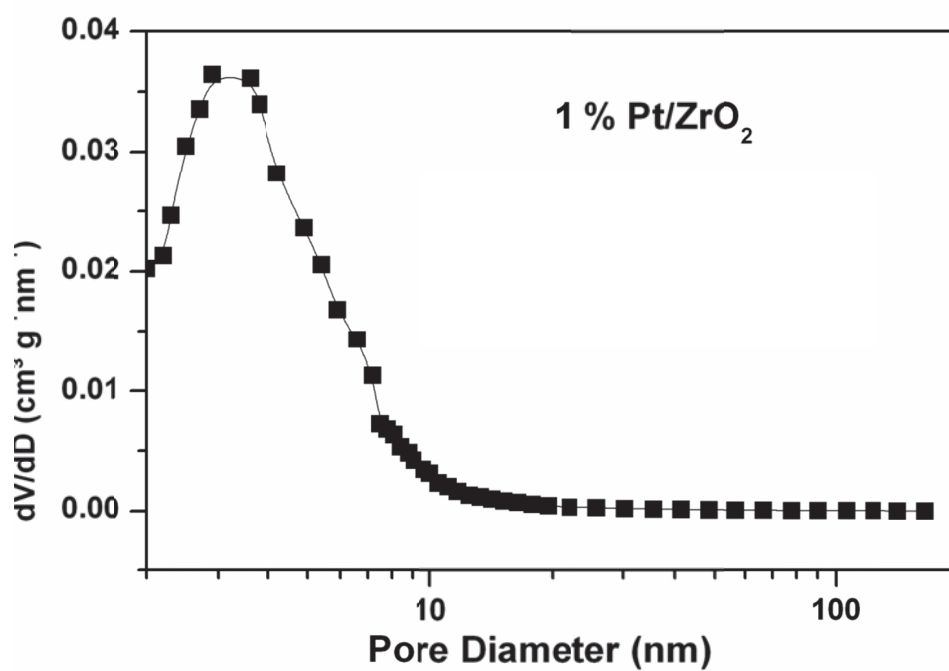
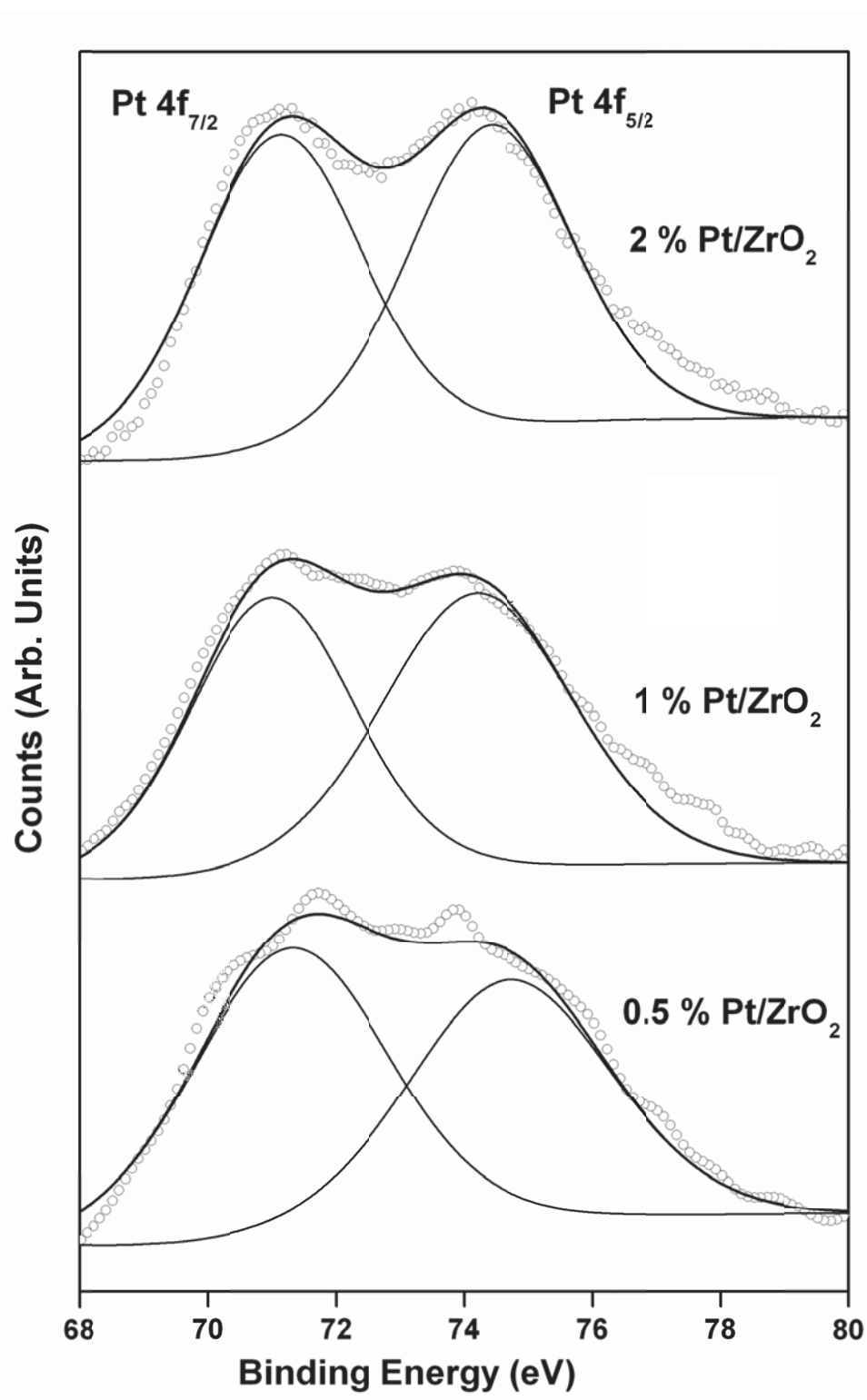


Fig 5.17: Pore size distribution for 1% Pt/ZrO<sub>2</sub> catalyst

### 5.3.2.5 X-ray Photoelectron spectroscopy

XPS measurements for all three Pt/ZrO<sub>2</sub> catalysts were carried in constant analyzer energy mode. The survey scan of all the three catalysts showed peaks corresponding to zirconium, oxygen, platinum and carbon (adventitious aliphatic carbon). The correction for charging effect due to insulating nature of the samples was carried out using carbon as internal reference (284.5 eV). The XPS spectra in the spectral region of Pt-4f and Zr-3d are shown in Fig. 5.18 and 5.19 respectively.

Pt 4f spectra for all three samples can be deconvoluted into 4f<sub>5/2</sub> and 4f<sub>7/2</sub> bands with respective binding energies of about 71.1 and 74.4 eV ( $\pm 0.1$ eV) as shown in Fig. 5.18. These values of binding energy are in good agreement with that reported in literature for platinum with zero oxidation state [134,153]. Thus XPS studies confirms the presence of platinum in zero oxidation state which is required the catalytic activity. Zr-3d spectra of three samples as shown in Fig. 5.19, shows 3d<sub>3/2</sub> and 3d<sub>5/2</sub> peaks with binding energies at around 182.3 eV and 184.7 eV which correspond to +4 oxidation state of zirconium [158,159].



**Fig 5.18:** XPS spectra of Pt/ZrO<sub>2</sub> catalysts in the spectral region corresponding to Pt-4f.

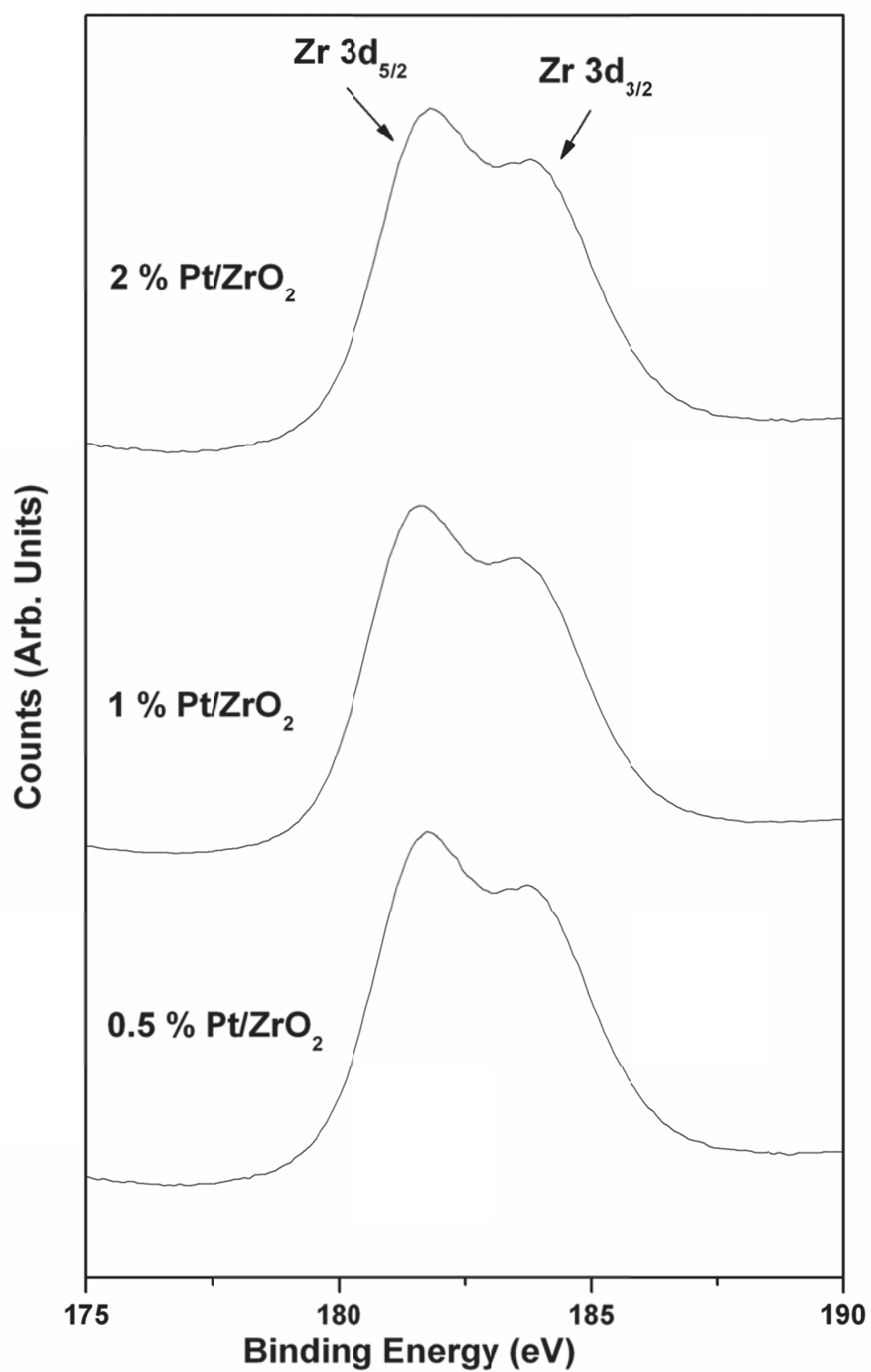


**Fig 5.19:** XPS spectra of Pt/ZrO<sub>2</sub> catalysts in the spectral region corresponding to Zr-3d.



## Chapter 5

---

### 5.3.2.6 Catalytic activity of the catalyst

The catalysts prepared were evaluated for their activity for liquid phase HI decomposition reaction. After carrying out the reaction for a particular time and at a particular temperature (2h, 120 °C), the solution was filtered. The eluent recovered was analysed for concentrations of  $H^+$ ,  $I^-$  and  $I_2$  present in it and change in their concentrations was used to calculate the percentage conversions. The conversion values thus obtained are shown below in Table No. 5.4.

Catalyst	Conversion ( % )
Blank	2.9
ZrO <sub>2</sub>	6.3
0.5 Pt/ZrO <sub>2</sub>	13.9
1.0 Pt/ZrO <sub>2</sub>	16.5
2.0 Pt/ZrO <sub>2</sub>	18.7

**Table 5.4:** *Percentage conversion values for the different catalysts*

From Table 5.4, it can be seen that the percentage conversion of HI into hydrogen and iodine with zirconia alone was found to be 6.3 , which increases significantly upon use of a platinum based catalyst. Also, it can be seen that the percentage conversion increases on increasing of the noble metal loading. This highlights the role of platinum

## Chapter 5

---

metal and its requirement in the supported catalyst system to show appreciably high levels of conversion.

The conversion value for 1 % Pt/ZrO<sub>2</sub> catalyst is comparable to mesoporous Pt/carbon catalyst with same noble metal loading like Pt/MCM-C and Pt/SBA-C (Chapter 4). The conversion was higher as compared to other Pt/Carbon catalysts Pt/AC and PT/RC (Chapter 3) and Pt/FSC (Chapter 4).

This 1 % Pt/ZrO<sub>2</sub> catalyst was also evaluated for its activity at 120 °C as a function of time, i.e. the reaction was carried out for different time intervals from 1 hr to 4 hrs and percentage conversion was measured and it was found to be increasing almost linearly with time as shown in Fig. 5.20. The linearity in the conversion with time also confirms that the reaction product does not have any deterring effect as the conversion increases.

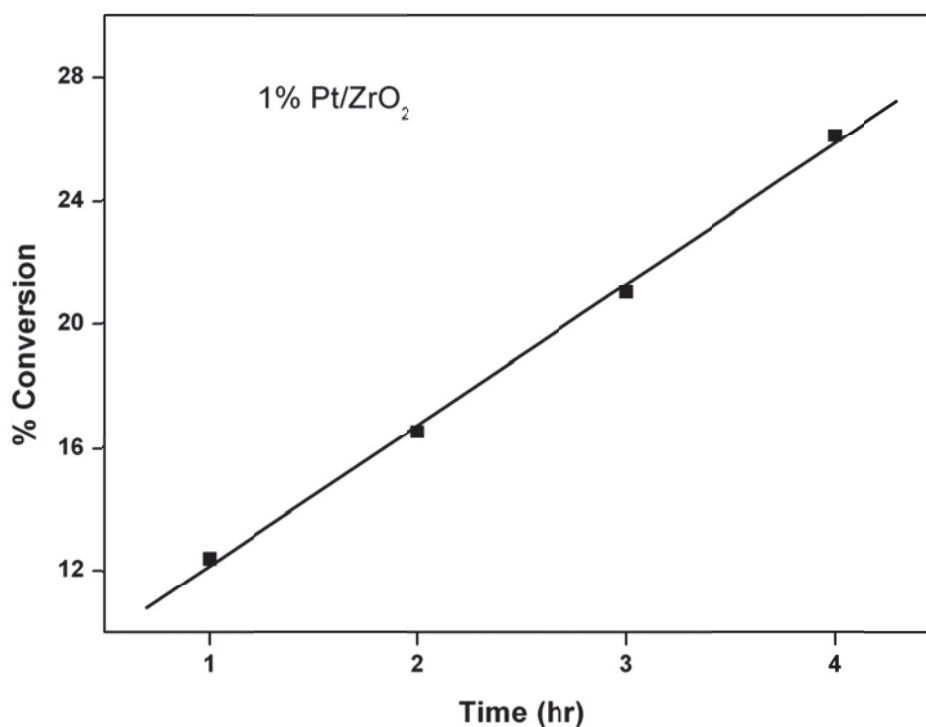


**Fig 5.20:** Percentage conversion for 1 % Pt/ZrO<sub>2</sub> with time at 120 °C

### 5.3.2.7 Stability of the Catalyst

After a typical study of 2 hours the used catalysts recovered from HI solution, were washed thoroughly and dried. These catalysts were characterized by XRD. Fig. 5.21 shows the XRD patterns for different used Pt/ZrO<sub>2</sub> catalysts.

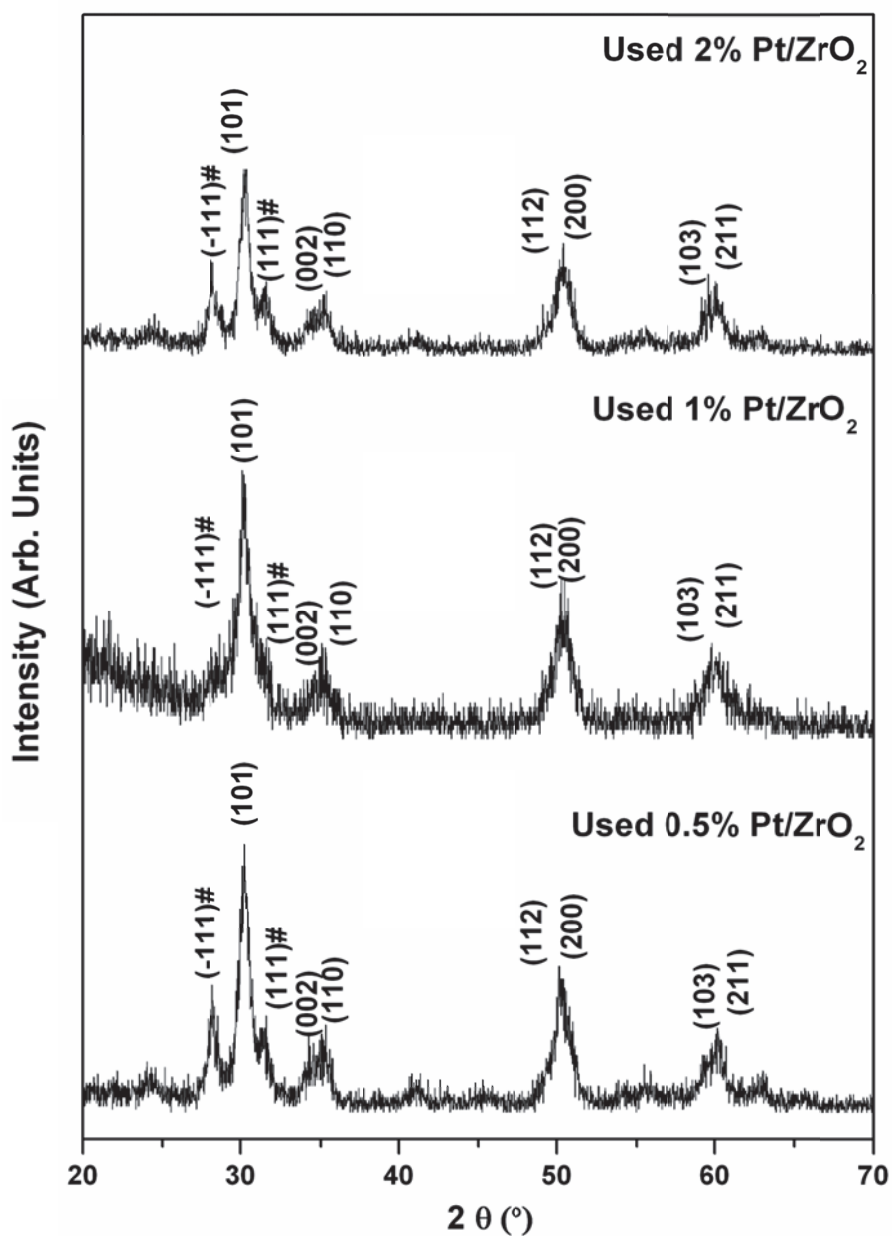


Fig 5.21: XRD patterns of used Pt/ZrO<sub>2</sub> catalysts

## Chapter 5

---

Here, there is no shift in peak positions corresponding to zirconia as compared to the fresh catalysts; the biphasic nature of zirconia is also same after the reaction. It indicates that there is no change in structure of the catalyst support during the reaction. As observed for fresh catalyst, the used catalyst also does not show any XRD line for platinum, hence confirming for the unchanged uniform dispersion. Thus we can say that the prepared catalysts are stable under the harsh conditions of liquid phase HI decomposition reaction conditions.

The eluent solution, when analysed for presence of Platinum by ICP-AES, did not exhibit the presence of the noble metal. This confirms for the stability of these catalyst against noble metal leaching under the reaction conditions.

### 5.3.3 Conclusion

Mesoporous zirconium oxide supported platinum catalysts were successfully prepared and applied to the liquid phase HI decomposition reaction of the Sulphur-Iodine process. There is a significant increase in percentage conversion of HI to  $H_2$  and  $I_2$  in presence of Pt/ZrO<sub>2</sub> catalyst. Percentage conversion is very low when the reaction is carried out in presence of only ZrO<sub>2</sub>, the support. Also, the conversion is found to increase with the increase in the noble metal loading in the catalyst, again highlighting the role of platinum in the catalytic decomposition of HI over these supported noble metal catalyst.

The results of XRD, EDS and SEM show that the loading of platinum metal over zirconia enhances the sintering resistance of the noble metal thereby increasing life of the catalyst. Moreover, the dispersion of Pt over the supports is found to be uniform. It can

## ***Chapter 5***

---

also be concluded from the results of activity evaluation that the percentage conversion of HI increases with the increase in loading percentage of the noble metal over support. The catalyst was also found to be stable under the liquid phase HI decomposition reaction conditions. All the results signify the potential for use of platinum supported on mesoporous zirconia catalysts for HI decomposition reaction of Sulphur-Iodine cycle for large scale production of hydrogen.

# Chapter 6

## Iodine Speciation Studies

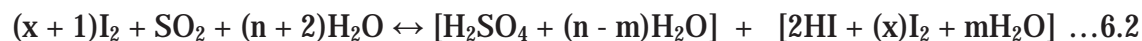
---

### 6.1 Introduction

Bunsen reaction is one of the three steps of sulphur – iodine cycle for thermochemical splitting of water, where  $\text{SO}_2$  is passed into the aqueous solution of iodine to produce hydriodic acid and sulphuric acids. The reaction involved can be presented as follows:



For practical purposes this reaction is carried out in liquid water media with an excess of both iodine and water with respect to their stoichiometric values. This is done to enhance separation of the two products into two corresponding liquid phases, namely a sulfuric acid rich phase and a  $\text{HI}_x$  phase. This also makes it possible to drive the reaction thermodynamically. Thus nearly all excess iodine is present in the heavier  $\text{HI}_x$  phase, while water is present in both liquid phases. Accordingly, the process can be schematized as follows:



Sulfuric acid phase

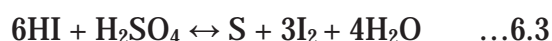
$\text{HI}_x$  phase

## Chapter 6

---

where  $x$  and  $n$  are the iodine and water molar excess quantities, respectively, in the reactant phase and  $m$  is the molar quantity of the excess water that ends up in the product  $\text{HI}_x$  phase.

However, along with the above reaction, the following two side reactions have also been found to occur producing elemental sulfur  $\text{S}$  and hydrogen sulfide  $\text{H}_2\text{S}$  [160]:



Therefore for the optimization of the S-I process, optimization of Bunsen section is of great importance. The sustainability of the whole S-I process is dependent of several factors involved in the Bunsen section for example composition of the  $\text{H}_2\text{SO}_4$  and  $\text{HI}_x$  phase, excess iodine and water in the feed and side reactions.

Lot of work has been carried out on the Bunsen section investigating the liquid-liquid equilibrium (LLE) phase separation performance [161-164]. Effect of  $\text{HI}$  and  $\text{I}_2$  concentration in a quaternary system  $\text{H}_2\text{SO}_4/\text{HI}/\text{I}_2/\text{H}_2\text{O}$  has also been investigated in the temperature range 25–120 °C. It was found that the LLE phase separation improved with a decrease of water and an increase of iodine content in the mixture [165]. Range of iodine content allowable (lower limit for liquid-liquid phase separation and upper one for iodine precipitation) has also been calculated at different temperatures. Norman et al [30] have reported the following optimum composition for the Bunsen reaction.



## Chapter 6

---

The excess iodine added, has dual role of facilitating segregation of the two product acids into two corresponding liquid phases and minimizing the side reactions between iodine and sulfur compounds by driving reactions 6.3 and 6.4 backwards[166,167].

Due to presence of excess iodine in  $HI_x$  phase, various polyiodide species are generated during the separation process. The formation of various polyiodide species can be explained as follows:



These polyiodide species need to be identified for complete understanding of the mechanism involved and kinetics followed in the processes. Lot of research works are reported in literature for identification of polyiodide species [168-171]. Most of the work reported in the literature is related to separation and identification of salts and complexes of these polyiodides in molten and solid form, only few of them are for aqueous solutions [172,173]. The methods employed range from vibrational spectroscopy, Mossbauer spectroscopy, NMR, ESR, ESCA, UV/Visible spectroscopy, electro-analytical techniques and X ray based methods.

In addition to the above facts, formation of polyiodide species is important in case of liquid phase HI decomposition where iodine (one of the product) get dissolved in HI. Therefore an attempt was made to identify the different polyiodide species of  $HI_x$  phase of Bunsen reaction. Also effect of presence of sulfuric acid has also been studied because



## **Chapter 6**

---

it may be present in the HI phase as an impurity. The spectroscopic techniques based on molecular absorbance in UV-visible spectroscopy and Raman spectroscopy were used to exploit change in symmetry for different HI<sub>x</sub> species.

### **6.2 Experimental**

#### **6.2.1 Preparation of solutions**

Different stock solutions of HI, KI and I<sub>2</sub> were prepared by dissolving the appropriate amount of the reagents in distilled water. HI and KI, both were easily soluble in water while I<sub>2</sub> requires sonication for dissolution. Thereafter these solution were mixed in different ratios for recording Raman and UV-visible spectra of different solutions with different I<sub>2</sub>:I<sup>-</sup> ratios.

#### **6.2.2 Raman spectroscopy**

Laser Raman spectra of the solutions containing varying amounts of HI, KI and I<sub>2</sub> were recorded on a LABRAM-1 spectrometer (ISA) in a back-scattering geometry, at a spectral resolution of 2 cm<sup>-1</sup>. An Ar<sup>+</sup> ion laser (488 nm) was used as an excitation source.

#### **6.2.3 UV-visible Spectroscopy**

The UV/Visible spectra of the solutions containing varying amounts of HI, KI and I<sub>2</sub> were recorded using a JASCO Spectrophotometer (Model V-650), JAPAN.

### **6.3 Results and discussion**

#### **6.3.1 Raman spectroscopy**

Raman spectra were recorded for 0.1 M HI with iodine concentration ranging from 0.1 to 0.6 M, i.e. the spectra were obtained for I<sub>2</sub>:I<sup>-</sup> ratio of 1 to 6. No spectral features were observed for both pure I<sup>-</sup> and pure I<sub>2</sub> solutions. The solution with HI:I<sub>2</sub> ratio

## Chapter 6

of 1:1 exhibits a strong broad Raman band in region 40 to 180  $\text{cm}^{-1}$  peaking at 113  $\text{cm}^{-1}$  (Fig. 6.1). This is attributed to presence centrosymmetric ( $D_{3h}$ )  $\text{I}_3^-$  species [168,174,175]. Triiodide species has a Raman active symmetric stretching band at  $\nu_1$  at 110  $\text{cm}^{-1}$  and two IR active bands at 50-70 and 130-140  $\text{cm}^{-1}$  corresponding to doubly degenerate bending and asymmetric stretch modes,  $\nu_2$  and  $\nu_3$ , respectively. Appearance of peak at 60  $\text{cm}^{-1}$  and 130  $\text{cm}^{-1}$  is indicative of change in symmetry of the  $\text{I}_3^-$  species due to anion-anion or anion-solvent interaction [175]. Presence of donor  $\text{I}_2$  adduct has also been reported to play a major role in appearance of  $\nu_3$  band [178].

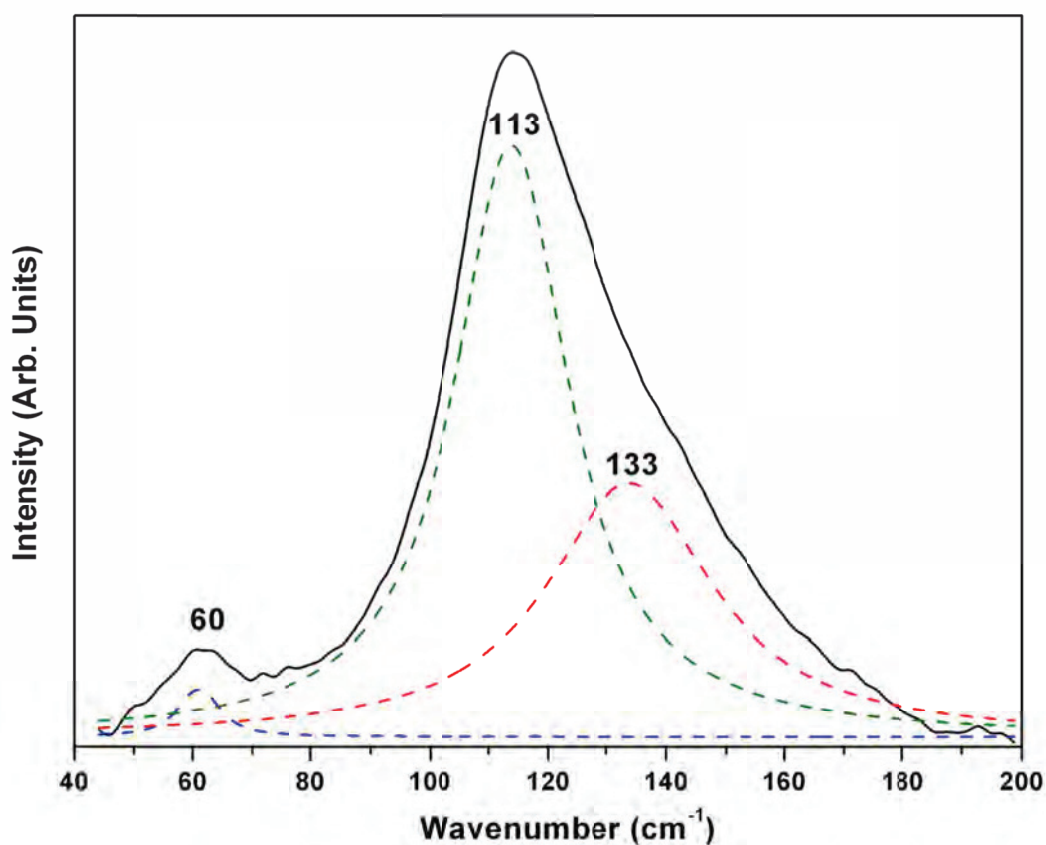


**Fig. 6.1:** Raman spectra of HI:I<sub>2</sub> 1:1 solution with deconvolution showing  $\nu_1$ ,  $\nu_2$  and  $\nu_3$  peaks

## Chapter 6

Fig. 6.2 shows overlay of Raman spectra obtained for increasing concentration of iodine from 0.1 M to 0.6 M in 0.1 M HI solution. The broad peak obtained for 1:1 HI:I<sub>2</sub> solution is found to decrease as HI:I<sub>2</sub> ratio increases to 1:4 and is constant for HI:I<sub>2</sub> ratio upto 1:5 and then again decreases for 1:6 ratio solution. Considering that 113 cm<sup>-1</sup> peak corresponds to I<sub>3</sub><sup>-</sup> species this decrease indicates for conversion of this species into higher polyiodides either by disproportionation or by adduct formation with iodine as shown below:

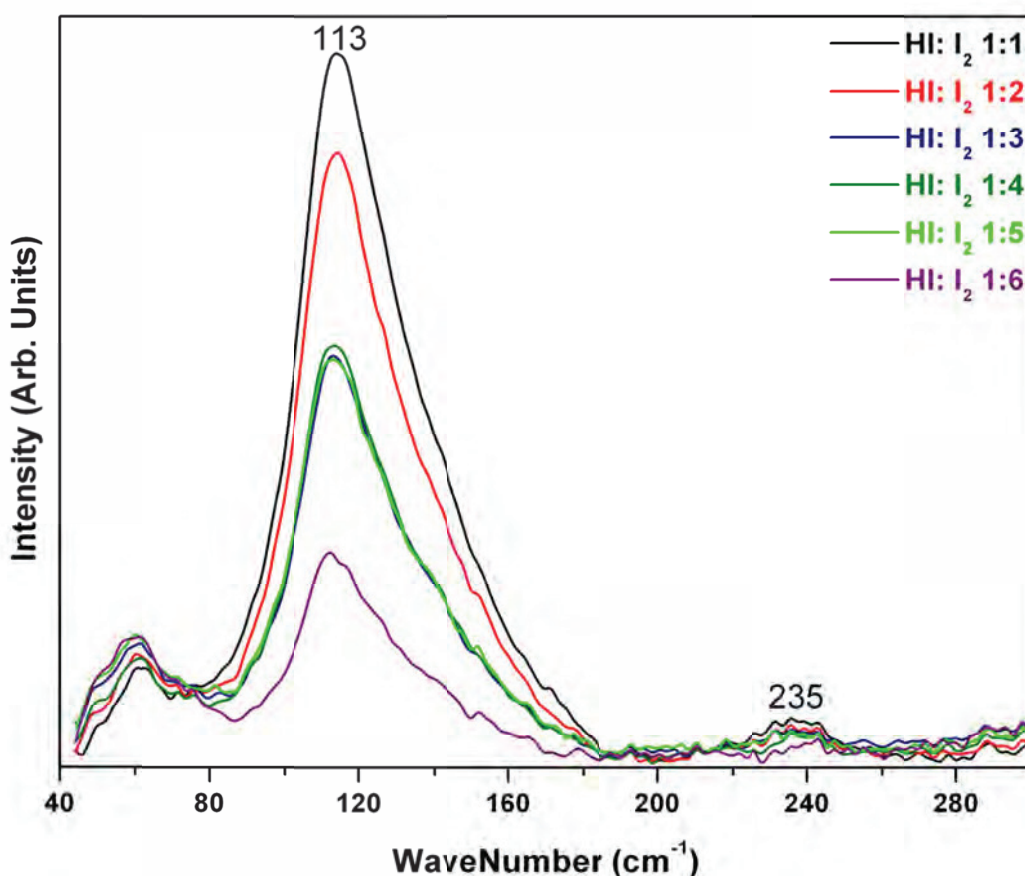


Fig. 6.2: Raman spectra for different HI:I<sub>2</sub> ratio solutions.

## Chapter 6

---

For understanding of this variation in the Raman spectra the change in intensity of three deconvoluted peaks as shown in Fig. 6.3 was plotted. The peak corresponding to the  $\nu_1$  band shows drastic decrease with increasing iodine concentration up to 1:3 HI : I<sub>2</sub> ratio and then remains constant for ratio up to 1:5 before decreasing further for 1:6 ratio. Similar trend is observed for  $\nu_3$  band, too. Compared to these the  $\nu_2$  band exhibits consistent increase with increasing HI:I<sub>2</sub> ratio. Such a pattern can be explained by taking into consideration the presence of I<sub>5</sub><sup>-</sup> species. It is reported by Sharp et al [174] that various bands exist at 165, 55, 146 and 114 cm<sup>-1</sup> and 157, 90, 143, 110 cm<sup>-1</sup> for linear and bent pentaiodide species, respectively. This system can be understood in terms of a disproportionation and coupled equilibrium initiated by the liquidification of a triiodide system as given below [168]:



Taking these information into account attempt was made to deconvolute Raman spectra corresponding to HI:I<sub>2</sub> ratio of 1:3 and multiple deconvolutions could be obtained for five peaks as shown in Fig. 6.4. Though not very conclusive it does indicate towards presence of higher polyiodides in equilibrium with the triiodide for increasing iodine concentration.

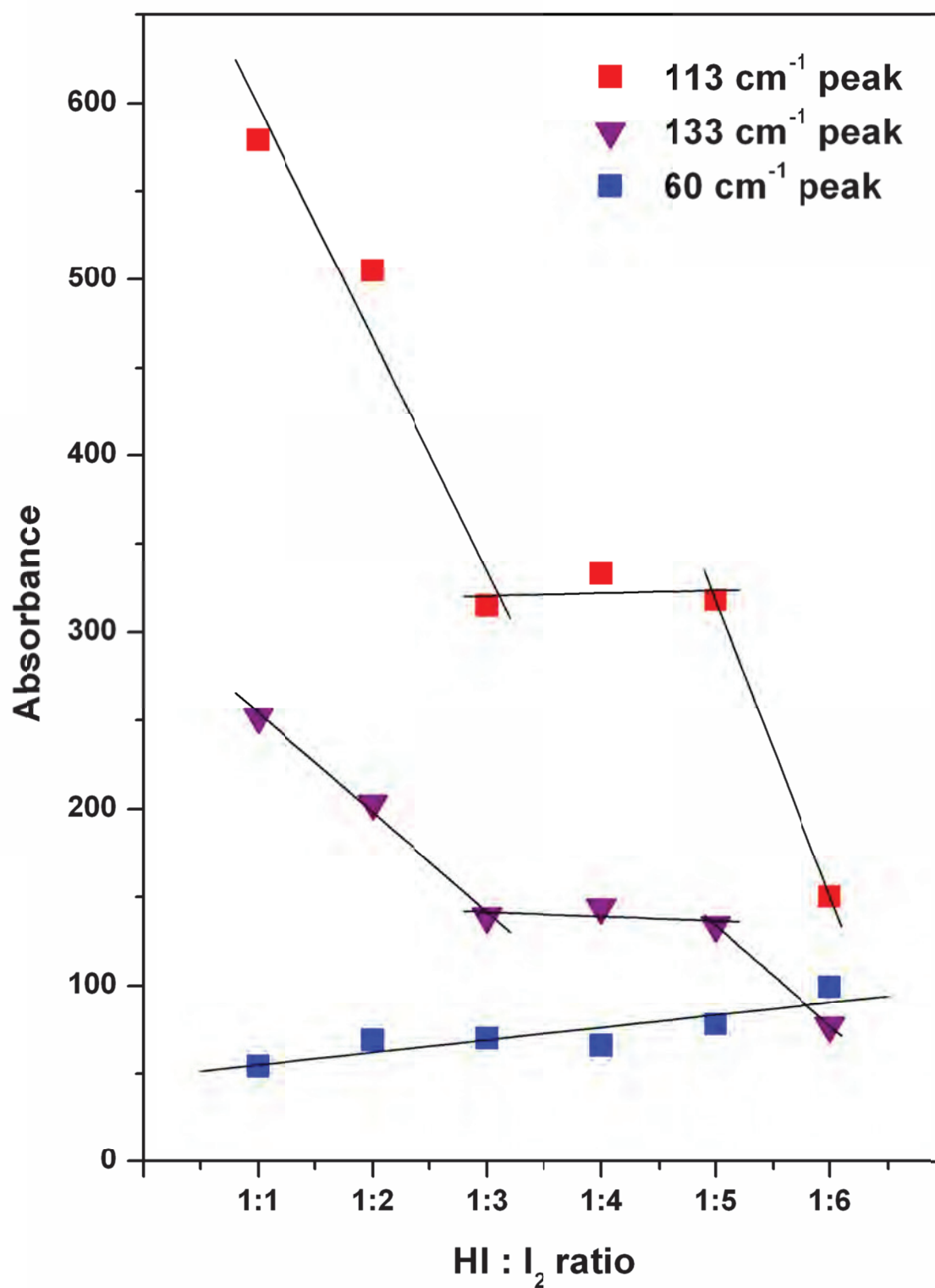


Fig. 6.3: Variation of intensity of  $\nu_1$ ,  $\nu_2$  and  $\nu_3$  peaks for different HI:I<sub>2</sub> ratio solutions.

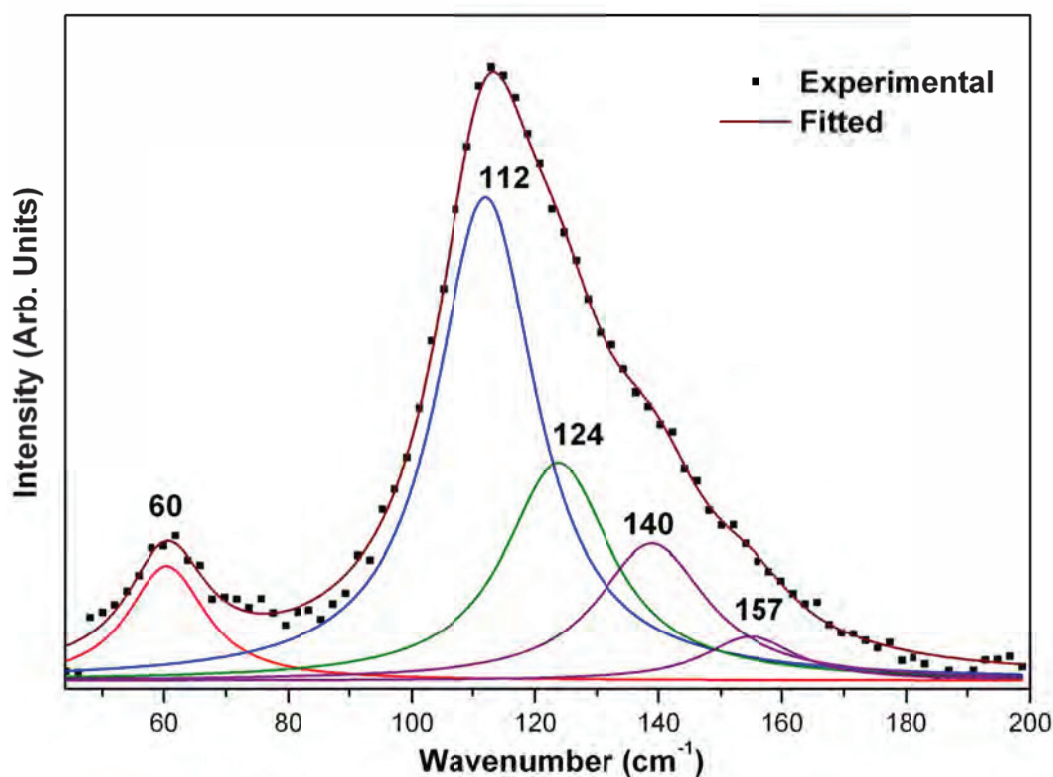


Fig. 6.4: Multiple deconvolutions corresponding to HI:I<sub>2</sub> ratio of 1:3.

As discussed in the introduction part, sulfuric acid may be present in the HI phase as an impurity. Therefore Raman spectra of the iodine iodide mixture has also been recorded in presence of sulphuric acid to see the effect of presence of sulfuric acid as well as effect of its concentration on the triiodide formation. For this purpose varying concentrations of sulfuric acid (0.1M to 0.6M) were added to a 1:1 HI:I<sub>2</sub> solution (Fig.6.5). It was observed that the Raman spectrum is free from any interference from sulfuric acid, as there was no change in position as well the height of the most prominent peak ( i.e. peak corresponding to I<sub>3</sub><sup>-</sup>).

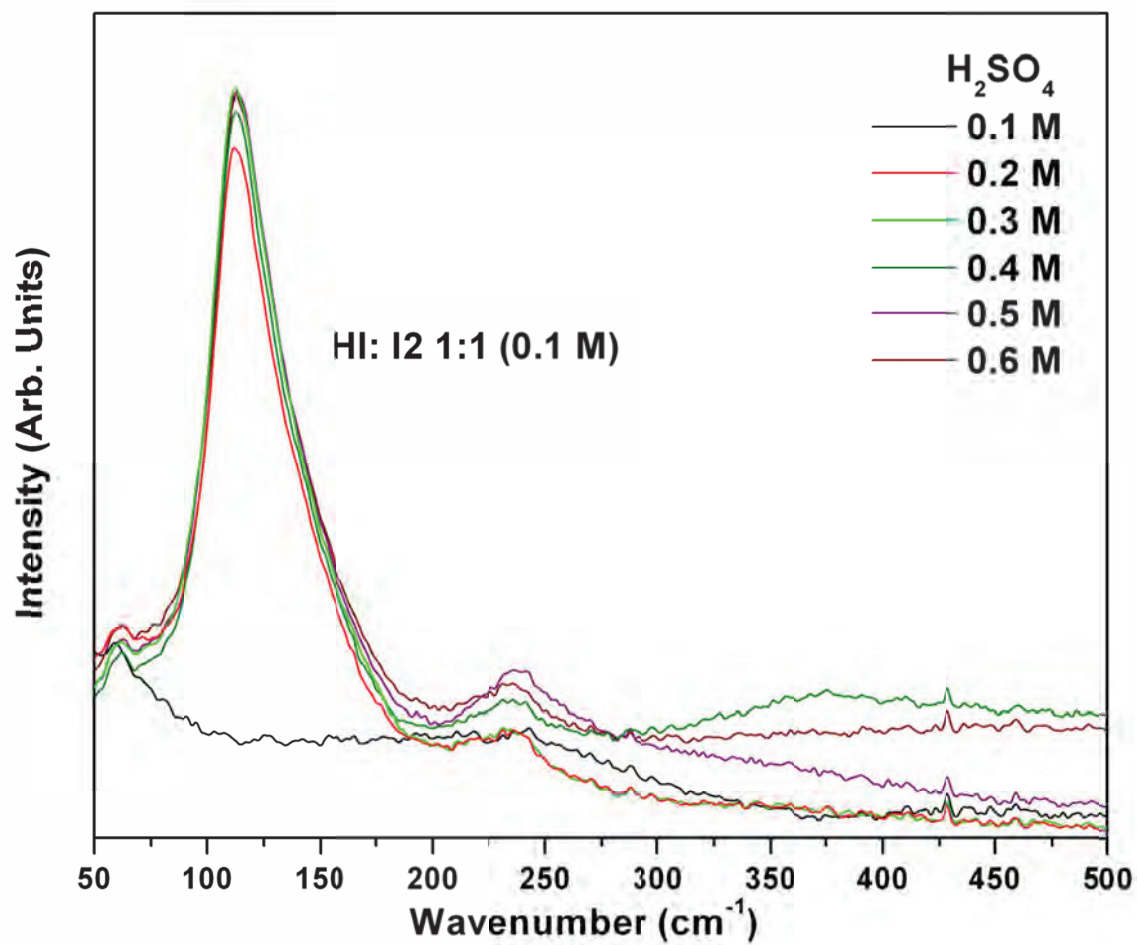


Fig. 6.5: Raman spectra in presence of different concentrations of sulfuric acid, depicting  
no effect of its presence

## Chapter 6

---

### 6.3.2 UV-visible spectroscopy

Similar measurements on iodine-iodide solutions were carried out using UV-visible spectroscopy. Only difference here is that lower concentration (in the range of  $10^{-4}$  M) are used to avoid saturation of absorbance signal. For this KI solutions of known concentration were mixed with Iodine solution to obtain final solutions of  $2 \times 10^{-4}$  M in terms of KI with KI:I<sub>2</sub> ratio varying from 1:0 to 1:10.

UV-visible absorption spectra for the above mentioned samples with KI:I<sub>2</sub> ratio varying from 1:0 to 1:10 is shown in Fig. 6.6. Absorption spectrum for iodine solution of  $2 \times 10^{-4}$  M concentration is also shown in Fig. 6.6. Fig. 6.6 c shows spectrum obtained for KI:I<sub>2</sub> 1:1 solution. It exhibits two peaks with maxima at 288 nm and 358 nm. Peak pertaining to 358 nm is reported to be of I<sub>3</sub><sup>-</sup> species [170]. This peak is found to decrease with increasing I<sup>-</sup>/I<sub>2</sub> ratio from 1:1 to 1:10. This is attributed to conversion of I<sub>3</sub><sup>-</sup> species to higher polyiodides, a trend similar to that obtained with Raman spectroscopy. However, this spectrum shows an additional peaks at ~288 nm and this peak is absent from spectrum as recorded for respective KI and iodine solutions. As observed in Fig. 6.7, this peak also follows a pattern of decrease in absorbance value with increasing I<sub>2</sub>:KI ratio as observed for 358 nm peak. It again indicates towards presence of I<sub>3</sub><sup>-</sup> species for its genesis.



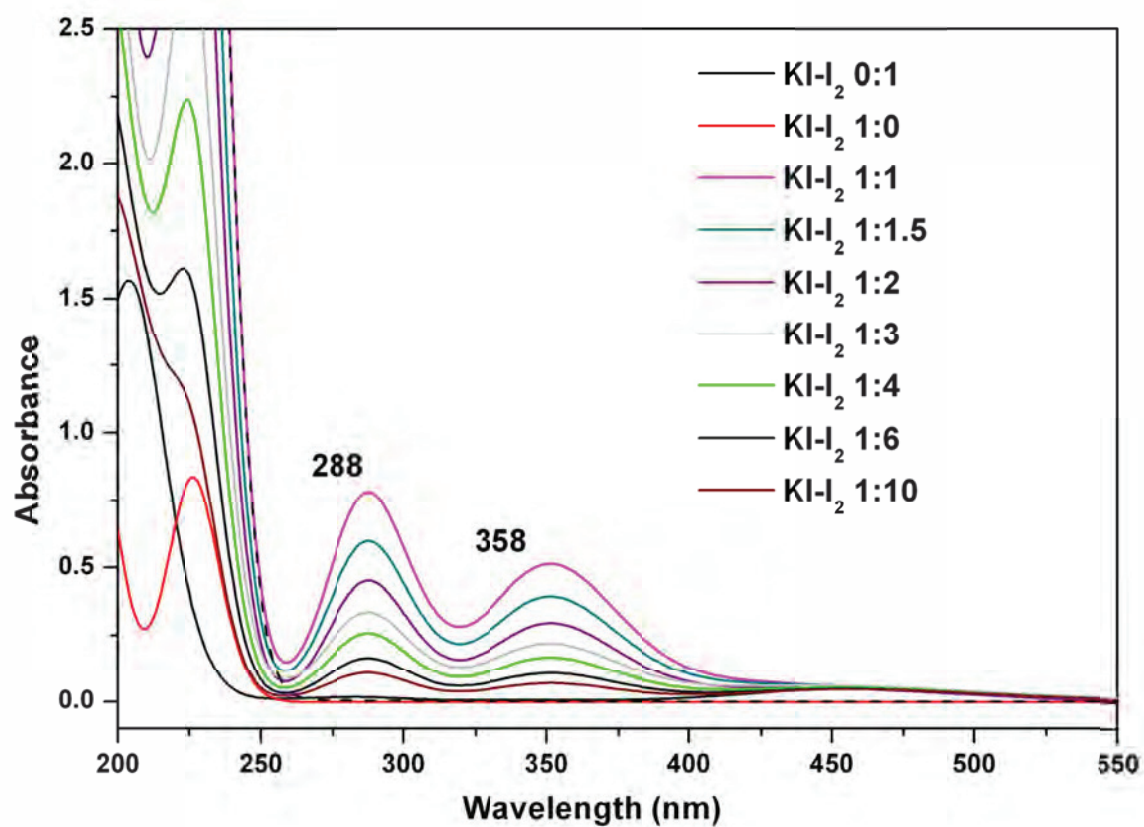


**Fig. 6.6:** *UV-visible spectra for different KI-I<sub>2</sub> solutions.*

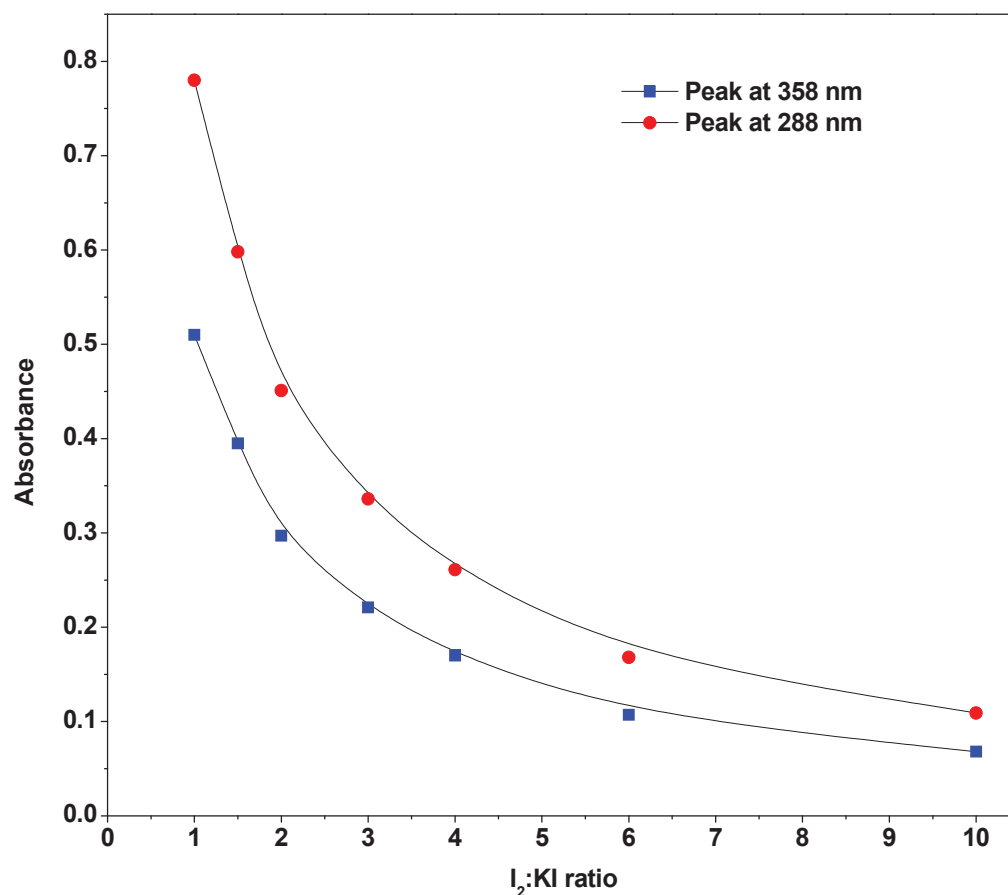


**Fig. 6.7:** Variation in absorbance value of 358 and 288 nm peaks with increasing iodine concentration in KI-I<sub>2</sub> solution.

When similar measurements were carried out for HI-I<sub>2</sub> solution of  $2 \times 10^{-4}$  M concentration, similar absorbance patterns are observed, though with a reduced absorbance values (Fig. 6.8). For these solutions the lower wavelength peaks at  $\sim 200$  nm and  $\sim 225$  nm, which were out of scale for KI based solutions, can be observed clearly. Both these peaks are different from earlier mentioned peaks at 288 nm and 358 nm, in the sense that they appear in case of pristine HI (204 nm) and iodine (227 nm) solutions too, respectively.

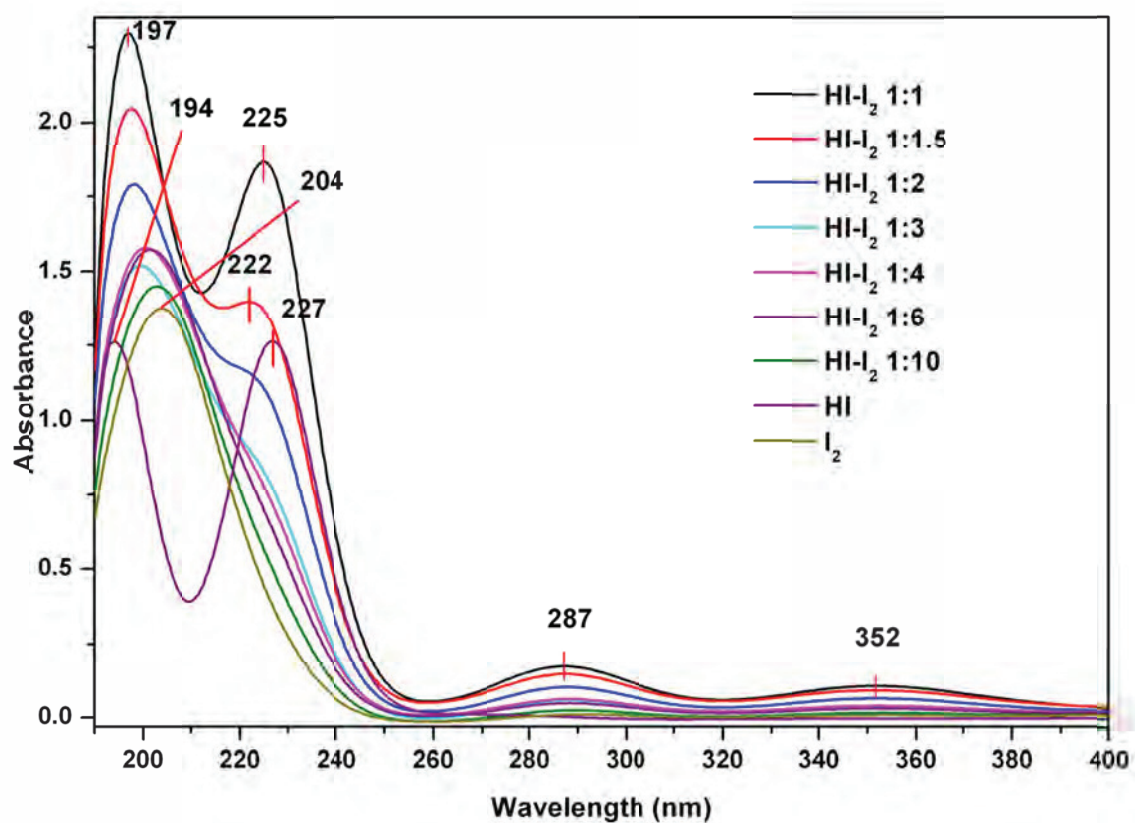


**Fig.6.8:** UV-visible spectra for different HI:I<sub>2</sub> ratio solutions

The peaks are appearing at 287 and 352 in this case are same as that for KI-I<sub>2</sub> solution mixture, where these peaks appear at 288 nm and 358 nm. These peaks also follow the same trend of absorbance upon increasing iodine concentrations as shown in Fig. 6.9.

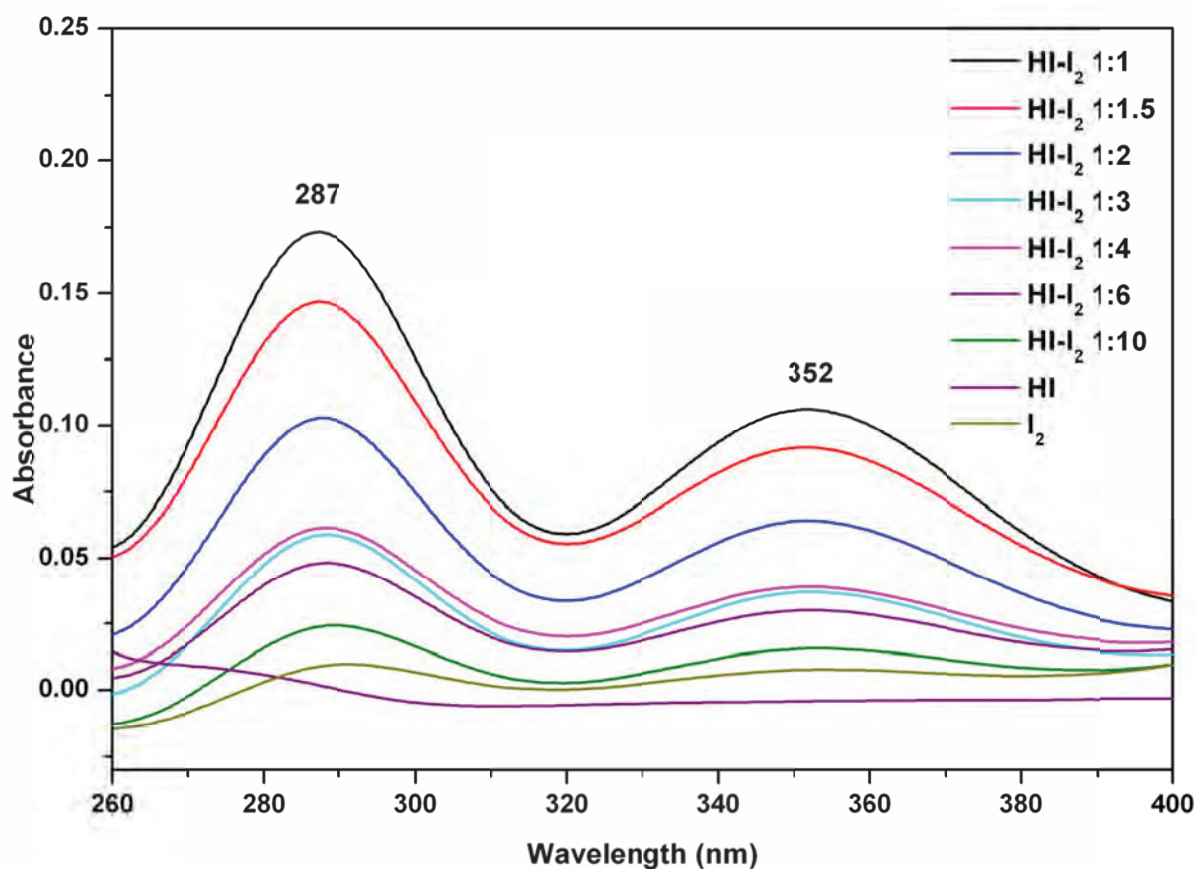


**Fig.6.9:** UV-visible spectra for different HI:I<sub>2</sub> ratio solutions in range of 260-400 nm

When this data is analysed for change in absorbance value of these peaks with respect to increasing I<sub>2</sub> concentration in HI solution a plot similar to Job's plot is obtained (Fig. 6.9) with maxima for 1:1 HI : I<sub>2</sub> concentration. Maxima for 1:1 composition again points towards assigning of these peaks to I<sub>3</sub><sup>-</sup> type of species. Due to their very high absorbance value these peaks can be very efficiently utilized for detection of triiodide species with high sensitivity.

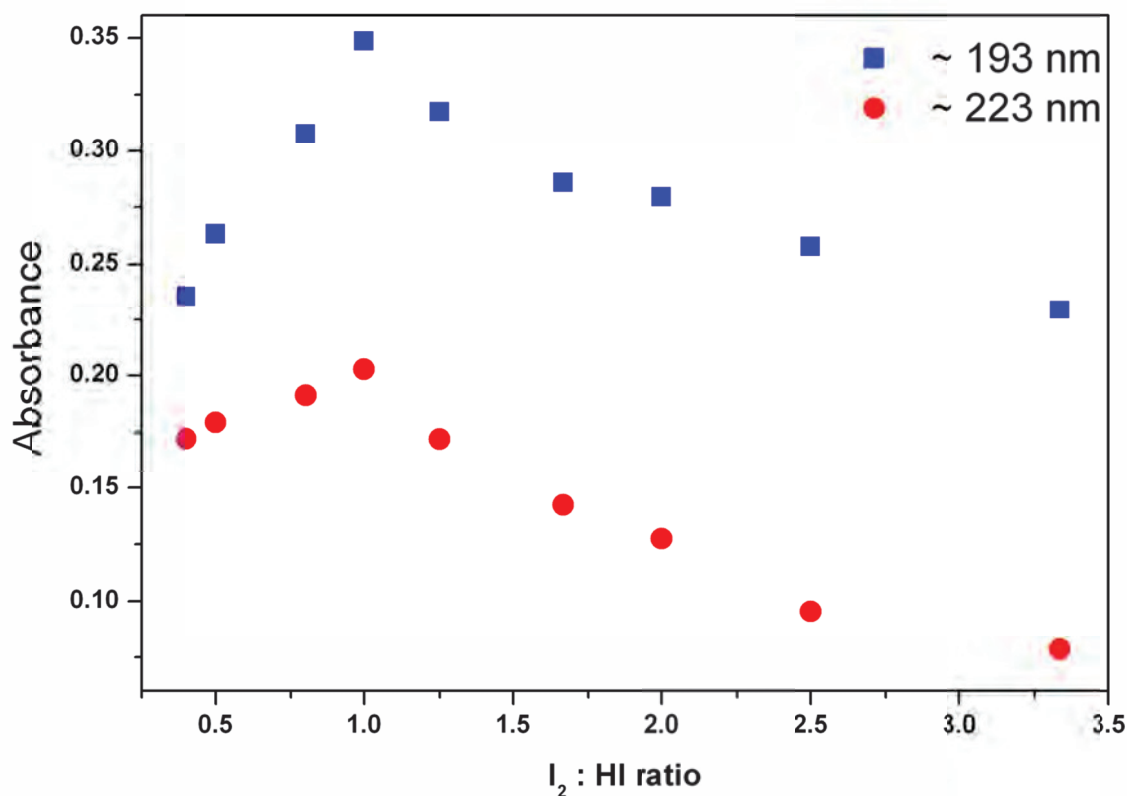


**Fig. 6.10:** Variation in absorbance values of 193 nm and 223 nm peaks with respect to iodine-HI ratio.

### 6.4 Conclusion

Presence of  $I_3^-$  and higher polyiodides in the  $HI_x$  phase of Bunsen reaction of sulfur Iodine thermochemical cycle was confirmed by UV visible and Raman studies. As far as  $I_3^-$  is concerned, direct evidence of its formation on addition of iodine to iodide solution is obtained from Raman as well as UV-Visible spectroscopy. Though there is no direct evidence for presence of higher polyiodides is obtained, still their formation could be indirectly inferred from these studies.

# Chapter 7

## Conclusions and Future Scope

---

### 7.1 Conclusions

The studies carried out in this thesis have contributed to fundamental understanding as well as development of heterogeneous catalysis for the major goal of hydrogen generation. Thermochemical water splitting by Sulfur Iodine thermochemical cycle is proposed for the large scale production of hydrogen using nuclear or solar heat (Chapter 1). This thesis reports development of catalysts for hydriodic acid decomposition reaction: the hydrogen producing step of S-I thermochemical cycle as well as other iodine based cycles (Chapter 3, 4, and 5). This thesis also includes the details of speciation studies carried out for polyiodide species generated during Bunsen reaction/ $\text{HI}_x$  separation (Chapter 6). Here, in this chapter we summarize the objective, approach towards the problem and major findings of the work, along with scope for the future work.

The main objective of these studies was to develop a suitable catalyst for hydriodic acid decomposition reaction which is active as well as stable under the harsh reaction environment. Hydriodic acid decomposition reaction is important in case of

## ***Chapter 7***

---

thermochemical water splitting research since it is the hydrogen producing step of the S-I cycle which is one of the most promising method for large scale hydrogen production using nuclear or solar heat. Majority of work and catalytic systems for HI decomposition reported in open literature are for vapor phase decomposition, while we have carried out detailed study of various catalysts for liquid phase HI decomposition reaction. Another objective of the study related to iodine speciation was to establish the presence of polyiodide species in Bunsen reaction mixture and their identification. These studies are also relevant to liquid phase HI decomposition reaction because iodine being one of the products is present in the reaction mixture along with the reactant HI, hence formation of polyiodides is possible.

Carbon with different properties was first of all explored as a catalyst support for platinum metal. Choice of carbon is based in its properties like stability, high volume to weight ratio, tunability of surface area and porosity. Mesoporous and microporous carbon supports were prepared by hard templating route using porous silica templates. Along with them, activated carbon and graphitic carbon were also explored as support for catalysts. For graphitic carbon based catalysts, the effect of noble metal loading was also studied and it was observed that percentage conversion increase with the platinum loading, however the increase is not linear. It has been observed that 1 wt % loading of platinum gives maximum conversion in terms of per unit weight of platinum. The stability of the catalysts in presence of excess iodine was also established (Chapter 3).

In case of porous carbon supported catalysts prepared by hard templating method, platinum can be added at two different steps. The step at which platinum is added affects

## *Chapter 7*

---

the stability of catalysts against platinum leaching, whereas activity of catalysts is similar in both cases. Catalyst where platinum precursor is added along with the carbon precursor is having better platinum retention as compared to the case where platinum is loaded after formation of carbon. Also it was observed that the catalysts with microporous nature of support have lower activity in spite of having high surface area, while the catalysts with mesoporous support have higher activity (Chapter 4). Therefore mesoporous carbon supported catalysts where platinum was added at the first stage catalyst were found to be the better as compared to others in terms of activity as well as stability. Overall catalysts with mesoporous nature or mixed porosity or planar type of support exhibit higher catalytic activity (Chapters 3 and 4).

Oxides were also explored as catalyst support for platinum. Three different oxides (Titania, Ceria and Zirconia) were used as support for preparation of catalysts for HI decomposition reaction. Chemical reduction method was used for reducing platinum to zero oxidation state. Effect of platinum loading was studied and it was found that the percentage conversion increase with increasing noble metal loading, in this case also the increase was not linear.

In terms of catalytic activity, it was observed that ceria supported catalysts exhibit highest conversion followed by zirconia and then titania. But ceria support was found to be unstable under in reaction conditions, due to dissolution of support in HI as most of the catalyst gets dissolved. Among zirconia and titania, zirconia based catalysts exhibits higher stability against platinum leaching, with no platinum coming into the HI solution. Mesoporous nature of zirconia support may also played important role in enhancing



## Chapter 7

---

catalytic activity and stability of zirconia supported catalysts. Therefore zirconia was found to a better support for platinum catalysts for liquid phase HI decomposition reaction (Chapter 5).

Overall conclusion from catalyst development studies for liquid phase HI decomposition reaction is that the following catalysts were found to be better in terms of activity as well as stability as compared to others: (i) Graphitic carbon, (ii) Mesoporous carbon and (iii) Zirconia supported catalysts. Keeping in mind the goal of large scale production of hydrogen, large scale production of catalyst is also required. For this purpose mesoporous carbon seems to be a less attractive option because preparation of mesoporous carbon is time consuming and costly affair. Graphitic carbon supported catalyst is a suitable candidate for large scale production purposes. Zirconia based catalyst with simple chemical reduction method is also attractive candidate as it can also be prepared in large scale.

For speciation studies, presence of  $I_3^-$  and higher polyiodides in the  $HI_x$  phase of Bunsen reaction of sulfur Iodine thermochemical cycle was confirmed by both UV visible absorption spectroscopy and Raman spectroscopy studies. As far as  $I_3^-$  is concerned, direct evidence of its formation on addition of iodine to iodide solution is obtained from Raman as well as UV-Visible spectroscopy. Though there is no direct evidence for presence of higher polyiodides is obtained, still their formation could be indirectly inferred by these studies.

## ***Chapter 7***

---

### **7.2 Future Scope**

Future scope of this work includes use of these catalysts for vapor phase HI decomposition reaction and the comparison of the results with that for liquid phase. Also based upon the activity and stability results and also considering the scalability for large scale production of catalysts, Platinum-zirconia and platinum-graphitic carbon based catalysts can be explored for large scale HI decomposition. Detailed studies on kinetics of HI decomposition on these two catalysts can be carried out to understand the mechanism of this reaction. Nickel based catalysts can also be explored to bring down the cost of the catalyst.

# References

---

- [1] BP Statistical Review of World Energy 2014, Source <http://www.bp.com/content/dam/bp/pdf/Energy-economics/statistical-review-2014/BP-statistical-review-of-world-energy-2014-full-report.pdf>
- [2] The OECD environmental outlook to 2050: Key findings on climate change, Source [http://www.oecd.org/env/cc/Outlook 20to 202050 Climate 20Change 20Chapter H IGLIGHTS-FINA-8pager-UPDATED 20NOV2012.pdf](http://www.oecd.org/env/cc/Outlook%20to%202050%20Climate%20Change%20Chapter%20HIGHLIGHTS-FINA-8pager-UPDATED%20NOV2012.pdf)
- [3] B. Suresh, M. Yoneyama, S. Schlag, *CEH Marketing Research Report Abstract. Hydrogen. Chemical Industries Newsletter October 2007, 7-8, SRI Consulting. Source* <http://www.sriconsulting.com/nl/Public/2007Oct.pdf>
- [4] International Energy Agency (IEA). *IEA Energy Technology Essentials. Hydrogen Production & Distribution. April 2007. AECD/IEA, 2007. Source* <http://www.iea.org/techno/essentials5.pdf>
- [5] C.E. Bamberger, D.M. Richardson, *Cryogenics*, **1976**, *16*,197-208.
- [6] J.E. Funk, *International Journal of Hydrogen Energy*, **2001**, *26*, 185-190.
- [7] S. Abandes, G. Flamant, *Solar Energy*, **2006**, *80*, 1611-1623.
- [8] I. Dincer, M.T. Balta, *International Journal of Energy Research*, **2011**, *35*,123-137.
- [9] R.R. Sadhankar, *International Journal of Energy Research*, **2007**, *31*, 1131-1141.
- [10] M.A. Rosen, G.F. Natere, C.C. Chukwu, R. Sadhankar, S. Suppiah, *International Journal of Energy Research*, **2012**, *36*,456-465.

## References

---

- [11] S. Licht, *Chemical Communications*, **2005**, 37, 4635-4646.
- [12] A. Noglik, M. Roeb, C. Sattler, R. Pitz-Paal, *International Journal of Energy Research*, **2011**, 35, 449-458.
- [13] M.T. Balta, I. Dincer, A. *International Journal of Energy Research*, **2010**, 34, 757-775.
- [14] J.E. Funk, R.M. Reinstrom, *Ind. Eng. Chem. Process Des. Dev.*, **1966**, 5, 336-342.
- [15] J.L. Russell, J.T. Porter, *Proceedings of Hydrogen Energy Miami Energy Conference (Ed by T. N. Verziroglu)*, Plenum Press Newyork, **2007**, 517-529.
- [16] R.E. Chao, *I & EC Product Research Development*, **1974**, 13, 94-101.
- [17] L.C. Brown, J.F. Funk, S.K. Showalter, *General Atomics Report GAA23373*, **2000**.  
Available at <http://web.gat.com/pubs-ext/miscpubs/A23373.pdf>
- [18] M.A. Rosen, G.F. Naterer, R. Sadhankar, S. Suppiah, S., *Canadian Hydrogen Association Workshop*, Quebec, October 19-20, **2006**.
- [19] M. Lewis, J. Masin, Argonne National Laboratory, University of Chicago, November **2005**.
- [20] G.F. Naterer, S. Suppiah, M. Lewis, K. Gabriel, I. Dincer, M.A. Rosen, M. Fowler, G. Rizvi, E.B. Easton, B.M. Ikeda, M.H. Kaye, L. Lu, I. Pioro, P. Spekkens, P. Tremaine, J. Mostaghimi, J. Avsec, J. Jiang, *International Journal of Hydrogen Energy*, **2009**, 34, 2901-2917.
- [21] R.D. Doctor, D.C. Wade, M.H. Mendelsohn, *Proceedings of the American institute of chemical engineers spring national meeting*, New Orleans, March 10-14, **2002**.

## References

---

- [22] R.D. Doctor, D.T. Matonis, D.C. Wade, *Proceedings of nuclear hydrogen production, OECD nuclear energy agency second information exchange meeting, Argonne National Laboratory, October 2-3; 2003.*
- [23] R.D. Doctor, D.T. Matonis, D.C. Wade, A.V. Moiseyev, J.J. Sienicki, R. Faibish, *Proceedings of the spring national meeting of the American institute of chemical engineers, April 25-29; 2004.*
- [24] M. Sakurai, E. Bilgen, A. Tsutsumi, Y. Yoshida, *SolarEnergy*, **1996**, *57*, 51-58.
- [25] F. Lemort, P. Charvin, C. Lafon, M. Romnicanu, *Int. J. Hydrogen Energy*, **2006**, *31*, 2063-2075.
- [26] F. Lemort, C. Lafon, R. Dedryv re, D. Gondeau, *Int. J. Hydrogen Energy*, **2006**, *31*, 906-918.
- [27] G.E. Beghi, *Int. J. Hydrogen Energy*, **1986**, *11*, 761-771.
- [28] C. Marchetti, G. de Beni,. *EU/C-IS/722/72.e.*, *Commission of the European Community, EURATOM Joint Research Center, Ispra, Italy, 1972.*
- [29] E.B. Lee, C.K. Wu, *Westinghouse Electric Corp., Patent 3,888,750, June 10, 1975.*
- [30] J.H. Norman, G.E. Besenbruch, L.C. Brown, D.R. O'Keefe, C.L. Allen, *Final Report for the Period February 1977 through December 31, 1981General Atomic Company Report GA-A16713, 1981.*
- [31] Norman JH, Besenbruch GE, O'Keefe DR. GRI-80/ 0105, **1981.**
- [32] C. Forsberg, P.S. Pickard, P. Peterson, *Nuclear News*, **2003**, 30-32.
- [33] H. Nakajima, K. Ikenoya, K. Onuki, S. Shimizu, *Kagaku Kougaku Ronbunshu*, **1998**, *24*, 352-359.

## References

---

- [34] K. Onuki, S. Shimizu, H. Nakajima, S. Fujita, Y. Ikezoe, S. Sato, S. Machi, *Proceeding of the 8th World Hydrogen Energy Conference, Honolulu, 1990*, 547-556.
- [35] K. Onuki, H. Nakajima, S. Shimizu, S. Sato, I. Tayama, *J Hydrogen Energy System Society of Japan*, **1993**, 18, 49-56.
- [36] H. Nakajima, M. Sakurai, K. Ikenoya, G.J. Hwang, K. Onuki, S. Shimizu, *Proceedings of the 7th International Conference on Nuclear Engineering,, ICONE-7104Tokyo, Japan, 1999*.
- [37] M. Sakurai, H. Nakajima, K. Onuki, S. Shimizu, *J. Membr. Sci.*, **1999**, 156, 61-71.
- [38] X. Vitart, A. Le Duigou, P. Carles. *Energy conversion and management*, **2006**, 47, 2740-2747.
- [39] T. Drake, B.E. Russ, L. Brown, G. Besenbruch, *AIChE 2007 Fall Annual Meeting*, **2007**, 566.
- [40] S. Kubo, H. Nakajima, S. Kasahara, S. Higashi, T. Masaki, H. Abe, *Nucl. Eng. Des.*, **2004**, 233, 347-354.
- [41] J.H. Norman, K.J. Mysels, R. Sharp, D. Williamson, *Int. J. Hydrogen Energy*, **1982**, 7, 545-556.
- [42] P. Zhang, S.Z. Chen, L.J. Wang, T.Y. Yao, J.M. Xu, *Int. J. Hydrogen Energy*, **2010**, 35, 10166-10172.
- [43] G. Cerri, C. Salvini, C. Corngale, A. Giovannelli, D.D.L. Manzano, A.O. Martinez, A.L. Duigou, J. Borgard, C. Mansilla, *Int. J. Hydrogen Energy*, **2010**, 35, 4002-4014.
- [44] A. Le Duigou, J.M. Borgard, B. Larousse, D. Doizi, R. Allen, B. Ewan, *Int. J. Hydrogen Energy*, **2007**, 32, 1516-29.

## References

---

- [45] N. Sakaba, S. Kasahara, K. Onuki, K. Kunitomi, *Int. J. Hydrogen Energy*, **2007**, *32*, 4160-4169.
- [46] B.J. Lee, H. No, H.J. Yoon, H.G. Jin, Y.S. Kim, J. . Lee, *Int. J. Hydrogen Energy*, **2009**, *34* , 2133-2143.
- [47] S. Kasahara, S. Kubo, R. Hino, K. Onuki, M. Nomura, S. Nakao, *Int. J. Hydrogen Energy*, **2007**, *32*, 489-496.
- [48] T. Pregger, D. Graf, W. Krewitt, C. Sattler, M. Roeb, S. Mooller, *Int. J. Hydrogen Energy*, **2009**, *34*, 4256-4267.
- [49] D. Graf, N. Monnerie, M. Roeb, M. Schmitz, C. Sattler, *Int. J. Hydrogen Energy*, **2008**, *33*, 4511-4519.
- [50] A. Giaconia, G. Caputo, A. Ceroli, M. Diamanti, V. Barbarossa, P. Tarquini, S. Sau, *Int. J of Hydrogen Energy*, **2007**, *32*, 531-536.
- [51] D. O'Keefe, C. Allen, G. Besenbruch, L. Brown, J. Norman, R. Sharp, *Int. J of Hydrogen Energy*, **1982**, *7*, 381- 92.
- [52] G. Arifal, G.J. Hwang, K. Onuki, *Journal of Membrane Science*, **2002**, *210*, 39-44.
- [53] K. Onuki, G.J. Hwang, G. Arifal, S. Shimizu, *Journal of Membrane Science*, **2001**, *192*,193-199.
- [54] B. Belaissaoui, R. Thery, X.M. Meyer, M. Meyer, V. Gerbaud, X. Joulia, *Chemical Engineering and Processing*, **2008**, *47*, 396-407.
- [55] G.J. Hwang, K. Onuki, *Journal of Membrane Science*, **2001**, *194*, 207-215.
- [56] M. Roth, K.F. Knoche, *Int. J of Hydrogen Energy*, **1989**, *14*, 545-549.
- [57] C.E. Bamberger, *Cryogenics* ,**1978**, *18*, 170-183.

## References

---

- [58] Y. Shindo, N. Ito, K. Haraya, T. Hakuta, H. Yoshitome, *Int. J of Hydrogen Energy*, **1983**, 8, 509-513
- [59] T. Kumagai, S. Mizuta, *Industrial & Engineering Chemistry Process Design and Development*, **1985**, 24, 795-802.
- [60] I. Berzelius, *Berz. Jahresbericht*, 15 **1834/1835**) 237.
- [61] V. Smil, *Nature*, **1999**, 400, 415.
- [62] R. Pearce, W. R. Patterson, *Catalysis and chemical processes*, Leonard Hill, Scotland, **1981**.
- [63] G. A. Somorjai, *Introduction to surface chemistry and catalysis*, John Wiley Sons, Inc., New York, **1994**, 444.
- [64] P.H. Emmett, *CRC Crit. Rev. Solid State Sci.*, **1973**, 4, 127-150.
- [65] G.C. Bond, *Principles of Catalysis*, London Chemical Society, London, **1972**.
- [66] D. K. Chakrabarty, *Adsorption and catalysis by solids*, Wiley Eastern Limited, New Delhi, **1991**.
- [67] G. C. Bond, *Catalysis by Metals*, Academic Press, New York, **1962**.
- [68] S. J. Thomson and G. Webb, *Heterogeneous catalysis*, Oliver and Boyd, Edinburgh, **1968**.
- [69] B. Gates, J.R. Katzer, G.C.A. Schuit, *Chemistry of catalytic processes*, McGraw-Hill, New York, **1979**.
- [70] S. Roy, Morrison, *The Chemical Physics of Surfaces*, Plenum, New York, **1977**.
- [71] D.R. O'keefe, J.H. Norman, D. G. Williamson, *Catalysis Reviews: Science and Engineering*, **1980**, 22, 325-369.



## References

---

- [72] D.M. Ginosar, L.M. Petkovic, A.W. Glenn, K.C. Burch, *Int. J. Hydrogen Energy*, **2007**, *32*, 482-488.
- [73] L.M. Petkovic, D.M. Ginosar, H.W. Rollins, K.C. Burch, P.J. Pinhero, H.H. Farrell, *Appl. Catal. A: Gen*, **2008**, *338*, 27-36.
- [74] B.M. Nagaraja, K.D. Jung, B.S. Ahn, H. Abimanyu, K.S. Yoo, *Ind. Eng. Chem. Res.*, **2009**, *48*, 1451-1457.
- [75] M. Dokiya, T. Kameyama, K. Fukuda, Y. Kotera, *Bull. Chem. Soc. Jpn.*, **1977**, *50*, 2657-2660.
- [76] M. Bodehstein, *Z. Phys. Chem.*, **1899**, *3*, 295.
- [77] G. B. Kistiakowsky, *J. Am. Chem. Soc.*, **1928**, *50*, 2315.
- [78] J. H. Sullivan, *J. Chem. Phys.*, **1959**, *30*, 1292.
- [79] J. H. Sullivan, *J. Chem. Phys.*, **1959**, *30*, 1577.
- [80] J. H. Sullivan, *J. Chem. Phys.*, **1962**, *36*, 1925.
- [81] J. H. Sullivan, *J. Chem. Phys.*, **1967**, *46*, 73.
- [82] Y. Shindo, N. Ito, K. Haraya, T. Hakuta, H. Yoshitome, *Int J Hydrogen Energy*, **1984**, *9*, 695-700.
- [83] C.N. Hinshelwood , C.R. Prichard, *J. Chem. Soc.*, **1925**, *127*,1552.
- [84] C. N. Hinshelwoodand, R. E. Burke, *J. Chem. Soc.*, **1925**, *127*, 2896.
- [85] J.L. Holmes and L.S.M. Ruo, *J. Chem. Soc.*, **1968**, 1231 (1968).
- [86] J.M. Kim, J.E. Park, Y.H. Kim, K.S. Kang, C.H. Kim, C.S. Park, K.K. Bae, *Int J Hydrogen Energy*, **2008**, *33*, 4974-4980.

## References

---

- [87] Z.C. Wang, L.J. Wang, P. Zhang, S.Z. Chen, J.M. Xu, J. Chen, *Chinese Chemical Letters*, **2009**, *20*, 102-105
- [88] Y.W. Zhang, J. Zhou, Z. Wang, J. Liu, K. Cen, *Int J Hydrogen Energy*, **2008**, *33*, 2211-2217.
- [89] Y.W. Zhang, Z. Wang, J. Zhou, J. Liu, K. Cen, *Int J Hydrogen Energy*, **2008**, *33*, 602-607.
- [90] Y. Chen, Z. Wang, Y. Zhang, J. Zhou, K. Cen, *Int J Hydrogen Energy*, **2010**, *35*, 445-451.
- [91] Z. Wang, L. Wang, S. Chen, J. Xu, J. Chen, *Int J Hydrogen Energy*, **2010**, *35*, 8862-8867.
- [92] D.M. Ginosar, L.M. Petkovic, K.C. Burch, *AIChE Annual Meeting*, **2007**.
- [93] L.M. Petkovic, D.M. Ginosar, H.W. Rollins, K.C. Burch, C. Deiana, H.S. Silva, M.F. Sardella, D. Granados, *Int J Hydrogen Energy*, **2009**, *34*, 4057-4064
- [94] L. Wang, Q. Han, D. Li, Z. Wang, J. Chen, S. Chen, P. Zhang, B. Liu, M. Wen, J. Xu, *Int J Hydrogen Energy*, **2013**, *38*, 111-116.
- [95] Z. Wang, Y. Chen, C. Zhou, R. Whiddon, Y. Zhang, J. Zhou, K. Cen, *Int J Hydrogen Energy*, **2011**, *36*, 216-223.
- [96] P. Favuzza, C. Felici, L. Nardi, P. Tarquini, A. Tito, *Applied Catalysis B: Environmental*, **2011**, *105*, 30-40.
- [97] M. Lanchi, G. Caputo, R. Liberatore, L. Marrelli, S. Sau, A. Spadoni, P. Tarquini, *Int J Hydrogen Energy*, **2009**, *34*, 1200-1207.

## References

---

- [98] Y. Zhang, J. Zhou, Y. Chen, Z. Wang, J. Liu, K. Cen, *Int J Hydrogen Energy*, **2008**, *33*, 5477-5483.
- [99] P. Favuzza, C. Felici, M. Lanchi, R. Liberatore, C.V. Mazzocchia, A. Spadoni, P. Tarquini, A.C. Tito, *Int J Hydrogen Energy*, **2009**, *34*, 4049-4056.
- [100] Y. Zhang, Z. Wang, J. Zhou, J. Liu, K. Cen, *Int J Hydrogen Energy*, **2009**, *34*, 8792-8798.
- [101] Y. Zhang, Z. Wang, J. Zhou, J. Liu, K. Cen, *Int J Hydrogen Energy*, **2009**, *34*, 5637-5644.
- [102] I.V. Dulera, R.K. Sinha, *J. of Nucl. Mater.*, **2008**, *383*, 183–188.
- [103] A.M. Banerjee, M.R. Pai, K. Bhattacharya, A.K. Tripathi, V.S. Kamble, S.R. Bharadwaj, S.K. Kulshreshtha, *Int J Hydrogen Energy*, **2008**, *33*, 319-326
- [104] A.M. Banerjee, A.R. Shirole, M.R. Pai, A.K. Tripathi, S.R. Bharadwaj, D. Das, P.K. Sinha, *Applied Catalysis B: Environmental*, **2012**, *127*, 36-46.
- [105] A.M. Banerjee, M.R. Pai, S.S. Meena, A.K. Tripathi, S.R. Bharadwaj, *Int J Hydrogen Energy*, **2011**, *36*, 4768-4780.
- [106] J. Haber, J.H. Block, B. Delmon, *Pure & Appl. Chem.*, **1995**, *67*, 1257-1306.
- [107] R. Ryoo, S.H. Joo, M. Kruk, M. Jaroniec, *Adv. Mat.*, **2001**, *13*, 677-681.
- [108] F. Sch th, W. Schmidt, *Adv. Mat*, **2002**, *14*, 629-638.
- [109] H.P. Klug, L.E. Alexander, *X-ray Diffraction Procedures for Polycrystalline and Amorphous Materials*, John Wiley & Sons, Inc., NY, London, **1974**.
- [110] B. D. Cullity, *Elements of X-ray diffraction*, Addison-Wilson Publishing Comp. Inc., USA, **1959**.

## References

---

- [111] C. Suryanarayana, M.G. Norton, *X-ray diffraction: A Practical approach*, Springer Science Business Media, 1998.
- [112] S. Brunauer, P. Emmett and E. Teller, *J. Amer. Chem. Soc.*, **1938**, *60*, 309-319.
- [113] J.H. de Boer, B.C. Lipens, B.G. Lippens, J.C.P. Broekhoff, A.V. Heuvel, T.V. Osinga, *J. Colloid Interface Sci.*, **1966**, *21*, 405-414.
- [114] E.P. Barrett, L.G. Joyner, P.P. Halenda, *J. Amer. Chem. Soc.*, **1951**, *73*, 373-380.
- [115] D. Dollimore, G.R. Heal, *J. Appl. Chem.*, **1964**, *14*, 109-114.
- [116] R.W. Cahn, P. Haasen, E.J. Kramer, *Material Science and Engineering: Characterisation of Materials*, VCH Publisher Inc., New York, 1991.
- [117] D.B. William, C.B. Carter, *Transmission Electron Microscopy*, Plenum Press, New York, 1996.
- [118] D.A. Long, *The Raman Effect: A Unified Treatment of the Theory of Raman Scattering by Molecules*, John Willey Sons Ltd., 2002.
- [119] B. Schrader, *Infrared and Raman Spectroscopy—Methods and Applications*, VCH Publishers Inc. New York, USA, 1995.
- [120] G. Herzberg, *Molecular Spectra and Molecular Structure—II Infrared and Raman Spectra of Polyatomic Molecules*, D. Van Nostrand Company, Inc. USA, 1945.
- [121] J.R. Ferraro, *Introduction to Raman Spectroscopy*, Elsevier, 2003.
- [122] P. Serp, J.L. Figueiredo, *Carbon Materials for Catalysis*, John Wiley Sons, 2008.
- [123] E. Furimsky, *Carbons and Carbon Supported Catalysts in Hydroprocessing*, Royal Society of Chemistry, 2008.
- [124] T.F. Fuller, P. Strasser, *Carbon*, **2014**, *75*, 5-42,

## References

---

- [125] E. Antolini, *Applied Catalysis B: Environmental*, **2009**, *88*, 1-24.
- [126] V. Machek, B.N. Kuznetsov, Y.A. Ryndin, V.I. Kovalchuk, J. Chlebek, *React. Kinet. Catal. Lett.*, **1981**, *18*, 253-256.
- [127] E. Lam, J.H.T. Luong, *ACS Catal.*, **2014**, *4*, 3393-3410.
- [128] H. J ntgen, *Fuel*, **1986**, *65*, 1436-1446.
- [129] R.J. Mammone, M. Binder, D. Chu, *Army Research Laboratory Report*, ARL-TR-934, 1996.
- [130] V. Lordi , N. Yao, J. Wei, *Chem. Mater.*, **2001**, *13*, 733-737.
- [131] J.H. Vleeming, B.F.M. Kuster, G.B. Marin, F. Oudet, P. Courtine, *Journal of Catalysis*, **1997**, *166*, 148-159.
- [132] S. Ikeda, S. Ishino, T. Harada, N. Okamoto, T. Sakata, H. Mori, S. Kuwabata, T. Torimoto, M. Matsumura, *Angewandte Chemie*, **2006**, *118*, 7221-7224.
- [133] Y. Wang, D.C. Alsmeyer, R.L. McCreery, *Chem. Mater.*, **1990**, *2*, 557-563.
- [134] A.K. Shukla, M. Neergat, P. Bera, V. Jayaram, M.S. Hegde, *Journal of Electroanalytical Chemistry*, **2001**, *504*, 111-119.
- [135] J.J. Shao, Z.J. Li, C. Zhang, L.F. Zhang, Q.H. Yang, *Journal of Materials Chemistry A*, **2014**, *2*, 1940-1946.
- [136] Y. Oosawa, T. Kumagai, S. Mizuta, W. Kondo, Y. Takemori and K. Fujii, *Bull. Chem. Soc. Jpn.*, **1981**, *54*, 742-748.
- [137] S.K. Sonkar, M. Saxena, M. Saha, S. Sarkar S, *J Nanosci Nanotechnol.*, **2010**, *10*, 4064-4067
- [138] J. Fu , H. Qiao , D. Li , L. Luo , K. Chen, Q. Wei, *Sensors*, **2014**, *14*, 3543-3556.

## References

---

- [139] M. E. Davis, *Acc. Chem. Res.*, **1993**, *26*, 111-115.
- [140] A. Corma, *Chem. Rev.*, **1995**, *95*, 559-614.
- [141] J.S. Beck, J.C. Vartuli, W.J. Roth, M.E. Leonowicz, K.D. Schmidt, C.T.W. Chu, D.H. Olson, E.W. Sheppard, S.B. McCullen, J.B. Higgins, J.L. Schlenker, *J. Am. Chem. Soc.*, **1992**, *114*, 10834-10843.
- [142] A. Vinu, P. Srinivasu, M. Takahashi, T. Mori, V.V. Balasubramanian, K. Ariga, *Micro. Meso. Mat.*, **2007**, *100*, 20-26.
- [143] M. Ignat, C.J. Van Oers, J. Vernimmen, M. Mertens, S.S. Potgieter-Vermaak, V. Meynen, E. Popovici, P. Cool P., *Carbon*, **2010**, *48*, 1609-1618.
- [144] Z. Wu, Y. Yang, D. Gu, Y. Zhai, D. Feng, Q. Li et al., *Top Catal.*, **2009**, *52*, 12-26.
- [145] M.A. Pimenta, G. Dresselhaus, M.S. Dresselhaus, L.G. Cancado, A. Jorio A, R. Saito, *Phy. Chem. Chem. Phys.*, **2007**, *9*, 1276-91.
- [146] V.L. Zholobenko, A.Y. Khodakov, D. Durand, *Microporous and Mesoporous Materials*, **2003**, *66*, 297-302.
- [147] F.C. Tai, S.C. Lee, C.H. Wei, S.L. Tyan, *Materials Transactions*, **2006**, *47*, 1847.
- [148] A. Galarneau, D. Desplandier-Giscard, F. Di Renzo, F. Fajula, *Catalysis Today*, **2001**, *68*, 191-200.
- [149] V. Polshettiwar, D. Cha, X. Zhang, J.M. Basset, *Angewandte Chemie International Edition*, **2010**, *49*, 9652-9656.
- [150] H.W. Graham, W. Chun, R.W. McCabe, J.P. Cuif, S.E. Deutsch, O. Touret, *Catalysis Today*, **1999**, *50*, 309-328.
- [151] H. Knozinger, *Studies in Surface Science and Catalysis*, **1985**, *20*, 111-125.

## References

---

- [152] M. Gartner, V. Dremov, P. Muller, H. Kisch, *ChemPhysChem*, **2005**, 6, 714-716.
- [153] D. Cahen, J.E. Lester, *Chem Phys Lett*, **1973**, 18, 108-11.
- [154] A. Pfau, K.D. Schierbaum, *Surf. Sci.*, **1994**, 321, 71-80.
- [155] L. Qiu, F. Liu, L. Zhao, Y. Ma, J. Yao, *Applied Surface Science*, **2006**, 252, 4931-4935
- [156] H. Jensen , A. Soloviev, Z. Li, E.G. S gaard; *Applied Surface Science*, **2005**, 246, 239-249.
- [157] N.J. Price, J.B. Reitz, R.J. Madix, E.I Solomon; *Journal of Electron Spectroscopy and Related Phenomena*, **1999**, 98-99, 257-266.
- [158] D. Barreca, G.A. Battiston, R. Gerbasi, E. Tondello, P. Zanella, *Surf. Sci. Spectra*, **2000**, 7, 303-309.
- [159] M. Chun, M.J. Moon, J. Park, Y.C. Kang, *Bull. Korean Chem. Soc.*, **2009**, 30, 2729-2734.
- [160] M. Sakurai, H. Nakajima, R. Amir, K. Onuki, S. Shimizu, *Int J Hydrogen Energy*, **2000**, 25, 613-619.
- [161] H.F. Guo, P. Zhang, Y. Bai, L.J. Wang, S.Z. Chen, J.M. Xu, *Int J Hydrogen Energy*, **2010**, 35, 2836–2839.
- [162] Y. Bai, P. Zhang, H. Guo, S. Chen, L. Wang, J. Xu, *Chin J Chem Eng*, **2009**, 17, 160-166.
- [163] B. J. Lee, N.O.H. Cheon, Y.H. Joon, K.S. Jun, K.E. Soo, *Int J Hydrogen Energy*, **2008**, 33, 2000-2010

## References

---

- [164] D.H. Lee, K.J. Lee, Y.H. Kang, Y.H. Kim, C.S. Park, G.J. Hwang, *Trans Korean Hydrogen New Energ Soc*, **2006**, *17*, 395-402.
- [165] S. Colette, N.B. Mokrani, P. Carles, P. Fauvet, M. Tabarant, C.D. Rosset, *et al.*, *Proceedings of WHEC, France, Lyon*, **2006**.
- [166] M. Sakurai, H. Nakajima, K. Onuki, K. Ikenoya, S. Shimizu, *Int J Hydrogen Energy*, **1999**, *24*, 603-612.
- [167] M. Sakurai, H. Nakajima, K. Onuki, S. Shimizu, *Int J Hydrogen Energy*, **2000**, *25*, 605-611.
- [168] P. H. Svensson, L. Kloo, *Chemical Reviews*, **2003**, *103*, 1649-1684.
- [169] A.J. Blake, F.A. Devillanova, R.O. Gould, W.S. Li, V. Lippolis, S.S. Parsons, C. Radek, M. Schröder, *Chemical Society Reviews*, **1998**, *3*, 195-205.
- [170] E.H. Wiebenga, E.E. Havinga, K.H. Boswijk, *Advances in Inorganic Chemistry and Radiochemistry*, **1961**, *3*, 133-169.
- [171] A. Anderson, T.S. Sun, *Chemical Physics Letters*, **1970**, *6*, 611-616.
- [172] D. A. Palmer, R.W. Ramette, R.E. Mesmer, *Journal of Solution Chemistry*, **1984**, *13*, 673-683.
- [173] V.T. Calabrese, A. Khan, *J. Phys. Chem. A*, **2000**, *104*, 1287-1292.
- [174] S.B. Sharp, G.I. Gellene, *J Phys. Chem.*, **1997**, *101*, 2192-2197.
- [175] P. H. Svensson, L. Kloo, *J. Chem. Soc. Dalton Trans.*, **2000**, *14*, 2449-2455.
- [176] P. Deplano, J.R. Ferraro, M.L. Mercuri, E.F. Trogu, *Coord. Chem Rev*, **1999**, *188*, 71-95.